AD-A010 265

STRESS-CORROSION CRACKING OF METALLIC MATERIALS

PART III - HYDROGEN ENTRY AND EMBRITTLEMENT IN STEEL

OHIO STATE UNIVERSITY

PREPARED FOR
AIR FORCE MATERIALS LABORATORY

APRIL 1975

REPORT DOCUMENTATION PAGE

READ INSTRUCTIONS
BEFORE COMPLETING FORM

1. REPORT NUMBER	2. GOVT ACCESSION NO.	3. RECIPIENT'S CATALOG NUMBER
AFML-TR-72-102, Part III		AD A011 245

4. TITLE (and Subtitle)	5. TYPE OF REPORT & PERIOD COVERED
STRESS-CORROSION CRACKING OF METALLIC MATERIALS, PART III - Hydrogen Entry and Embrittlement in Steel	Final - December 15, 1968 through 31 Oct 1971
	6. PERFORMING ORG. REPORT NUMBER

7. AUTHOR(s)	8. CONTRACT OR GRANT NUMBER(s)
M. G. Fontana, R. W. Staehle	F33615-69-C-1258

9. PERFORMING ORGANIZATION NAME AND ADDRESS	10. PROGRAM ELEMENT PROJECT, TASK AREA & WORK UNIT NUMBERS
The Ohio State University Research Foundation 1314 Kinnear Road Columbus, Ohio 43212	Project No. 7312 Task No. 731202

11. CONTROLLING OFFICE NAME AND ADDRESS	12. REPORT DATE
Air Force Materials Laboratory Wright-Patterson Air Force Base, Ohio 45433	April, 1975
	13. NUMBER OF PAGES
	188 /9

14. MONITORING AGENCY NAME & ADDRESS(if different from Controlling Office)	15. SECURITY CLASS. (of this report)
	Unclassified
	15a. DECLASSIFICATION/DOWNGRADING SCHEDULE

16. DISTRIBUTION STATEMENT (of this Report)

Approved for public release; distribution unlimited.

DDC

MAY 27 1975

D

17. DISTRIBUTION STATEMENT (of the abstract entered in Block 20, if different from Report)

18. SUPPLEMENTARY NOTES

19. KEY WORDS (Continue on reverse side if necessary and identify by block number)

hydrogen embrittlement	hydrogen permeation	hydrogen entry
cathodic poisoners	stress corrosion cracking	
steel		

20. ABSTRACT (Continue on reverse side if necessary and identify by block number)

The chemical environment and metallurgical structure play important roles in the entry of hydrogen into iron and steel. In particular, the effect of compounds of sulfur, arsenic, phosphorus, selenium, and other elements, generally called "cathodic poisoners," is considered. The mechanism by which these substances act is not well understood, but several explanations of their behavior are offered in the text. Their effect is probably related to a perturbation of the surface layer of the metal, and this accelerates the hydrogen

DD FORM 1473 EDITION OF 1 NOV 65 IS OBSOLETE

20.

absorption kinetics significantly as the number of structural defects increases. The role of pH, electrochemical potential, stress, and temperature on the hydrogen entry kinetics is also considered. On the other hand, additions of certain compounds can decrease the kinetics. With regard to metallurgical factors that influence the hydrogen entry and permeation rates, these include the alloy composition (substitutional and interstitial atoms), annealing and tempering (temperature, time), grain size, and the microstructure (form and distribution of carbides, etc.). The literature regarding the stress corrosion cracking of high-strength steel is reviewed. Both metallurgical and environmental parameters are discussed in light of a hydrogen-induced slow crack growth process. Studies of slow crack growth in gaseous environments are reviewed, with a comparison of crack growth behavior in both gaseous and aqueous media. Although many similarities exist between crack growth in aqueous and gaseous environments, a recent observation of rapid crack propagation in pure Cl_2 gas questions the requirement for hydrogen as a critical species in gaseous environment slow crack growth.

FOREWORD

This report was prepared by Drs. Mars. G. Fontana and Roger W. Staehle of the Department of Metallurgical Engineering, The Ohio State University, Columbus, Ohio. The principal investigator for this project was Dr. Mars Fontana of the Department of Metallurgical Engineering, under Contract F33(615)-69-C-1258. This contract was initiated under Project No. 7312, "Metal Surface Deterioration and Protection," Task No. 731202, "Metal Surface Deterioration," during the period December 15, 1968 through October 31, 1971. This work was administered by the Advanced Metallurgical Studies Branch of the Metals and Ceramics Division, Air Force Materials Laboratory, Wright-Patterson Air Force Base, Ohio, under the direction of Dr. C. T. Lynch and the late Dr. H. B. Kirkpatrick (AFML/LLN).

The work reported herein consists of two review papers on the general problem of hydrogen entry and embrittlement of steel. Project funds supported research of the co-authors of these articles, who are former students in the Department and who are listed below.

1. Dr. George Kerns, whose Ph.D. dissertation was entitled, "Stress Corrosion Cracking in Gaseous and Aqueous Environments." At present Dr. Kerns is associated with the E. I. duPont de Nemours Co. Experimental Station, Wilmington, Delaware. He obtained his Ph. D. in March, 1973.

2. Dr. Ming T. Wang, whose Ph. D. dissertation was entitled, "Effect of Heat Treatment and Stress Intensity Parameters on Crack Velocity and Fractography of AISI 4340 and 18 Ni Maraging Steels." At present Dr. Wang is associated with the General Electric Company, Vallecitor Nuclear Center, Pleasanton, California. He obtained his Ph. D. in June, 1972.

3. Dr. R. Daniel McCright, whose Ph. D. dissertation was entitled, "Electro-Permeation of Hydrogen in Ferritic Structures." At present, Dr. McCright is an Adjunct Assistant Professor in the Department of Metallurgical Engineering at The Ohio State University. He obtained his Ph. D. in March, 1971.

This report was submitted by the authors in July, 1974.

NOTICE

When Government drawings, specifications, or other data are used for any purpose other than in connection with a definitely related Government procurement operation, the United States Government thereby incurs no responsibility nor any obligation whatsoever; and the fact that the government may have formulated, furnished, or in any way supplied the said drawings, specifications, or other data, is not to be regarded by implication or otherwise as in any manner licensing the holder or any other person or corporation, or conveying any rights or permission to manufacture, use, or sell any patented invention that may in any way be related thereto.

This report has been reviewed and cleared for open publication and/or public release by the appropriate Office of Information (OI) in accordance with AFR 190-17 and DOD 5230.9. There is no objection to unlimited distribution of this report to the public at large, or by DDC to the National Technical Information Service (NTIS).

This technical report has been reviewed and is approved for publication.

C. T. LYNCH
Senior Scientist
Metals Behavior Branch
Metals & Ceramics Division

FOR THE COMMANDER

N. G. TUPPER
Metals Behavior Branch
Metals Division

iv

TABLE OF CONTENTS

vii

LIST OF ILLUSTRATIONS - (Continued)

xi

LIST OF TABLES - Part I

xiv

LIST OF ILLUSTRATIONS - PART II

STRESS-CORROSION CRACKING OF METALLIC MATERIALS

INTRODUCTION

Hydrogen entry into steels and iron-base alloys is frequently responsible for the loss of useful physical and mechanical properties of these materials. This report is concerned with the problems of hydrogen absorption and permeation in steels, and of hydrogen embrittlement and related stress corrosion failure, particularly in the high-strength steels. This report is divided into two parts: the first part is addressed to hydrogen embrittlement and the second to hydrogen entry. These parts were presented at the International Conference on Hydrogen Embrittlement and Stress Corrosion Cracking of Iron Base Alloys, held in Unieux, France, in June, 1973, and will appear in the proceedings of that conference. The proceedings will be published in late 1974. The present report constitutes the third and final volume of the final report of the project, "Stress Corrosion Cracking of Materials."

PART I - STRESS CORROSION CRACKING AND HYDROGEN EMBRITTLEMENT IN HIGH-STRENGTH STEELS

G. E. Kerns
M. T. Wang
R. W. Staehle

INTRODUCTION

The purpose of this review is to characterize the stress-corrosion cracking and hydrogen embrittlement behavior of high- (and ultra-high) strength steels with regard to both metallurgical and environmental parameters. Despite the high-strength levels attainable for these steels, their industrial application is quite limited by susceptibility to delayed failure. Cracking has been observed in both distilled water and low-pressure hydrogen gas environments (in the absence of chloride or sulfide additions), as well as in marine atmospheres.

The steels examined in this review include low- and high-alloy martensitic steels, as well as martensitic and precipitation-hardenable stainless steels, at strength levels of 150 ksi or greater. Typical compositions are given in Table I. Maraging steels will be reviewed by D. Dautovich and S. Floreen.

The early studies in the environmental instability of steels were by A. R. Troiano, as summarized in the 1959 Campbell Memorial Lecture.[2] Similar delayed failure studies were conducted by Bastein et al.[3] Later studies, involving the exposure of smooth, self-stressed specimens to marine or industrial environments are typified by the work of Phelps and Liginow.[4] The later introduction of linear elastic fracture mechanics to stress-corrosion investigations was initiated by Brown.[5] Although the evolution of new testing procedures has permitted more detailed investigations, the static fatigue and stress-corrosion cracking phenomena for these steels are, in reality, the same. This is substantiated by effects of strength level, microstructure, and environmental variables.

There are indeed other effects observed in hydrogen-containing environments, such as blistering, micro-fissuring, etc. However, these processes are not strong functions of material strength level, as is the stress-corrosion cracking problem. Such additional phenomena will be treated in detail by M. Smialowski and others, and will not be discussed in this review.

Stress-corrosion cracking, delayed failure, hydrogen embrittlement, and sulfide cracking are then felt to be the result of the same phenomenon. The environments, per se, are simply believed to alter the effective hydrogen fugacity, as illustrated schematically in Fig. 1.

Preceding page blank

Table I - Typical Compositions of High Strength Steels [From the work of Sandoz (1)]

Type or Designation	C	Cr	Ni	Mo	Mn	Co	Cu	Al	Ti	Si	V	Other	Range of Nominal Tensile and Yield Strength, ksi	
													TS	YS
Low-Alloy Martensitic														
HY-130	0.12	0.6	5.0	—	0.9	—	—	—	—	0.2	—	—	145-155	130-145
4130	0.30	1.0	—	0.2	0.5	—	—	—	—	0.3	—	—	200-300	180-250
4340	0.40	0.8	1.9	0.25	0.7	—	—	—	—	0.6	—	—		
D6AC	0.45	1.15	0.55	1.0	0.8	—	—	—	—	0.25	0.05	—		
H-11	0.40	5.0	—	1.3	0.3	—	—	—	—	0.90	0.50	—		
High-Alloy Martensitic														
HP 9-4-45	0.45	0.3	8.5	0.20	0.10	3.75	—	—	—	0.10	0.10	—	185-250	170-220
HP 9-4-25	0.25	0.50	8.5	0.50	0.10	3.75	—	—	—	0.10	0.10	—		
HP 9-4-20	0.20	0.80	9.0	1.0	0.3	4.5	—	—	—	0.10	0.10	—		
10Ni-2Cr-1Mo-8Co	0.11	2.20	10.0	1.0	0.06	8.0	—	—	—	0.1	—	—		
Martensitic Stainless														
410	0.12	12.0	—	—	0.5	—	—	—	—	0.35	—	—	120-200	100-150
431	0.15	16.0	2.0	—	0.5	—	—	—	—	0.35	0.25	—	60-220	130-210
12Mo-V	0.26	12.3	0.75	1.0	0.5	—	—	—	—	0.3	0.29	—		
Precipitation-Hardening Stainless														
AM 364 (M)*	0.011	11.1	11.2	—	0.05	—	—	0.61	0.22	0.05	—	—	180-270	175-220
Custom 455 (M)	0.014	11.8	8.5	—	0.03	—	2.2	—	1.3	0.15	—	0.25Cb		
PH 13-8-Mo (M)	0.04	13.0	8.0	2.0	0.10	—	—	1.0	—	<0.10	—	—		
PH 14-8-Mo (SA)	0.035	14.5	8.5	2.2	0.85	—	—	1.2	—	0.05	—	—		
PH 15-7-Mo (SA)	0.07	15.0	7.0	2.2	0.60	—	—	1.0	—	0.30	—	—		
15-5-PH (M)	0.66	15.0	4.6	—	0.25	—	3.3	—	—	0.40	—	0.25Cb		
17-4-PH (M)	0.04	16.0	4.0	—	0.50	—	3.3	—	—	0.30	—	0.25Cb		
17-7-PH (SA)	0.07	17.0	7.0	—	0.25	—	—	1.0	—	0.30	—	—		
AM 350 (SA)	0.10	16.5	4.3	2.7	0.75	—	—	—	—	0.30	—	0.10N		
AM 355 (SA)	0.13	15.5	4.3	2.7	0.75	—	—	—	—	0.30	—	0.12N		
AFC 260 (SA)	0.07	15.0	1.8	4.5	—	13.0	—	—	—	0.13	0.25	0.15Cb		
AFC-77 (M)	0.15	14.0	0.2	5.0	0.2	13.0	—	—	—	—	—	—		

4
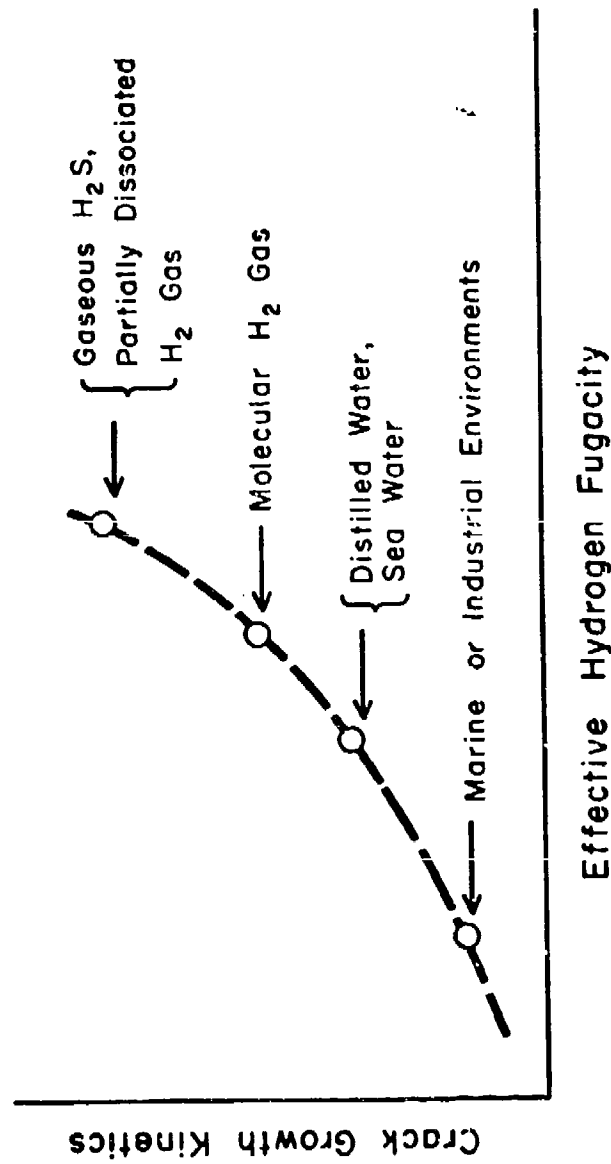
Fig. 1. Schematic Illustration of Severity of Stress Corrosion Cracking Environments

5

Early work by Phelps et al.[4] has indicated that both anodic dissolution and cathodic hydrogen embrittlement processes can result in the stress-corrosion cracking of high-strength steels. However, it now appears reasonable to view both stress-corrosion cracking and hydrogen embrittlement as the same process. This clarification is attributed to Brown et al.,[6] who measured the pH and potential values at the tips of growing stress-corrosion cracks, finding them to be sufficient for the production of hydrogen.

The primary goal in stress-corrosion cracking studies is to obtain reproducible test results. The use of smooth tensile or bent beam specimens does not satisfy this requirement. This is seen in early studies based on measured parameters of applied stress and time to failure.[7] The principal reason for such difficulties was felt to be a variation in the initiation time for stress-corrosion cracks. Thus, the application of fracture mechanics (with pre-cracked specimens) led to greater reproducibility. Additional studies, via fracture mechanics techniques, have permitted the measurement of crack velocity as a function of applied stress intensity. In summary, typical test data obtained using each technique are shown in Fig. 2. Generally, as seen in Fig. 2(c), three crack velocity regimes (I, II, III) are observed for high-strength steels in aqueous environments.

It is clearly established in the electrochemical literature that hydrogen reduction will occur in aqueous media at potentials more active (-) than the oxidation potential of the hydrogen electrode, $E° = 0.0 - 0.059$pH (for equilibrium with 1 atm gaseous H_2). Figure 3 shows the pH dependence of this potential, superimposed on the Pourbaix diagram for iron. At low pH values, the oxidation of iron in a deaerated solution must then give a potential between that for iron ($Fe \rightarrow Fe^{++}$) and the hydrogen electrode potential. Such is found to be the case in the stress-corrosion cracking of high-strength steels in neutral or acidic solutions.[8] The reduced hydrogen (atomic) can then re-combine (to give H_2 gas) or enter the steel. The uncombined hydrogen species is responsible for stress-corrosion cracking and delayed failure phenomena. The role of cathodic poisons is in affecting the residence time of dissociated hydrogen on the metal surface, but will be discussed in further detail by R. D. McCright.

This review will focus on the basic metallurgy of high-strength steels, test procedures, metallurgical effects on stress-corrosion behavior, environmental effects on cracking behavior, and proposed cracking mechanisms.

PHYSICAL METALLURGY AND MECHANICAL
PROPERTIES OF HIGH-STRENGTH STEELS

The physical metallurgy of high-strength steels has been discussed in the literature.[11-15] The high-strength steels will be reviewed, with regard to their general behavior.

(a)
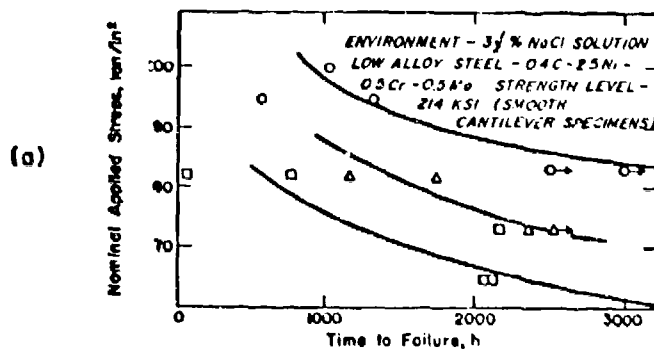
Effect of Stress on Time to Failure [From the work of Hughes et al. (7)]

(b)
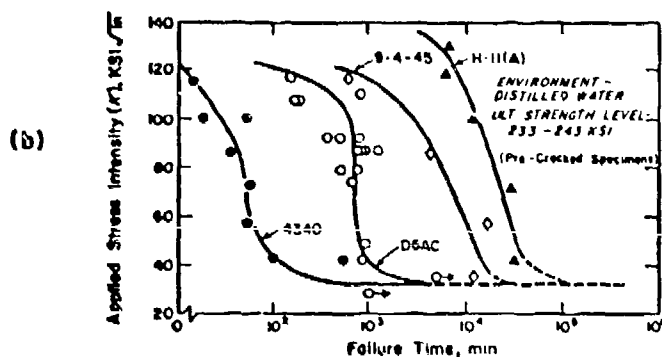
Effect of Stress Intensity on Time to Failure [From the work of Steigerwald and Benjamin (8)]

(c)
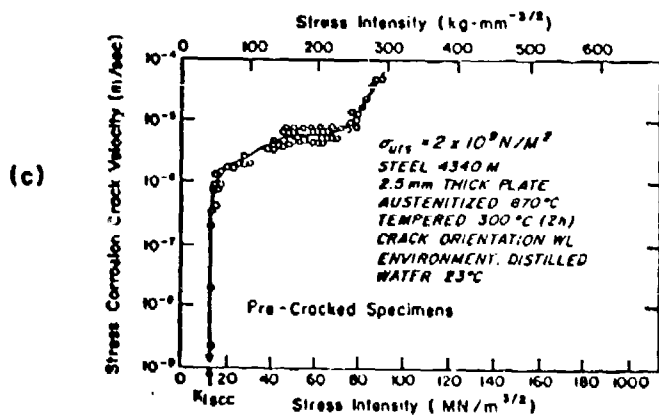
Effect of Applied Stress Intensity on Crack Velocity [From the work of Speidel (9)]

Fig. 2. Methods of Presenting Stress Corrosion Data

Stable Phases
Fe, Fe^{++}
Fe_3O_4, Fe_2O_3
H_2, O_2, H_2O
$HFeO_2^-$

O_2

ⓑ

Potential (vs SHE)

H_2O

ⓐ

0

Fe^{++}

H_2

Fe_2O_3

Fe_3O_4

Fe

$HFeO_2^-$

$\bar{0}$

7

$1\bar{4}$

pH
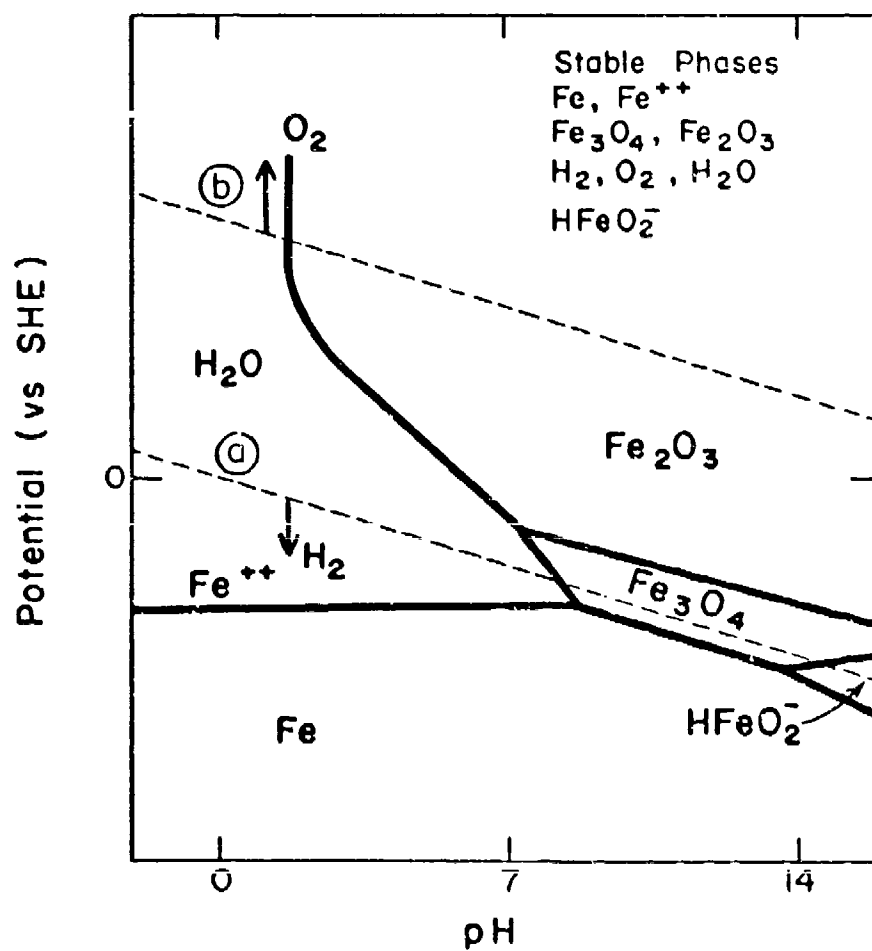
Fig. 3. Pourbaix Diagram for Iron-Water System at 25°C
[From the work of Pourbaix and de Zoubov (10)]

8

Low-alloy, high-strength steels are primarily heat treated by a quench and temper procedure, as shown for AISI 4340 steel in Fig. 4. Tensile properties and fracture toughness values are shown, as functions of tempering temperature, in Fig. 5. The as-quenched structure is martensite, with possible retained austenite. Upon tempering at temperatures up to 300°F, ϵ-carbide is precipitated at martensite plate or twin boundaries.[11] High dislocation densities are present in the martensite structure. Tempering above 400°F results in a resolution of ϵ-carbide, with concurrent Fe_3C precipitation. Carbide precipitation in 4340 steel has been studied by Klinger et al.[17] The carbide species and fracture toughness are shown in Fig. 6 as a function of tempering parameters. It is clear that martensitic structures tempered below 600°F have minimal fracture toughness (Fig. 5), with either ϵ-carbide or platelet cementite within the microstructure (Fig. 6).

Tempering of H-11 steel differs from that of 4340 in that carbides of the type M_2C, M_7C_3, M_6C, and $M_{23}C_6$ precipitate during the tempering process.[11] Tensile properties are shown as functions of tempering temperature in Fig. 7. Figure 8 shows the effect of tempering temperature on impact strength and tensile properties for Type 410 stainless steel. Both steels exhibit high strength levels at tempering temperatures up to 900°F.

Precipitation hardening stainless steels differ from martensitic stainless grades in that copper additions (17-4pH) and aluminum additions (17-7pH) promote age hardening during martempering. The effect is retained high strength levels at tempering temperatures up to 900°F. High-alloy martensitic steels (9Ni-4Co series) derive their strength from solid solution strengthening (carbon) and by carbide dispersion strengthening during tempering.[13]

The isothermal transformation diagram for a 0.1C-12Cr hardenable stainless steel is shown in Fig. 9. Since no "bainite knee" is observed, the use of marquenching procedures, with isothermal holds for up to several minutes below 800°F, are feasible during the hardening operation for 12Cr martensitic stainless steels.

The phenomenon of temper embrittlement is encountered in the majority of high-strength steels. Banerjee[11] has shown that 500°F embrittlement is observed with 4340 steel, as well as 900°F embrittlement for the cases of H-11 and Type 422 steels. Figure 10 shows the effect of tempering temperature on impact strength for 4340, H-11, and 300M steels. Type 410 stainless steel was found to exhibit 900°F embrittlement,[13] as shown in Fig. 8. In summary, the medium- or high-alloy steels generally exhibit 900°F embrittlement, while 500°F embrittlement is observed in low-alloy steel. Such behavior is shown schematically in Fig. 11. The 9Ni-4Co alloys, however, exhibit no significant temper embrittlement behavior.[13]

9
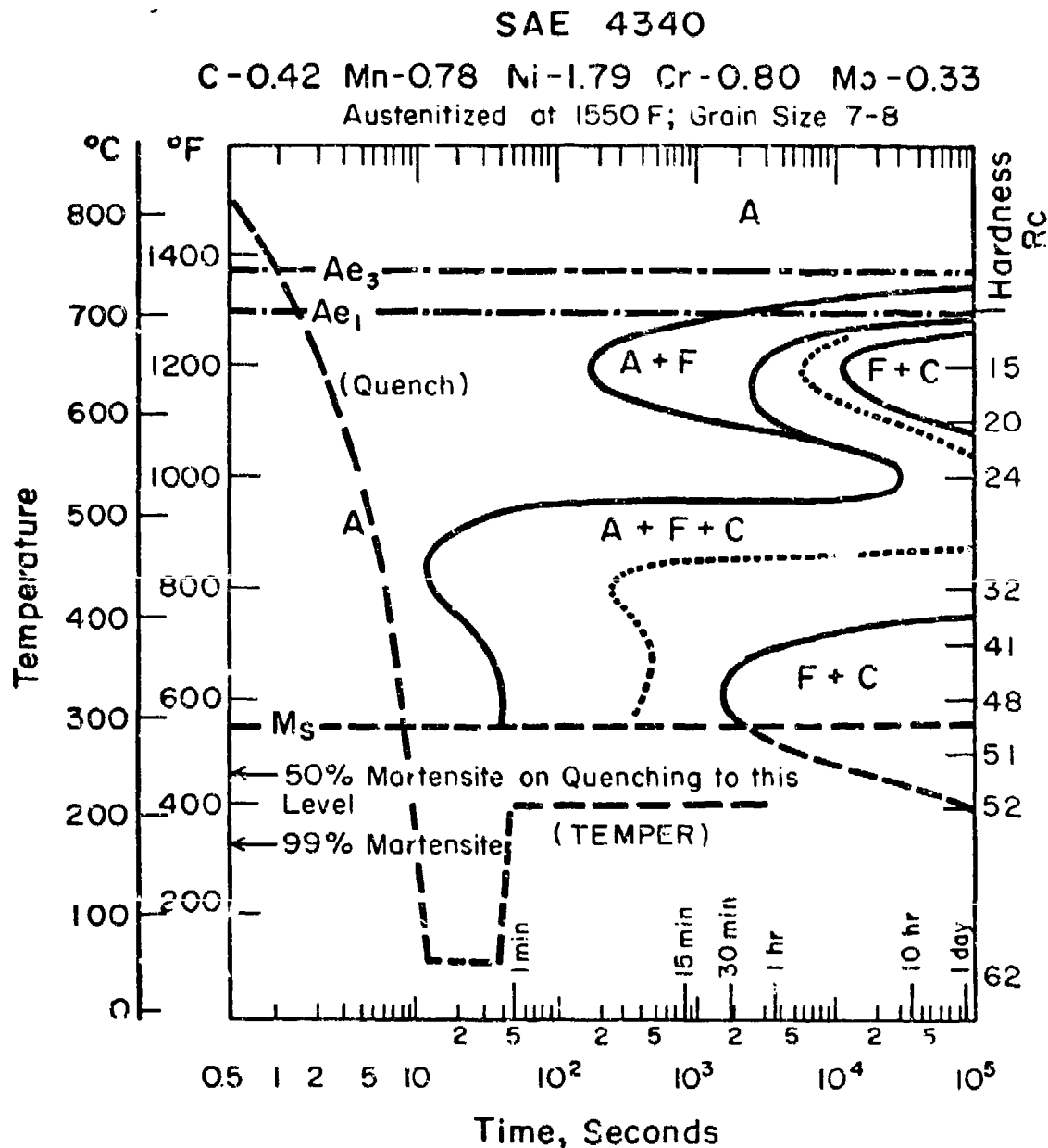
Fig. 4. Isothermal Transformation Diagram for SAE 4340 Steel [From published data (16)]

10

(a)

2 Hr at Tempering Temperature (°F)

(AIR-MELTED)   (VACUUM-INDUCTION)
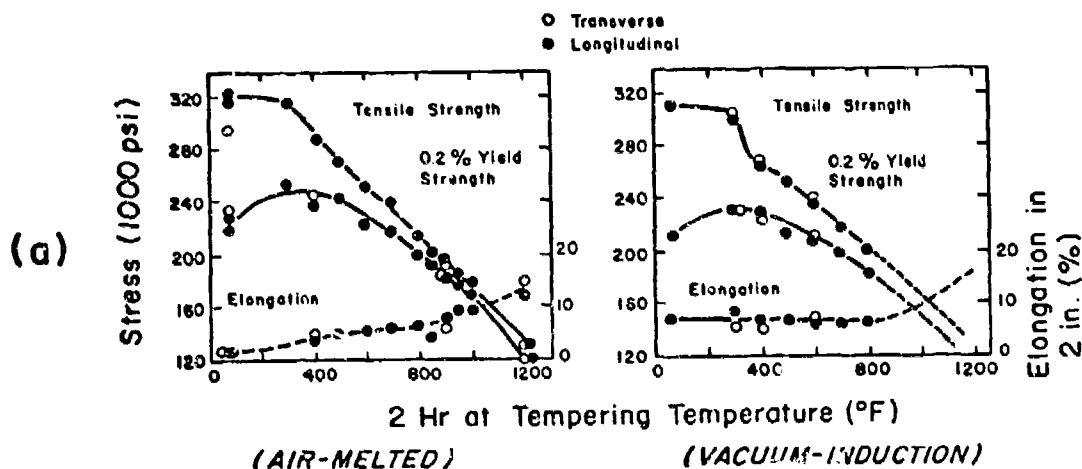
Tensile Properties of AISI 4340 Steel as Functions of Tempering
Temperature [From the work of Banerjee (11)]

(b)
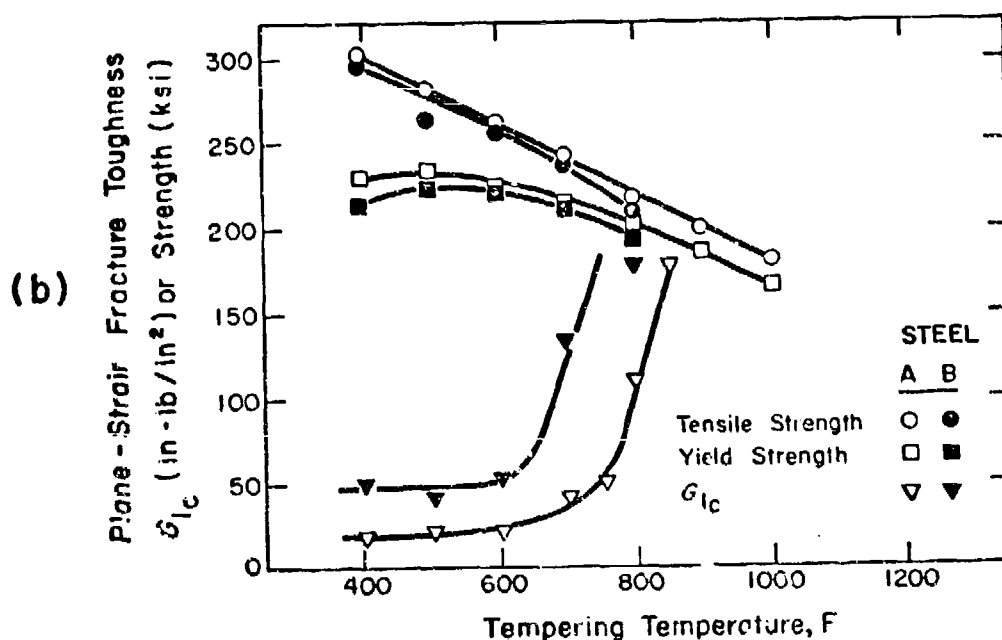
Tensile Properties and Fracture Toughness of AISI 4340 Steel
as Functions of Tempering Temperature [From the work of
Baker et al. (12)]

Fig. 5.   Mechanical Properties of AISI 4340 Steel
as Functions of Tempering Temperature

11
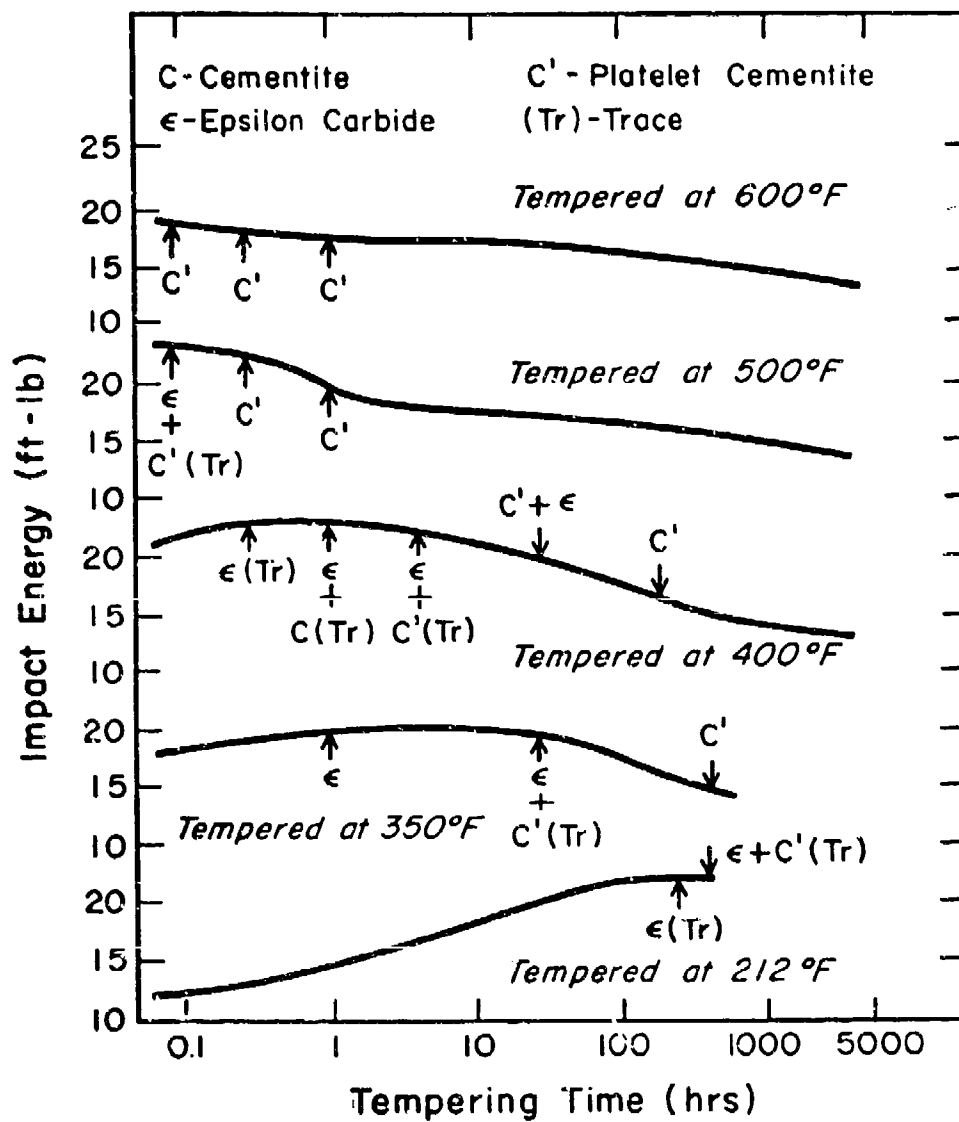
Fig. 6. Effect of Tempering Parameters on the Transition
Carbides and Impact Toughness of AISI 4340 Steel
[From the work of Klinger et al. (17)]
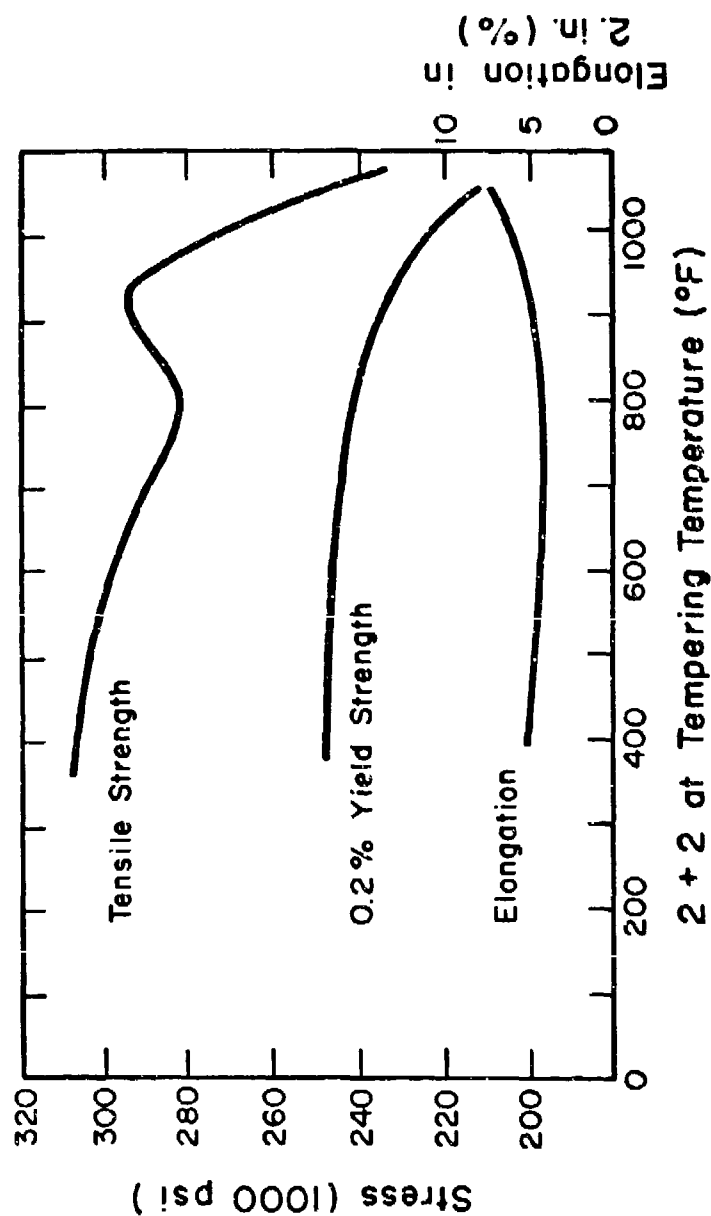
Fig. 7. Tensile Properties of H-11 Steel as Functions of Tempering Temperature [From the work of Banerjee (11)]

13

(a)
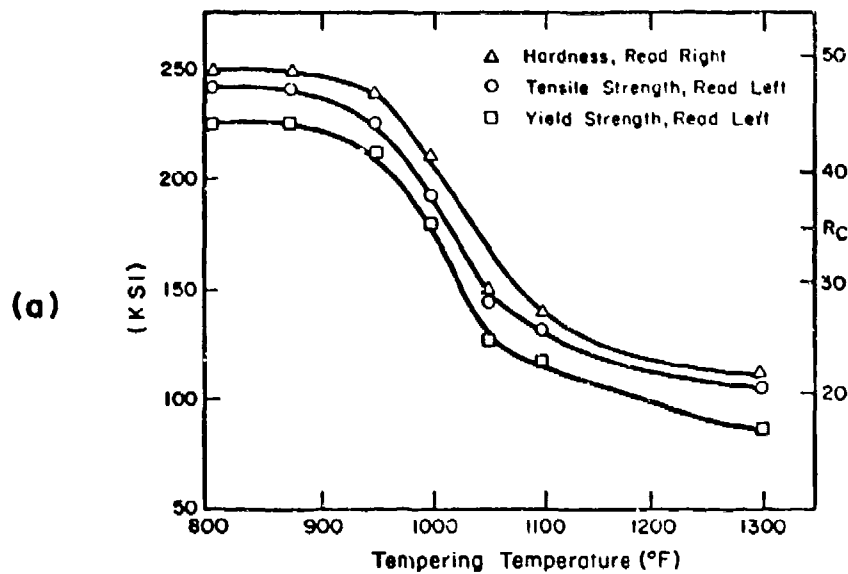
Effect of Tempering Temperature on the Tensile Properties
of Type 410 Stainless Steel [From the work of McGuire
et al. (18)]

(b)

SMOOTH BENT BEAM SPECIMENS
STRESS - 100 KSI CHARGED IN
0.IN H_2SO_4 + 3mg As/Hr.
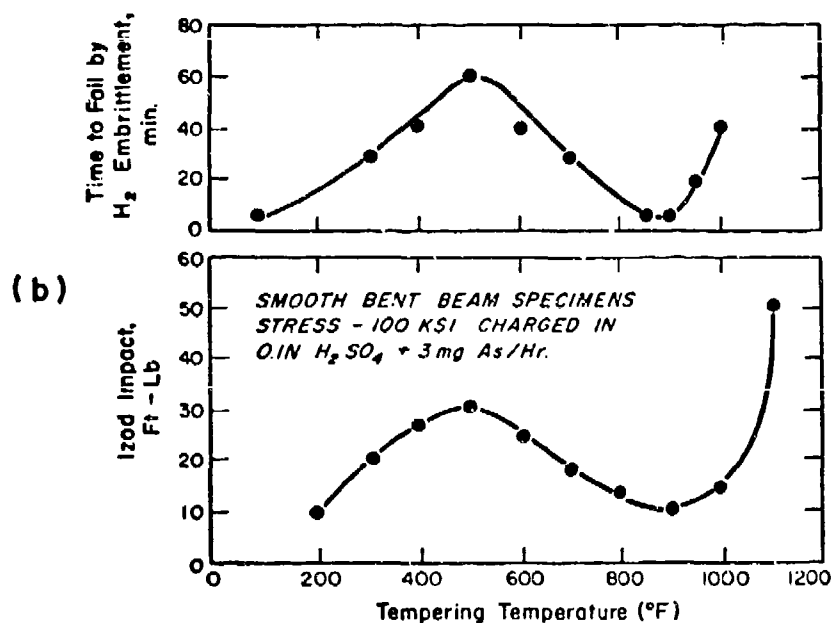
Effect of Tempering Temperature on Notch Impact Strength
and H_2 Embrittlement Susceptibility of Type 410 Stainless
Steel [From the work of Lillys and Nehrenberg (19)]

Fig. 8.   Effect of Tempering Temperature on Mechanical
Properties of Type 410 Stainless Steel

14
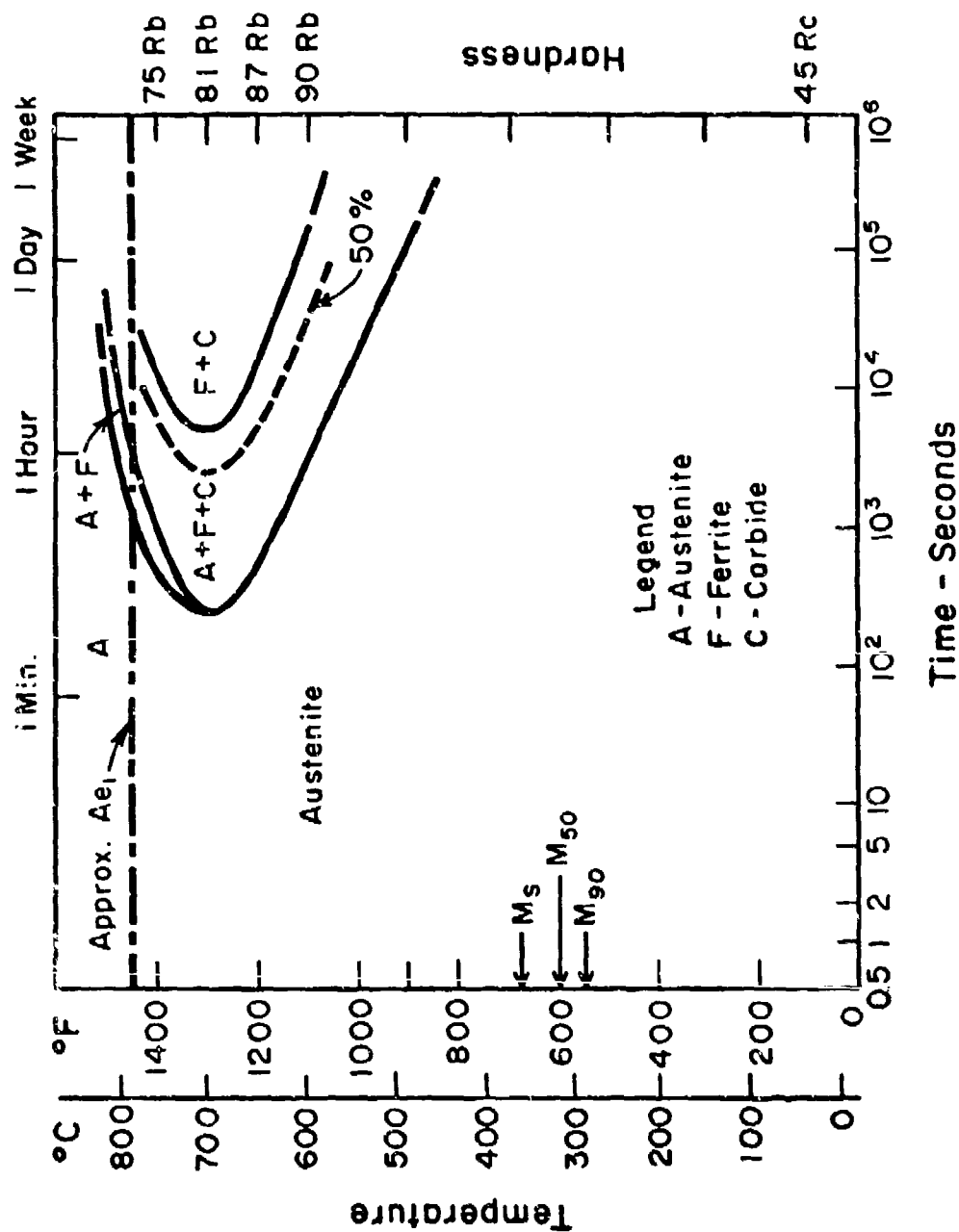
Fig. 9. Isothermal Transformation Diagram for Hardenable 12-Cr Stainless Steel [From the work of Rickett et al. (20)]

15
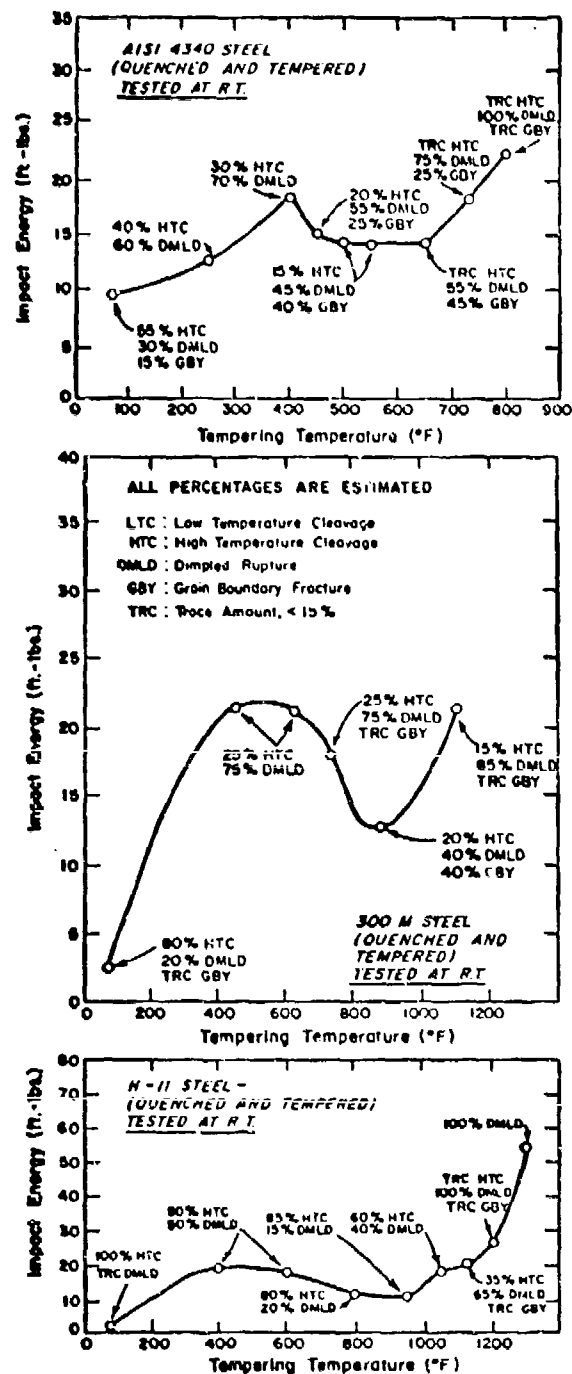
Fig. 10. Effect of Tempering Temperature
on Impact Toughness of 4340,
300M, and H-11 Steels [From
the work of Bucher et al. (21)]

16
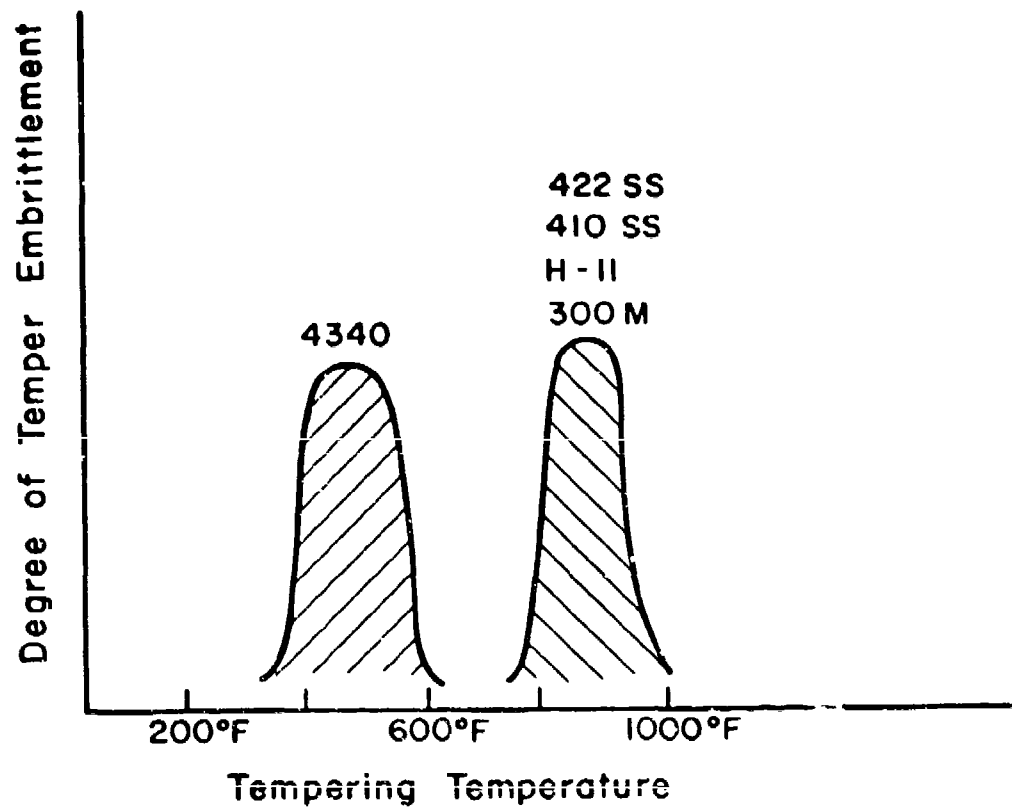
Fig. 11.   Schematic Illustration of Temperature Ranges
for Temper Embrittlement Phenomena

STRESS-CORROSION TEST METHODS

Stress-corrosion testing has involved the use of numerous specimen geometries. Early studies were based on self-stressed U-bend specimens, such as those described by Phelps et al.[4] and Davis.[22] Initial application of fracture mechanics involved the use of single-edge-notched specimens, as described by Proctor and Paxton,[23] and Carter.[24] Other geometries include the center-cracked sheet specimen, described by Hancock and Johnson,[25] and the double cantilever beam specimens, of the type used by Van der Sluys.[26] Figure 12 shows a schematic diagram of the self-stressed U-bend specimen. Fracture mechanics specimen geometries, and applicable stress intensity relationships, have been discussed by Brown,[28] and are shown in Figs. 13 and 14. Further discussion of such specimen geometries may be found elsewhere.[5,26,29,30] The use of fracture mechanics specimen geometries, with the associated pre-fatigue cracking procedure, has then minimized the variable of crack initiation time in stress-corrosion testing.

Two considerations are outstanding in the application of fracture mechanics to stress-corrosion cracking studies; i.e., (1) the stress state at the crack tip, and (2) the absence of ideal elastic behavior at the crack tip region. The existence of a triaxial stress state has been shown to greatly increase the effect of hydrogen on mechanical properties.[2] Therefore, the most severe stress corrosion test procedures include plane strain conditions at the crack tip. The specimen thickness requirement for plane strain is given[31] as

$$B \geq 2.5 \left(\frac{K_{Ic}}{\sigma_{ys}}\right)^2 ,$$

where

$B =$ specimen thickness (in.),

$K_{Ic} =$ critical stress intensity for catastrophic failure, and

$\sigma_{ys} = 0.2\%$ yield strength for the steel.

In reality, ideal elastic conditions do not exist at the crack tip. However, for the steels of interest in this review, the region of plasticity is not significant. The over-riding advantage of the fracture mechanics approach is that the applied stress intensity (K) concept provides a means of defining stress-corrosion behavior in terms of stress and flaw size, and in a reproducible manner.

18
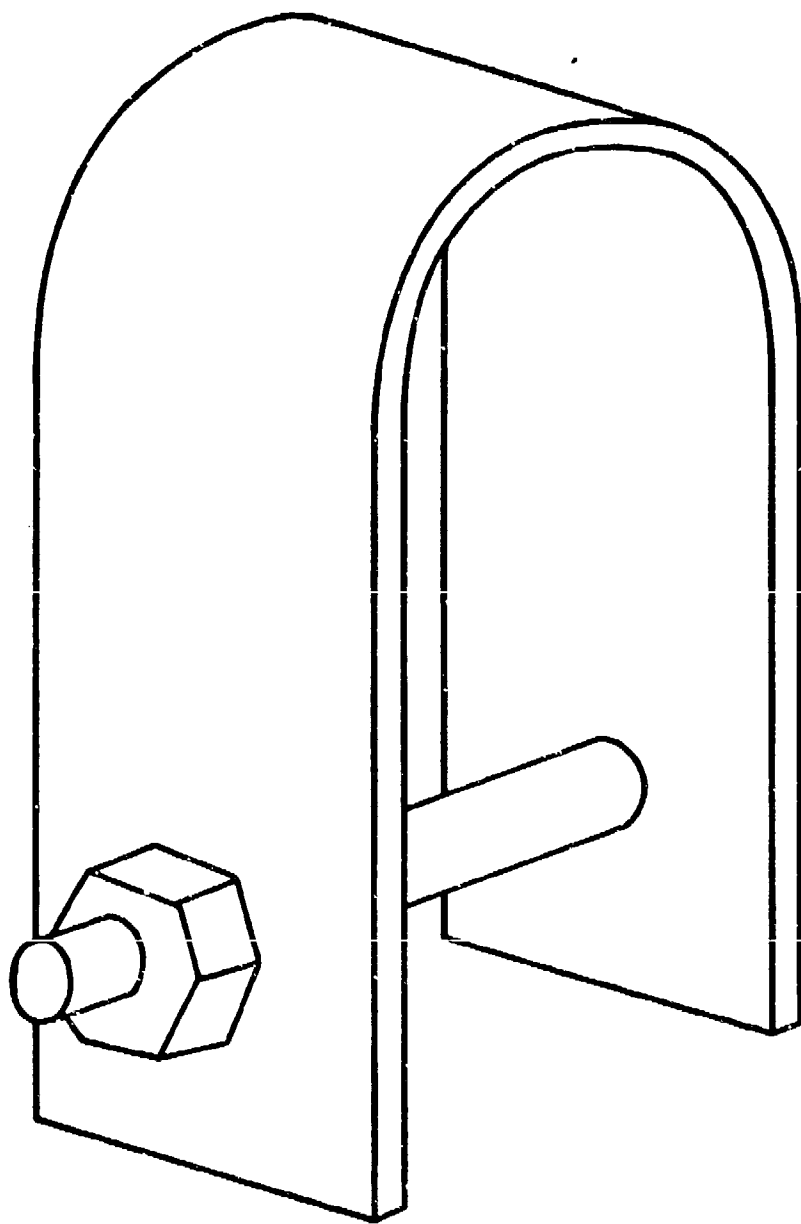
Fig. 12. Schematic Diagram of U-Bend
Specimen [From Logan (27)]

Specimen Type : (a) Center - Cracked Tension
(b) Single Edge Notched - 3 Point Loading
(c) Single Edge Notched - 4 Point Loading
(d) Single Edge Notched - Tension

(a)

$5 < W/B < 10$
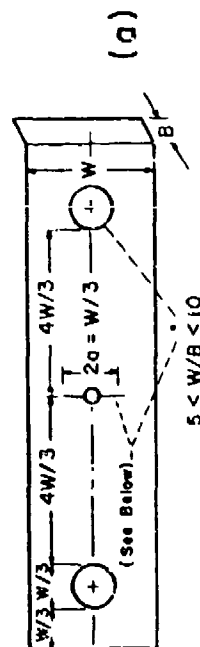
$$K_1 = \frac{P}{B}\frac{a^{\frac{1}{2}}}{W}\left[1.77 + 0.227\left(\frac{2a}{W}\right) - 0.510\left(\frac{2a}{W}\right)^2 + 2.7\left(\frac{2a}{W}\right)^3\right]$$

for range $\frac{2a}{W} = 0$ to 0.7

* *Surface Must be Symmetric to Specimen Centre Line within W/1000*

(b)

$2 < W/B < 8$

$$K_1 = \frac{6M}{B}\frac{a^{\frac{1}{2}}}{W^2}\left[1.96 - 2.75\left(\frac{a}{W}\right) + 13.66\left(\frac{a}{W}\right)^2 - 23.98\left(\frac{a}{W}\right)^3 + 25.22\left(\frac{a}{W}\right)^4\right]$$

for $\frac{a}{W} = 0$ to 0.5

(c)

$2 < W/B < 8$
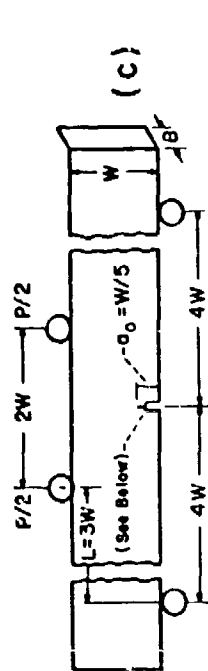
$$K_1 = \frac{6M}{B}\frac{a^{\frac{1}{2}}}{W^2}\left[1.99 - 2.47\left(\frac{a}{W}\right) + 12.97\left(\frac{a}{W}\right)^2 - 23.17\left(\frac{a}{W}\right)^3 + 24.80\left(\frac{a}{W}\right)^4\right]$$

for $\frac{a}{W} = 0$ to 0.6

Where $M = \frac{PL}{2}$

(d)

$4 < W/B < 8$
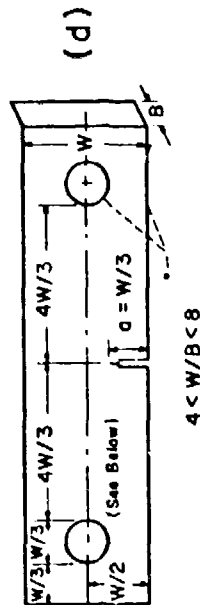
$$K_1 = \frac{P}{B}\frac{a^{\frac{1}{2}}}{W}\left[1.99 - 0.4124\left(\frac{a}{W}\right) + 18.70\left(\frac{a}{W}\right)^2 - 38.48\left(\frac{a}{W}\right)^3 + 53.85\left(\frac{a}{W}\right)^4\right]$$

for range $\frac{a}{W} = 0$ to 0.6

* *Surfaces Must be True to Specimen Centre Line Within W/1000*

Fig. 13. Specimen Geometry and Stress Intensity Relationships for Stress Corrosion Test Specimens [From the review by Brown (28)]

20

(a)
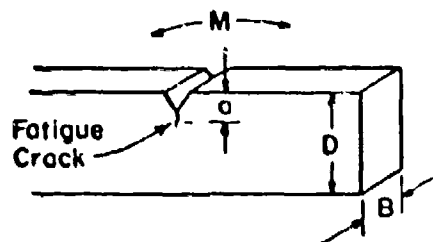
$$K_1 = \frac{4.12\, M\sqrt{\alpha^{-3} - \alpha^3}}{B D^{3/2}}$$

$$\alpha = 1 - \frac{a}{D}$$

(b)
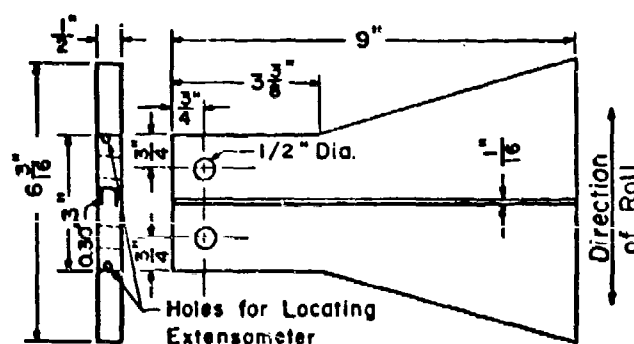
$$K = \frac{2P\left[3(a+a_0)^2 + h^2\right]^{\frac{1}{2}}}{\sqrt{b_n}\, b\, h^{3/2}\, (1 - \nu^2)^{1/2}}$$

(c)
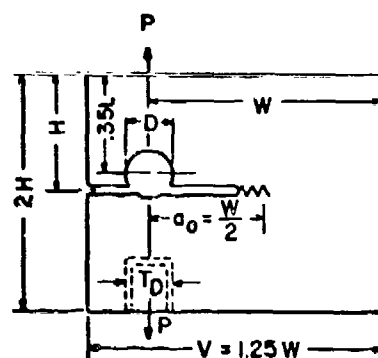
$$B = a_0$$
$$W = 2H = 2.0\,B$$
$$D = 0.6\,B$$
$$T_D = 0.5\,B$$
For a/W from 0.25 to 0.65

$$K_1 = \frac{P}{B}\,\frac{a^{1/2}}{W}\left[39.70 - 294\cdot2\left(\frac{a}{W}\right) + 1118\left(\frac{a}{W}\right)^2 - 1842\left(\frac{a}{W}\right)^3 + 1159\left(\frac{a}{W}\right)^4\right]$$

Fig. 14. Specimen Geometry and Stress Intensity Relationships for Stress Corrosion Test Specimens [From the review by Brown (28)]

EFFECT OF ALLOY STRENGTH LEVEL

The dominant metallurgical parameter in defining the susceptibility of high-strength steels to stress-corrosion cracking is strength level.[30] The classical approach to reducing the stress-corrosion cracking problem has been to lower the strength level. The strength level effect is clearly shown by the data of Brown[33] in Fig. 15. It is significant that the extrapolation of the K_{Iscc} curve, to intersect the K_{Ic} curve, defines the critical strength level at which there is a substantial chemical effect on the fracture of the steel. This is shown schematically in Fig. 16, and is a strong function of metallurgical and environmental parameters. It is important to realize that stress-corrosion cracking will occur below this strength level. However, the environmental effect on the fracture process is considerably less. The increase of strength level has been shown to decrease the threshold stress intensity for cracking (K_{Iscc}) and to increase crack growth kinetics in both gaseous and aqueous environments.

Smooth (unnotched) specimens of quenched and tempered AISI 4340 steel were tested by Hughes et al.[7] using 3% NaCl or 0.1N HCl aqueous environments. Failure times were strongly decreased by an increase of strength level in either environment, as shown by the data in Fig. 17.

Sandoz[34] has investigated the effect of strength level in 4340 steel, finding increased strength level to be detrimental in both gaseous and aqueous environments. The effect of strength level on the threshold stress intensity for cracking is shown in Fig. 18. The data were obtained using pre-cracked specimens of the single cantilever beam geometry. The data show that the threshold stress intensity for cracking is lowered by galvanic coupling to a more active metal (Mg) and raised by coupling to a more noble metal (Cu).

Crack velocities, for the same applied stress intensity, are substantially increased by increasing the strength level of the steel. Colangelo and Ferguson[35] observed higher velocities with increasing strength level for quenched and tempered AISI 4340 steel in a 3.5% NaCl solution; this is shown in Fig. 19. Crack velocities in dry hydrogen gas environments were found by Kerns[36] to be a strong function of strength level for quenched and tempered AISI 4335V and D6AC steels. The data, obtained using pre-cracked double cantilever beam specimens, are shown in Figs. 20 and 21. It is, however, an erroneous approach to define stress-corrosion cracking susceptibility as a function of strength level alone. The microstructure of high-strength steels is also affected on tempering of the martensitic structure.

EFFECT OF MICROSTRUCTURE

Sub-structure Effects

The particular susceptibility of high-strength martensitic steels to stress-corrosion cracking has been attributed to the presence
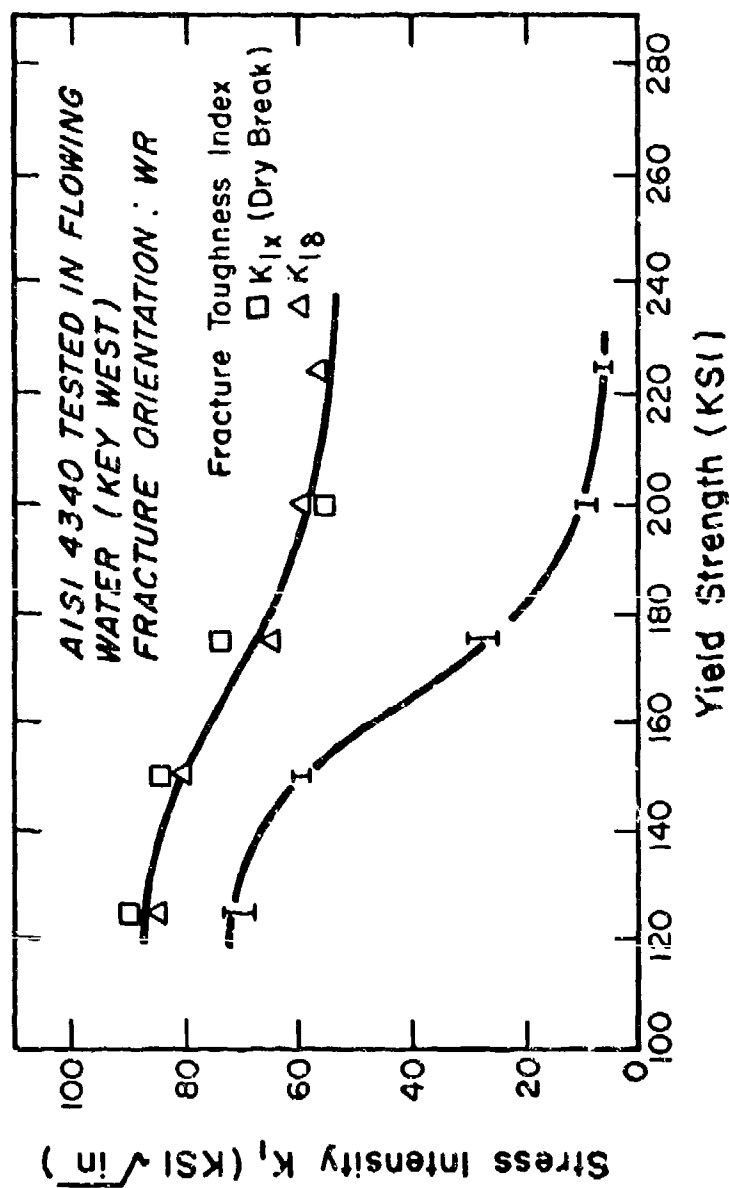
Fig. 15. Effect of Strength Level on K_{Ic} and K_{Iscc} for AISI 4340 Steel [From the work of Brown (33)]
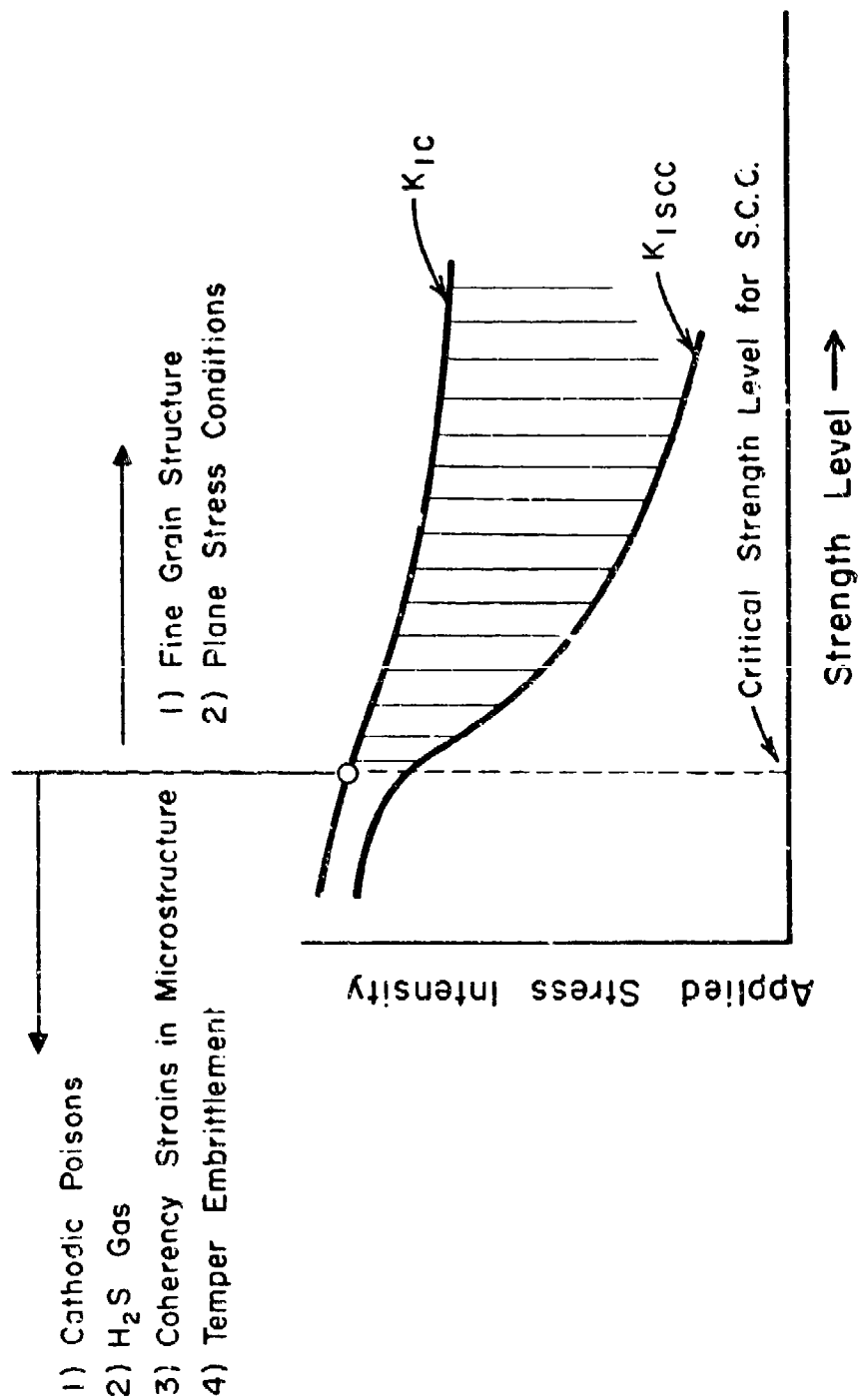
Fig. 16. Schematic Diagram Showing Effect of Metallurgical and Environmental
Variables on Critical Strength Level for Stress Corrosion Cracking
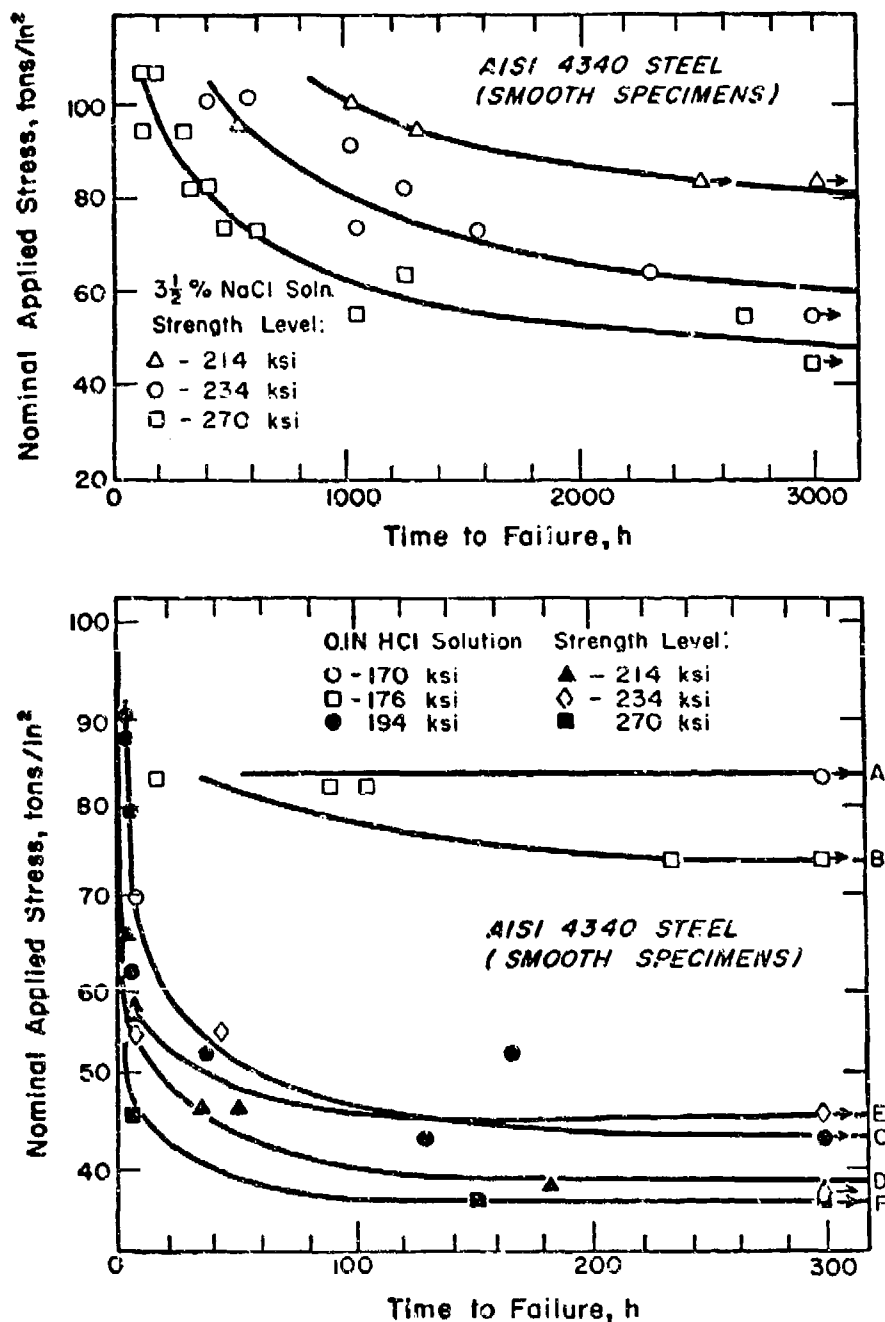
Fig. 17. Effect of Strength Level on Delayed Failure
on AISI 4340 Steel in Aqueous Solutions
[From the work of Hughes et al. (7)]

25
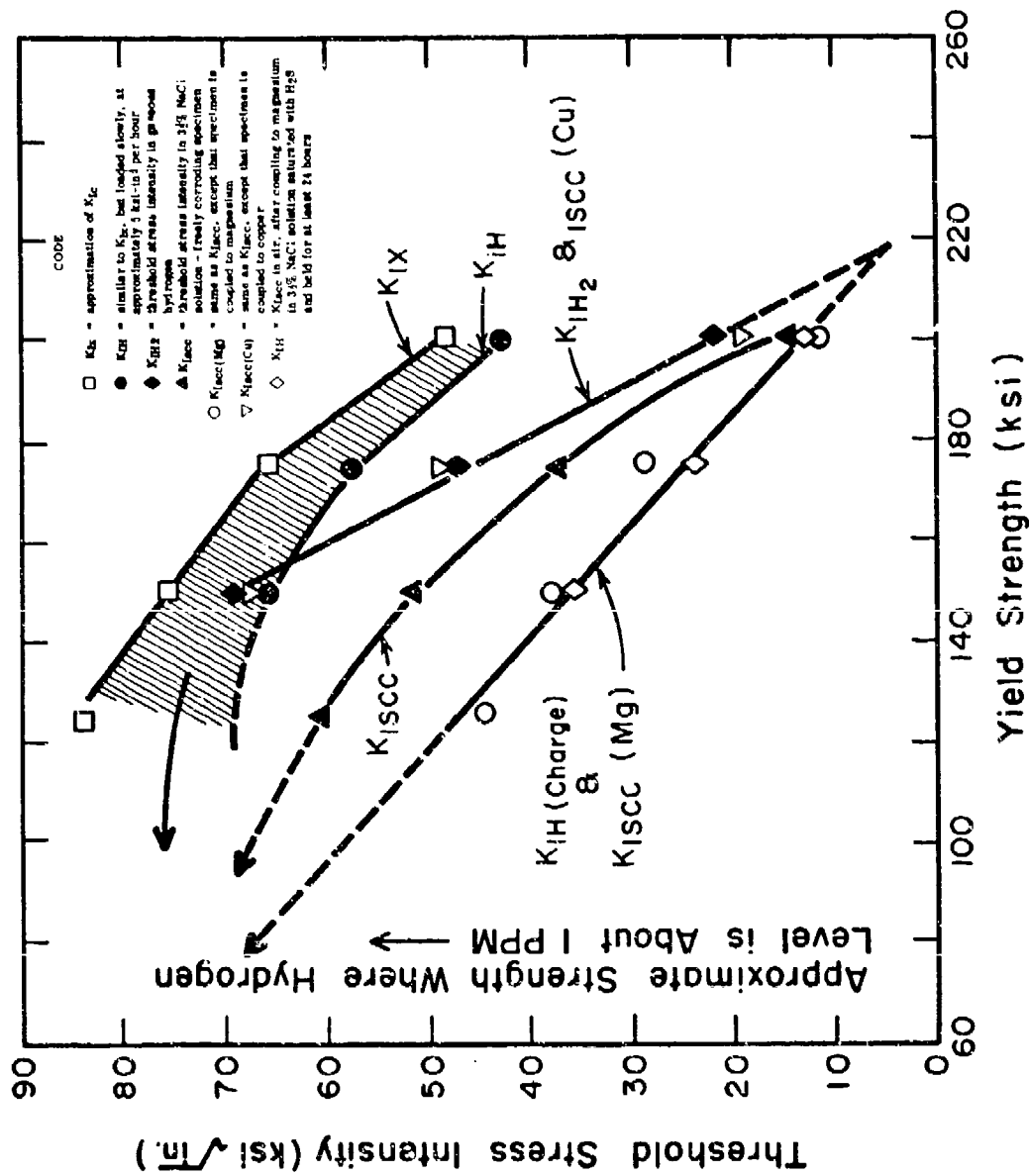
Fig. 18. Effect of Yield Strength on Threshold Stress Intensity for Crack Growth in Commercial AISI 4340 Steel [From the work of Sandoz (34)]
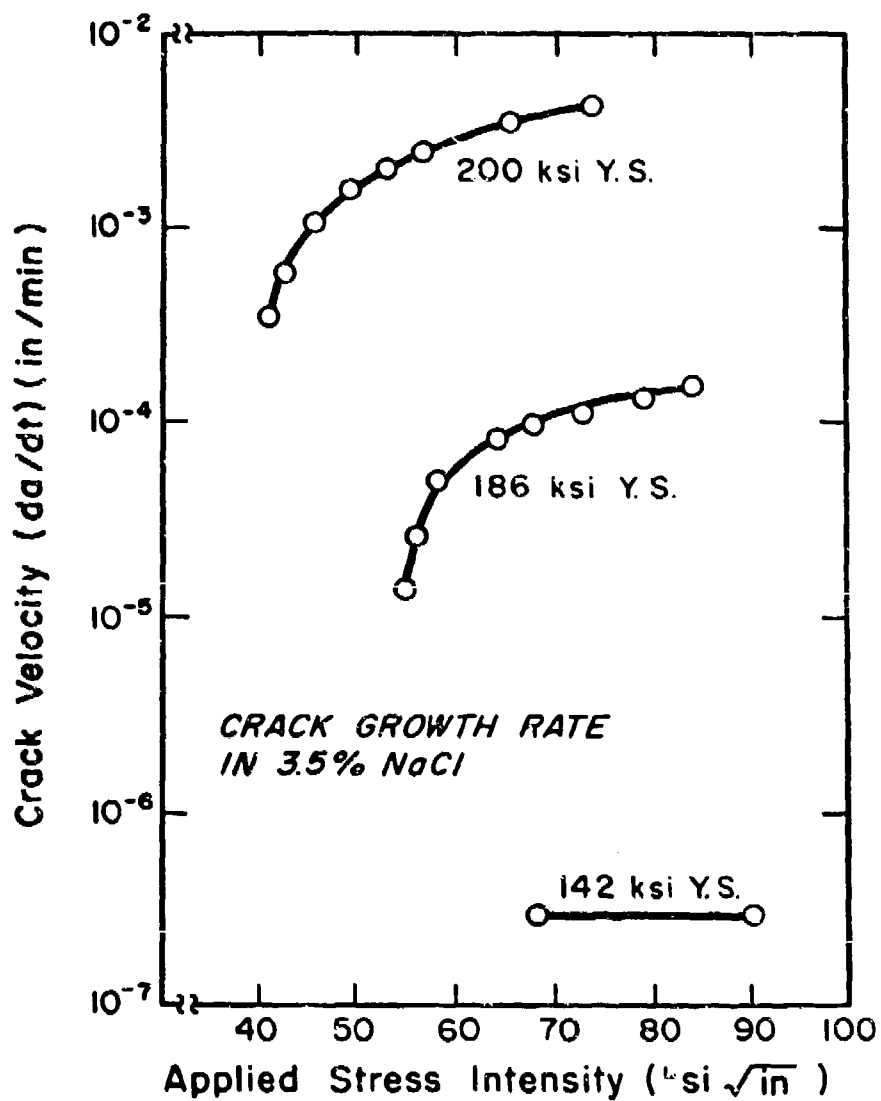
Fig. 19. Effect of Applied Stress Intensity on Crack Velocity for AISI 4340 Steel [From the work of Colangelo and Ferguson (35)]

27
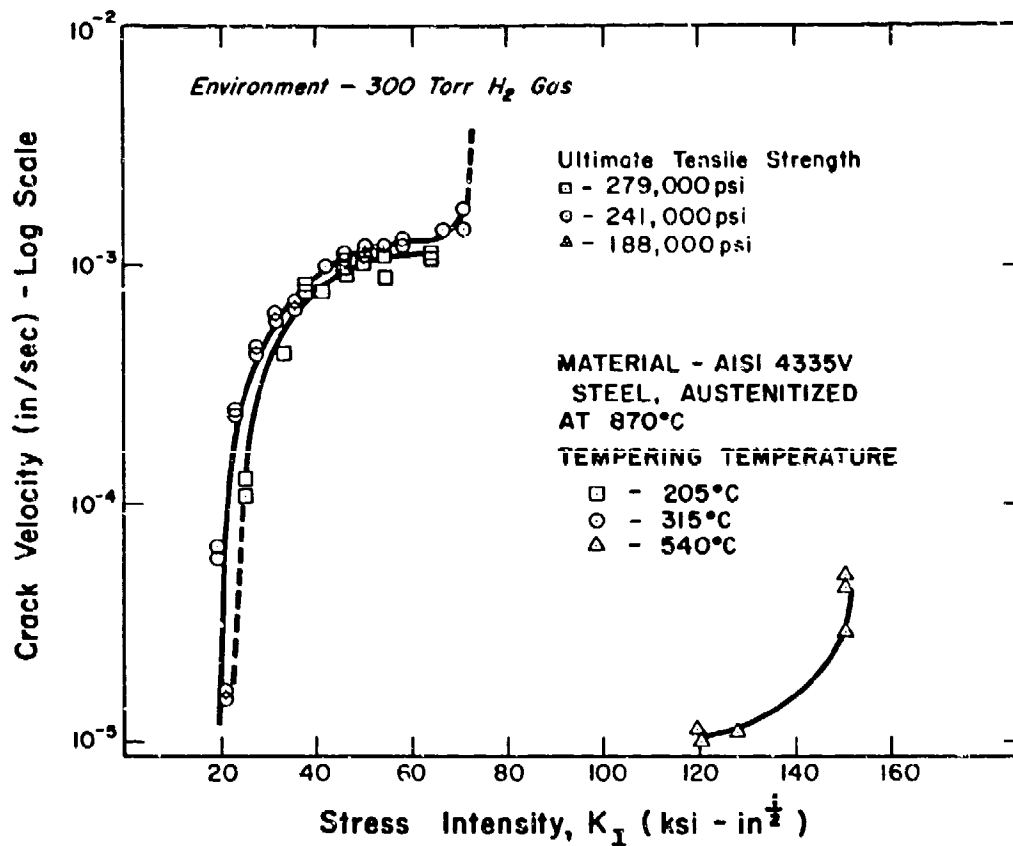
Fig. 20. Crack Velocity, as a Function of Tempering Temperature and Applied Stress Intensity for AISI 4335V Steel in Dry H_2 Gas [From the work of Kerns (36)]
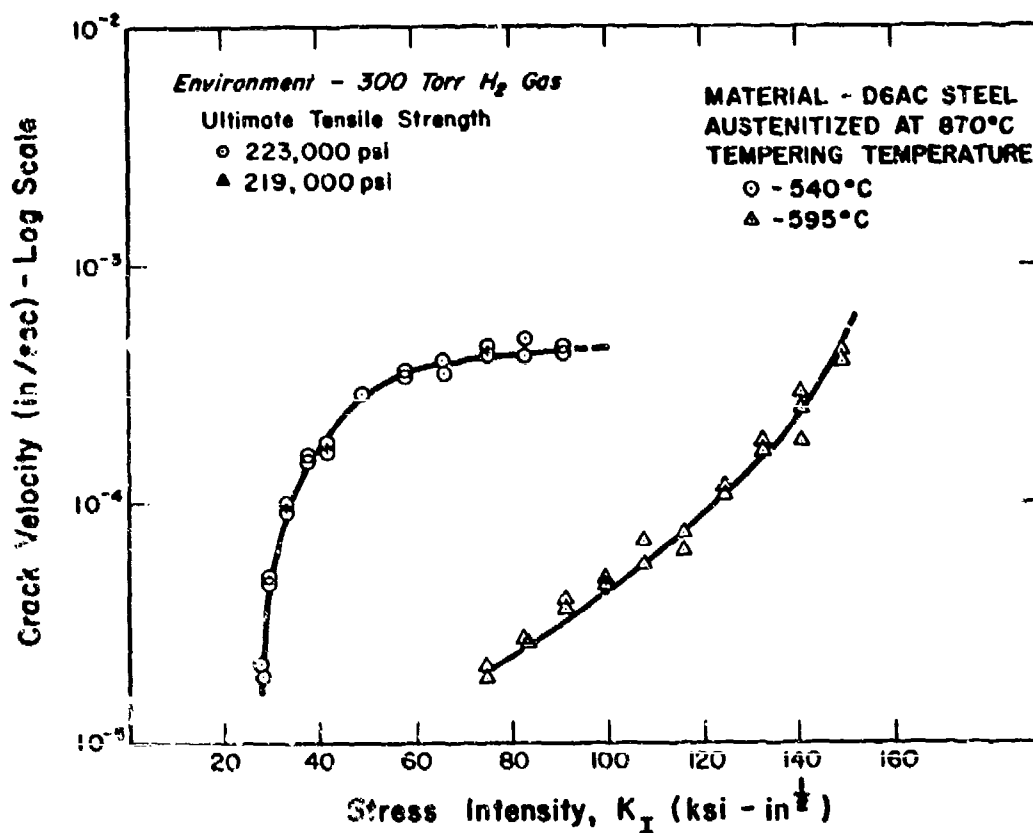
Fig. 21. Crack Velocity, as a Function of Tempering Temperature and
Applied Stress Intensity for D6AC Steel in Dry H_2 Gas
[From the work of Kerns (36)]

29

of c-carbides, high dislocation densities, and coherency strains between twinned martensite platelets.

Wang and Staehle[37] have shown that, for the same strength level, crack velocities are more than an order of magnitude greater for 4340 steel with a tempered martensite structure than for the lower bainite structure. Figure 22 shows crack velocity as a function of applied stress intensity for martensitic and bainitic steels. The difference was attributed to more effective trapping of hydrogen at coherently twinned interfaces in the plate martensite structure, as opposed to the incoherent bainite laths. It is also seen in Fig. 22 that the range of stress intensities required for cracking is notably lower for the martensite structure.

Vaughan and Phalen[38] have shown that the microstructure of tempered 4340 steel plays a significant role in the entry of hydrogen into the steel. The dislocation sub-structure of as-quenched martensite was found to be partially removed by tempering at temperatures up to 600°F. Subsequent hydrogen charging of steels tempered in this range, however, was found to regenerate the martensite sub-structure. Hydrogen charging of steels tempered at 800 or 1300°F showed blistering or grain boundary broadening, with no evidence of structural damage due to hydrogen entry into the grains. Details of the charging procedures were not given.[38] The regeneration of sub-structure was attributed to the ease of hydrogen entry into martensite tempered at low temperatures. Baker et al.[13] have described the microstructural changes in AISI 4340 steel brought about by tempering above 600°F as (1) recovery processes which lower the dislocation density in the martensite, (2) disappearance of twin boundary structure, and (3) spherodization of carbides precipitated at twin boundaries between martensite plates.

The susceptibility of martensitic 400-series stainless steels to both stress-corrosion cracking and to temper embrittlement occur within a range of tempering temperatures which promotes the re-solution of one carbide species, and the simultaneous re-precipitation of another. Banerjee[11] has shown that H-11 and Type 422 stainless steel undergo temper embrittlement in the 900 to 1000°F tempering range. Studies with 4340 steel[11] have shown 500°F embrittlement to occur. For each steel, carbide analysis was performed by electron and x-ray diffraction analysis, in addition to electron microprobe analysis. The relative carbide intensities are shown in Fig. 23 for each steel, as a function of tempering temperature. The temper-embrittled structures exhibited high dislocation densities, with dislocation pinning by precipitated carbides. Such carbides were of the M_3C for 4340 steel and $M_{23}C_6$ for Type 422 stainless steel. Unnotched bent-beam specimens of martensitic stainless steels (Types 410, 420, 422, and 436) were tested by Lillys and Nehrenberg[13] in a 5% salt spray environment. Minimum failure times were observed after a 900°F temper. Additional studies were conducted with Type 410 stainless steel by charging stressed specimens (100 ksi) in 0.1N H_2SO_4, containing 3 mg As/ℓ. The delayed failure results (Fig. 8b) indicate minimum failure times for a 900°F temper. The two
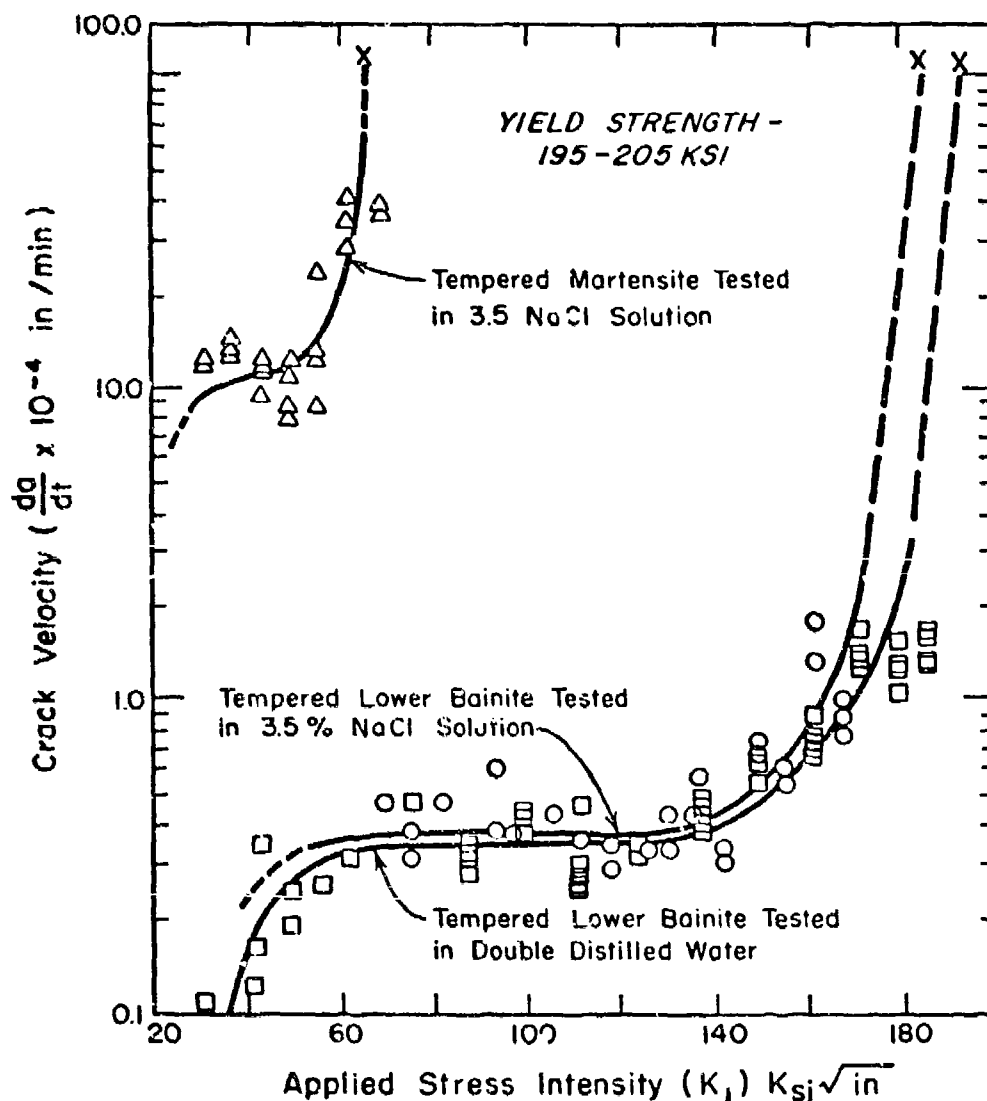
Fig. 22. Crack Velocity vs. Stress Intensity for AISI 4340 Steel (Martensitic and Bainitic Structures) in $3\frac{1}{2}\%$ NaCl Solution (pH = 6.0) or Double Distilled Water [From the work of Wang and Staehle (37)]
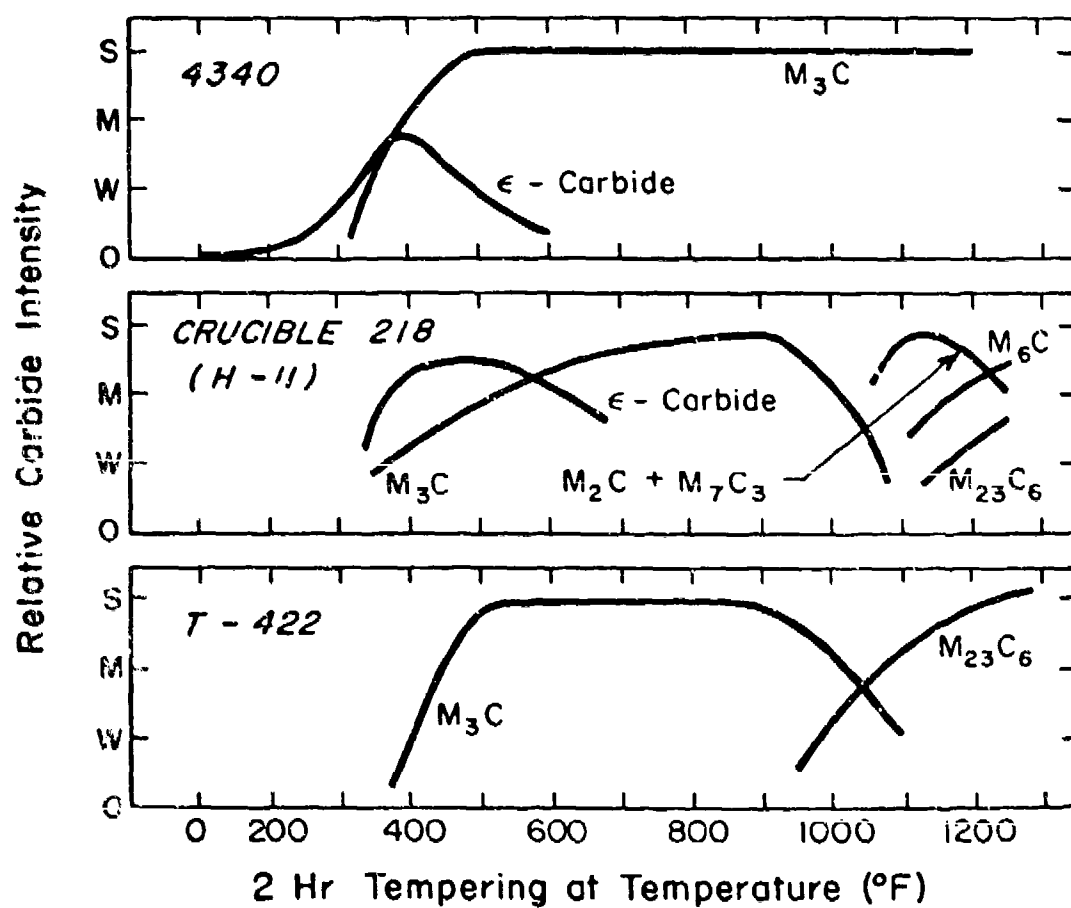
Fig. 23. Relative Carbide Intensities in Low Alloy and Stainless Steels as a Function of Tempering Temperature [From the work of Banerjee (11)]

studies[11,19] show that temper embrittlement and susceptibility to stress-corrosion cracking occur over the same range of tempering temperatures.

Zackay et al.[39] have shown a markedly greater resistance to delayed failure for a TRIP (TRansformation Induced Plasticity) steel, as compared to a tempered martensitic steel of the same strength level. The steel compositions and heat treatments are given in Table II. Pre-fatigue cracked SEN (single edged notched) specimens of TRIP steel were pre-loaded to a fraction of the critical stress intensity for unstable fracture (K_{Cr}). Both martensitic and TRIP steel specimens were then charged in 4 wt% H_2SO_4 solution, containing a poison (white phosphorus dissolved in CS_2). Following Cd-plating and baking, the specimens were statically loaded. No failures were observed for the TRIP steel at loads corresponding to $0.8\ K_{Cr}$ and times of up to 510 minutes. The martensitic steel failed rapidly, as shown in Table III. Microscopic examination of TRIP steel specimens showed that hydrogen cracking was limited to the crack tip region (transformed to martensite on pre-loading), with no observable macroscopic crack extension.

Ausforming of D6AC steel, prior to quenching, has been found to both refine the final microstructure and increase delayed failure times in a distilled water environment by an order of magnitude. Ault et al.[40] have investigated aus-bay quenching and ausforming processes for D6AC, using the treatments in Table IV. Plane strain fracture toughness values were obtained using pre-fatigue cracked notched round specimens. Figure 24 shows the improvement in toughness obtained by ausforming; Fig. 25 shows the delayed failure times for un-notched specimens in a distilled water environment. Microstructural observations revealed that both martensite platelet and carbide sizes were reduced in the ausformed steel, with a more uniform carbide distribution.

Table II - Composition and Heat Treatment of
Martensitic and TRIP Steels
[From the work of Zackay et al. (39)]

| Steel | Composition (w/o) | | | | | | Heat Treatment |
	C	Mn	Si	Cr	Ni	Other	
TRIP	0.25	2.1	2.0	8.8	8.3	3.7 Mo	Solution annealed at 1175°C for 1 hr, ice brine quenched, and 80% warm rolled at 425°C
Tempered Martensite	0.46	0.4	2.1	0.5	12.0	4.0 Co	Austenitized at 1000°C for 1/2 hr, oil quenched, and tempered at 450°C for 2 hr + 2 hr

Table III - Hydrogen Charging Conditions, Stress Levels, and Loading Times for Martensitic and TRIP Steels [From the work of Zackay et al. (39)]

Specimen	σ(ult)	K_{ci}, ksi$\sqrt{in}$	Plastic Zone loaded at 1b (Pct) f_{ci}	Hydrogen Charging Conditions			Bake Time, min	Dead Weight Helium Condition		
				Thick., mm	Current Density ma/in²	(J)Pitted		Dur., min	load, lb	Pct K_{ci}
1	102	139		50	125	No	0	60	3560	70
2	101	135		50	125	No	0	240	4165	80
3	103.0	144				No	0			
4	102.2	138	80	50	125	No	0	210	4150	80
5	102.6		80	50	125	No	0	450	3700	76
6	97.7		90	50	125	No	0	420	3870	80
7	95.2	—	60	120	500	Yes	0	450	3950	80
10	93.0		80	120	500	Yes	2350	450	3670	80
11	94.0		80	120	500	Yes	2720	420	3900	80
12	95.8		80	120	500	Yes	30	480	3960	50
13	100.3		80	120	500	Yes	120	510	3900	80
14	95.2	—								
Martensitic Steel 1	78.7	48		50	125	No	0	342	1050	45
Y.S. 2	78.5	74	—	50	125	No	0	—	—	—
3	71.8	90				No	0			
4	71.2	83				No	0			

TRIP Steels
≈ 220 ksi

Martensitic Steel
Y.S. ≈ 228 ksi

[1] Based upon the engineering stress level (notch plus fatigue crack). Slow crack growth continued in the region near the surface until the critical point of the true K_{ci} may be stable.
[2] Stress intensity after the crack grew 0.15 mm, at which point failure occurred at one jumping hole.
[3] Must initiate at one jumping hole.

Table IV - Thermal-Mechanical Processing Treatments for
D6AC Steel [From the work of Ault et al. (40)]

Ausformed

1. Austenitized at 1650°F in air for 2 hours
2. Air cooled to 1050°F, held at 1000°F for 1/2 hour
3. Reduced 65% by press forging
4. Oil quenched
5. Stress-relieved at 350°F for 2 hours
6. Specimens cut out and finish ground
7. Tempered for 2 + 2 hours

Conventional

1. Austenitized at 2000°F in air for 1 hour
2. Reduced 65% by press forging
3. Air cooled
4. Specimens cut out and machined 0.025 in. oversize
5. Austenized at 1650°F in air for 2 hours
6. Oil quenched
7. Stress-relieved at 350°F for 2 hours
8. Specimens finish machined to size
9. Tempered for 2 + 2 hours

Aus-bay

1. Steps 1 through 8 of conventional treatment
2. Austenitized at 1650°F in salt for 1 hour
3. Transferred rapidly to 950°F salt bath
4. Held in 950°F salt for 5 minutes
5. Quenched in 150°F oil
6. Tempered for 2 + 2 hours
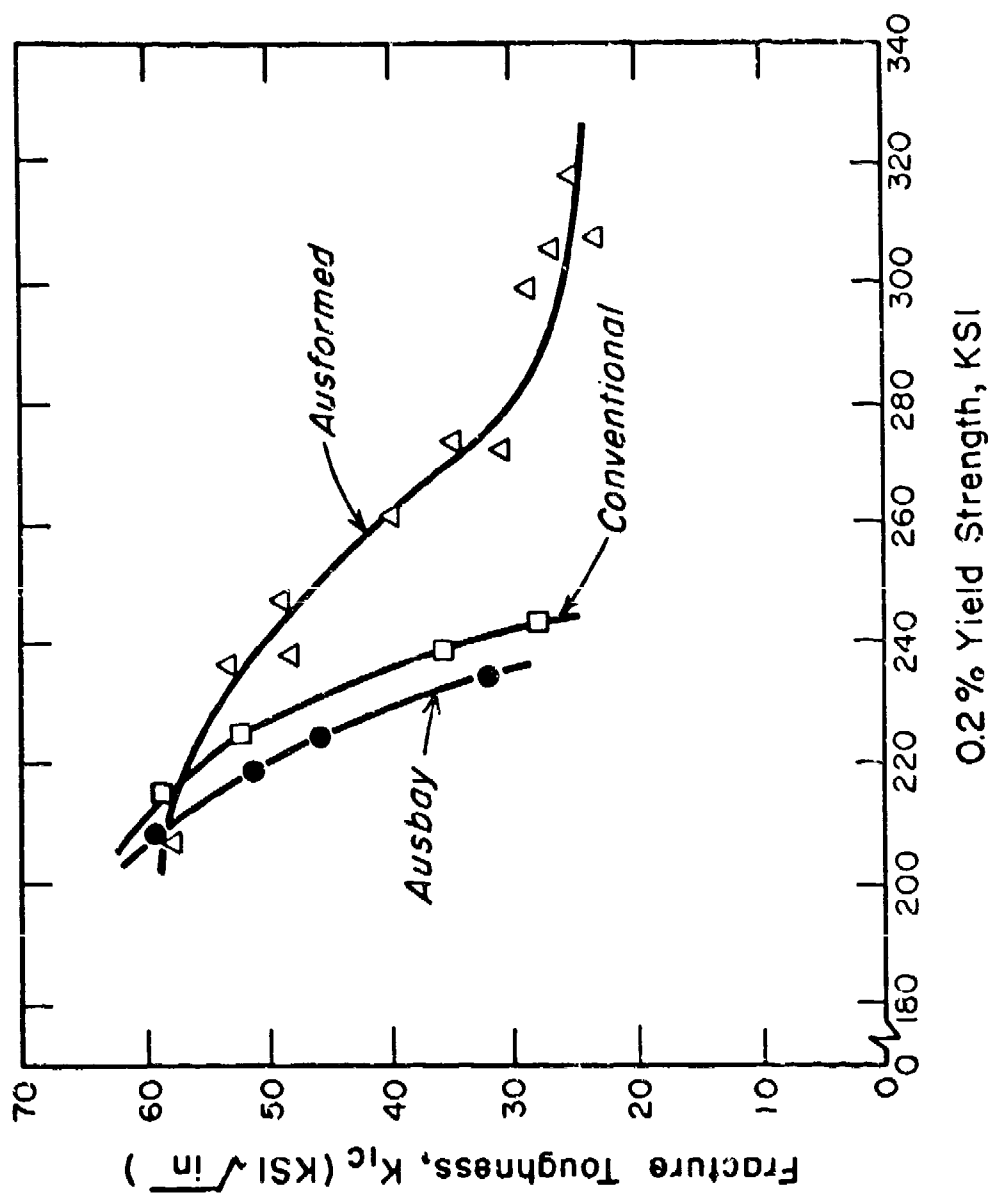
Fig. 24. Effect of Thermal-Mechanical Processing on Fracture Toughness of D6AC Steel [From the work of Ault et al.(40)]
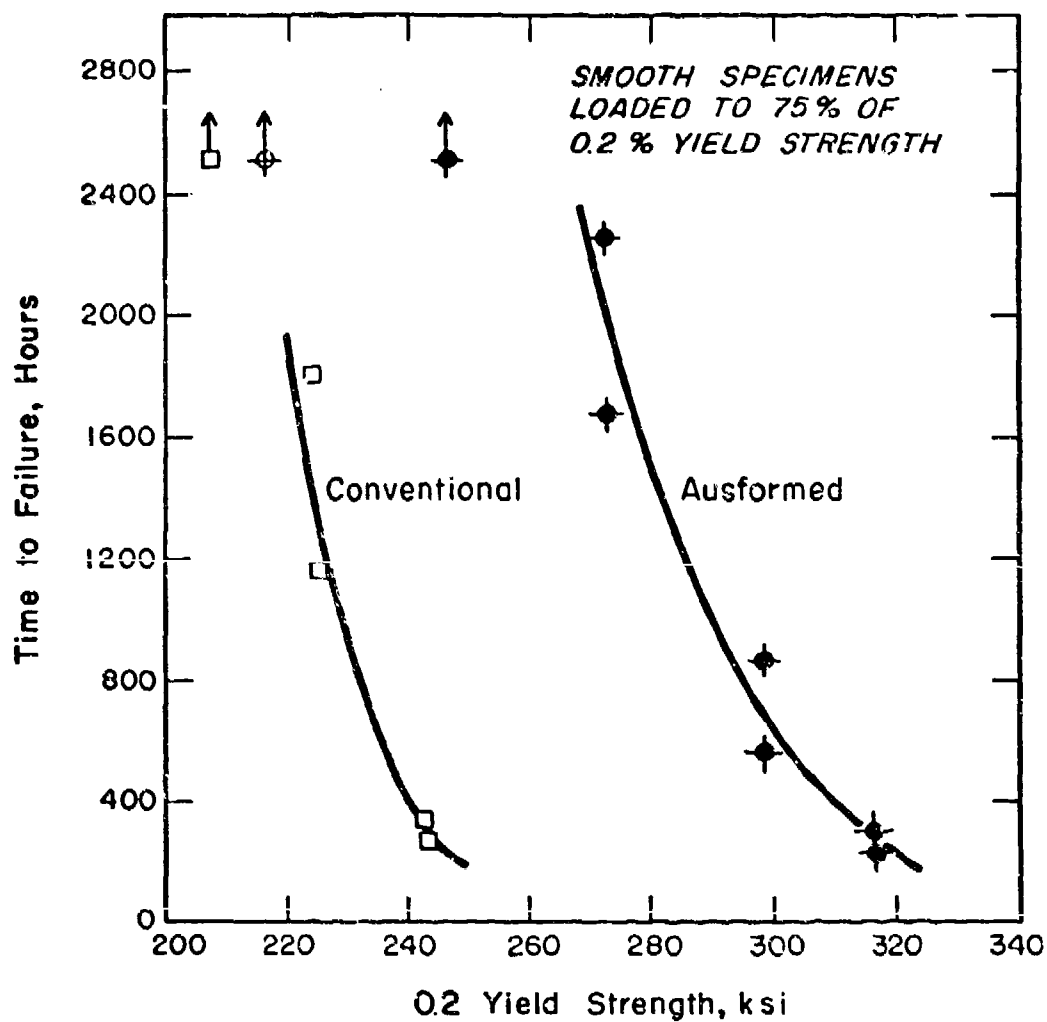
Fig. 25. Effect of Prior Ausforming Process on Delayed Failure of D6AC Steel in Distilled Water Environment [From the work of Ault et al. (40)]

Marquenching of Type 410 stainless steel has been used to improve the resistance to delayed failure. Bressanelli[40] has studied the effect of marquenching on the H_2 embrittlement susceptibility of Type 410 stainless steel tempered at 900°F. Strip specimens were tested in bending after immersion in a 1:1 HCl solution containing 2% SeO_2. Bend angle at fracture was the measured parameter. The post-charging bend angle is shown in Fig. 26 for oil-quenched and marquenched specimens. Isothermal holds of 10 minutes, at 400 to 600°F, during quenching were found to exhibit the greatest effect. The improved cracking resistance of marquenched steel was attributed to a nonuniform carbide distribution. Regions of martensite not strengthened by carbide precipitation were felt to provide barriers to crack propagation.

EFFECT OF PRIOR AUSTENITE GRAIN SIZE

In neutral or acidic aqueous environments, the delayed failure of high-strength steels generally exhibits an intergranular fracture mode, along prior austenite grain boundaries.[19,22,26] In gaseous environments (H_2, H_2S), intergranular cracking is also observed.[38,42,43] Therefore, the effect of prior austenite grain size on stress-corrosion cracking behavior is of obvious importance.

A decrease in prior austenite grain size has been found to increase both the fracture toughness (K_{Ic}) and the threshold stress intensity value for stress-corrosion cracking (K_{Iscc}) for high-strength steels.

Proctor and Paxton[44] have studied the effect of grain size on the delayed failure of AISI 4340 steel in 3.5% NaCl solution. The heat treatments, strength levels, and resulting grain sizes are given in Table V. Pre-fatigue cracked single cantilever beam specimens were used in the investigation. Failure times, as a function of initial applied stress intensity, are shown in Fig. 27. A coarse grain size results in a shorter failure time than that for fine-grained (higher-strength level) steel. There is no significant effect of such grain size variation on either fracture toughness (K_{Ic}) or the threshold stress intensity for cracking (K_{Iscc}).

Webster[45] has conducted an extensive study of grain size effects on the fracture toughness and K_{Iscc} values for a 14Cr-13Co-5Mo precipitation-hardening stainless steel (AFC77). Grain diameter was varied from 2.3 to 60 μm, using the thermal-mechanical treatments illustrated in Fig. 28. Figure 29 shows the effect of grain size on the fracture toughness (K_{Ic}) of the steel. Fracture toughness values were determined both by Charpy impact tests and by 0.5" thick SEN slow bend specimens, loaded in three-point bending. For the same tempering temperature, the threshold stress intensity values for stress-corrosion cracking are 25 to 33% higher in the fine-grained steel. This is shown in Fig. 30.

38
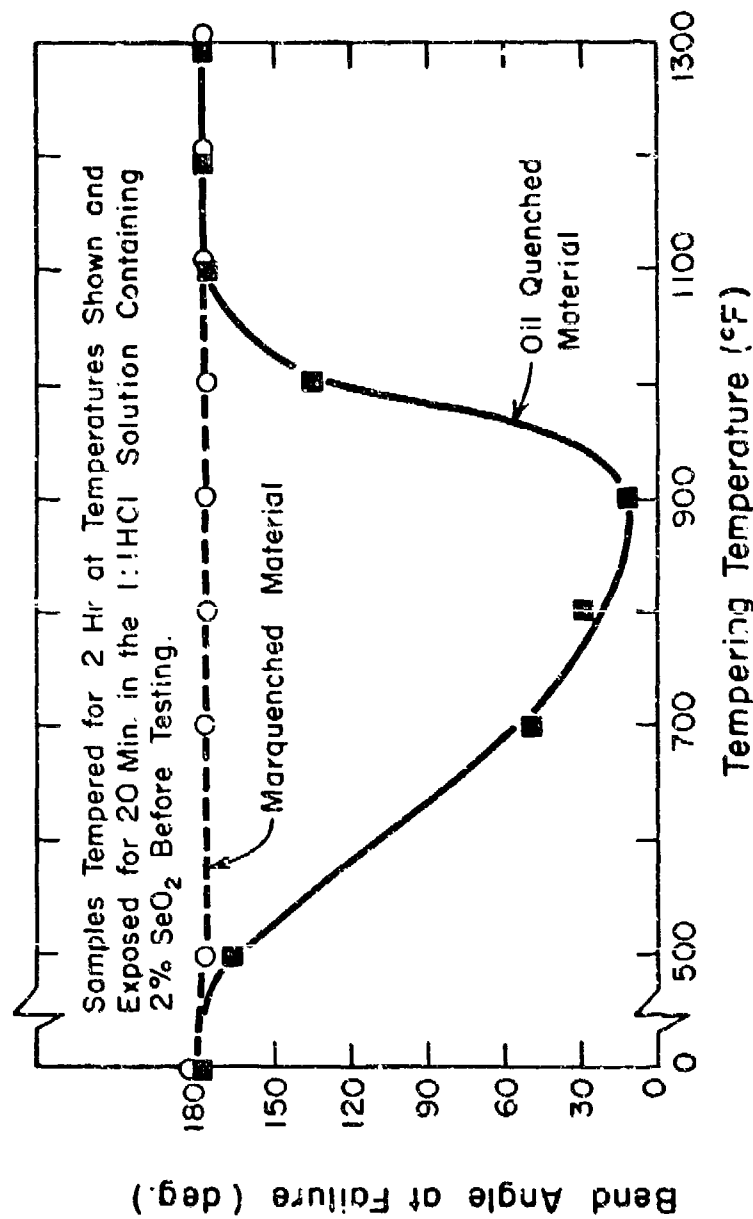
Fig. 26. Effect of Tempering Temperature on Hydrogen Embrittlement Susceptibility of Marquenched and Oil-Quenched Type 410 Stainless Steel [From the work of Bressanelli (41)]

39

Table V - Heat Treatments Used to Obtain Variable Prior
Austenite Grain Size in AISI 4340 Steel
[From the work of Proctor and Paxton (44)]

I. Conventional heat-treatments:

   (a) Normalize for 1 hr at 900°C (1650°F) and air cool

   (b) Austenitize for 2 hr at T C and oil quench
       Steel A: T = 915°C (1680°F)
       Steel B: T = 805°C (1480°F)

   (c) Refrigerate in liquid nitrogen for 15 min

   (d) Temper 1 hr + 1 hr at 205°C (400°F) and oil quench

II. Repetitive austenitizing heat-treatments:

   (a) Normalize for 1 hr at 900°C (1650°F) and air cool

   (b) Homogenize for 1 hr at 800°C (1580°F) and oil quench

   (c) Austenitize for 90 sec at 815°C (1500°F) and oil quench
       Steel C: step (c) was repeated once (i.e., total
                 of 2 cycles)
       Steel D: step (c) was repeated four times (i.e.,
                 total of 5 cycles)

   (d) Refrigerate in liquid nitrogen for 15 min

   (e) Temper 1 hr + 1 hr at 205°C (400°F) and oil quench

Steel Designation	ASTM (grain size)	Yield Strength (ksi)	Tensile Strength (ksi)
A	7	245	270
B	8.5	249	271
C	10.5	259	276
D	12	265	280
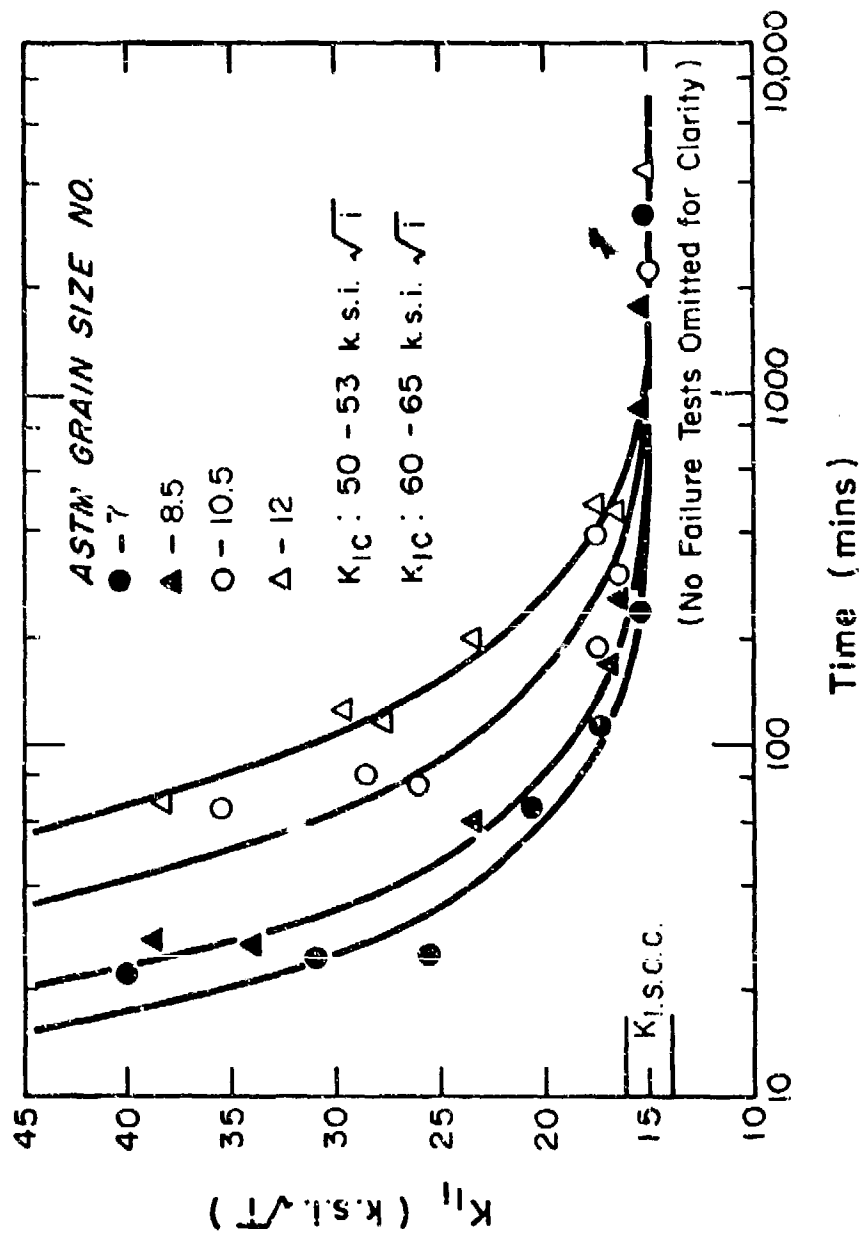
Fig. 27. Effects of Grain Size and Initial Stress Intensity on Delayed
Failure Time for AISI 434C Steel [From the work of
Prcctor and Paxton (44)]

Fig. 28. Thermal-Mechanical Processes Used to Obtain Variation
of Grain Size in AFC 77 Steel [From the work of
Webster (45)]
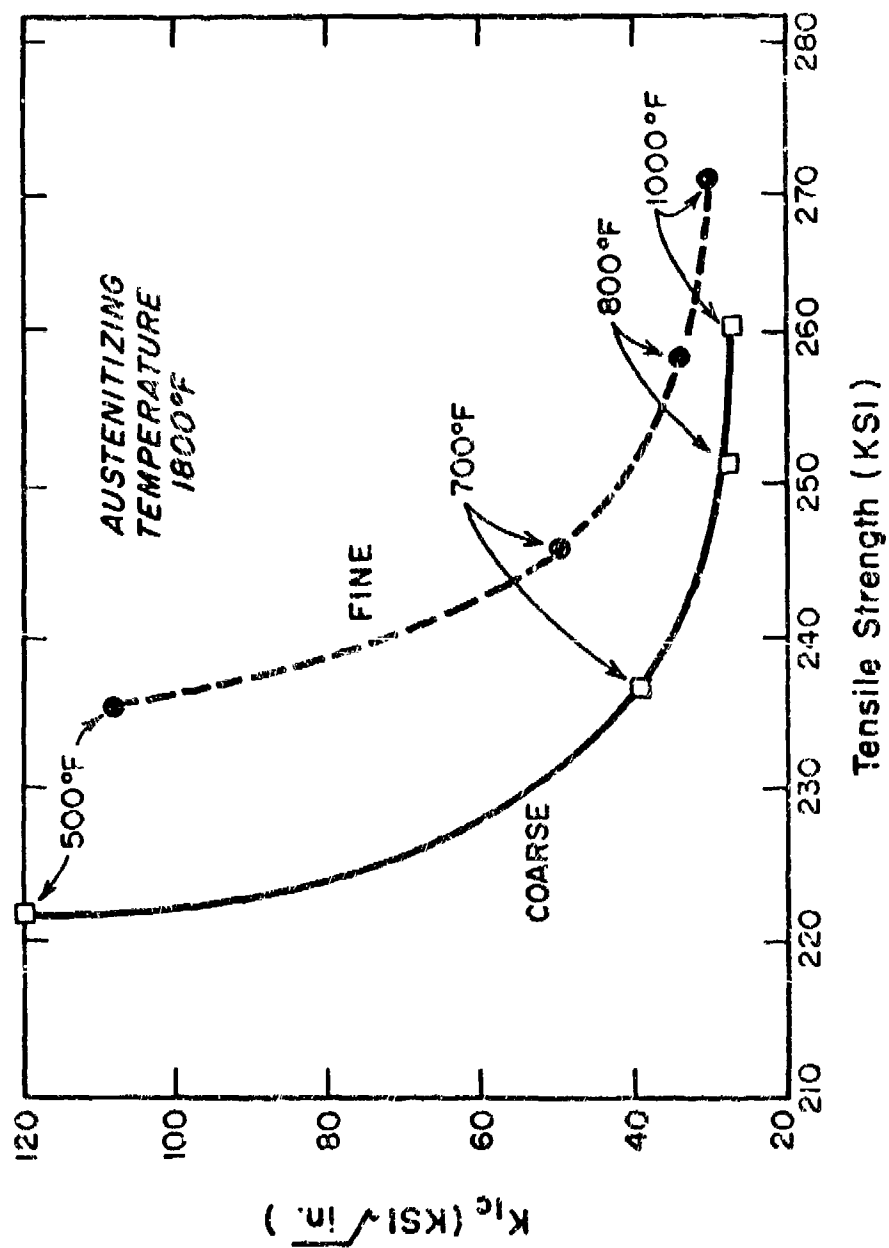
Fig. 29. Effect of Grain Size on Fracture Toughness of AFC-77 Steel Tempered at Various Temperatures [From the work of Webster (45)]

43

I HR Austenitizing at 1800°F
2 + 2 HR Temper

(a) 500°F TEMPER

(b) 1000°F TEMPER
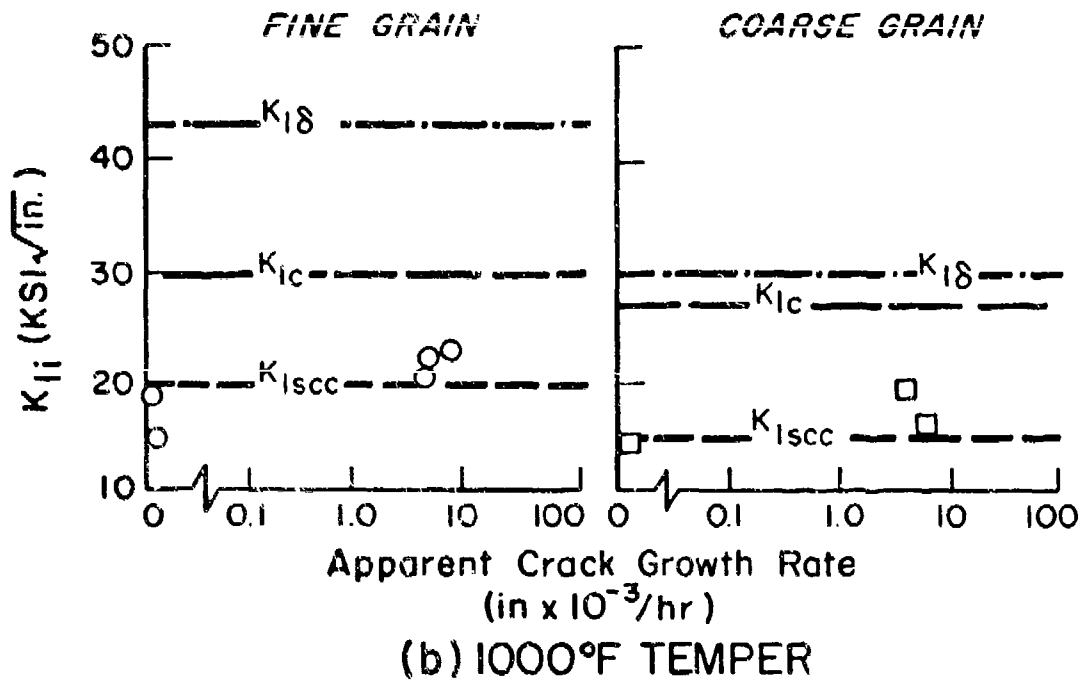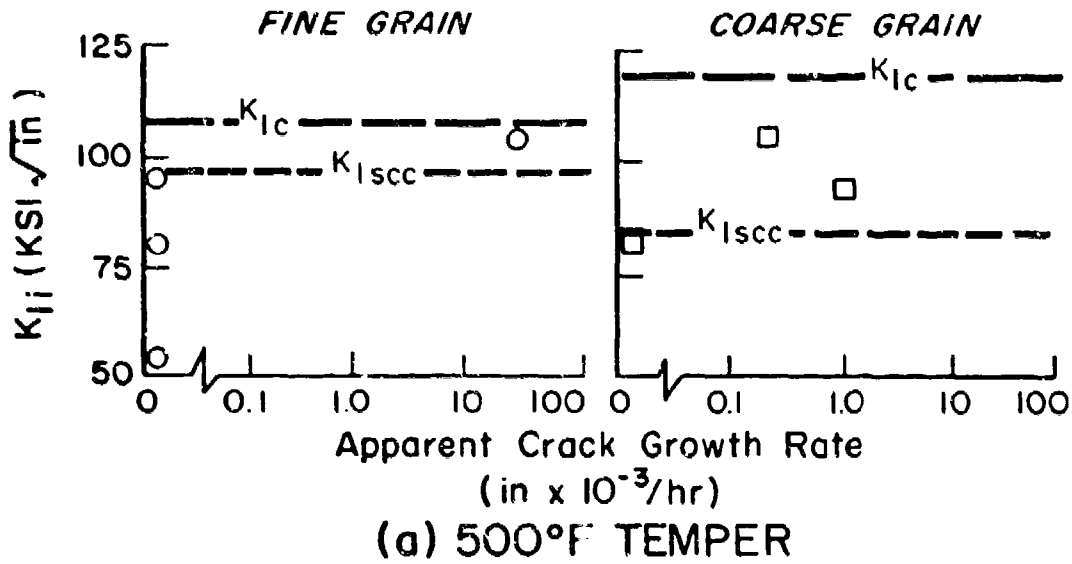
Fig. 30.   Effect of Prior Austenite Grain Size on K_{1scc} for
AFC 77 Steel [From the work of Webster (45)]

44

EFFECT OF STEEL COMPOSITION

Stress-corrosion behavior is strongly affected by the chemical composition of high-strength steels. Carbon additions (up to 0.4%) and manganese additions (up to 2.5%) are found to lower the K_{Iscc} value for AISI 4340 steel in 3.5% NaCl solution. Delayed failure times for pre-cracked specimens of medium- and high-alloy martensitic steels (9Ni-4Co, H-11) in a distilled water environment are substantially greater than failure times for low-alloy steels (4340, D6AC). Silicon additions (1.6% or more) to AISI 4340 steel have been found to substantially lower the stress-corrosion crack velocities in a 3.5% NaCl solution.

The fracture toughness and stress-corrosion cracking susceptibility of high-strength steels have been extensively reviewed by Sandoz.[1] The general behavior shows a decrease in K_{Iscc} with increasing strength level, for the case of aqueous environments. However, certain martensitic steels were found to be superior to AISI 4340 at strength levels below 200 ksi. These include HY-130, HY-150, HP 9-4-20, and HP 9-4-25. Other steels were found to exhibit K_{Iscc} values close to those of 4340 steel. The latter include H-11, D6AC, 300M, HP 9-4-45, and 4340V.

At moderate strength levels, high-alloy martensitic and precipitation-hardening stainless steels were found to exhibit greater cracking resistance than low-alloy martensitic grades.[1]

The effect of major compositional changes on stress-corrosion behavior was also investigated by Benjamin and Steigerwald.[18] Center-notch pre-fatigue cracked specimens of six high-strength steels had been heat treated to give ultimate strength levels in the range 233-244 ksi, and statically loaded in a distilled water environment. The resulting delayed failure data, as a function of normalized initial stress intensity (K_i/K_c), are presented in Fig. 31. Yield strength values for the steels ranged from 194 to 229 ksi. A detailed microstructural comparison of the steels was not made. It is clear, however, that the delayed failure kinetics are substantially lower in 9Ni-4Co and H-11 steels, as compared to 4340 steel.

Alloying element additions to 4340-type steel by Sandoz[34] have shown detrimental effects for C and Mn. The additions of P, S, Cr, Mo, and Ni showed no substantial effects on stress-corrosion cracking behavior. Pre-fatigue cracked single cantilever beam specimens were tested in both sea water and aqueous 3.5% NaCl solutions. The additions of carbon (up to 0.4%) or manganese (up to 2.5%) were found to lower K_{Iscc} in the test environments, as shown in Fig. 32.

The specific effect of silicon additions on the stress-corrosion cracking of AISI 4340 steel was investigated by Carter.[46] Pre-fatigue cracked single cantilever beam specimens were used in the study. The stress-corrosion environment was an aqueous 3.5% NaCl solution. For material having ultimate strength levels of 280-300 ksi, additions of
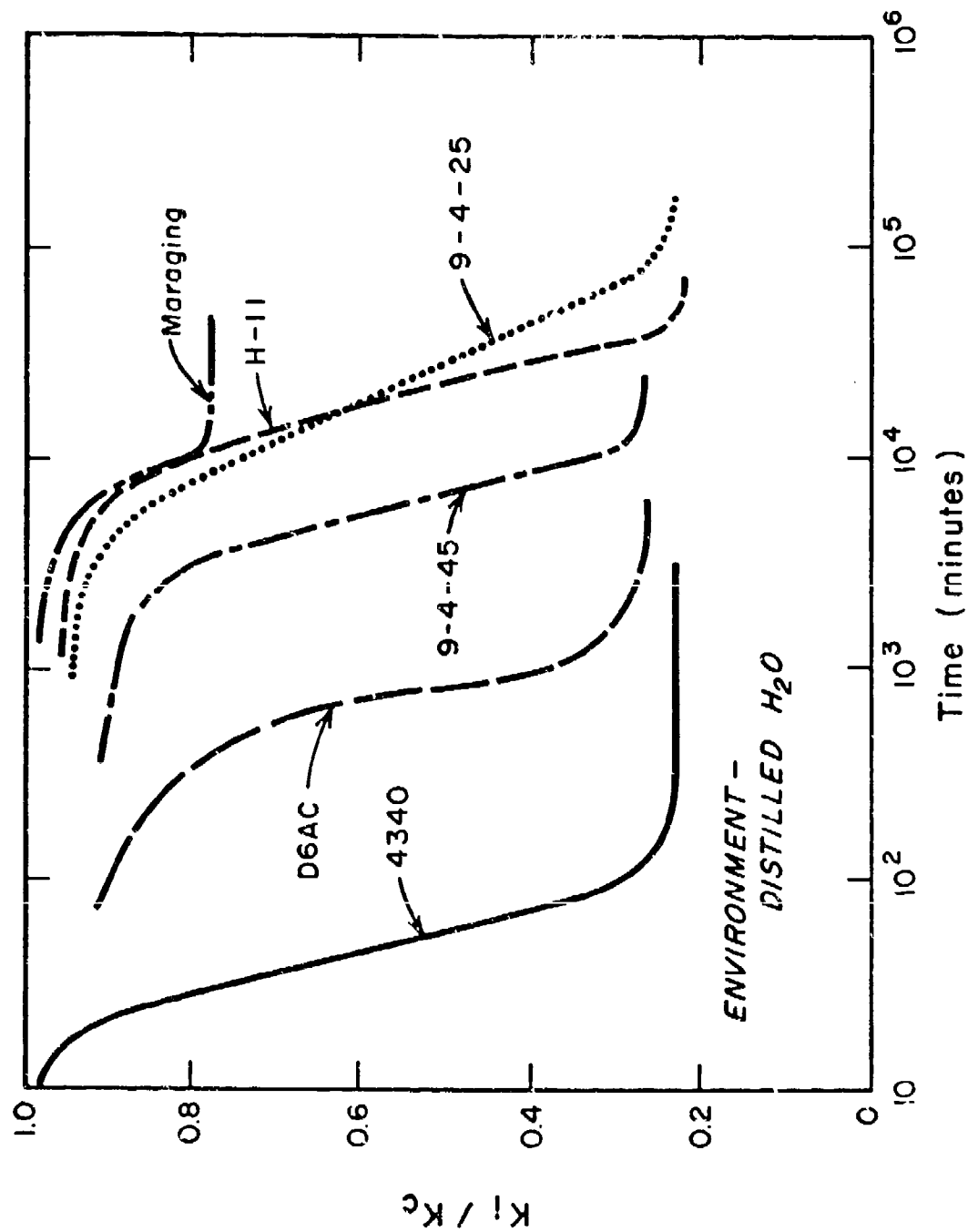
Fig. 31. Effect of K_i/K_c Ratio on Failure Times for Six High Strength Steels [From the work of Benjamin and Steigerwald (16)]
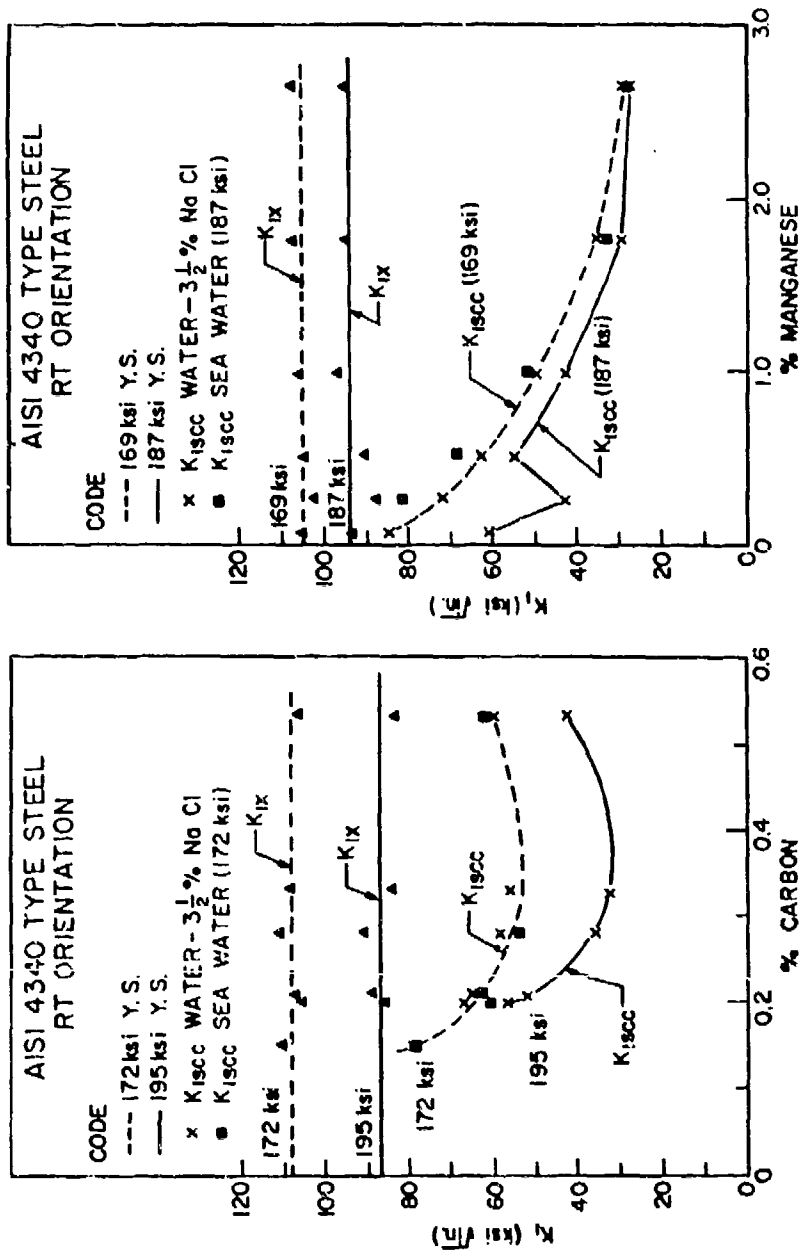
Fig. 32. Effects of Carbon and Manganese on the Threshold
Stress Intensity for Crack Growth in AISI 4340
Steel [From the work of Sandoz (34)]

silicon up to 2.15% showed no measurable effect on K_{Iscc}, but resulted in a pronounced decrease in K_{Ic} with silicon levels of less than 0.5%. These effects are shown in Fig. 33. Delayed failure times, at $K_I = 32$ ksi-in.$^{1/2}$, are increased by silicon additions greater than 1%, as shown in Fig. 34. The addition of silicon to lower-strength 4340 steel (230-240 ksi strength level) showed a slight increase in K_{Iscc} for silicon levels up to 1%. No effect of silicon content on K_{Ic} was observed up to 1.58% Si. The latter effects are shown in Fig. 35.

Crack velocity measurements, as a function of silicon content and applied stress intensity, revealed significantly lower crack velocities for silicon contents of 1.58% or more in the lower strength level 4340 steel. The crack velocity effect is shown in Fig. 36.

ENVIRONMENTAL EFFECTS

Significant effects on stress-corrosion cracking behavior have been observed for the case of aqueous environment variables. Low solution pH, applied cathodic potentials, and the addition of cathodic poisons accelerate the failure of smooth specimens in aqueous media. Anion or cation additions have increased the delayed failure times for AISI 4340 foil specimens in chloride solutions.

For the case of pre-cracked specimens, applied potential and pH changes also show substantial effects on crack growth rates.

Addition of Cathodic Poisons to
Aqueous Environments

Cathodic poisons, containing elements from Groups V and VI of the periodic table, have been show to promote hydrogen entry into iron or steel from aqueous media. Radhakrishnan and Shrier[1] have studied the enhanced permeation of hydrogen through 0.002" thick low-strength steel foil as a function of cathodic poison additions to a 0.1N H_2SO_4 solution. Permeation kinetics were increased (during charging) on the addition of As (as sodium arsenite), Se (as selenous acid), and Te. Sulfur compounds (sodium sulfide, carbon   .fide, and thiourea) were found to enhance permeation kinetics in the absence of an applied potential. Additions of As, Se, and Te were less than 100 μg/ml. The effectiveness of each poison species is revealed by its relative enhancement of the hydrogen permeation rate, shown in Fig. 37. The poisons were rated, in order of effectiveness in promoting hydrogen entry, as

$$As > Se > Te > S .$$

Cathodic poison additions have been clearly shown to both increase hydrogen entry into high-strength steel, in conjunction with lowering the stress required for delayed failure in aqueous media.
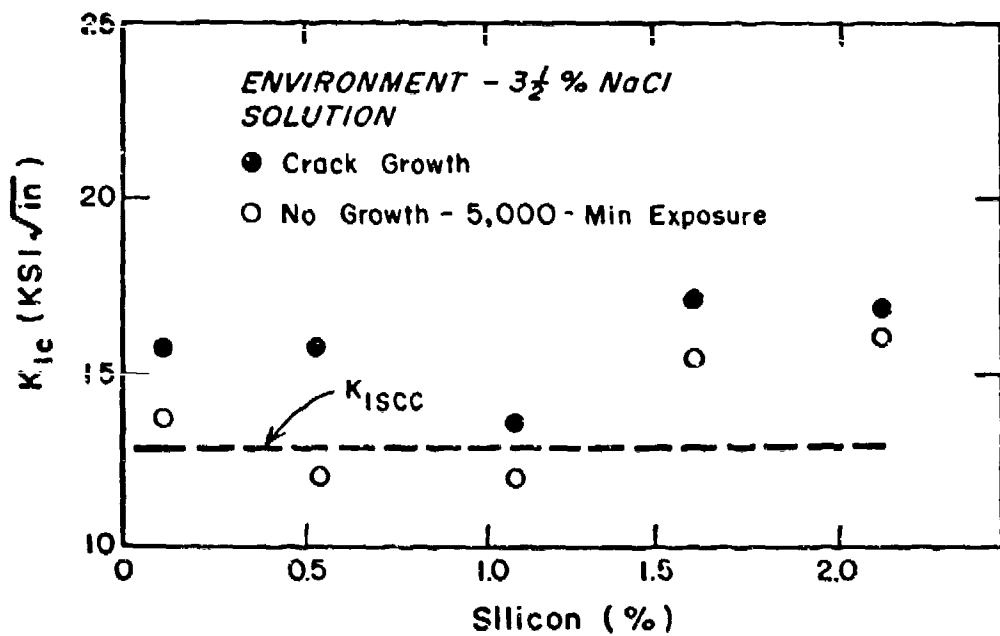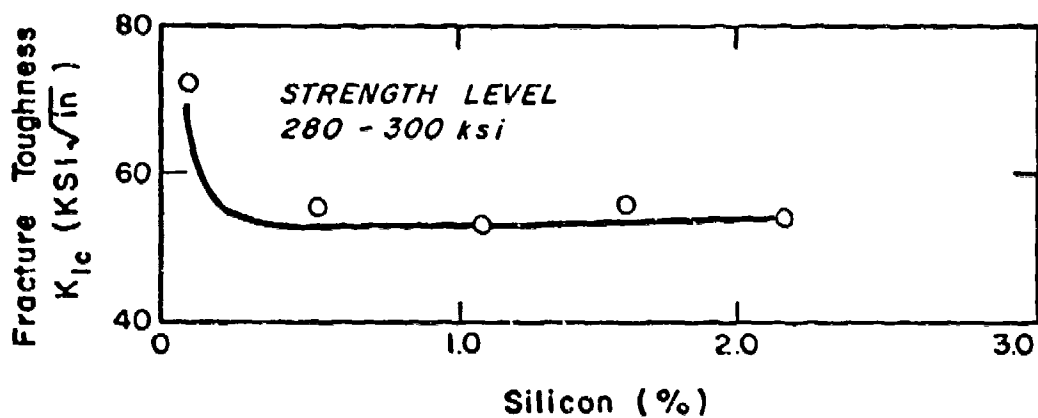
Fig. 33. Effect of Silicon Content on Fracture Toughness
and Threshold Stress Intensity for Crack Growth
in AISI 4340 Steel [From the work of Carter (46)]
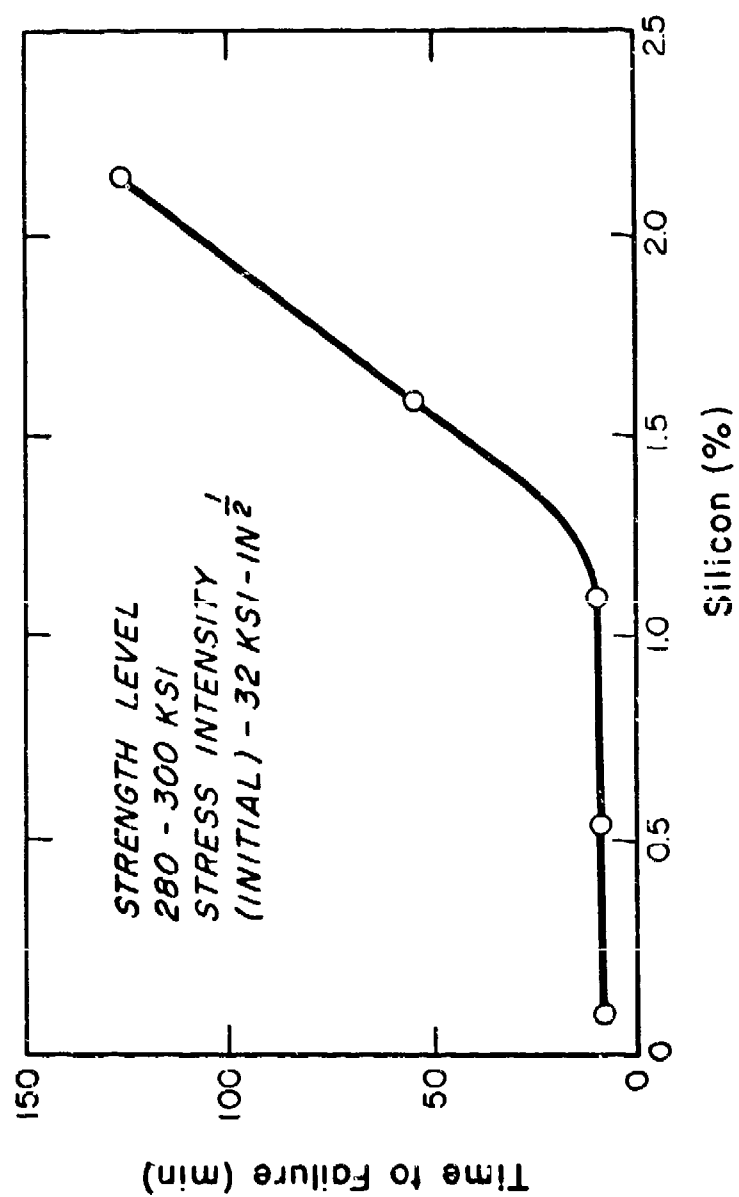
Fig. 34. Effect of Silicon Content on the Delayed Failure Time of AISI 4340 Steel in 3½% NaCl Solution [From the work of Carter (46)]
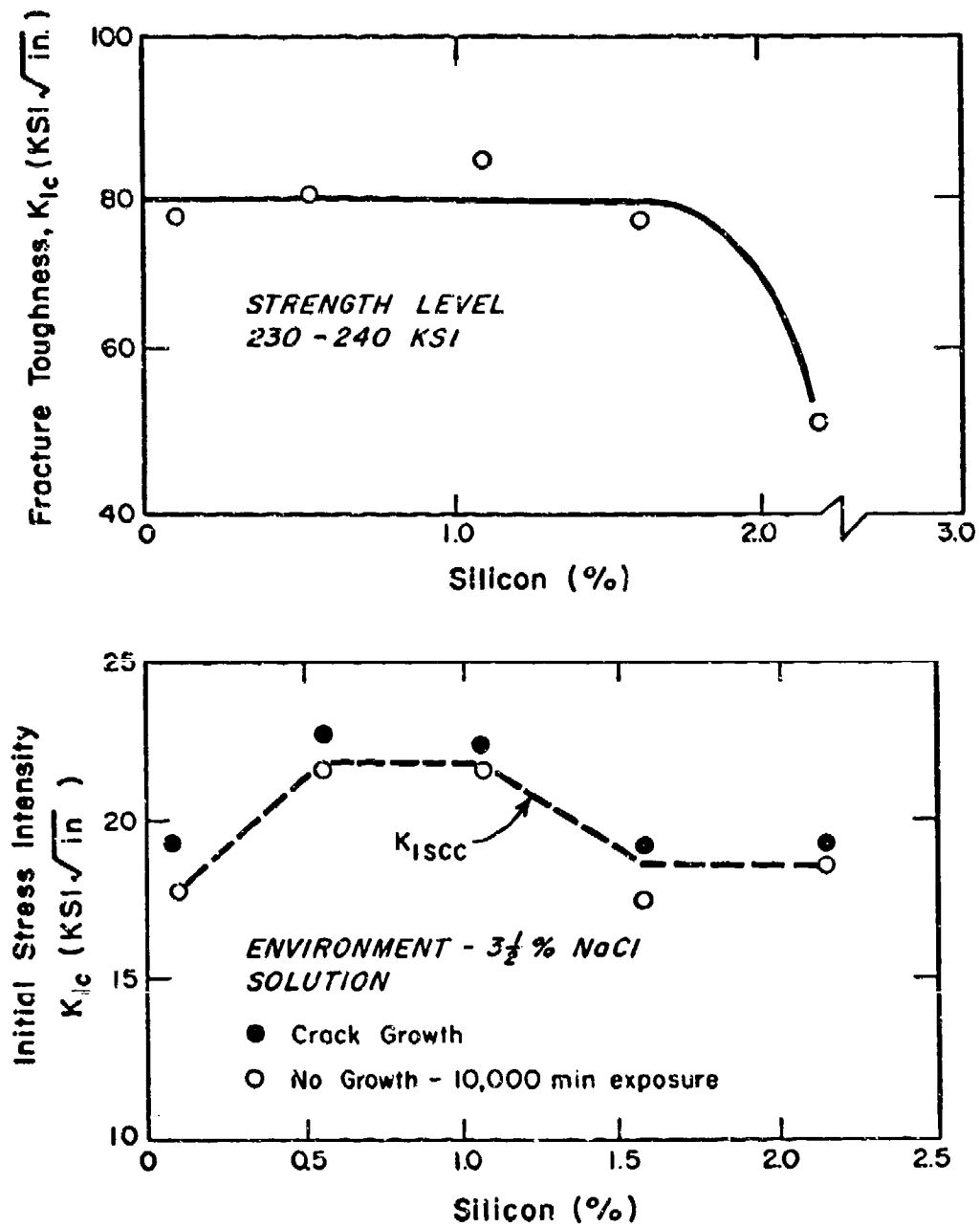
Fig. 35. Effect of Silicon Content on Fracture Toughness and
Threshold Stress Intensity for Crack Growth in
AISI 4340 Steel [From the work of Carter (46)]

51
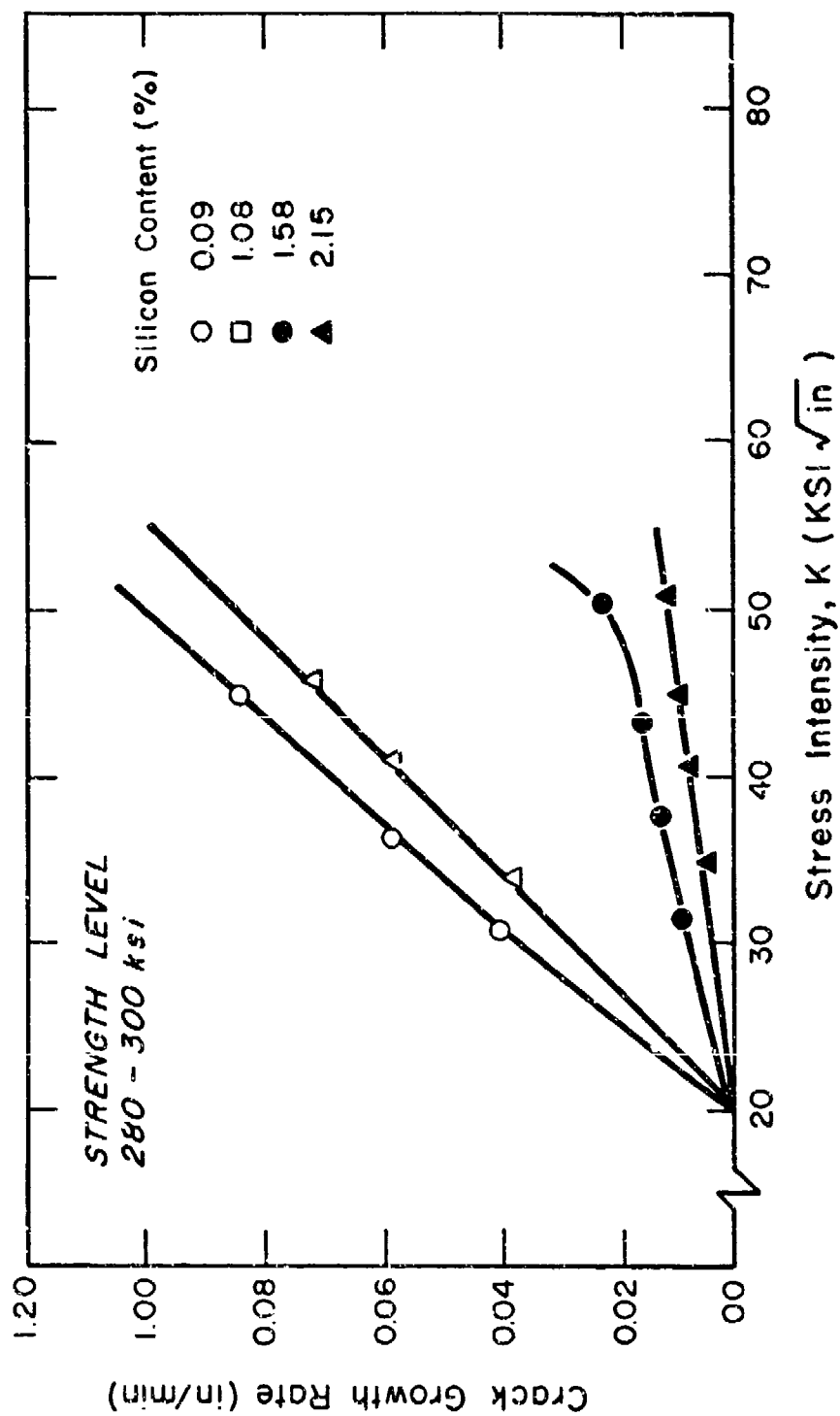
Fig. 36. Effect of Silicon Content on Crack Velocity in AISI 4340 Steel [From the work of Carter (46)]
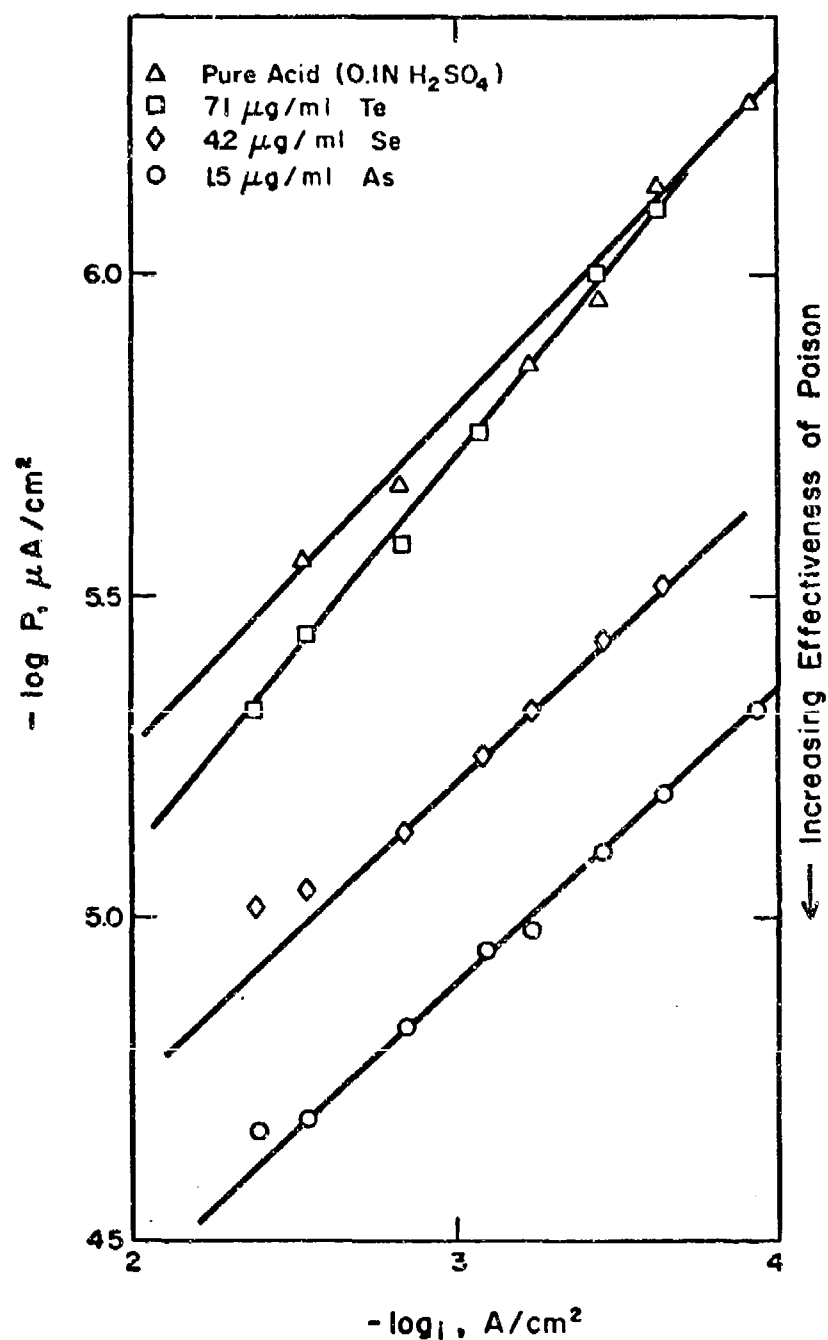
Fig. 37. Effects of Applied Cathodic Current and Poison Additions on the Permeation Rate of Hydrogen Through Low Strength Steel [From the work of Radhakrishnan and Shreir (47)]

Wood[48] found that the addition of a poison (P in CS_2) to a 4% H_2SO_4 charging bath increased the hydrogen content of 4130 steel by an order of magnitude. The strength level of the steel was 229-234 ksi. In similar work, Farrell[49] has found that the addition of arsenic metal (0.5 mg/ℓ) to a 4% H_2SO_4 charging solution increased the hydrogen absorption of low-alloy high-strength steel (strength level 270 ksi), as seen in Fig. 38. The detrimental effect of hydrogen content on the fracture stress of un-notched tensile specimens is shown in Fig. 39.

Hydrogen sulfide additions to neutral or acidic aqueous environments will strongly accelerate the delayed failure kinetics of high-strength steels. Treseder and Swanson[50] showed that H_2S additions to a 0.5% acetic acid solution reduced the fracture stress for exposed specimens of 9-Ni high-strength steel by a factor of 5. Hudgins et al.[51] reported a similar effect of H_2S on the delayed failure of low-alloy high-strength steel specimens (notched-ring geometry) in a 5% NaCl solution. The effect of H_2S additions, shown in Fig. 40, appears most significant in the pH range 3-7.

Effect of Ionic Additions to Aqueous Solutions

The addition of ionic species to the aqueous stress-corrosion environment has, in general, shown a pronounced effect on delayed failure kinetics.

Tirman, Haney, and Fugassi[52] have studied the effect of prior treatment of 4340 steel foil in aqueous and non-aqueous sulfur-containing solutions on the subsequent delayed failure in 0.6M NaCl solution (acidified to pH 1.5 with HCl). Pre-treating solutions, and the effect on subsequent failure times, are given in Table VI. The tensile strength of the 0.002" thick foil specimens was 220-264 ksi; the foil specimens were stressed to 75% of the yield strength. The effect of such pre-treatment was attributed to the formation of local sulfided areas on the steel surface which retard the re-combination of atomic hydrogen. In later work, Fugassi and Haney[53] studied the effect of heavy metal ion additions on the stress-corrosion cracking of AISI 4340 steel in dilute HCl solutions. Specimens of 4340 steel foil (yield strength of 203 ksi) were stressed to 75% of the yield strength. The effects of various metallic salt additions on the delayed failure time in dilute HCl solution (pH 1.5) are given in Table VII. Additions of $SnCl_2$ (10^{-1} mole/ℓ), $Pb(C_2H_3O_2)_2$ (10^{-2} mole/ℓ), and $CaCl_2$ (10^{-2} mole/ℓ) increased the delayed failure time by more than one order of magnitude. The effect of such heavy metal ion additions was attributed to dissolution of sulfides from the steel, giving HS^- ions, with the precipitation of insoluble heavy metal sulfides. The process thereby removed the sulfide areas on the steel believed to be responsible for accelerating hydrogen entry into the steel. Chloride ions, per se, have not produced any significant effect on the cracking susceptibility or kinetics in AISI 4340 steel,[37] as shown in Fig. 22.
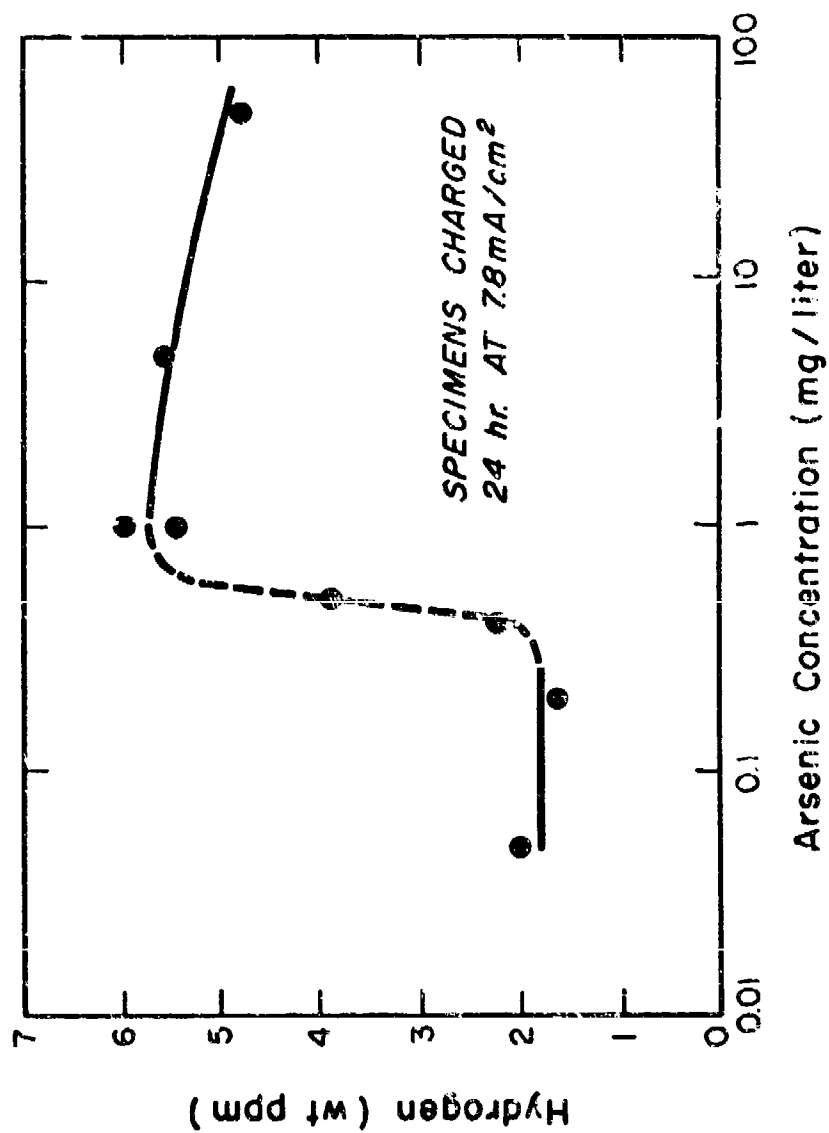
Fig. 38. Effect of Arsenic Additions in 4% H_2SO_4 on the Hydrogen Adsorption by High Strength Steel [From the work of Farrell (49)]

55
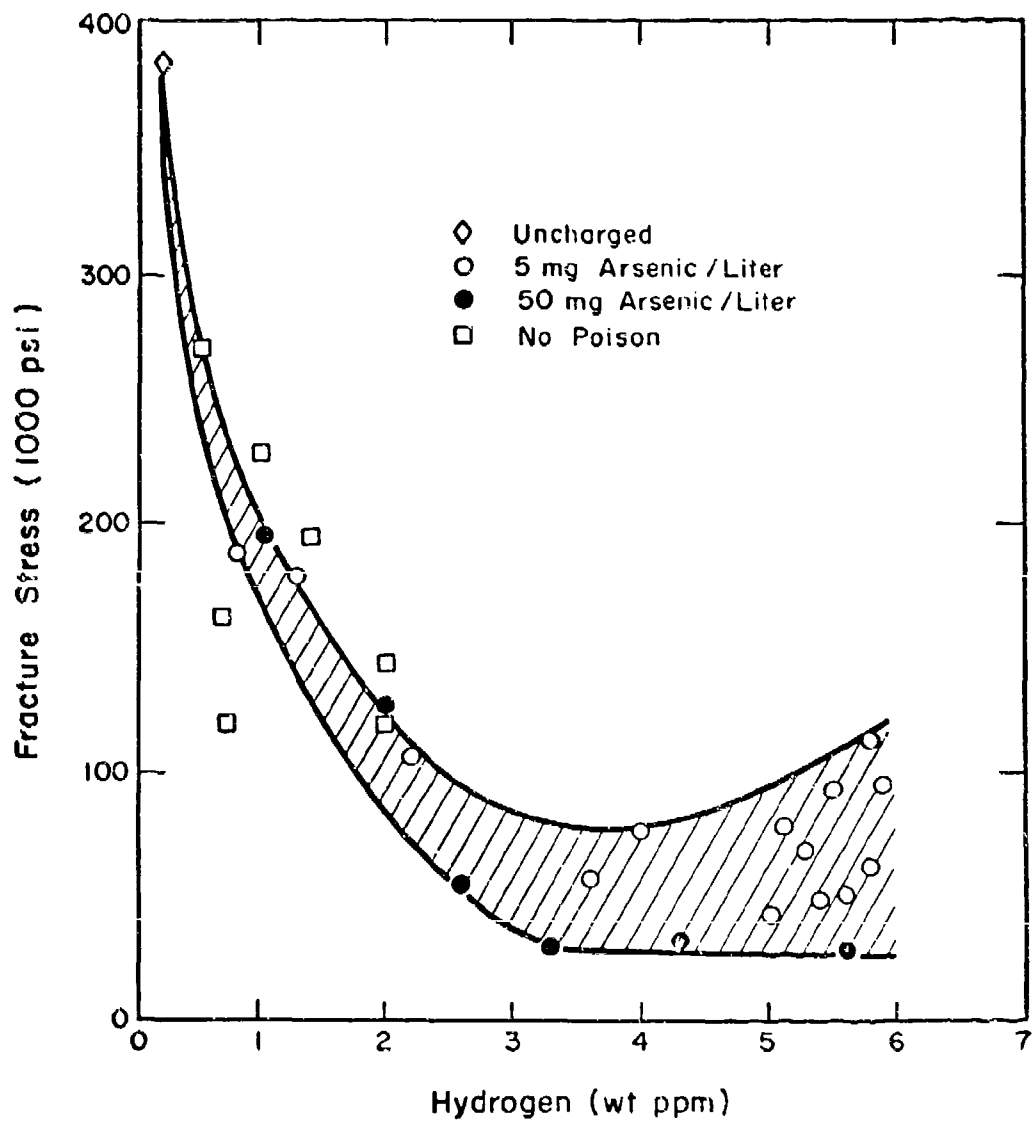
Fig. 39. Effect of Hydrogen Content on Fracture Stress of
Unnotched High Strength Steel Tensile Specimens
[From the work of Farrell (49)]
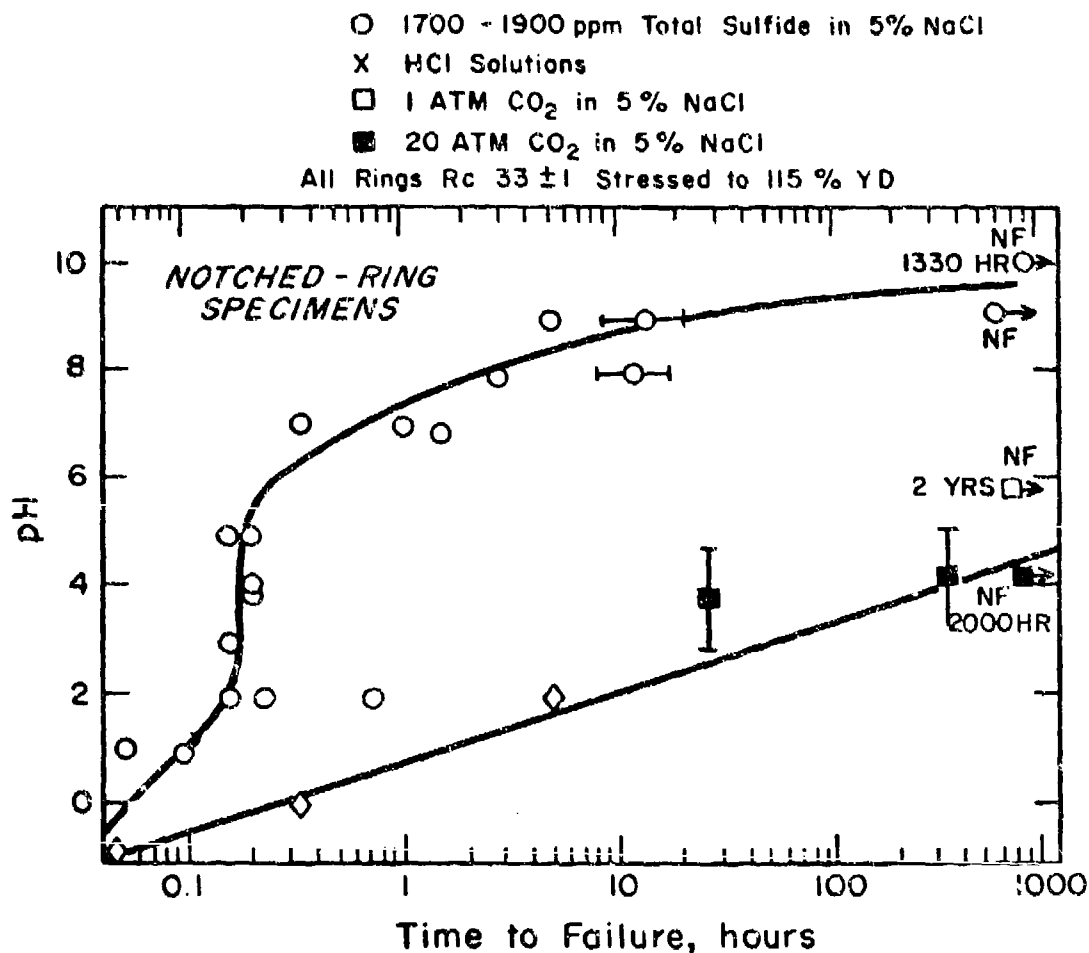
Fig. 40. Effects of Solution pH and H_2S Additions on Failure of Un-notched High Strength Steel Specimens in 5% NaCl Solution [From the work of Treseder and Swanson (50)]

Table VI – Effect of Prior Exposure to Sulfide, Sulfite, and Sulfate
Media on the Delayed Failure of AISI 4340 Steel Foil in
0.6M NaCl Solution [From the work of Tirman, Haney, and
Fugassi (52)]

Solution	Time Treatment (min)	% Change Time to Failure
H_2S in H_2O (Sat'd)	30	-50
H_2S in H_2O "	40	-40
H_2S in H_2O "	120	-70
NaHS in H_2O	40	-50
NaHS in H_2O	120	-50
Thionex' in C_6H_6	120	-60
Thionex in C_3H_5	720	-60
CS_2 in C_3H_6	120	-20
CS_2 in C_6H_6	720	-60
H_2SO_3 in H_2O*	40	-70
H_2SO_3 in H_2O**	40	-60
$NaHSO_3$ in H_2O*	40	-70
Na_2SO_3 in H_2O*	40	+10
$NaHSO_4$ in H_2O*	40	-50
Na_2SO_4 in H_2O*	40	+10

'Tetramethylthiuram monosulfide
*0.1M
**0.01M

Table VII - Effect of Metal Salt Additions on Delayed Failure
of AISI 4340 Steel Foil in Aqueous HCl Solutions
[From the work of Fugassi and Haney (53)]

Compound	Concentration (m/ℓ)	% Change Time to Failure
None		0
Na_2SO_4	10^{-2}	-10
NaCl	$2 \cdot 10^{-2}$	-20
$NiCl_2$	10^{-2}	-50
$PbSO_4$	$1.4 \cdot 10^{-4}$ (sat'd)	1500
$PbSO_4$	$1.4 \cdot 10^{-5}$	40
$PbCl_2$	10^{-3} (sat'd)	900
$PbCl_2$	10^{-4}	700
PbC_2O_4	$3 \cdot 10^{-6}$ (sat'd)	10
PbC_2O_4	$3 \cdot 10^{-7}$	-50
$Pb(C_2H_3O_2)_2$	10^{-2}	2000
$Pb(C_2H_3O_2)_2$	10^{-3}	1000
$PbCrO_4$	$1.4 \cdot 10^{-8}$ (sat'd)	-10
$ZnCl_2$	10^{-1}	200
ZnO	$3.6 \cdot 10^{-5}$ (sat'd)	400
$CdCl_2$	10^{-2}	2000
$CdCl_2$	10^{-3}	300
$CdCl_2$	10^{-4}	50
$SnCl_2$	10^{-1}	4500
$SnCl_2$	10^{-2}	3000
$SnCl_2$	10^{-3}	1500
$SnCl_2$	10^{-4}	900

EFFECTS OF pH AND APPLIED POTENTIAL

The delayed failure of smooth or notched specimens of high-strength steel in aqueous media is rapidly accelerated by a decrease of solution pH. The effect of pH on crack velocity, however, is not as significant. Applied potentials, both anodic and cathodic, have been found to accelerate the delayed failure of non-precracked specimens of high-strength steel.

Hughes et al.[7] have shown a severe effect of solution pH for notched-ring specimens stressed in a 5% NaCl solution containing H_2S. The effect is shown in Fig. 40. Treseder and Swanson[51] have shown a strong effect of pH on the delayed failure of high-strength steel specimens of a bent beam geometry. Figure 41 shows such a pH effect on the delayed failure stress for a quenched and tempered low-alloy steel (0.3C-1.5Mn-0.2Si-0.25Mo). Both studies[50,51] show a decrease of failure time in sulfide environments with decreasing solution pH.

The effect of pH on crack growth kinetics in AISI 4340 steel was studied by Van der Sluys.[26] Using double cantilever beam specimens, the author investigated pH, applied potential, and strain energy release rate (G) effects on crack velocity. Figure 42 shows that the effect of pH on crack velocity is significant only at large cathodic potentials.

It has been shown by Brown[54] that impressed potentials (either anodic or cathodic) strongly increase the crack velocity in a variety of high-strength steels. Figure 43 shows such an effect for pre-cracked specimens. Additional studies by Brown et al.[6] have shown, however, that the pH and potential conditions at the tip of a growing stress-corrosion crack in AISI 4340 steel permit hydrogen evolution. Similarly, Brown[55] has found such electrochemical conditions in a variety of high-strength steels, as shown on the Pourbaix diagram of Fig. 44. Thus, it is clear that the effects of pH and potential on crack velocities in these steels (Figs. 42 and 43) are not fully explainable at this time.

The measured effect of potential on delayed failure times has shown that either anodic or cathodic potentials decrease the failure time for some high-strength steels in aqueous solutions. McGuire et al.[56] have shown that hydrogen-induced stress-corrosion cracking can occur with Type 410 stainless steel. Figure 45 shows the effect of impressed potential on both the delayed failure times for 0.008" thick U-bend specimens, and the rate of hydrogen permeation through the steel. Electrochemical polarization (anodic or cathodic) is found to accelerate both delayed failure and hydrogen permeation. On anodic polarization, stress-corrosion cracks were found to initiate at the base of corrosion pits.

The effect of potential on hydrogen permeation and delayed failure for AISI 4340 and HP 9-4-45 steels was studied by Barth et al.[5] Failure times for both steels were decreased by cathodic polarization. The steels had an approximate tensile strength of 245 ksi. The steels
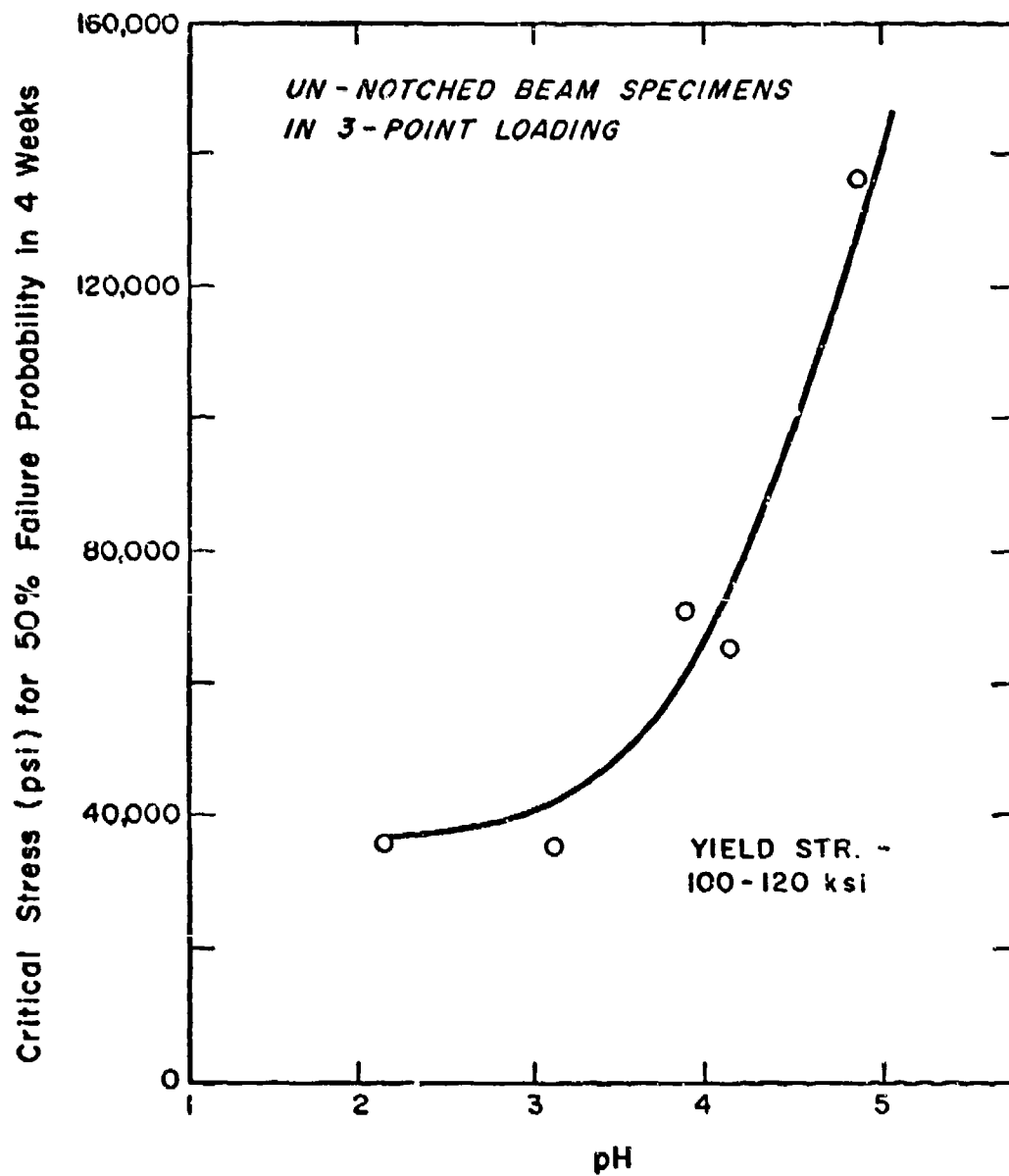
Fig. 41. Effect of pH on Delayed Failure Stress for Low Alloy Steel in H_2S Saturated Acetic Acid Solution Containing Sodium Acetate Buffer [From the work of Treseder and Swanson (50)]
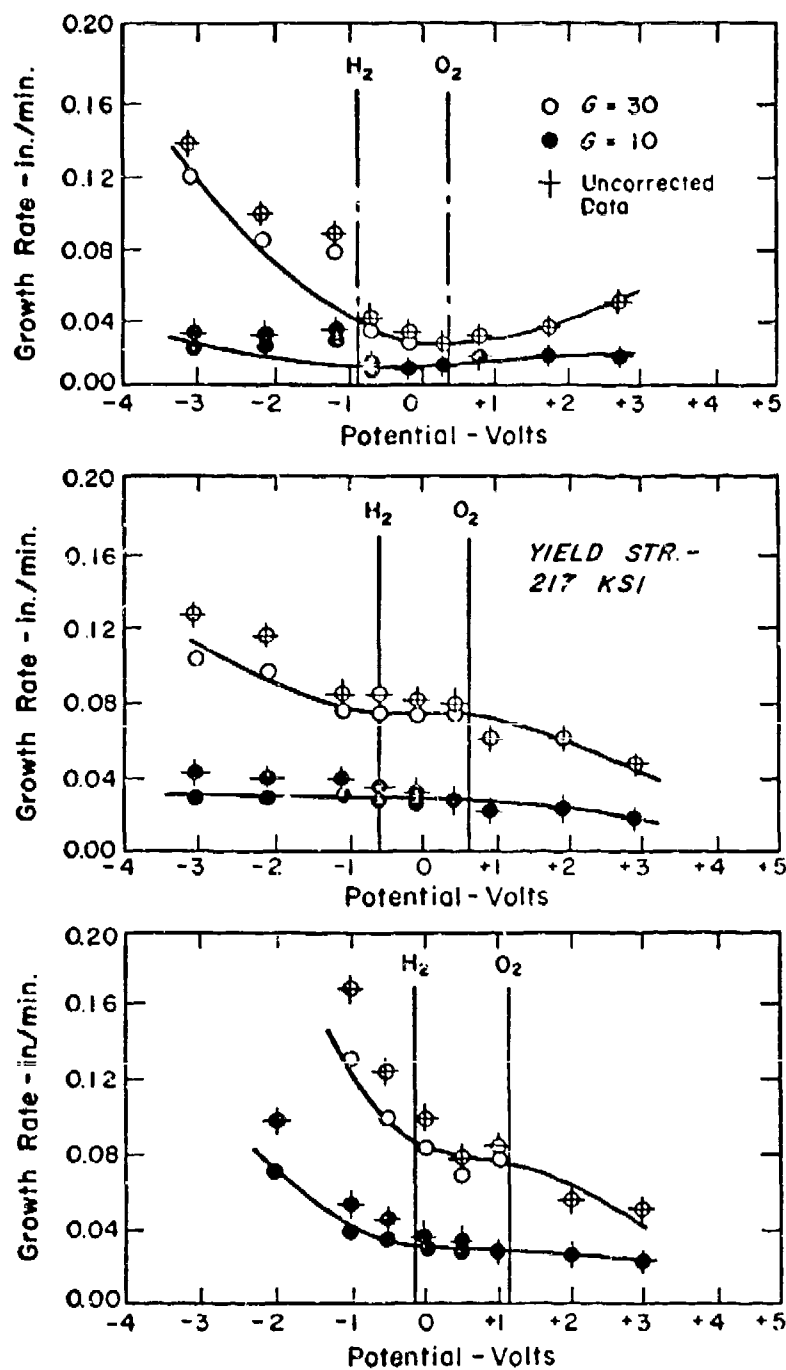
Fig. 42. Effects of pH, Applied Potential, and
Strain Energy Release Rate (G) on
Crack Velocities in AISI 4340 Steel
[From the work of Van der Sluys (26)]

62
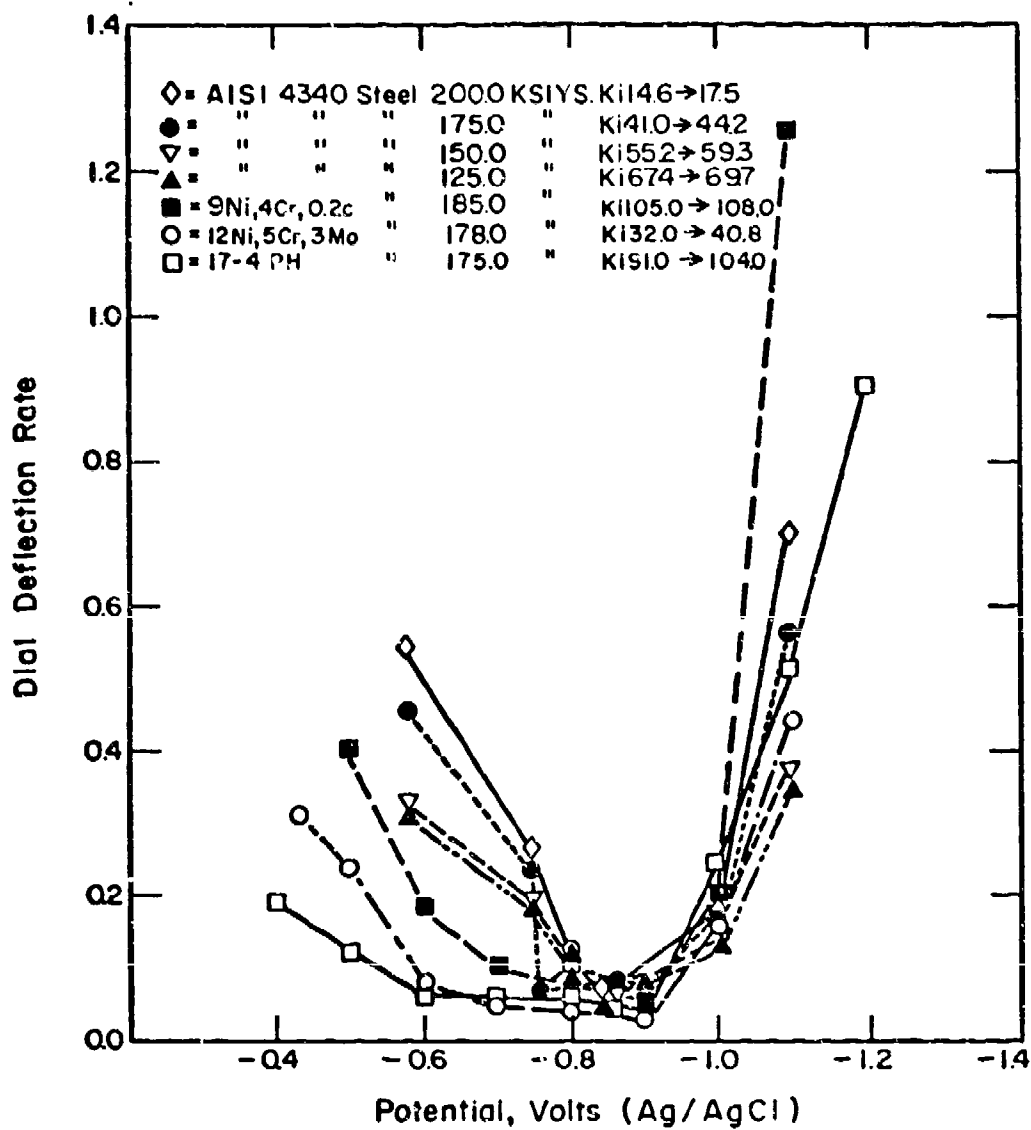
Fig. 43. Effect of Applied Potential on Crack Growth Rates in
Aqueous Chloride Environment [From the work of
Brown (54)]

63
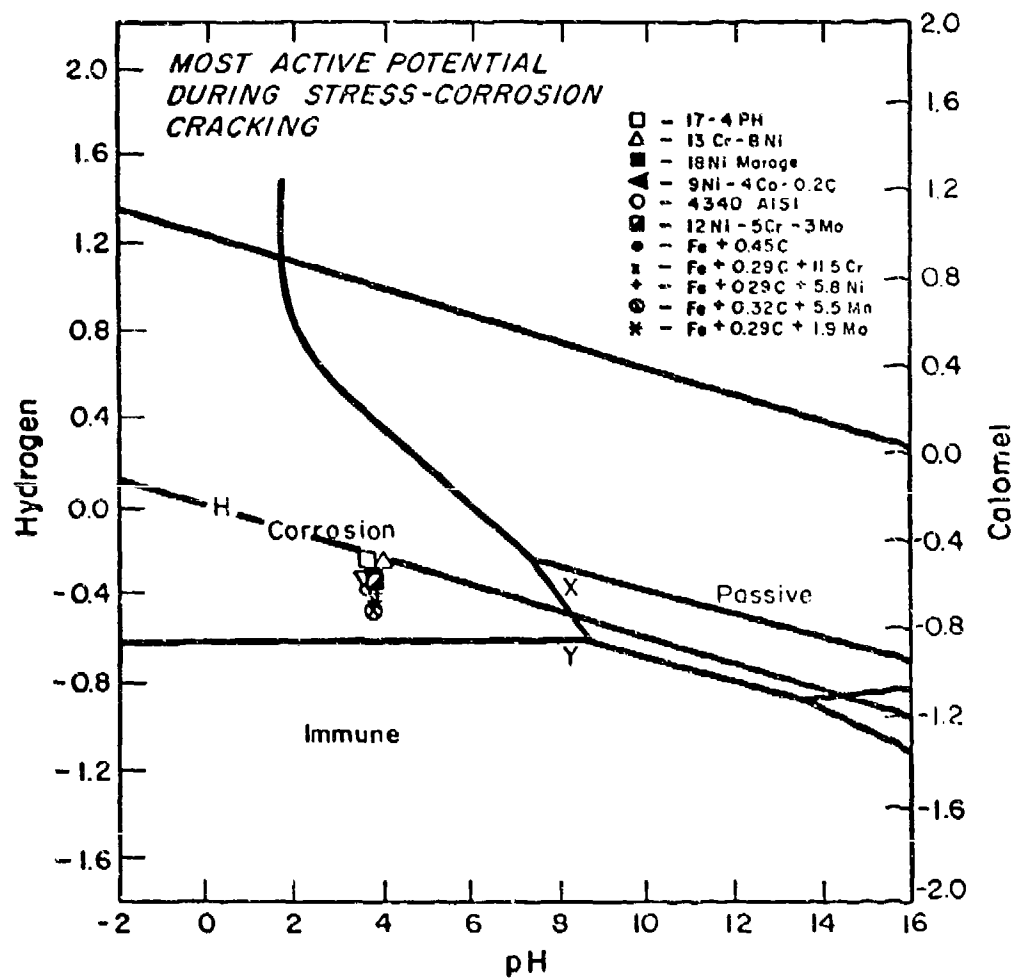
Fig. 44. Potential and pH Conditions for Active Stress
Corrosion Cracks in High Strength Steels
[From the work of Brown (55)]

(a)

STEEL	Y.S (ksi)
O 410	225
□ 410	225
△ 410	210
▽ 410	180
● 430	60

AERATED $3\frac{1}{2}$ %
NaCl SOLUTION
(pH = 6.5) AT 100°C
[U-BEND SPECIMENS]

Failure Time (minutes)

1000
100
10
1

Applied Potential (Millivolts vs SCE)

-200   -600   -1000   -1400

(b)

Hydrogen Permeation Rate $\dfrac{Std.cm^3 \times 10^6}{cm^2\ sec}$

AERATED $3\frac{1}{2}$ %
NaCl SOLUTION
(pH = 6.5)
AT 100°C

1000
100
10
1

E_{corr}

STEEL	Y.S. (ksi)
O 410	225
△ 410	270
▽ 410	275
● 430	60

Applied Potential (Millivolts vs SCE)

-200   600   -1000   -1400

Fig. 45. Effect of Applied Potential on Delayed
Failure Times and Hydrogen Permeation
Rates for Types 410 and 430 Stainless
Steel [From the work of McGuire et al. (56)]

65

were tested as 0.030" foils, stressed to 50 ksi. Figure 46 shows the
effects of applied potential on hydrogen permeation and delayed failure
times. For the case of HP 9-4-45, the decrease in failure time by
anodic polarization was accompanied by pitting corrosion. The occurrence
of pitting is expected[58] to produce similar electrochemical conditions,
at the base of the pit, as those found at stress-corrosion crack tips.[3,55]
Thus, hydrogen-induced cracking is not eliminated as a possible failure
mechanism.

EFFECT OF APPLIED STRESS INTENSITY
ON CRACK GROWTH RATE

Increases of stress or applied stress intensity increase the
kinetics of delayed failure. The critical role of stress in delayed
failure is shown by the effect of notch radius on both the notch ten-
sile strength and delayed failure times for high-strength steel in a
distilled water environment. The effect of increasing notch acuity on
delayed failure of 300M steel is shown in Fig. 47. The effect of
gross section stress, per se, on delayed failure has been shown in
Fig. 2(e). The effect of applied stress intensity on crack growth
kinetics in aqueous solutions will, in general, show three distinct
regions of stress intensity dependence (I, II, and III).

Speidel[9] has shown that such regions exist for quenched and
tempered AISI 4340M steel in a distilled water environment. Such
behavior is shown in Fig. 2(c). At low stress intensities (Region I),
crack velocity if strongly increased by increasing applied stress
intensity. At intermediate stress intensity values, crack velocity is
a weak function of K_I, giving Region II behavior. At high stress
intensity values (near K_{Ic}), the strong dependence of crack velocity
on K_I constitutes Region III behavior. Figure 48 shows the results of
Spiedel[60] for AFC-77 steel, again exhibiting distinct regional behavior.
Crack branching was observed by Spiedel in Region II.[60] Regions I, II,
and III were observed   ng and Staehle[57] for bainitic structures as
well, as seen in Fig. __. Regions I and II were observed in high-
strength level 4340 steel by Colongelo and Ferguson,[55] as shown for a
salt water environment in Fig. 19.

Mostovoy et al.[61] have shown Region I - Region II behavior for
quenched and tempered 300M and bainitic HP 9-4-45 steels in an aqueous
3.5% NaCl environment. Yield strength levels were 233 ksi and 200 ksi,
respectively. The crack velocity   stress intensity data are shown
in Figs. 49 and 50. Figure 51 shows the stress intensity dependence
of crack velocity for 300M in a distilled water environment. Crack
velocity measurements for 250-grade maraging steel also exhibited
Region I - Region II cracking behavior. Microscopic examination of a
250 maraging steel specimen, following crack growth in a 3.5% NaCl
solution, was found[1] to exhibit crack micro-branching at Region II
stress intensity values. This is in agreement with the observations
of Spiedel. In addition, the presence of chloride in the environment
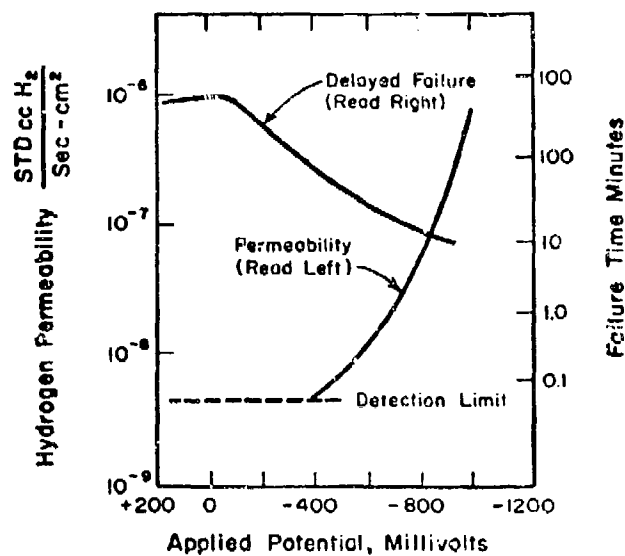
4340 Steel
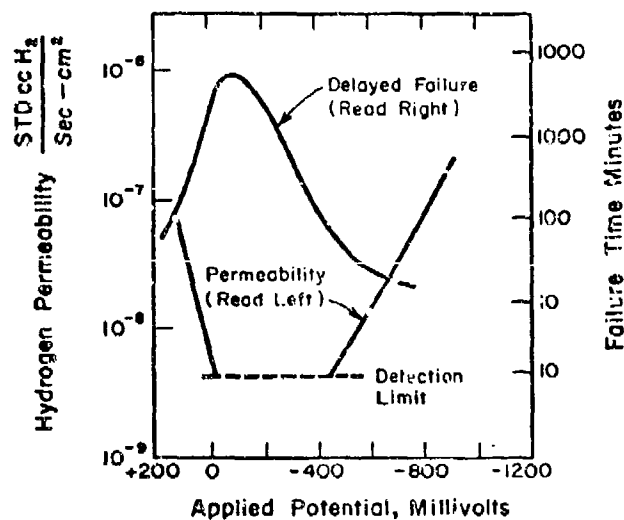
HP 9-4-45 Steel

Fig. 46. Effect of Applied Potential on Delayed
Failure Time and Hydrogen Permeation
Rate for Stressed Foils (50 ksi) of
AISI 4340 and HP 9-4-45 Steels in
3.0N NaCl Solution [From the work of
Barth et al. (57)]
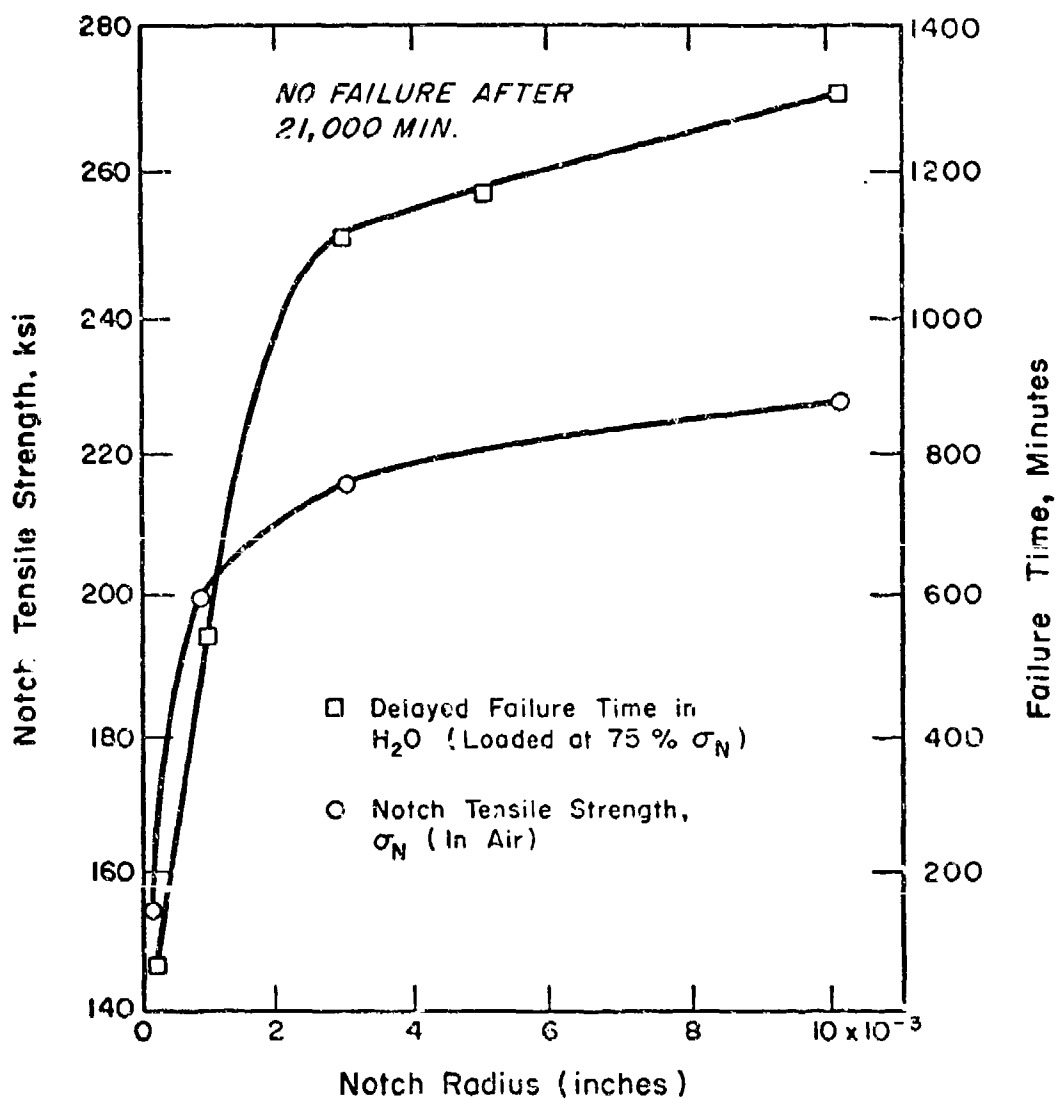
Fig. 47. Effect of Notch Radius on Notch Tensile Strength and
Delayed Failure Characteristics of 300M Steel,
220 ksi Strength Level at 68°F [From the data of
Hanna et al. (59)]

68
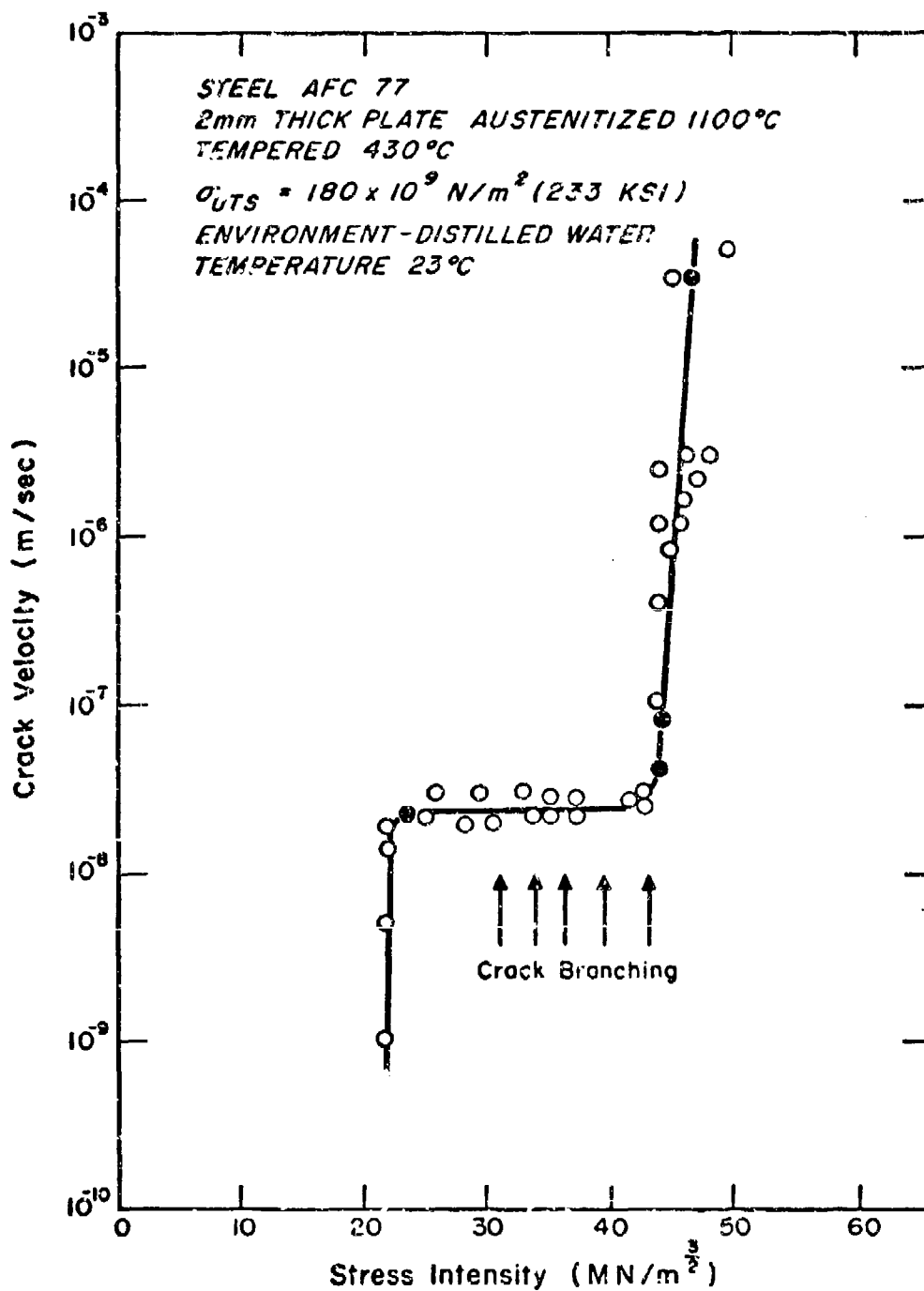
Fig. 48. Effect of Applied Stress Intensity on Crack Velocity for AFC 77 Steel in Distilled Water [From the work of Speidel (60)]
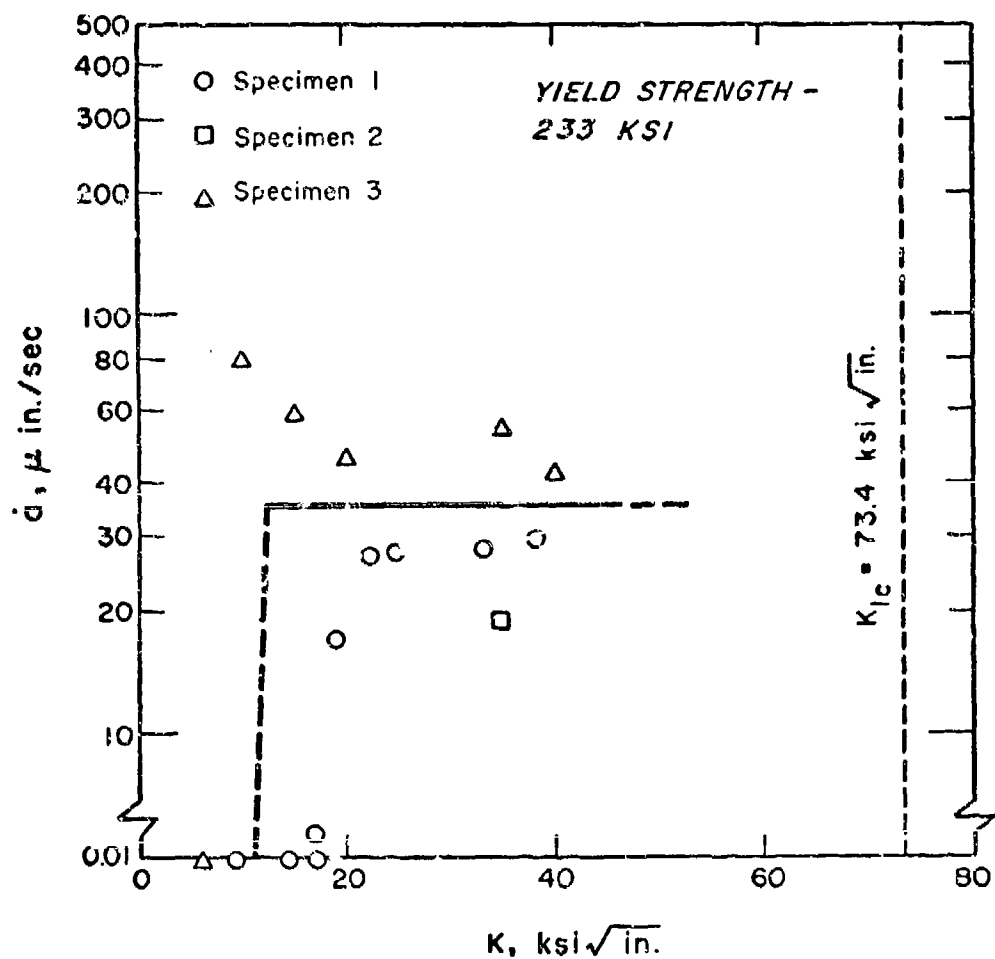
Fig. 49. Effect of Applied Stress Intensity on Crack
Velocity for 300M Steel in $3\frac{1}{2}\%$ NaCl Solution
[From the work of Mostovoy et al. (61)]
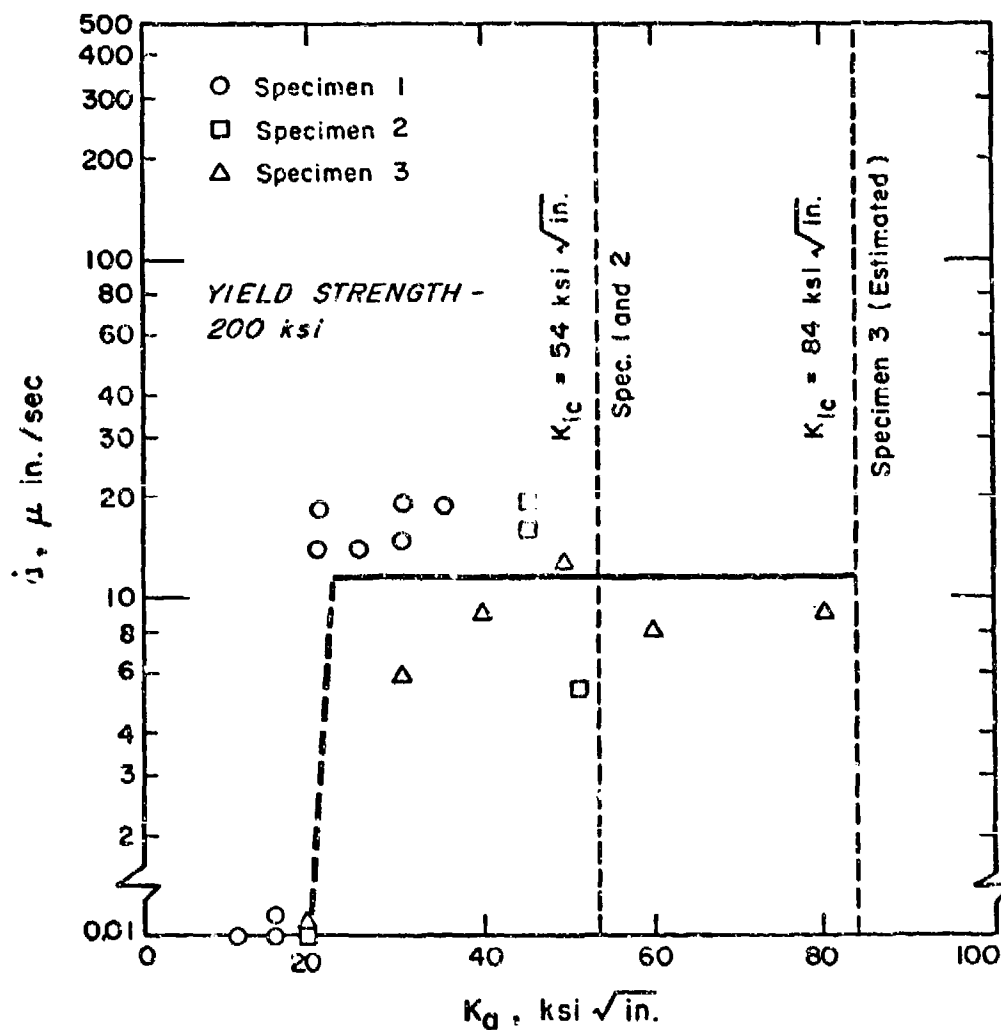
Fig. 50. Effect of Applied Stress Intensity on Crack
Velocity for HP 9-4-45 Steel in $3\frac{1}{2}\%$ NaCl
Solution [From the work of Mostovoy et al. (61)]
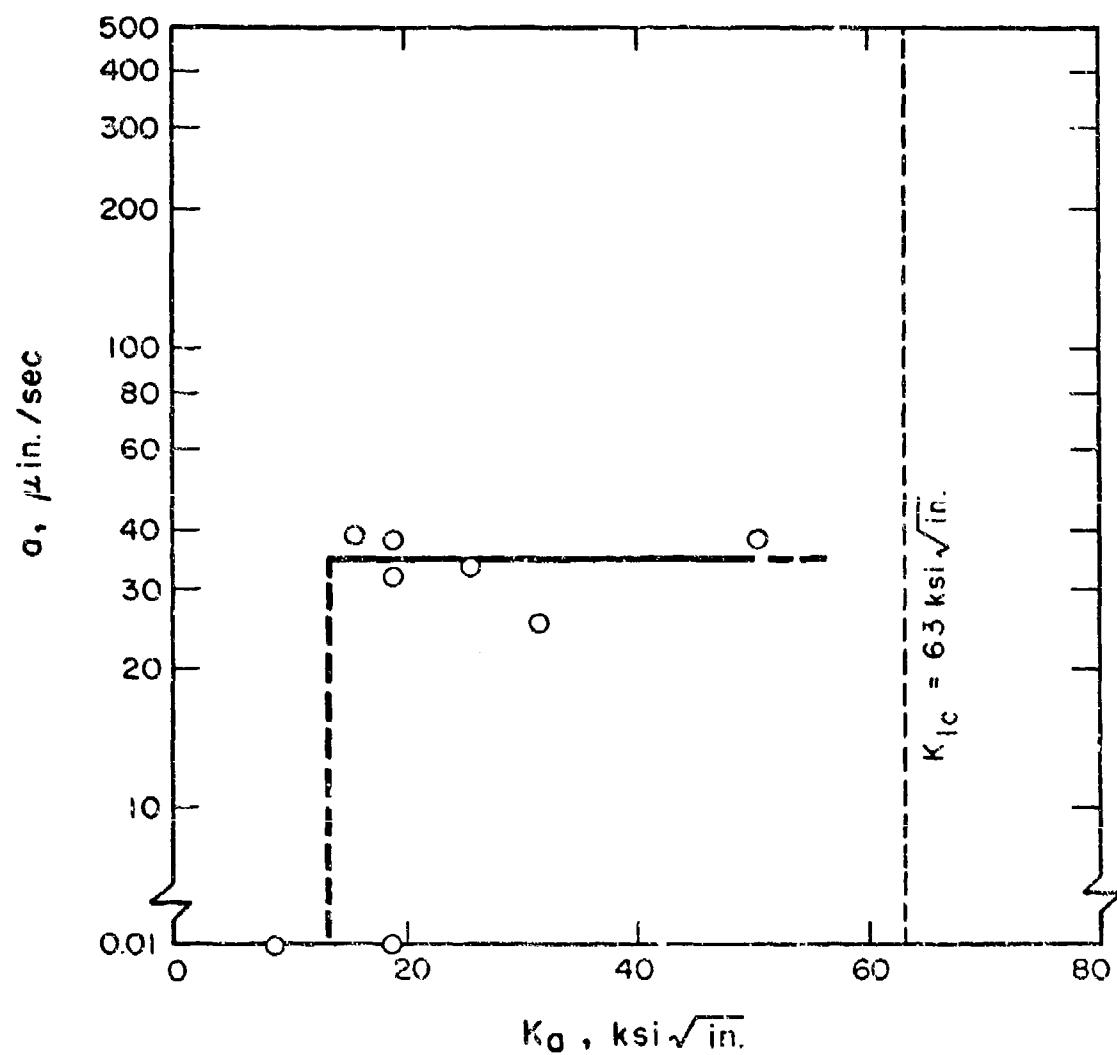
Fig. 51. Effect of Applied Stress Intensity on Crack Velocity
for 300M Steel in Distilled Water Environment [From
the work of Mostovoy et al. (61)]

72

does not show a significant effect on crack velocity (Figs. 49 and 51). This agrees with the results of Staehle and Wang[37] shown in Fig. 22.

The Region II crack velocity is a significant parameter in that it pertains to the majority of stress and flaw-size conditions over which environmentally induced slow crack growth can occur. Of the steels presented here, 4340M shows the highest velocity, having a strength level of approximately 290 ksi.[9] For the same yield strength (200 ksi), the data for martensitic 4340 steel[35,37] show very similar Region II crack velocities (Figs. 19 and 22), on the order of 10^{-3} in./min. It is significant that AFC-77 steel, at the same strength level as 4340 steel[35,50] shows a Region II crack velocity approximately one order of magnitude lower.

The dependence of crack velocity on applied stress intensity is similar in both gaseous and aqueous environments. Landes[62] has measured crack velocities for AISI 4340 steel (strength level - 302 ksi) in both distilled water and atmospheric pressure H_2 gas environments. In both media, a strong crack velocity dependence on K was observed. A lower dependence of crack velocity on K was found with increasing stress intensity. The data are shown in Fig. 52. Sawicki[13] has observed Region I - Region II behavior for H-11 steel (yield strength - 230 ksi) in 800 torr dry H_2 gas. The stress intensity range for Region I behavior is increased by an increase of test temperature. The crack velocity data are presented in Fig. 53. Region I - Region II behavior is also observed for high strength AISI 4335V and D6AC steels, as shown in Figs. 20 and 21.

McIntyre and Priest[63] have observed Region I - Region II behavior for slow crack growth in 835M30 steel in both gaseous H_2 and gaseous H_2S environments, as shown in Fig. 54. Kerns and Staehle[64] have also observed Region I - Region II behavior in both H_2 and H_2S gaseous environments, as shown in Fig. 55. The latter data (Fig. 55) show that crack velocities in low-pressure H_2S [10^{-3} atmospheres] far exceed those observed in aqueous solutions.

The data of Landes[32] and those of Kerns and Staehle[34] show lower apparent K_{Iscc} values for aqueous cracking than for slow crack growth in gaseous media. However, the studies by McIntyre and Priest[63] indicate that threshold stress intensities for aqueous cracking are equal to or greater than those required for cracking in gaseous environments are seen in Figs. 52, 54, and 55 to be at least one order of magnitude greater than the growth rates observed in aqueous solutions.

Slow Crack Growth in Gaseous Environments

Water Vapor

Johnson and Willner[65] have studied slow crack growth rates for H-11 steel (yield strength - 230 ksi) in moist argon environments. Crack velocity was found to increase with moisture content up to a

73
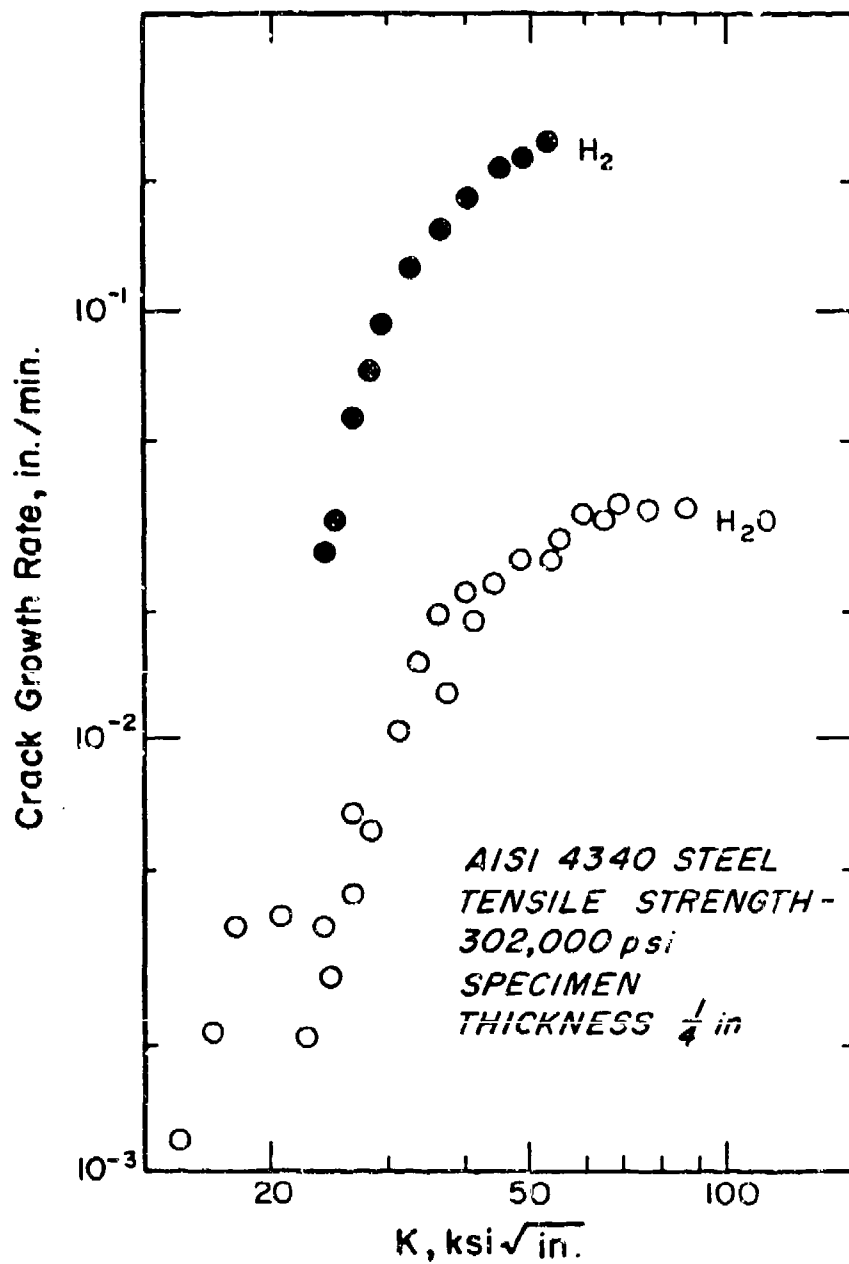
Fig. 52. Effect of Stress Intensity on Crack Velocity for AISI 4340 Steel in Distilled Water and Hydrogen Gas (1 atm) Environments [From the work of Landes (62)]
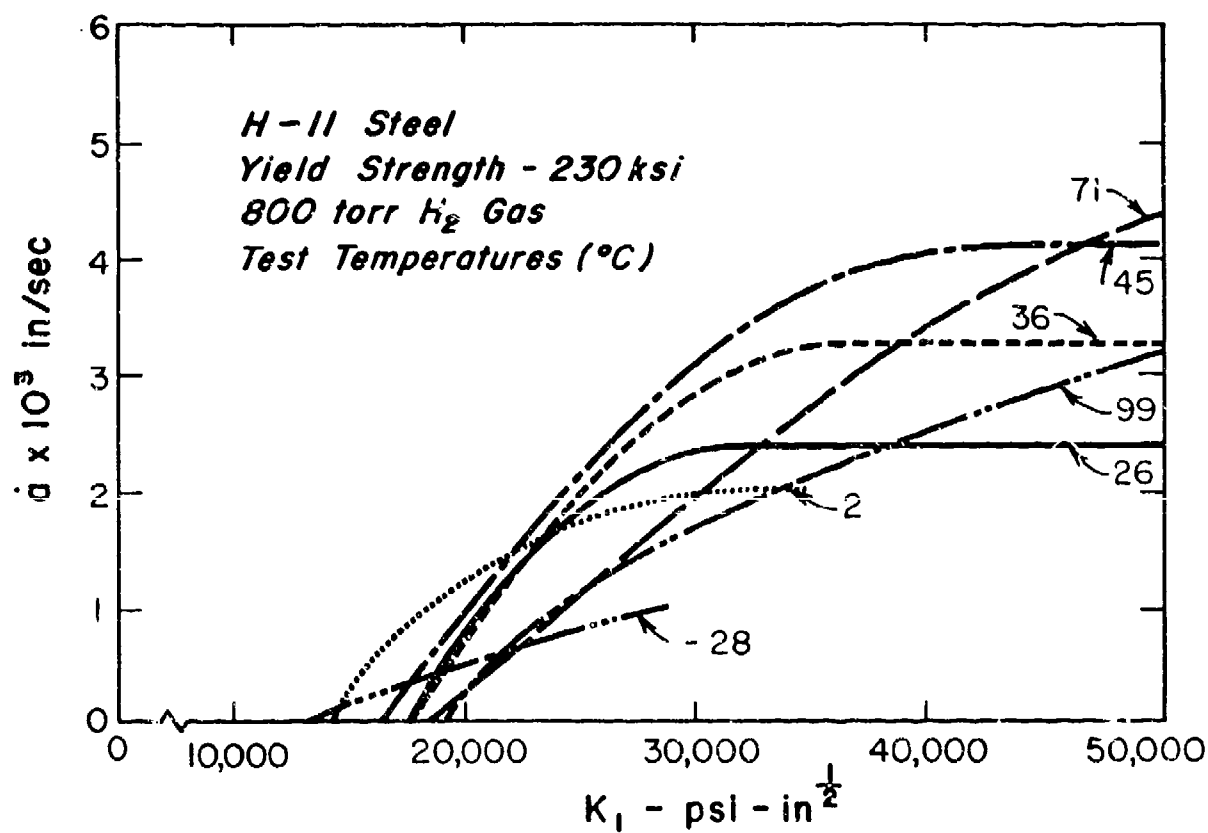
Fig. 53. Effects of Temperature and Applied Stress Intensity on Crack Velocity for H-11 Steel in Dry H_2 Gas [From the work of Sawicki (43)]
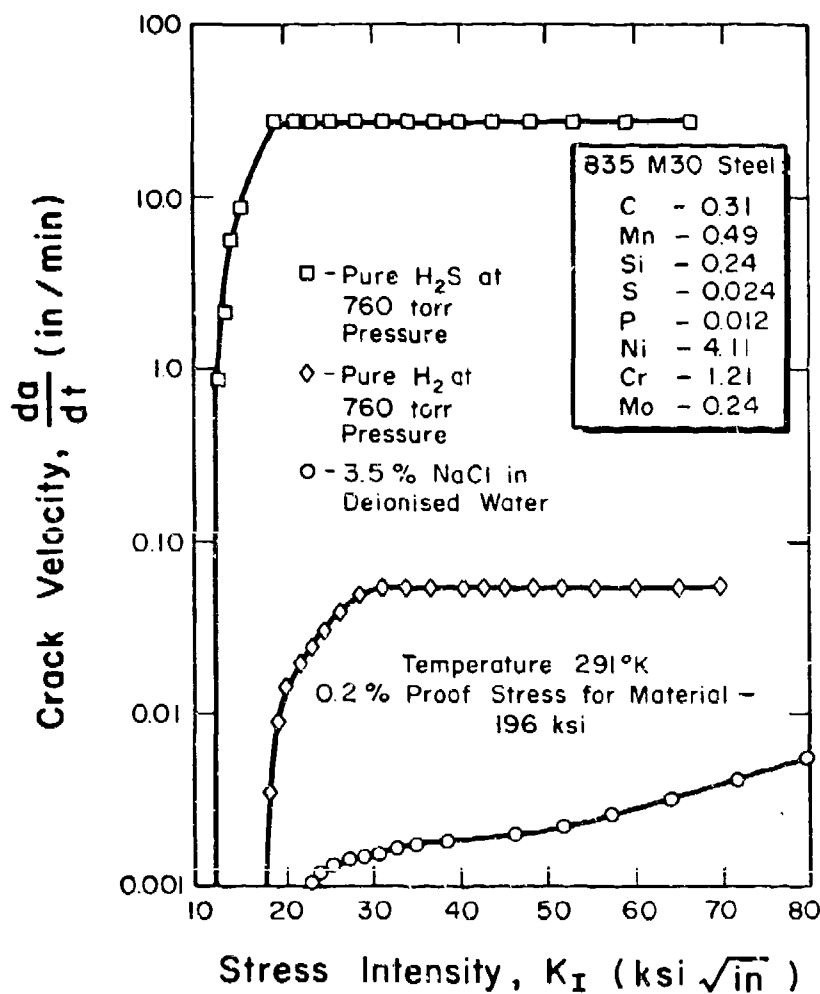
Fig. 54. Effect of Stress Intensity on Crack Velocity for 835M30 Steel in Aqueous NaCl, Gaseous H₂, and Gaseous H₂S Environments [From the work of McIntyre and Priest (63)]
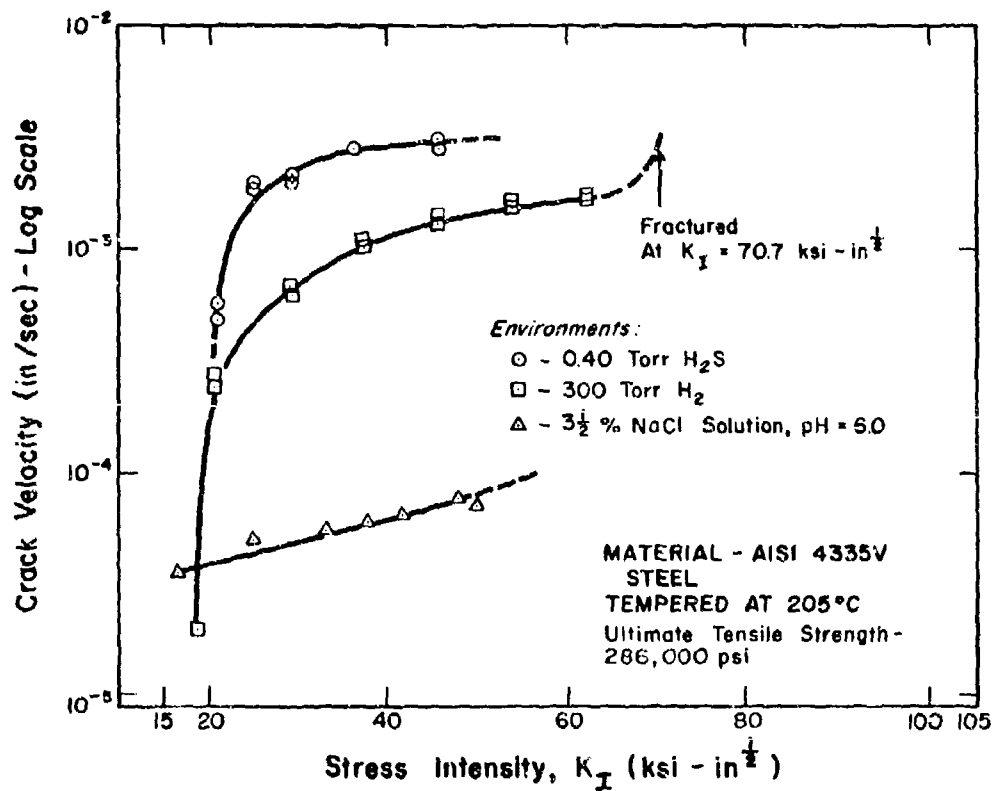
Fig. 55. Crack Velocity As a Function of Applied Stress Intensity for AISI 4335V Steel (Tempered at 205°C) in Salt Water, H₂ Gas, and H₂S Gas Environments [From the work of Kerns and Steehle (64)]

relative humidity of 60%. The effect of moisture on crack velocity is shown in Fig. 56. Crack velocities in water-saturated argon were found to be the same as those in liquid water. The latter result is shown in Fig. 57. The effect of water vapor was attributed to condensation of water vapor at the crack tip. Condensation of 60% relative humidity was the result of lowering the equilibrium vapor pressure of water by the low radius of curvature at the crack tip (solid-vapor interface).

H_2 Gas

The initial observations of crack growth in dry H_2 gas environments were by Hancock and Johnson,[25] showing significantly larger velocities than those observed in aqueous solutions. Crack velocity measurements in humidified argon or humidified hydrogen environments did not differ significantly from those observed for a distilled water environment. Figure 58 shows the greater velocities observed in dry H_2 gas, as compared to water or moist argon environments, for quenched and tempered H-11 steel.

The Effect of Gas Pressure on Crack Velocity

The dependence of crack velocity on gas pressure has been shown to be a function of both test temperature and applied stress intensity. Reported pressure dependencies for crack growth in H_2 gas range from $P_{H_2}^{1/2}$ to $P_{H_2}^{2}$.

The initial study of the crack velocity - H_2 pressure relationship was by Williams and Nelson.[40] Using fully hardened 4130 steel specimens (pre-fatigue cracked DCB geometry), the investigators measured the pressure dependence of crack velocity at test temperatures of -60°C, +23°C, and +60°C; the results are shown in Fig. 59. Sawicki[43] measured the H_2 pressure dependence of crack velocity in H-11 steel at +27°C, +47°C, and +80°C. In the latter study, a $P_{H_2}^{3/2}$ dependence was observed at +80°C, in agreement with the Williams and Nelson study.[40] Figure 60 shows the pressure dependencies observed by Sawicki.[43] At +27°C and +47°C, the pressure dependence was $P_{H_2}^{1}$, with no observation of a $P_{H_2}^{1/2}$ dependence at low temperatures.

Studies by Kerns[43] have shown that the H_2 pressure dependence, at 22°C to 27°C, is a function of applied stress intensity. Figures 61 and 62 show pressure dependencies for slow crack growth in 205°C tempered AISI 4335V steel at three stress intensity values. As seen in Fig. 20, the stress intensities lie in Region 1, Region II, and in the transition zone. Similar results are shown for 315°C tempered 4335V steel and for D6AC steel in Figs. 63, 64, and 65. The observed pressure dependence coefficient is shown as a function of crack velocity and stress intensity in Fig. 66.
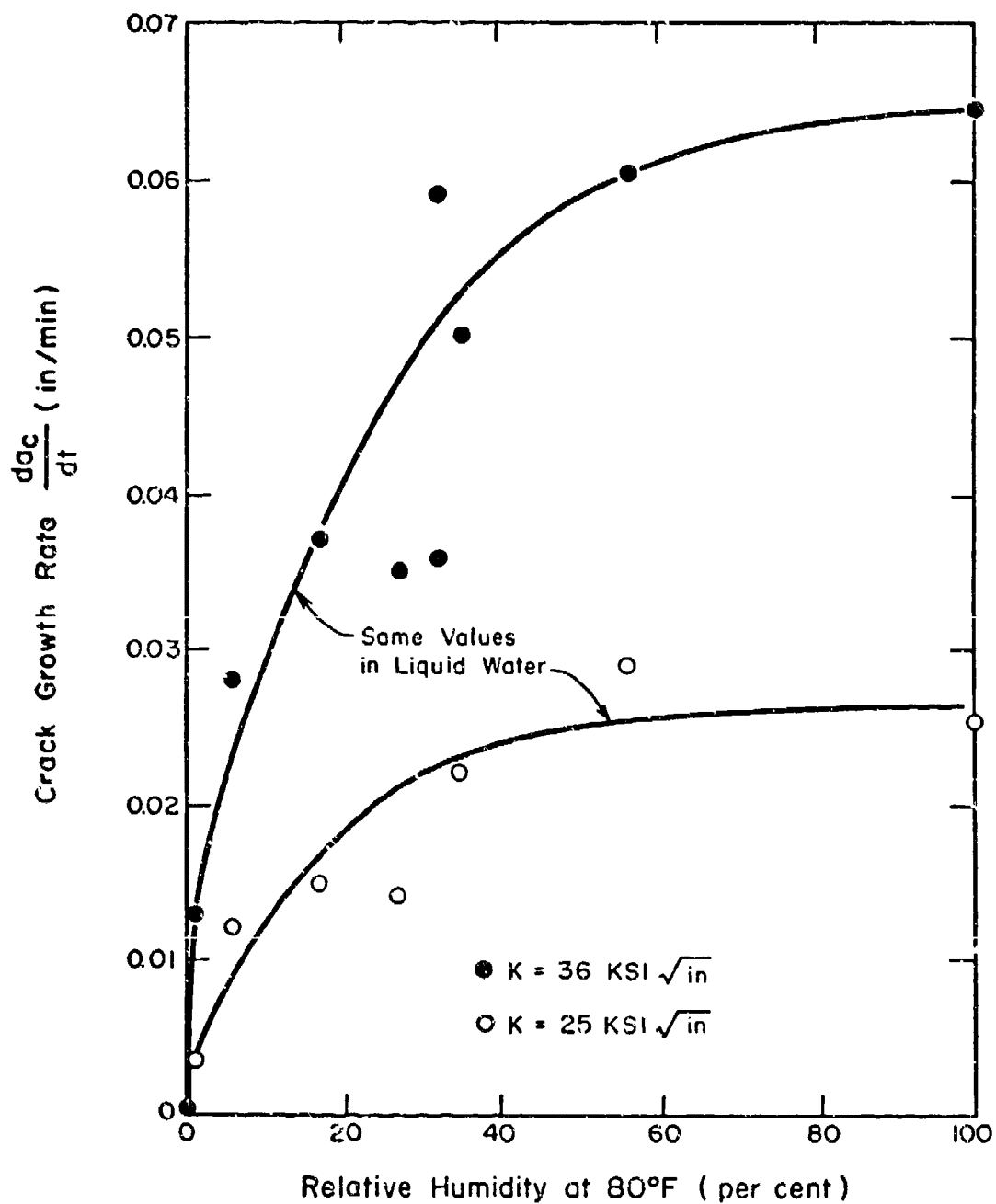
Fig. 56. Effect of Relative Humidity on Crack Velocity for H-11 Steel
(230 ksi y.s.) in Moist Argon Environments [From the work of
Johnson and Willner (65)]

79
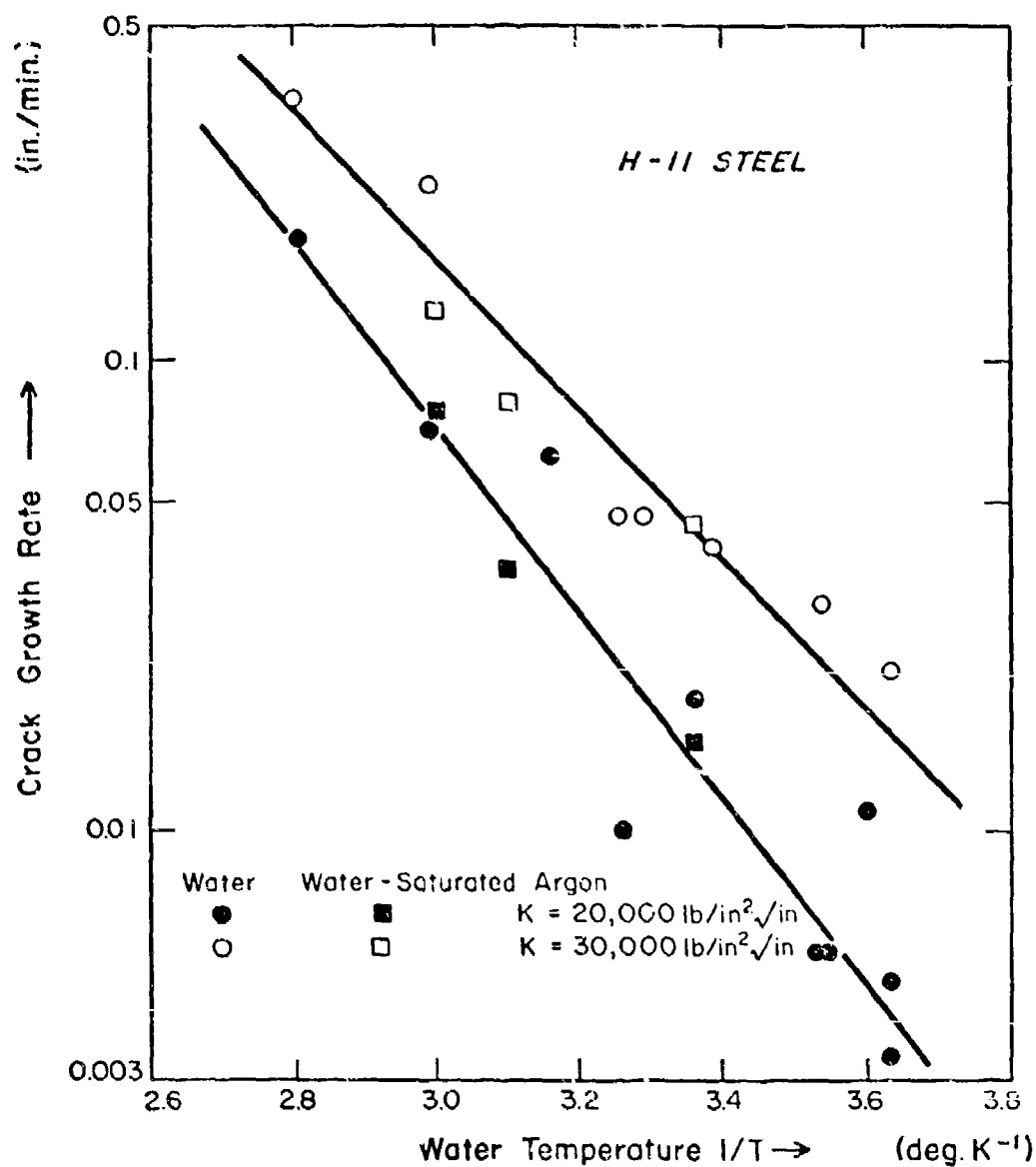
Fig. 57. Effects of Temperature and Stress Intensity on Crack
Growth Rate in Water and Water-Saturated Argon
Environments [From the work of Johnson and Willner
(65)]
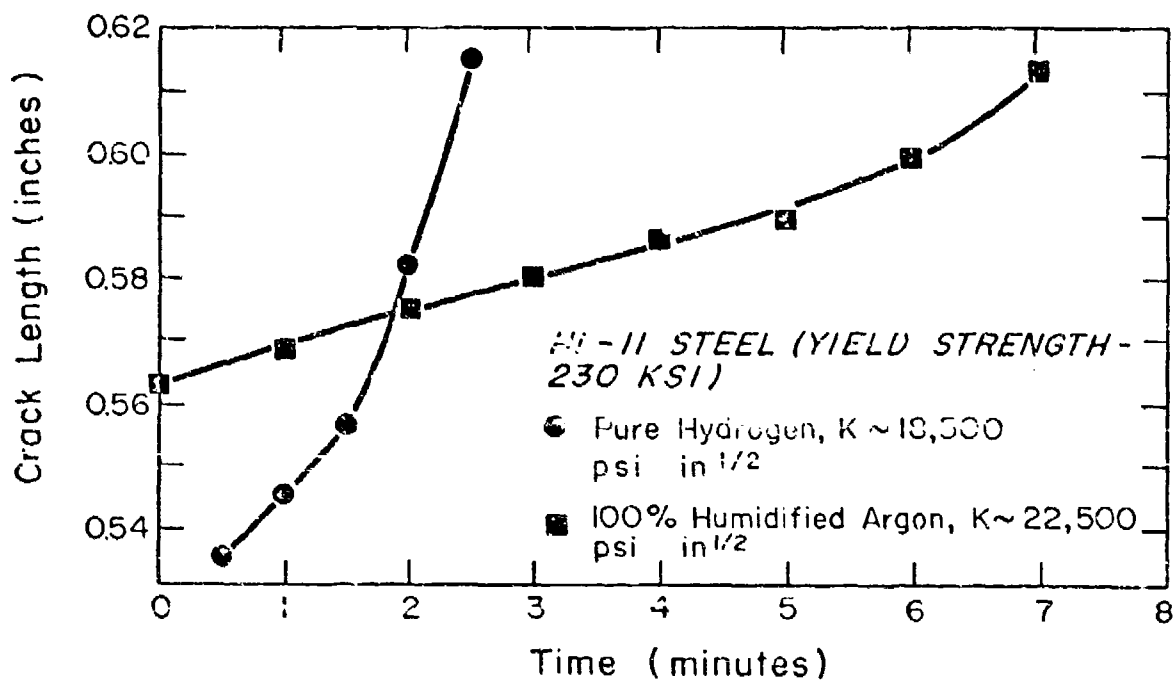
Fig. 58. Crack Velocities for H-11 Steel in Moist Argon and Dry Hydrogen
Gas Environments [From the work of Hancock and Johnson (25)]
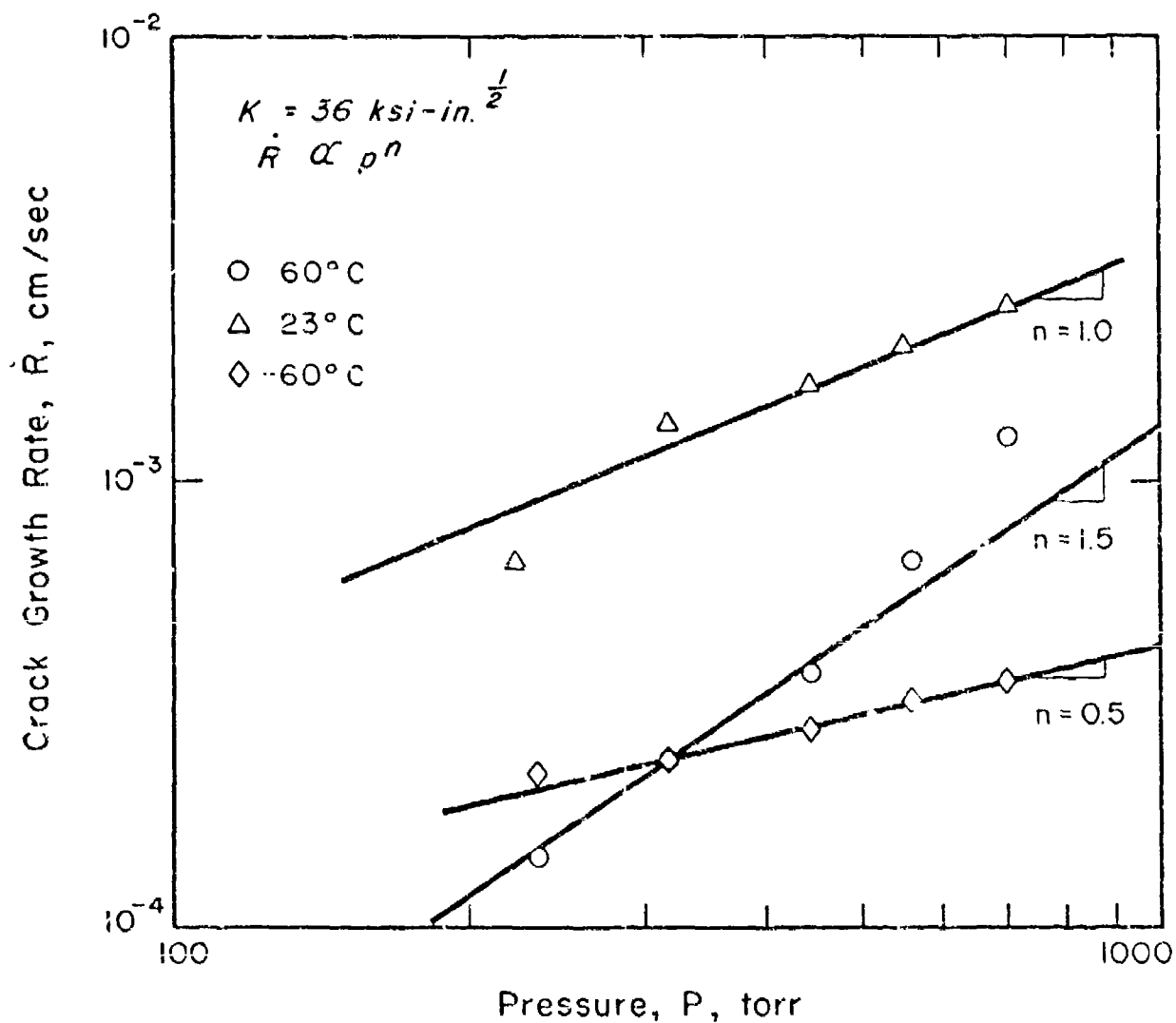
Fig. 59. Effect of Hydrogen Pressure on Crack Velocity in 4130 Steel at Various Temperatures [From the work of Williams and Nelson (42)]

82
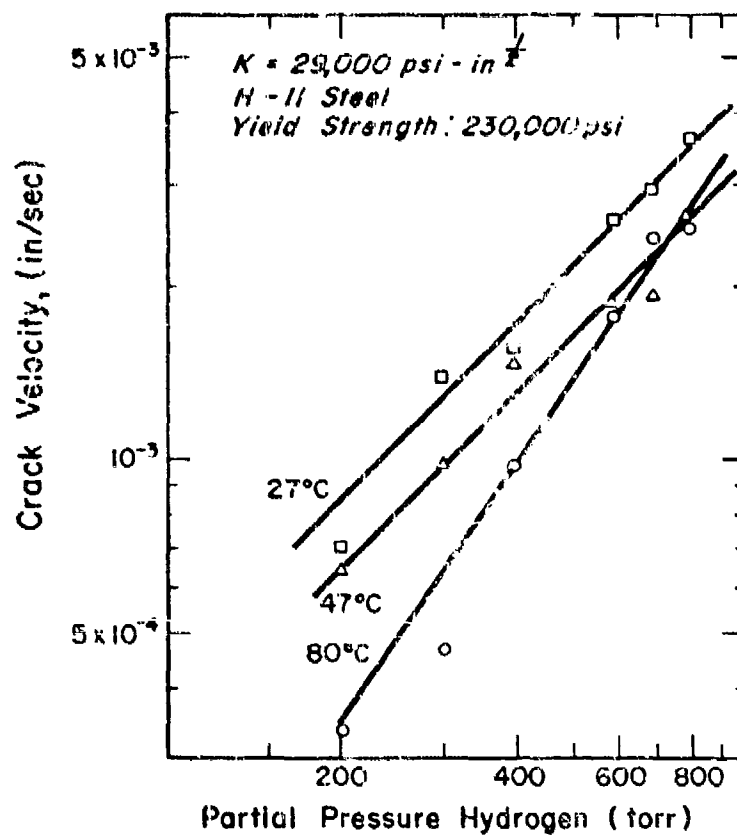
Fig. 60. Effect of Test Temperature on the Pressure
Dependence of Crack Velocity for H-11 Steel
Specimens in H_2 Gas [From the work of
Sawicki (43)]
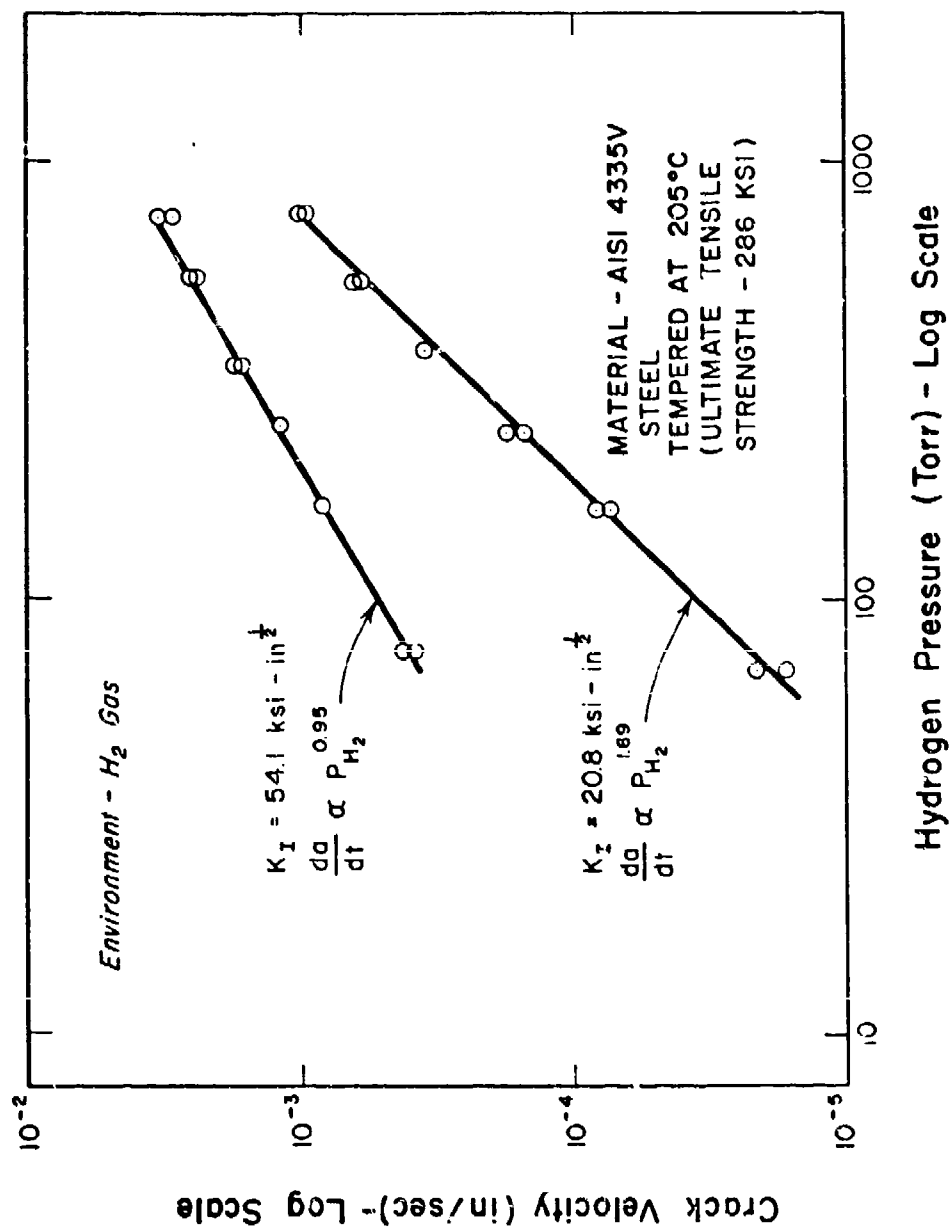
Fig. 61. Crack Velocity as a Function of H_2 Pressure and Applied Stress Intensity for 205°C Tempered AISI 433V Steel [From the work of Kerns (36)]

84

Environment – H_2 Gas

$K_I = 41.6$ ksi – in$^{\frac{1}{2}}$

$\frac{da}{dt} \propto P_{H_2}^{1.16}$

MATERIAL – AISI 4335V
STEEL
TEMPERED AT 205°C
(ULTIMATE TENSILE
STRENGTH – 279 KSI)

Crack Velocity (in/sec) – Log Scale

10^{-2}

10^{-3}

10^{-4}

10^{-5}

10   100   1000

Hydrogen Pressure (Torr) – Log Scale
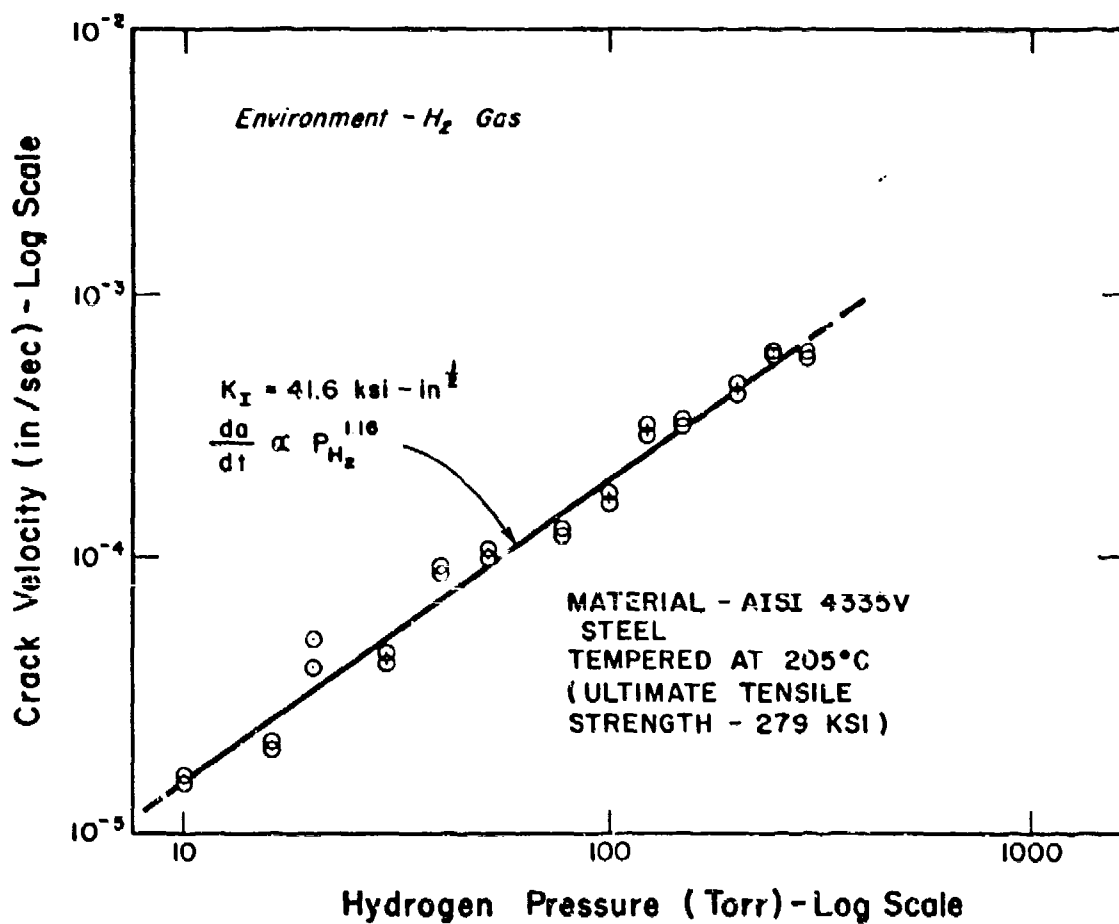
Fig. 62. Crack Velocity as a Function of Hydrogen Pressure for AISI
4335V Steel at K_I = 41.6 ksi-in.$^{\frac{1}{2}}$ [From the work of Kerns
(36)]
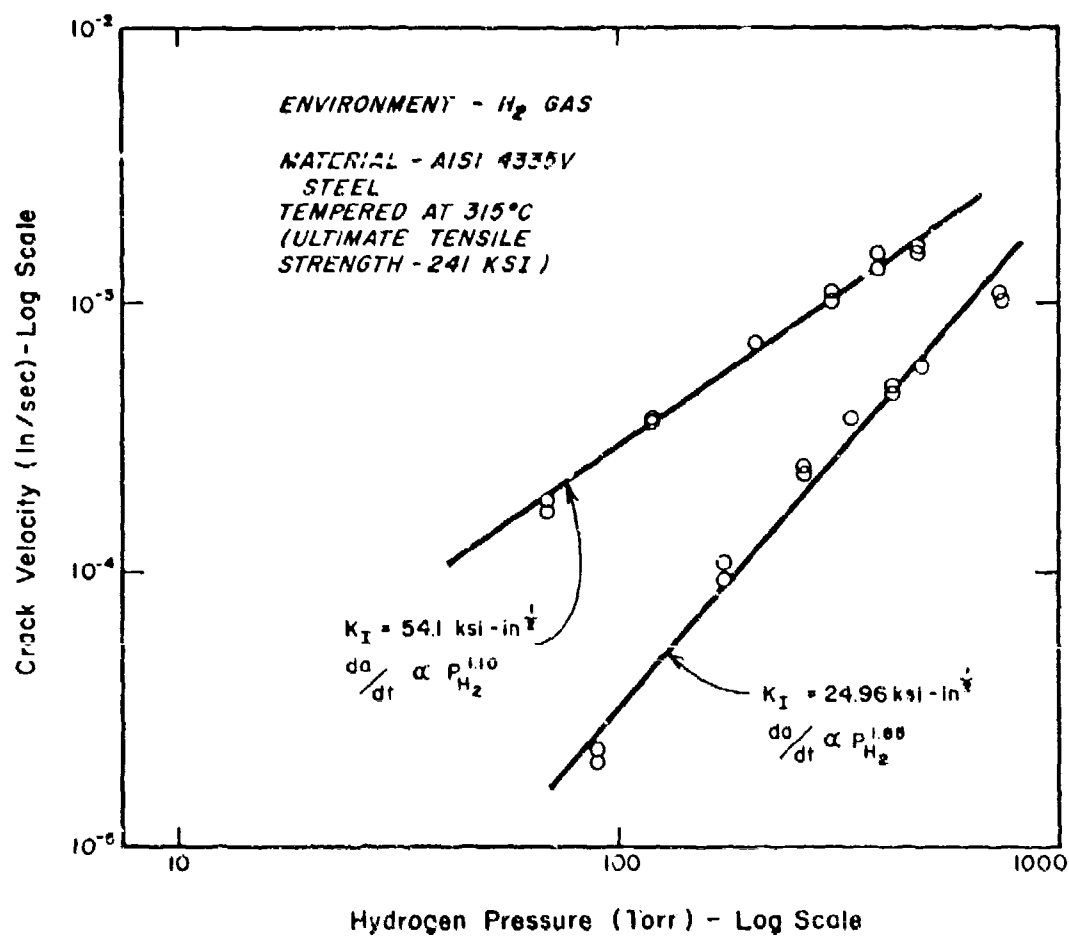
Fig. 63. Crack Velocity as a Function of H_2 Pressure and Applied
Stress Intensity for 315°C Tempered AISI 4335V Steel
[From the work of Kerns (36)]
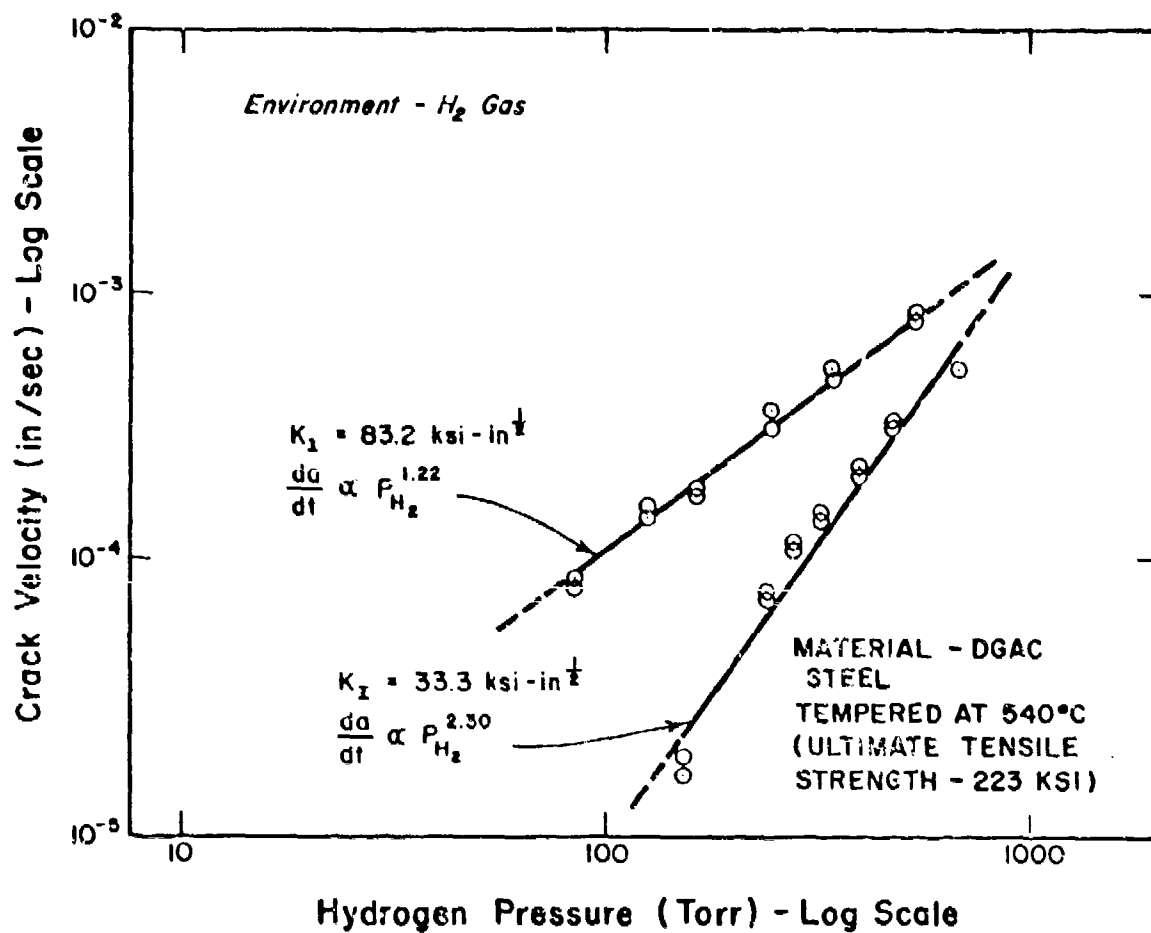
Fig. 64. Crack Velocity as a Function of H₂ Pressure and Applied Stress Intensity for 540° C Tempered D6AC Steel [From the work of Kerns (36)]
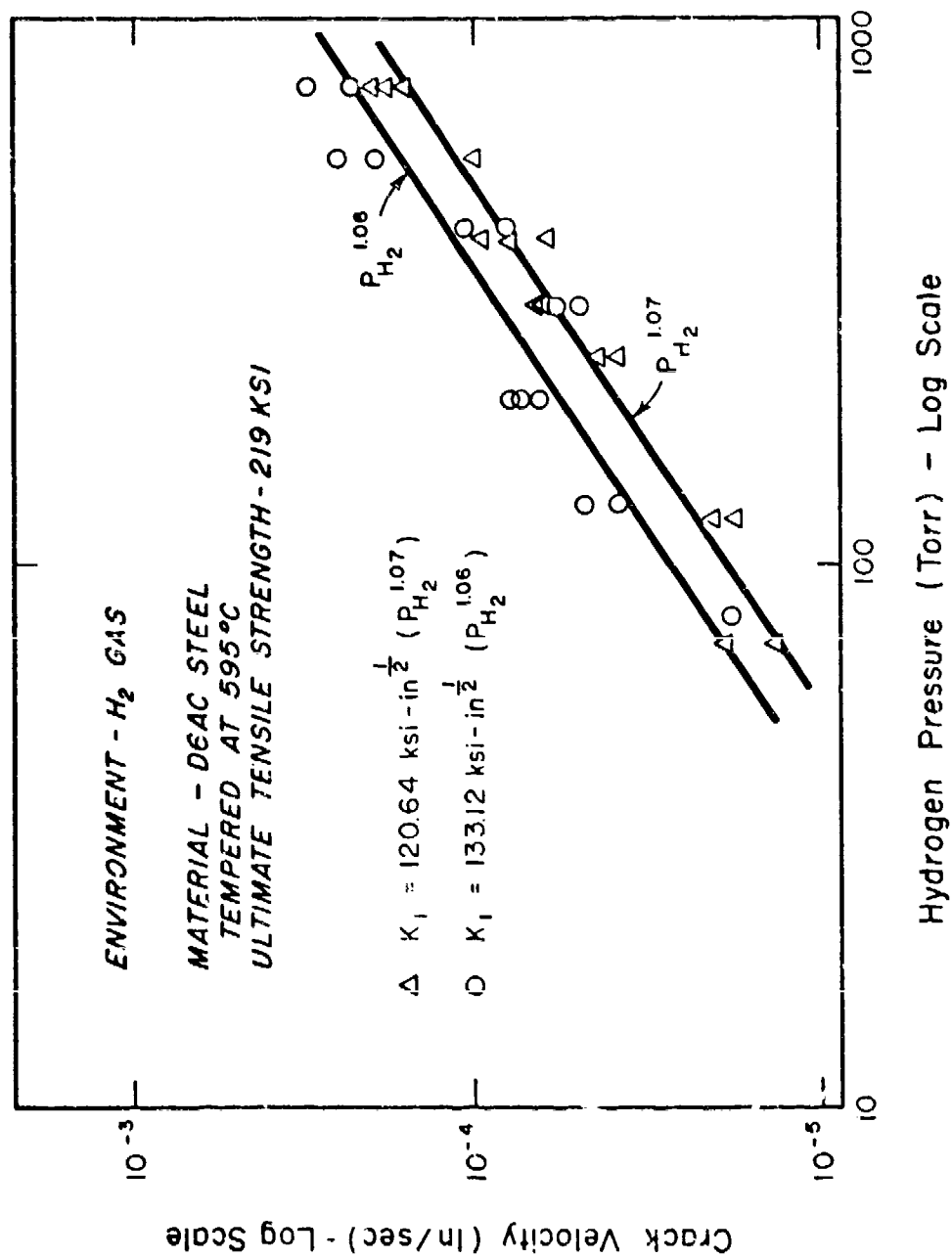
Fig. 65. Crack Velocity as a Function of H_2 Pressure and Applied Stress Intensity for 595°C Tempered D6AC Steel [From the work of Kerns (36)]
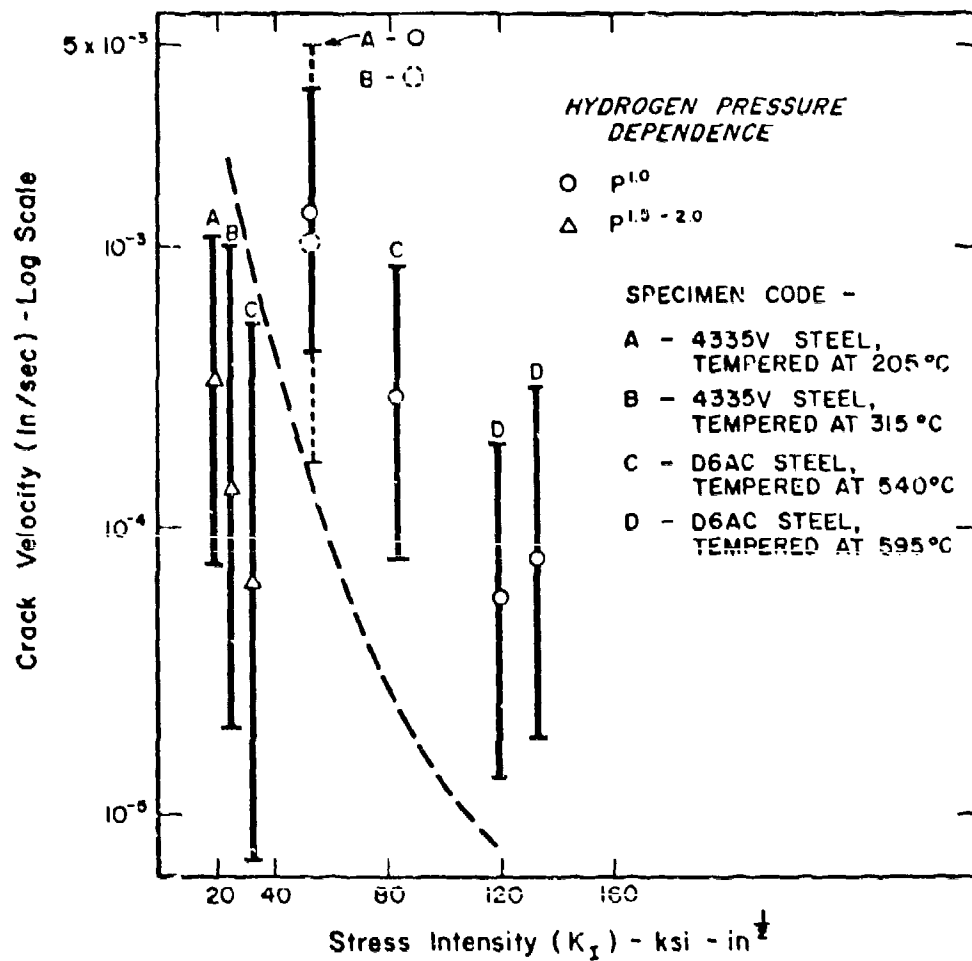
Fig. 66. Effects of Crack Velocity and Applied Stress Intensity on Observed Pressure Dependence Coefficient of Crack Velocity [From the work of Kerns (36)]

Crack velocity - hydrogen pressure studies by McIntyre and Priest[39] for high-strength 835M30 steel in 50-760 torr H_2 gas showed a $P_{H_2}^{1/2}$ dependence for crack velocity.

Investigation of the crack velocity dependence on H_2S pressure showed behavior similar to that for H_2 in the case of 205°C tempered 4335V steel.[94] The data are shown in Fig. 67. However, studies by McIntyre and Priest[39] for 835M30 steel in gaseous H_2S environments showed a $P_{H_2S}^{1/2}$ dependence of crack velocity.

The pressure dependence data are summarized in Table VIII. It is seen in the data of Sawicki,[43] shown in Fig. 53, that an increase of test temperature extends Region I behavior to higher stress intensity values. Therefore, for the same applied stress intensity, the pressure dependence of crack velocity pertains to Region II at low temperatures and Region I at high temperatures. The stress intensity chosen by Sawicki (29 ksi - in.$^{1/2}$), at 26°C, lies in the Region I - Region II transition zone (Fig. 53). At 71°C, the same stress intensity lies in Region I. The significance of such behavior is that, in general, it explains the increasing pressure dependence of crack velocity at high temperatures. The data of Williams and Nelson,[42] Sawicki,[43] and Kerns[36] are consistent if the Region II pressure dependence is $P_{H_2}^1$ and the Region I dependence is $P_{H_2}^{3/2}$ to $P_{H_2}^2$. A similar effect may apply for the case of H_2S gas environments. It is important that such a temperature dependence of Region I behavior does not explain the $P_H^{1/2}$ dependence for crack velocity at low and ambient temperatures,[42,39] nor the $P_{H_2S}^{1/2}$ dependence observed by McIntyre and Priest.[39]

EFFECT OF O_2 ADDITIONS ON SLOW CRACK
GROWTH IN GASEOUS ENVIRONMENTS

The addition of O_2 gas has been shown to halt cracking in dry H_2 gas environments. However, the critical amount of oxygen has not been clearly established. Hancock and Johnson[15] found that 0.7 vol% oxygen, added to hydrogen or water vapor environments, was sufficient to halt crack growth. The effect of oxygen was attributed to its preferential adsorption at the crack tip. In later work, Sawicki[43] reported that 0.4 vol% oxygen prevented cracking in H_2 gas environments at temperatures of -28°C to +100°C. Lesser oxygen levels (0.3 vol%) were found to increase the threshold stress intensity at which cracking was observed (23 ksi - in.$^{1/2}$ vs. 15 ksi - in.$^{1/2}$). Studies of slow crack growth in gaseous media by McIntyre and Priest[39] have shown that 1% oxygen was sufficient to halt crack growth in H_2 gas environments, but no oxygen effect was observed for slow crack growth in H_2S gas environments.

Recent studies by Kerns[36] have indicated that the absolute oxygen level is more significant than the O_2/H_2 ratio. The addition of 0.9 torr O_2 to 100 torr H_2 gas (0.9 vol%) showed no significant effect on the crack growth rate in AISI 4335V steel, as shown in Fig. 68. No crack growth was observed, however, on the addition of 4.7 torr O_2 to 665 torr H_2 (0.7%) for times up to 30 min.
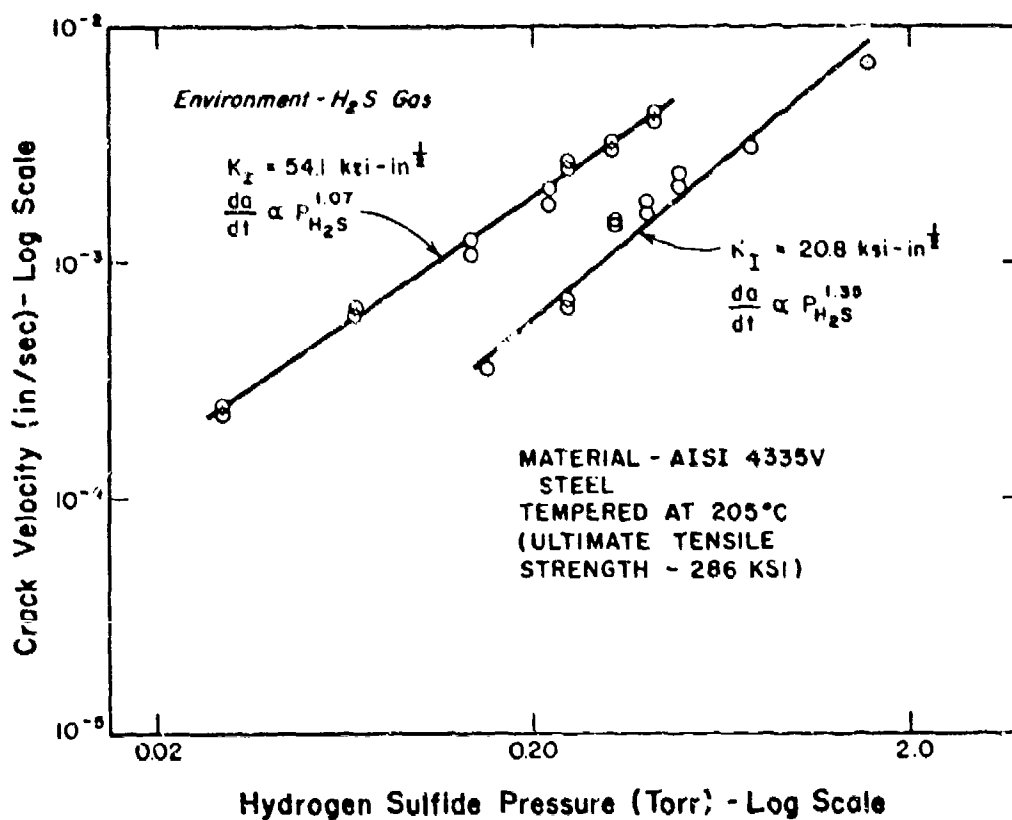
Fig. 67. Effects of Stress Intensity and Pressure on Crack Velocity for AISI 4335V Steel in H₂S Gas [From the work of Kerns and Staehle (64)]

91

Table VIII - Pressure Dependence Data for Crack Velocities in Gaseous Environments

Steel	Gas	Temperature	Stress intensity Range	Observed Dependence Coefficient $(n)_n$ for $da/dt \propto P_{H_2}, H_2S$	Reference
4130	H_2	-60°C	Not specified	1/2	Williams and Nelson (42)
"	"	+23°C	~ 2/3 K_{Ic}	1	"
"	"	+60	Not specified	3/2	"
H-11	"	+27°C	Region I-Region II transition	1	Sawicki (43)
"	"	+47°C	"	1	"
"	"	+80°C	Region I	3/2	"
4335V	"	22-27°C	Region I-Region II transition	1	Kerns (36)
"	"	"	Region II	1	"
"	"	"	Region I	2	"
D6AC	"	"	Region II	1	"
"	"	"	Region I	2	"
835M30	"	R.T.	Not specified	1/2	McIntyre et al. (63)
4335V	H_2S	22-27°C	Region II	1	Kerns (36)
"	"	"	Region I	1-3/2	"
835M30	"	R.T.	Not specified	1/2	McIntyre et al. (63)
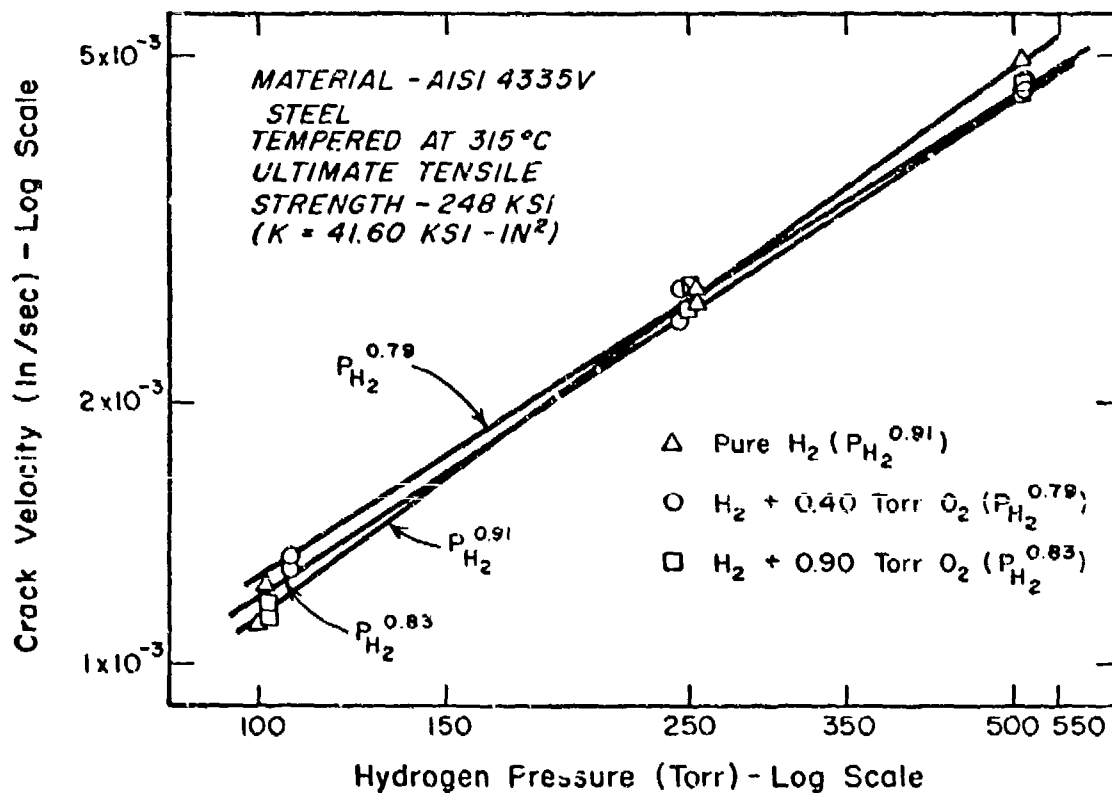
Fig. 68. Effect of Oxygen Additions on the Crack Velocity in Hydrogen Gas for AISI 4335V Steel Tempered at 315°C (From the work of Kerns (36)]

93

SLOW CRACK GROWTH IN OTHER GASEOUS ENVIRONMENTS

Crack growth has been observed in both Cl_2 and hydrogen halide gas environments, and at velocities more than two orders of magnitude greater than those observed in aqueous environments.

Kerns and Staehle[6] have observed crack velocities greater than 10^{-2} in./sec in HBr, HCl, and Cl_2 gaseous environments. However, tests in other gaseous media (NH_3, CH_4, and C_2H_2) revealed no evidence of significant slow crack growth. Studies in deuterium gas environments[36] have shown crack velocities 2.1 to 2.8 times lower than those observed in H_2 gas. The effects of such environmental species on crack velocity are shown in Fig. 69.

The crack growth observed in Cl_2 gas could not be attributed to impurity species. Table IX gives the expected crack velocities for various impurity species in the Cl_2 gas (99.97% pure), as well as the observed crack velocity in Cl_2 gas.

The reactivity of hydrogen halide gases was considered from the standpoint of a H_2 gas product, giving a hydrogen-induced cracking process. For the cracking found in gaseous H_2S, HCl, HBr, and H_2O environments, the reactions of the gas species with iron were considered to be:

$$2HCl_{(g)} + Fe_{(s)} \rightarrow FeCl_{2(s)} + H_{2(g)} ,$$

$$2HBr_{(g)} + Fe_{(s)} \rightarrow FeBr_{2(s)} + H_{2(g)} ,$$

$$H_2S_{(g)} + Fe_{(s)} \rightarrow FeS_{(s)} + H_{2(g)} , \text{ and}$$

$$4H_2O_{(\ell)} + 3Fe_{(s)} \rightarrow Fe_3O_{4(s)} + 4H_{2(g)} .$$
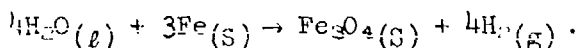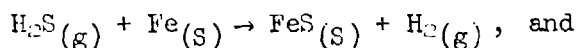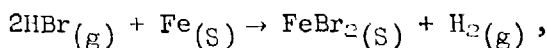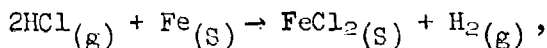
With the use of published thermodynamic data,[68-70] the equilibrium H_2 pressures were calculated, for a reacting gas pressure of 1/10 atm. The thermodynamic calculations for the water vapor environment were based on the liquid water species. The equilibrium H_2 pressures were then compared to observed crack velocities in each environment. For water vapor, the crack velocity in 3.5% NaCl solution (Fig. 55) was used. The velocity for an H_2S environment was obtained by extrapolation of the crack velocity -H_2S pressure dependence relationship for Region II (Fig. 67). The resulting hydrogen pressure and crack velocity data
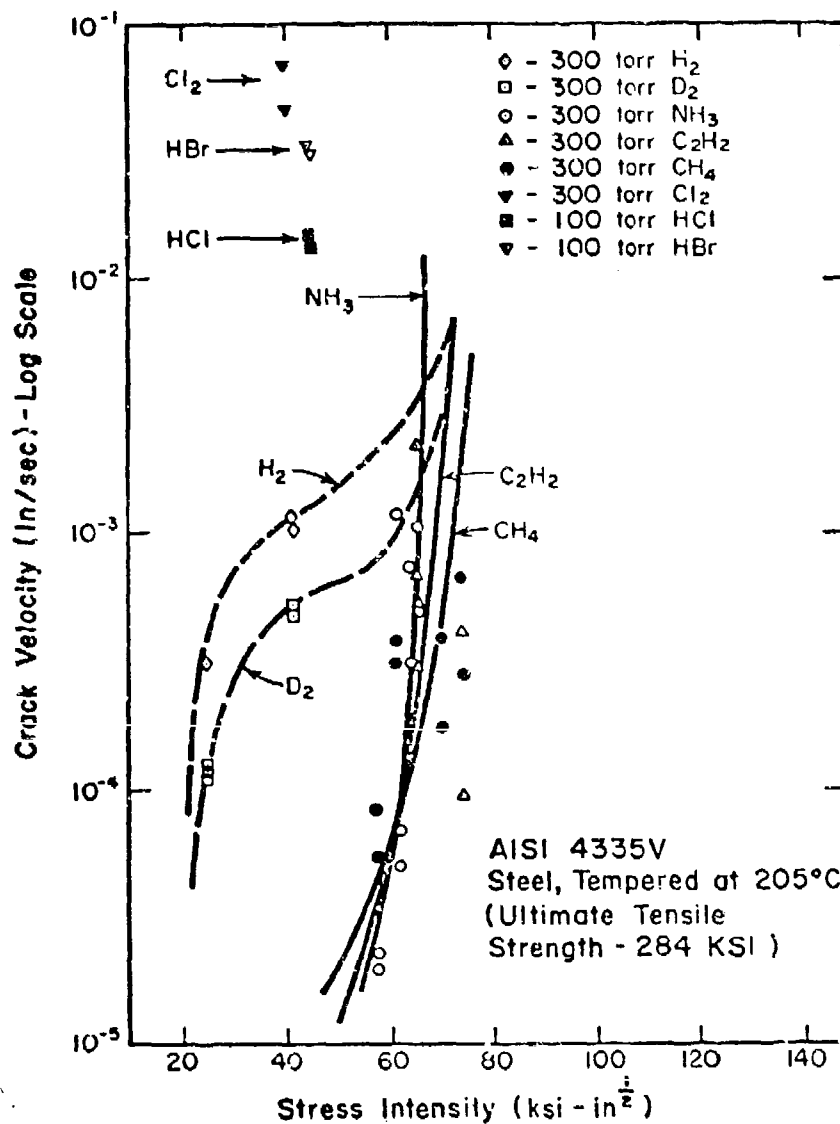
Fig. 69. Effect of Stress Intensity on Crack Velocity for
AISI 4335V Steel in Several Gaseous Environments
[From the work of Kerns and Staehle (67)]

95

Table IX - Crack Velocity Estimates Due to Residual
Contaminant Gases in Chlorine Gas Environment
[From the work of Kerns and Staehle (67)]

Impurity Vapor Species	Crack Velocity[a] (in./sec)
Water (liquid)	7×10^{-5}
Water (vapor at 9×10^{-2} torr pressure)	3×10^{-7}
Hydrogen (at 9×10^{-2} torr)	3×10^{-7}
Hydrogen chloride (at 9×10^{-2} torr)	1×10^{-5}
Dry chlorine (at 300 torr)	1×10^{-2}

[a]All at $K_1 = 45.8/47.8$ ksi-in.$^{1/2}$ stress intensity. Crack
velocity assumed to be linear function of gas pressure for
H_2 and HCl

[b]Crack velocity assumed to be linear function of water vapor
pressure, with equilibrium vapor pressure being 24 torr at
25°C; velocity in sodium chloride solution (pH = 6.0) is
taken as crack velocity in pure liquid water

are shown in Fig. 70. An apparent trend exists for H_2, HCl, and HBr
species, with H_2O and H_2S showing opposite deviations from such behavior.
In addition, the experimental H-dependence of crack velocity is shown
in Fig. 70 to be clearly different than that based on thermodynamic
calculations for H-containing gases.

The significant observations regarding slow crack growth in gaseous
environments are that (1) cracking is found to occur at very low pres-
sure (H_2S environment), and (2) hydrogen does not appear to be a
required species for slow crack growth (Cl_2 environment).

Studies by Williams et al.[71] have shown that the dissociation of
hydrogen gas greatly increases the crack growth kinetics in high-
strength steel exposed to the environment. Crack velocities were
measured for SAE 4130 steel (ultimate tensile strength - 220 ksi) in
a partially dissociated hydrogen gas environment. Using a heated
tungsten filament (2000°C), the authors produced partially dissociated
hydrogen (<1%) from molecular hydrogen gas at 8×10^{-3} torr pressure.
Crack velocities (at $K_I = 41$ ksi - in$^{1/2}$) were found to be approximately
three orders of magnitude greater than those predicted from prior
studies.[42]

TEMPERATURE DEPENDENCE OF SLOW CRACK GROWTH IN
HIGH-STRENGTH STEELS

The temperature dependence of crack velocity, for high-strength
steels in aqueous solutions, has resulted in activation energy values
comparable to that for hydrogen diffusion in steel. The temperature
dependencies observed for slow crack growth in gaseous environments
show clearly different behavior.
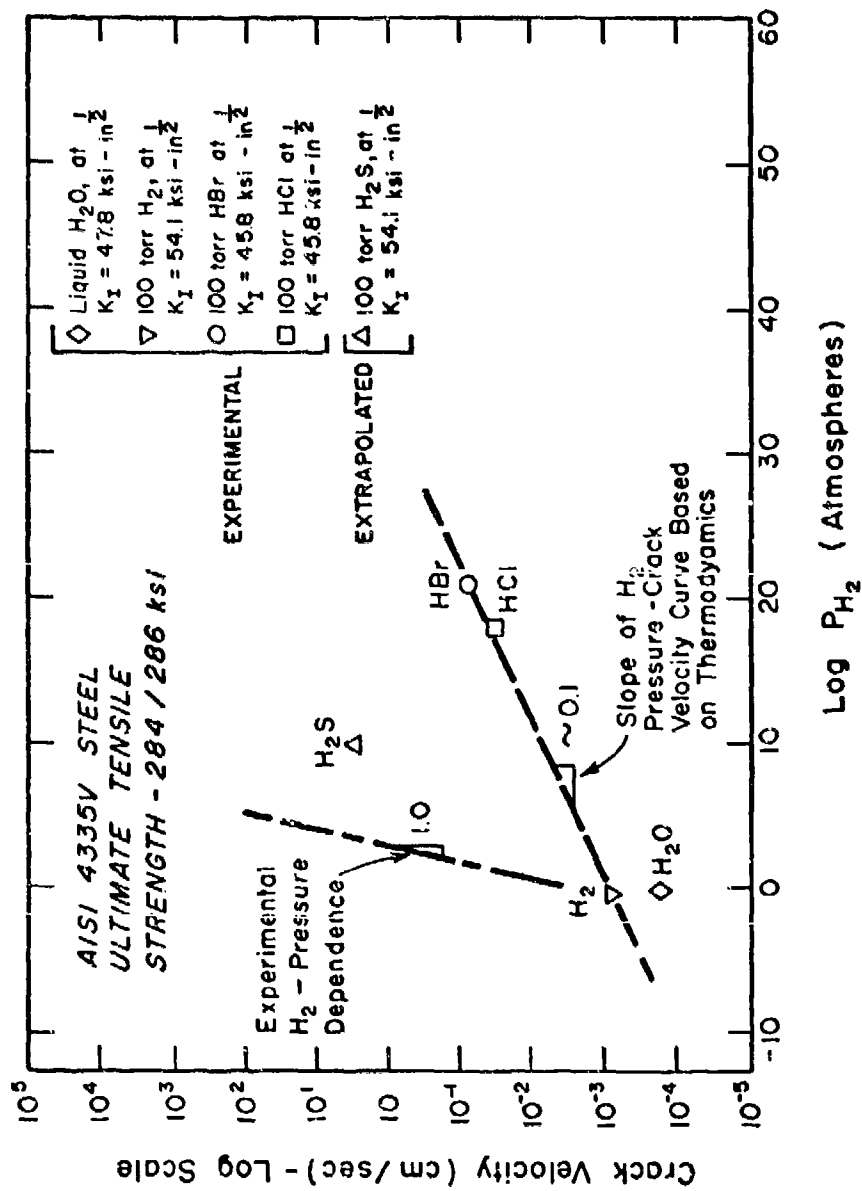
Fig. 70. Correlation of Observed Crack Velocities with Equilibrium Hydrogen Pressure for Slow Crack Growth of 4335V Steel in H-Containing Gaseous Environments [From the work of Kerns and Staehle (67)]

97

Johnson and Willner[75] have measured the temperature dependence of crack velocity for H-11 steel in water and moist argon environments. The data, shown in Fig. 57, give an activation energy for crack growth of approximately +9 kcal/mole. Van der Sluys[20] reported an activation energy of +8.1 to +8.7 kcal/g-mole, as shown in Fig. 71. Both results[20,65] show activation energies which closely agree with that observed by Beck et al.[72] for hydrogen diffusion through an AISI 4340 steel membrane (tensile strength - 260 ksi). The measured value was 9.2 kcal/mole.

The H_2 gas environment studies by Williams and Nelson[12] and Sawicki[13] both show a maximum in the temperature dependence of crack velocity. These results are shown in Figs. 72 and 73. The activation energies observed by McIntyre et al.[73] for crack growth in salt water, H_2 gas, and H_2S gas environments are shown in Fig. 74. No velocity maximum was observed for the temperature dependence in H_2 gas.[73] The temperature dependence data are summarized in Table X. The temperature dependencies show considerable disagreement for slow crack growth in hydrogen gas environments.

FRACTOGRAPHY AND CRACK BRANCHING AQUEOUS AND GASEOUS ENVIRONMENTS

The fracture mode for high-strength steels has been found to be predominantly intergranular in either aqueous or gaseous environments. The fractography is, however, a strong function of both the environmental species and the applied stress intensity.

Using high-strength AISI 4330M and AISI 4340 steels, Davis[22] showed that cracking of un-notched bent beam specimens occurs along prior austenitic grain boundaries for an aqueous 3.5% NaCl environment. Cathodic or anodic polarization showed no effect on fractography. Cathodic charging in 0.25N sodium sulfide solution greatly decreased the failure time, with no observable change in fractography. Fracture along prior austenite grain boundaries was also reported by Van der Sluys[20] for a distilled water environment.

Beachem[74] has shown that the fractography of quenched and tempered 4300 - type steels, fractured in an aqueous environment, is a strong function of applied stress intensity. Using wedge opening loaded (WOL) specimens, the author found that intergranular fracture occurs in high-strength steel (195 ksi yield strength) at low stress intensity values in 3.5% NaCl solution. For the same steel, ductile fracture (preceded by a mixed mode fracture) was observed with increasing values of applied stress intensity. At low K_I values, lower strength steel (172 ksi yield strength) exhibited a quasi-cleavage fracture. Upon galvanic coupling to a magnesium anode, the 172 ksi steel also exhibited intergranular fracture at low K_I values. The fractography transitions in the higher strength steel (195 ksi) were not affected by galvanic coupling. In the same study, 400°F tempered AISI 4340 steel was found to exhibit intergranular failure in a H_2 gas environment. Micro-void

98
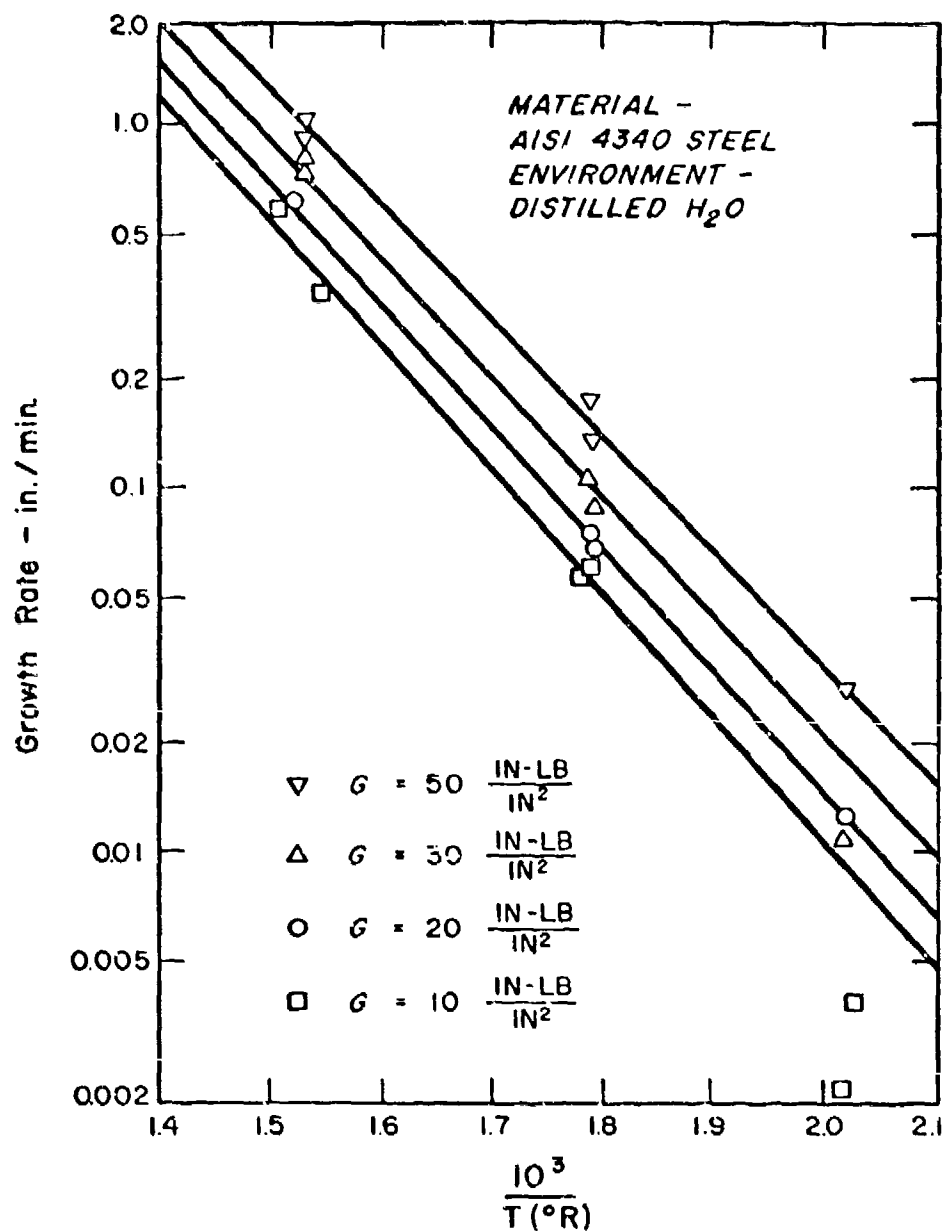
Fig. 71. Effects of Temperature and Crack Extension Force (G) on Crack Growth Rate [From the work of Van der Sluys (26)]

99
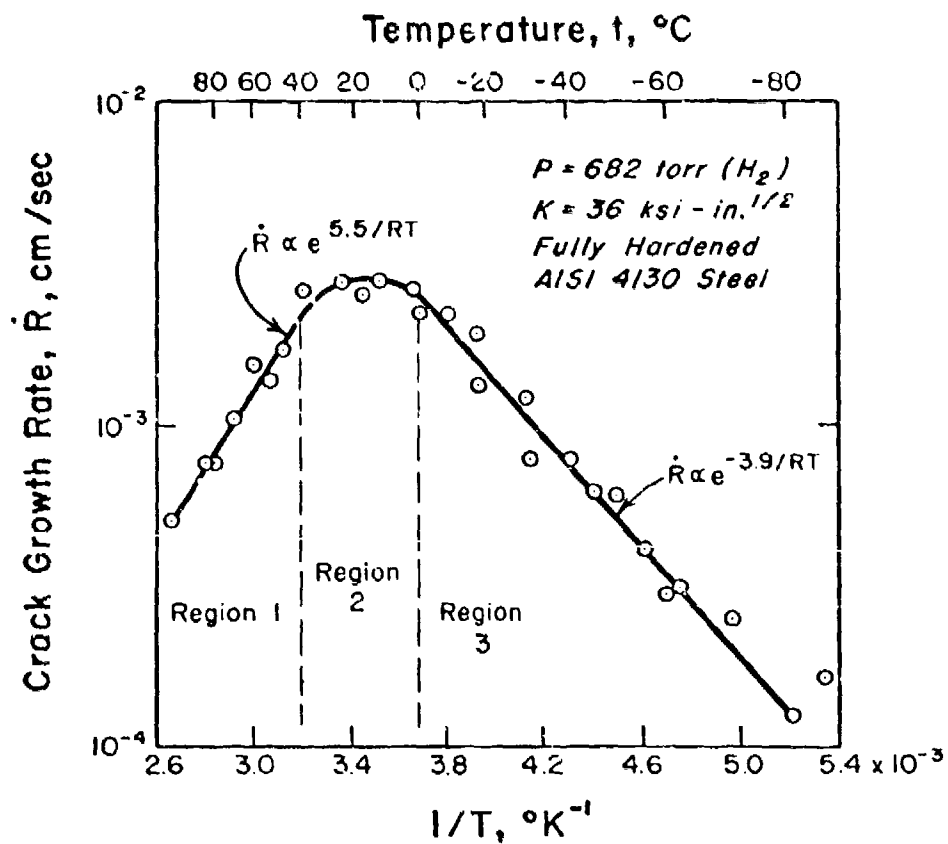
Fig. 72. Effect of Temperature on Crack Velocity for 4130 Steel in 682 Torr H_2 Gas [From the work of Williams and Nelson (42)]
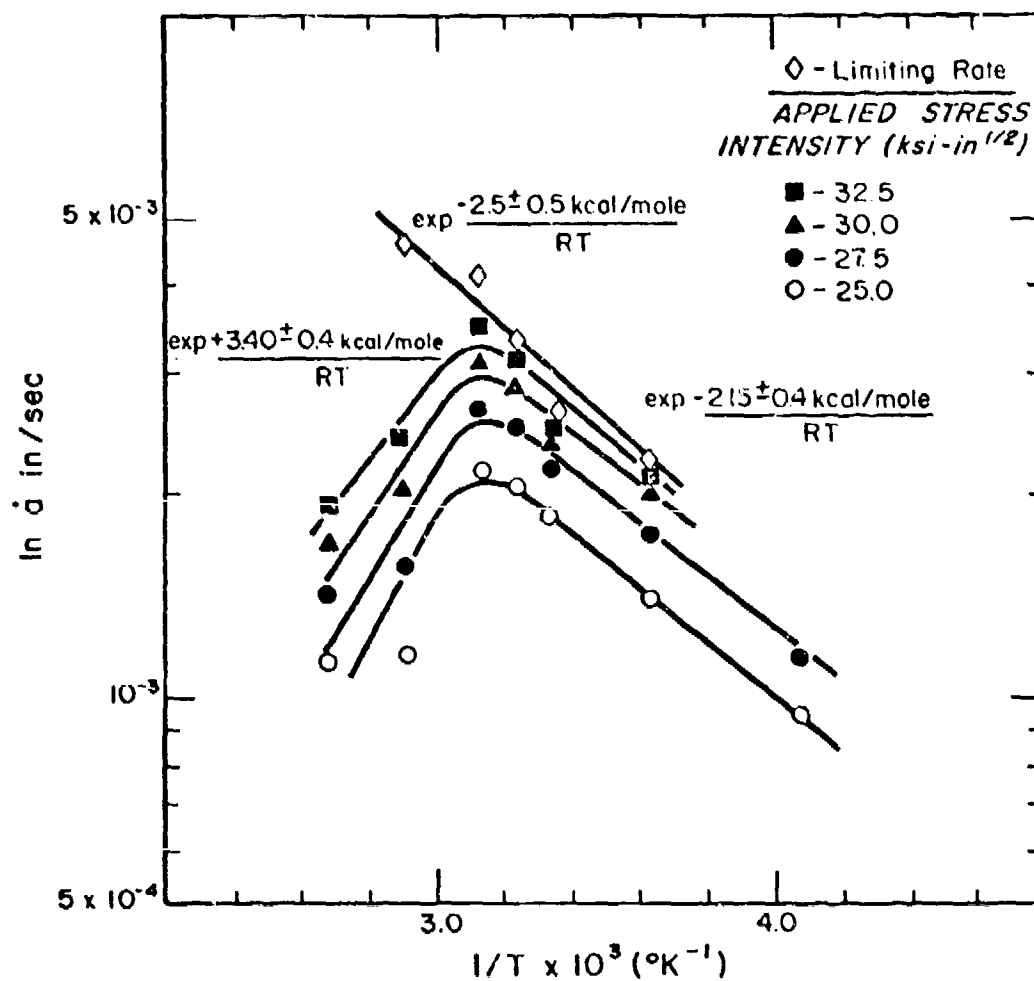
Fig. 73. Effect of Temperature on Crack Velocity for H-11 Steel in Dry H_2 Gas [From the work of Sawicki (43)]
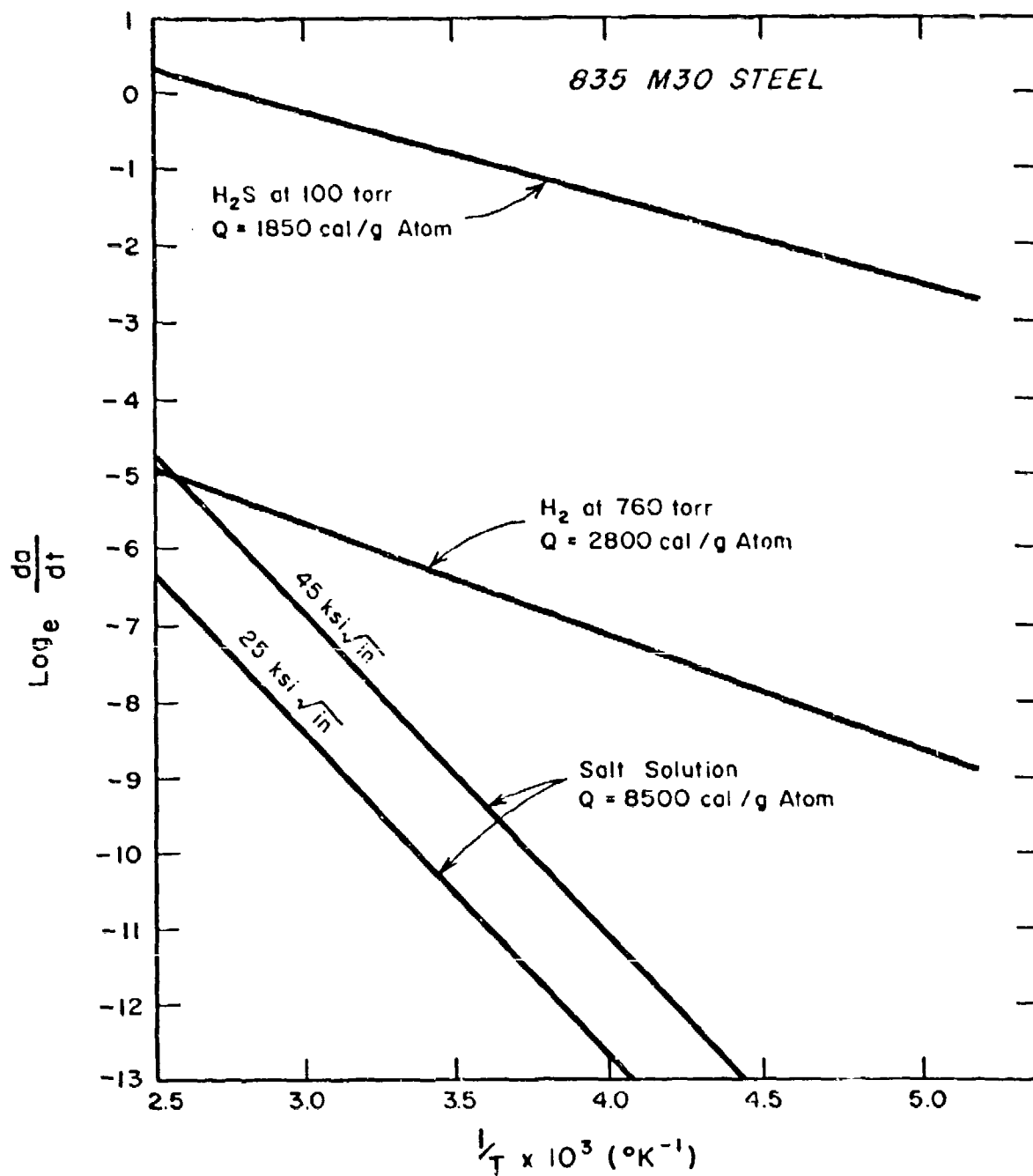
Fig. 74. Temperature Dependence of Crack Velocity for 835M30 Steel in Salt Water, H_2 Gas, and H_2S Gas Environments [From the work of McIntyre et al. (73)]

Table X - Activation Energies for Slow Crack Growth in Aqueous and Gaseous Environments

Steel	Environment	Temperature Range (°C)	Activation Energy (kcal/mole)	Reference
H-11	Distilled Water	+5 to +85	+9	Johnson and Willner (65)
4340	Distilled Water	+4 to +100	+8.1 to +8.7	Van der Sluys (26)
835M30	Salt Water	Not given	+8.5	McIntyre et al. (73)
4130 "	H_2 gas "	0 to -30 40 to 100	+3.9 -5.5	Williams and Nelson (42) "
H-11	H_2 gas	40 to -29 40 to 97	+2.2 ± 0.4 -3.4 ± 0.4	Sawicki (43)
835M30	H_2 gas	Not given	+2.8	McIntyre et al. (73)
835M30	H_2S gas	Not given	+1.9	McIntyre et al. (73)
4130	H_2 + H gas	-20 to +35	+6.8	Williams et al (71)

coalescence was the reported fracture mode for 1100°F tempered 4340 steel in a H_2 gas environment. Steel tempered at 600°F or 800°F exhibited a mixed fracture mode (intergranular, quasi-cleavage, and micro-void coalescence) in dry H_2 gas environments.

Changes in fracture mode with applied stress intensity have been observed by Wang and Staehle.[37] Martensite AISI 4340 steel exhibited intergranular fracture at low stress intensities in a 3.5% NaCl solution. An increase in stress intensity was found to increase the amount of dimpled rupture observed on the fracture surface. The increase of stress intensity for bainitic 4340 steel was found to produce a fracture mode transition from intergranular to transgranular.

Intergranular failure has been observed for Type 410 and Type 422 stainless steels in 5% salt spray environments.[19]

Crack branching is commonly observed in Region II for slow crack growth in aqueous environments. Speidel[50] has observed the branching phenomenon, as shown in Fig. 48. Crack microbranching, with crack branch separation distances on the order of one grain diameter, was observed at stress intensities of 1.4 K_{Iscc} or greater. Macro-branching was observed at stress intensities 1.4 times the minimum K value in Region II. Carter[5] has found crack branching in high-strength steels to occur at $K_{Br} = n K_{Iscc}$ where n varies from 2 to 4. The stress intensity values for branching in several high-strength steels are given in Table XI.

Fracture mode transitions have been observed in both H_2 and H_2S gas environments. Sawicki[43] has reported intergranular fracture for H-11 steel in dry H_2 gas at low K_I values. With increasing stress intensity values, the fractography exhibited increasing amounts of ductile tearing. Williams and Nelson[42] have reported intergranular fracture for 4130 steel in gaseous molecular H_2. The fractography in partially dissociated H_2 gas[1] showed either intergranular fracture or a mixed fracture mode (intergranular and ductile tearing). The fractography in both molecular and partially dissociated hydrogen gas environments was found to be a function of test temperature.[1] Ductile failure was observed above 120°C in molecular H_2 gas and below 0°C in partially dissociated H_2 gas.

Recent fractographic studies[96] have shown fracture mode transitions accompanying Region I - Region II behavior in H_2 gas environments. Region I fractures for 205°C or 315°C tempered AISI 4335V steel are characterized by primarily intergranular fracture. Mixed mode fractures, with dimpled rupture and secondary cracking, are observed in Region II. Figure 75 shows SEM fractographs (Regions I and II) for 205°C tempered 4335V steel. Fractographs for 315°C tempered steel are shown in Fig. 76. Mixed mode fractures were observed for 540°C tempered D6AC steel (Regions I and II), as shown in Fig. 77. Figure 78 shows the ductile failure observed with 595°C tempered D6AC steel.

Table XI - Conditions for Crack Branching in High Strength Steels
[From the work of Carter (75)]

Alloy	Heat Treatment	Yield Strength (ksi)	K_{Ic} (ksi√in.)	K_{Iscc} (ksi√in.)	K_{II} (ksi√in.)	K_{Ib} (ksi√in.)	K_{Ib}/K_{Iacc} (mean)	Crack Velocity Characteristics[a]
Conditions for Branching of Stress Corrosion Crack								
4340 (0.54% or 1.03% Si)	Q&T 750°/800°F	230	83	24	24.7 26.1 31.5	52.8 58.2 58.2 55.4 (mean)	2.4	Constant[a] (24)
9Ni-4Co-0.45C (martensitic)	Q&T 500°F	236	69	15	33.3 45.0 47.0 51.5	49.0 53.0 47.0 67.0 55.4 (mean)	3.5	Constant[b] (76)
350 grade maraging	Aged 8 hr at 900°F	335	36	10	12.5 15.3 20.5	25.6 22.7 31.2 26.6 (mean)	2.7	Constant[a] (77)
350 grade maraging	Aged 3 hr at 950°F	330	42	10	10.3 12.5 15.5 20.0	22.1 19.7 35.5 21.0 24.1 (mean)	2.4	Constant[a] (77)
Conditions for Branching at Tip of Fatigue Precrack								
300 grade maraging	Aged 6 hr at 900°F	289	89	12		45.0-50.8	3.8-4.2	Constant[a] (75)
9Ni-4Co-0.45C	475°F bainitic treatment	220	89	20		58.0-62.4	2.9-3.1	Constant[b] (76,78)
9Ni-4Co-0.30C	Q&T 950°F	200	116	35*		50.6-75.4	1.5-2.1	Constant[b] (76)
4330V	Q&T 500°F	196	103	25		43.9-49.9	1.8-2.0	Constant[a] (76)

[a] Determined by measurement
[b] Assumed from shape of K_{II} vs. time-to-failure curve
*Uncertain value
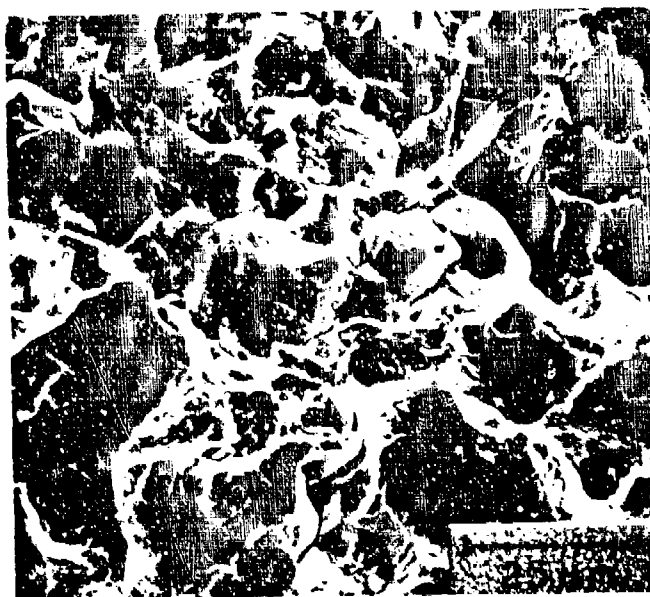
$K_I = 20.8$ ksi-in.$^{1/2}$ (Region I)
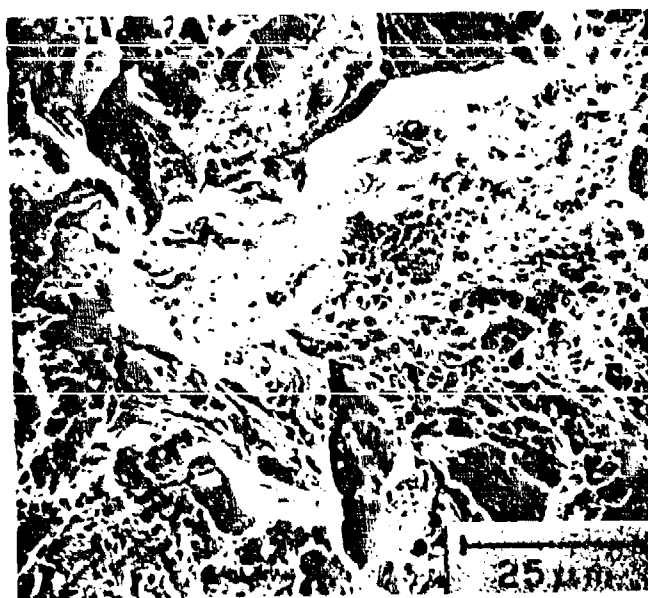
$K_I = 54.1$ ksi-in.$^{1/2}$ (Region II)

Fig. 75.   SEM Fractographs of AISI 4335V Steel (205°C temper) Tested in Dry H₂ Gas [From the work of Kerns (36)]
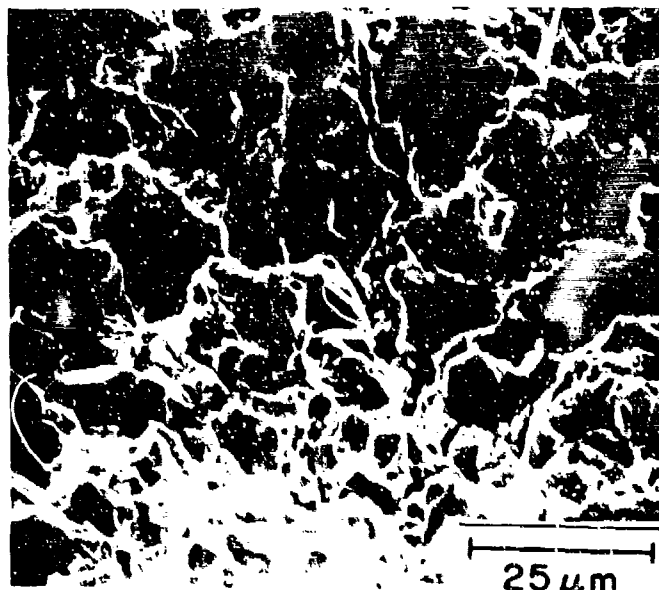
K_I - 20.8 ksi-in.$^{1/2}$ (Region I)
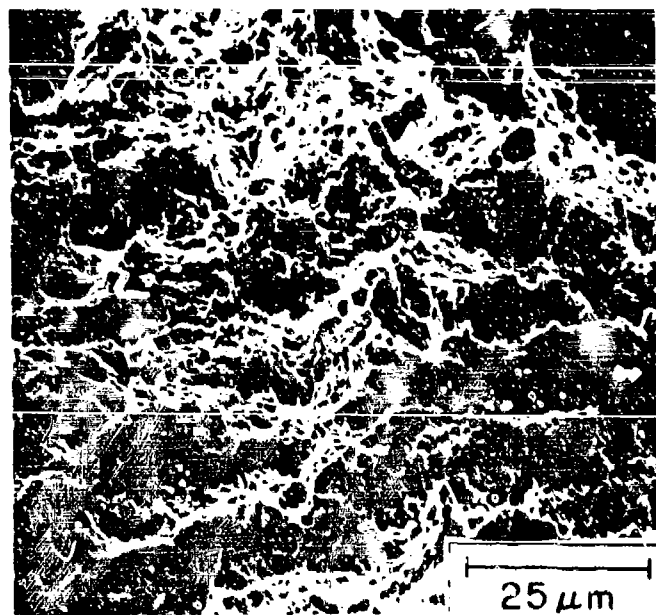
K_I - 54.1 ksi-in.$^{1/2}$ (Region II)

Fig. 76.   SEM Fractographs of AISI 4335V Steel (315°C temper)
Tested in Dry H_2 Gas [From the work of Kerns (36)]
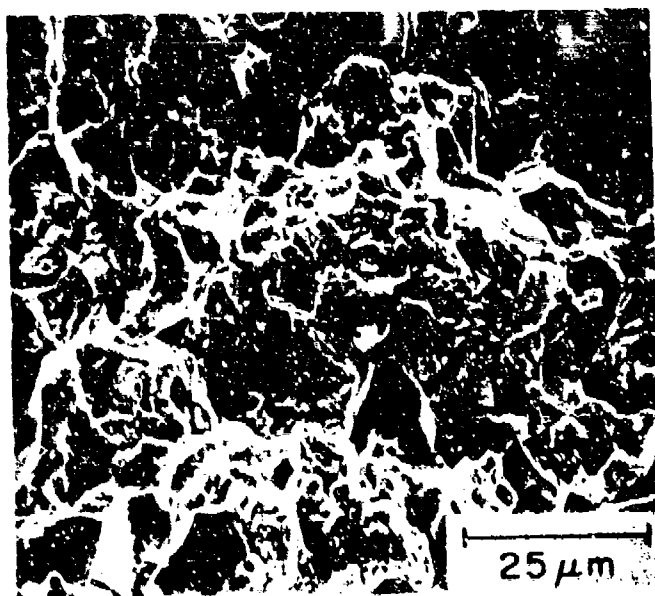
$K_I = 33.3$ ksi-in.$^{1/2}$ (Region I)
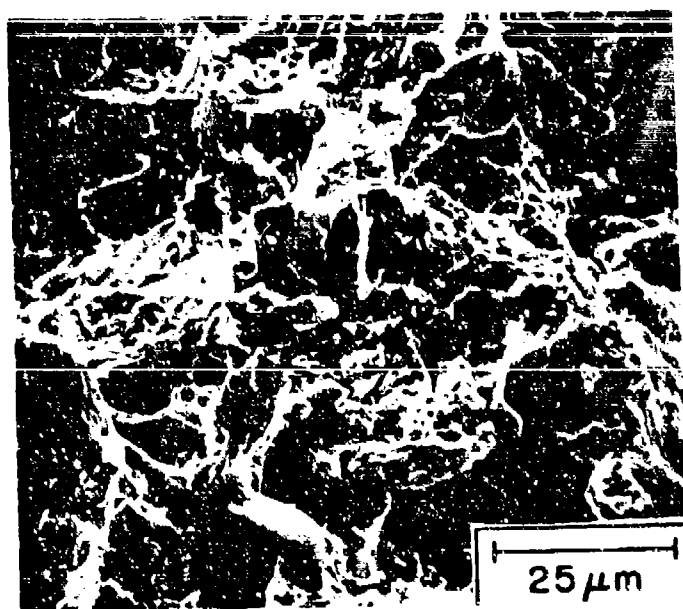
$K_I = 83.2$ ksi-in.$^{1/2}$ (Region II)

Fig. 77.   SEM Fractographs of D6AC Steel (540°C temper)
Tested in Dry H_2 Gas [From the work of Kerns (36)]
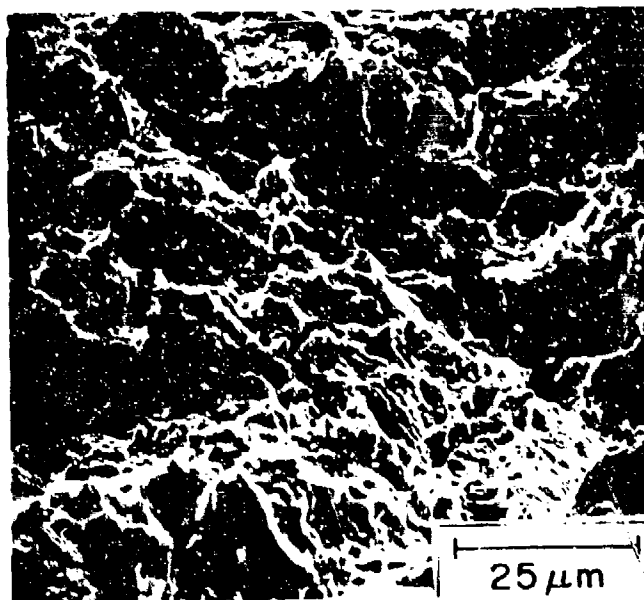
K_I = 121 ksi-in.$^{1/2}$
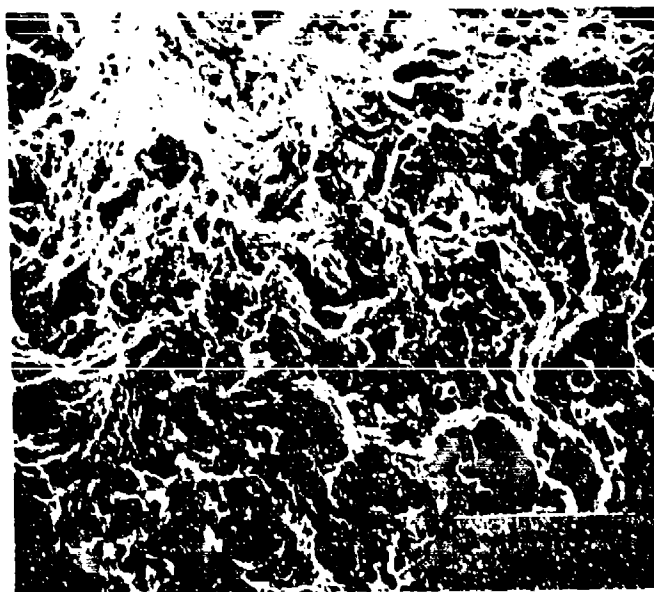
K_I = 133 ksi-in.$^{1/2}$

Fig. 78. SEM Fractographs of D6AC Steel (595°C temper) Tested in Dry H_2 Gas [From the work of Kerns (36)]

The fracture mode for 205°C tempered 4335V steel in H_2S gas was found to be intergranular in either Region I or Region II.[36] Figure 79 shows SEM fractographs for the H_2S environment. This is in contrast to the fracture behavior for the same steel in a H_2 gas environment (Fig. 75).

MECHANISM OF HYDROGEN EMBRITTLEMENT

In order to examine the stress-corrosion cracking of steels, it is necessary to review the possible mechanisms whereby hydrogen, as the critical species, assists in the fracture process. There are three outstanding theories; i.e.,

      (1)   pressure theory of Zapffe and Sims,
      (2)   adsorption theory of Petch and Stables, and
      (3)   lattice bond theory of Troiano.

Zapffe and Sims[79] have proposed that hydrogen embrittlement results from the precipitation of molecular hydrogen at structural defects in the steel. The resulting gas pressure exceeds the "elastic strength" of the steel. More recently, Tetelman[80] has proposed that pressures of molecular hydrogen, precipitated at defects (voids or micro-cracks) ahead of an advancing crack, will produce internal stresses in the steel. Such stresses reduce the required external stress for crack propagation.

The Troiano model[2] proposes that electrons donated from interstitial hydrogen atoms enter the d-band of transition metals. The increased electron density increases the inter-atomic spacing of the lattice, thereby reducing the cohesive strength of the metal.

The adsorption theory of Petch and Stables[81,82] proposes that the surface energy requirement for crack extension, in the Griffith criterion, is lowered by the adsorption of hydrogen gas at the crack tip.

The hydrogen embrittlement theories are seen to result from two approaches. The Zapffe and Sims[79] and Tetelman[80] concepts propose additional internal stresses which reduce the required external stress for fracture. The Petch and Stables concept[82] and the Troiano model[2] propose that the cohesive strength of the lattice is reduced, again giving a lower required stress for fracture.

It is equally significant to realize the shortcomings of the proposed hydrogen embrittlement models.

Crack propagation has been observed in high-strength steels exposed to molecular hydrogen gas at pressures down to 10 torr (Fig. 62). In such cases, no equilibrium hydrogen activity gradient exists (between the gas phase and the metal lattice) such that internal hydrogen pressures, sufficient for lattice bond de-cohesion, can eixst within the steel. Therefore, the validity of the pressure theory[79,80] is questioned.
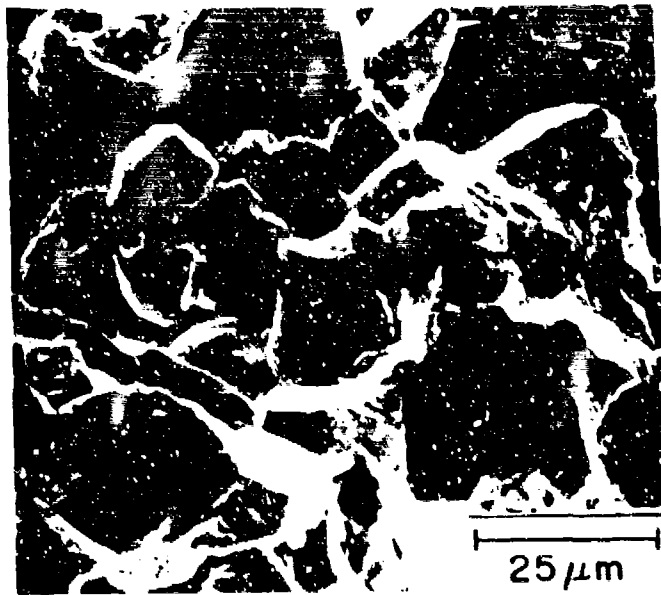
$K_I = 20.8$ ksi-in.$^{\frac{1}{2}}$ (Region I)

$K_I = 54.1$ ksi-in.$^{\frac{1}{2}}$ (Region II)

Fig. 79. SEM Fractographs of AISI 4335V Steel (205°C temper) Tested in H$_2$ Gas [From the work of Kerns (36)]

The Petch theory[81] is questioned from the standpoint of the fracture strength of real materials, as well as its inconsistency with observed cracking behavior in gaseous environments. Tetelman and McEvily[83] have stated that for materials having yield strength values less than the theoretical cohesive strength of the lattice, the effect of surface energy on the total energy required for fracture is negligible. Secondly, the lowering of surface energy (of the metal) by gas adsorption implies, via the Gibbs and Langmuir isotherms,[81] that a higher heat of adsorption for the gas species will result in a greater reduction of metal surface energy. This is predicted by Petch.[81] However, oxygen is known to adsorb on iron more strongly than hydrogen[84] and yet halts cracking in gaseous environments.[25,36,43,63] Therefore, the Petch and Stables theory does not fully explain the cracking behavior in steels.

There have been no observed effects of hydrogen, at levels less than 10 ppm, on the lattice bond energy of iron. Therefore, the Troiano model[2] has yet to be substantiated by experiment.

MODELS FOR SLOW CRACK GROWTH IN
HYDROGEN-CONTAINING ENVIRONMENTS

Several models have been proposed to describe the slow crack growth process for high-strength steels in either gaseous or aqueous environments.

Troiano and Fidelle[54] have related stress corrosion in high-strength steels to the stress-induced diffusion of hydrogen to the elastic-plastic interface below the crack tip. The accumulation of sufficient hydrogen at the interface (region of high triaxial stress) results in crack initiation, and an incremental advance of the main crack front. Such a model is consistent with the acoustic emission phenomena observed during discontinuous slow crack growth in high-strength steels.[85-88] It is also in agreement with the predicted effect of stress on the activity of hydrogen in steel.[53] The effect of strength level on cracking susceptibility is explained by the magnitude of elastic tensile stresses attainable at the plastic zone boundary, and their effect on the equilibrium hydrogen concentration at the elastic-plastic interface. The model does not, however, explain the effect of environment on the activity of hydrogen at the steel surface.

Beachem[74] has proposed that the fracture modes observed in aqueous media are primarily a function of the microstructure, with hydrogen assisting the fracture process. At low stress intensity values, intergranular fracture is felt to be the energetically favorable fracture process. Higher mechanical energy inputs (larger K values) favor the quasi-cleavage fracture mode. Sufficiently large plastic zone sizes (larger K values) may contain inclusions which then act as nucleation sites for fracture by micro-void coalescence. The significant feature of the Beachem model is that the hydrogen species can assist ductile failure by "unlocking dislocations," permitting plastic flow to occur

at reduced external stresses. Such "hydrogen-assisted" cracking is not in agreement with fractographic features observed in gaseous H_2S environments. The H_2S species has been shown to (1) rapidly dissociate on an iron surface,[10] and (2) accelerate the entry of hydrogen into iron.[11,12] In view of such behavior, and the high crack velocities for high-strength steels in H_2S environments, the Beachem model would suggest a more ductile fracture in H_2S environments (as compared to aqueous solutions or H_2 gas). Figures 75 and 79 clearly show that for the same applied stress intensity failures in H_2S gas environments are less ductile than those in H_2 gas.

Crack growth in molecular H_2 gas has been described by the chemisorption model of Williams and Nelson.[42] The rate-controlling process for slow crack growth was described as the activated adsorption of hydrogen adatoms on the surface of the steel. Porter and Tompkins[13] have previously described such hydrogen chemisorption by the activated surface migration of hydrogen atoms from "initial adsorption sites" to "final adsorption sites." Using the Porter and Tomkins rate equation, Williams and Nelson[42] have explained the isobaric temperature dependence of crack growth in dry H_2 gas (Fig. 72), and the pressure dependencies of crack velocity (Fig. 59). The cracking mechanism was attributed to a lowering of surface energy by the model of Petch and Stables.[81,82]

Oriani[14] has reviewed the Williams and Nelson mode, arriving at clearly different pressure dependence predictions for the rate of adsorption (hence, crack velocity). Additional examination of the chemisorption model by Johnson and Sawicki[15] has shown that the Porter and Tompkins chemisorption rate equation was applied[42] at much higher temperatures and pressures than those of its original derivation.

The fractional surface coverage by physically adsorbed molecular hydrogen has been described by the Langmuir isotherm, and included as an "effective area" term in H_2 permeation rate expressions[93] and in the chemisorption rate equation of Williams and Nelson.[42] Johnson and Sawicki[15] have shown that the use of such "effective area" expressions is inconsistent with thermodynamics.

The rate of gas impingement is not a reasonable explanation, since the H_2S pressures required for slow crack growth in high-strength steel are approximately three orders of magnitude lower than the H_2 pressures required for the same crack velocity (Figs. 61 and 67). The substantial effect of hydrogen dissociation, however, is observed in both Regions I and II. Williams et al.[71] have shown that partial dissociation of hydrogen accelerates cracking by several orders of magnitude at a stress intensity of 41 ksi - in.$^{1/2}$ (approximately 2/3 of K_{Ic} for the steel). On the basis of other data (Fig. 20), this stress intensity value appears to be in Region II. Other studies[36] have shown that the addition of H_2S (2 vol%) to hydrogen gas increases the Region I crack velocity by two orders of magnitude. Crack velocity data are given in Table XII, and may be compared to the expected H_2 gas environment

Table YII - Crack Velocities Observed in 0.42 Torr Hydrogen Sulfide Gas, Before and After Dilution with Pure Dry Hydrogen[a]

Initial Velocity (in./sec) in 0.42 Torr H_2S	Volume % H_2S after Dilution	Crack Velocity after Dilution	Final Velocity, Time to Reach Steady State
2.02×10^{-3}	4.4 (10 torr H_2)	6.8×10^{-4}	1.90×10^{-3} } 24 sec.
2.10×10^{-3}	4.4	6.8×10^{-4}	2.02×10^{-3}
2.20×10^{-3}	2.1 (20 torr H_2)	4.4×10^{-4}	1.80×10^{-3} } 86 sec.
2.22×10^{-3}	2.1	4.4×10^{-4}	2.00×10^{-3}

[a]Data obtained usir· AISI 4335V steel - (tempering temp., 315°C) at K_I = 25.0 ksi-in.$^{1/2}$

114

velocity from Figs. 20 and 62 for 20 torr H_2 gas and $K_I = 25$ ksi - in.$^{1/2}$. Thus, the addition of H_2S gas, with the established effect on hydrogen recombination kinetics,[91] greatly accelerates cracking in Region I.

It is then concluded that several inadequacies exist in the models for crack growth in dry H_2 gas environments. The isothermal variation of crack velocity pressure dependence with applied stress intensity has not been explained by either the Williams and Nelson[42] or Sawicki[43] models. The effect of secondary cracking, or bifurcation, has not been considered as affecting the stress intensity and crack growth behavior in Region II.

ROLE OF CATALYTIC POISONS IN ACCELERATING STRESS CORROSION CRACKING

The specific role of cathodic poisons in hydrogen permeation from aqueous media has been investigated by Smialowski[97] using an iron base 5% Ni alloy and rotating disc electrode techniques. Additions of cathodic poisons were found to enhance hydrogen permeation through the Fe-Ni alloy from a 0.1N Na_2SO_4 solution acidified to pH 2.6 with H_2SO_4. Above a limiting cathodic current density of 12 mA/cm^2, the poisoning effect of SeO_2 and thiourea additions strongly decreased; this is shown in Fig. 80. It is proposed[97] that hydrogen entry is promoted by hydride species (AsH_3, SbH_3, H_2S, H_2Se). The hydrides absorb on the metal surface, giving a detached hydrogen atom;

$$2M + AsH_3 \rightarrow M\ AsH_2 + MH .$$
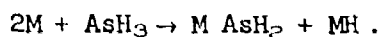
Such adsorption is believed to alter the surface structure of the metal, thus promoting hydrogen entry. Above a limiting cathodic current density, however, the solution becomes depleted in hydronium ions (hence, alkaline). Since H_2S and H_2Se are unstable in alkaline solutions, the poisoning effect ceases. The predicted stability for H_2S agrees with the minimal effect of H_2S additions on cracking in aqueous media for low pH values (Fig. 40).

A similar dissociative adsorption of H_2S gas has been found to occur on iron.[90] The effect of H_2S in promoting hydrogen entry from the gas phase has also been established[92] and agrees with the cracking behavior of high-strength steels in gaseous environments. However, the specific role of the hydride species in assisting hydrogen entry is not clear at this time.

INTERACTION OF HYDROGEN WITH THE MICROSTRUCTURE OF STEELS

The understanding of both hydrogen embrittlement and stress-corrosion cracking is hindered by a lack of knowledge as to the location of damaging hydrogen within the metallurgical structure. It has been
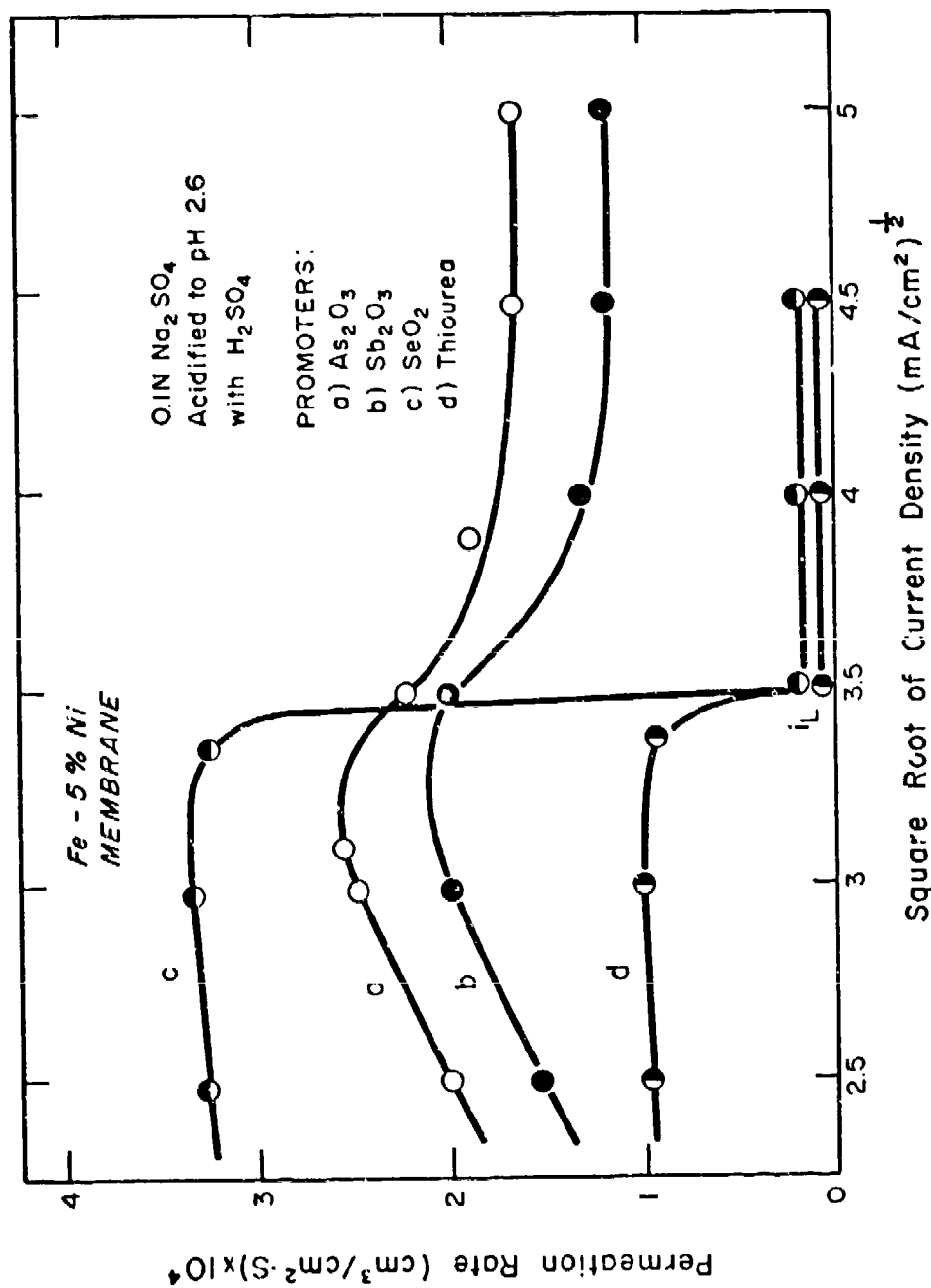
Fig. 80. Effect of Current Density on Hydrogen Permeation Rate in the Presence of Promoters [From the work of Smialowski (97)]

116

proposed that hydrogen traps exist within the structure of iron (or steel) thus explaining diffusion anomalies at low temperatures ($< 200°C$). However, the damaging hydrogen is clearly mobile and thus trapping does not offer a complete explanation for embrittlement.

The "trapping" concept was first introduced by Darken and Smith[98] and has since been applied in explaining the anomalously low diffusion coefficients for hydrogen at ambient temperatures in iron or steel.[99-102] Hill and Johnson[13] have shown that the activation energy for hydrogen diffusion in α-iron is +3.0 kcal/g-atom above 200°C. Below 200°C, however, the activation energy is +7.8 kcal/g-atom. The difference is attributed to trapping of hydrogen, with trapping energy for hydrogen of 4.8 kcal/g-atom. The nature of the traps was not specified.

Oriani[100] has related the trap density in steel to the non-ideal hydrogen diffusion coefficient observed at ambient temperatures. Trap density values were estimated to be on the order of $10^{19} cm^{-3}$ for a variety of steels. Solid-solid interfaces were proposed as trapping sites in non-cold worked steels, with micro-crack surfaces being more probably trapping sites than dislocations in cold-worked steel. Interaction energy estimates for trapped hydrogen were based on the results of other investigators, and ranged from 4.7 to 8.7 kcal/mole H.

Kim and Loginow[101] have related "trapping" effects to susceptibility to delayed failure. Using a martensitic 3.Ni-1.5Cr-0.5Mo-0.13C steel, the investigators varied the 0.2% yield strength level from 95 to 150 ksi. The amount of hydrogen absorption was determined, as a function of strength level, by immersion of 0.75" cube specimens in a 3% NaCl+ 0.5% acetic acid solution, saturated with H_2S. The saturation value for hydrogen adsorption was found to increase with strength level. Hydrogen diffusivity was measured using electrolytic permeation techniques and found to be inversely related to strength level. Lower apparent diffusivities of hydrogen were observed for higher strength steel and attributed to trapping of hydrogen. The delayed failure of unnotched tensile specimens in the same charging solution showed a decrease in failure time with increasing strength level. Estimates of lattice-dissolved hydrogen were found to be independent of strength level. Consequently, the delayed failure kinetics were attributed to trapped hydrogen in the steel. Interface boundaries, structure defects, impurity atoms, or internal free surfaces were suggested as possible trapping sites.

Kortovich and Steigerwald[103] have investigated hydrogen diffusivities and crack velocities for four martensitic high-strength steels. Pre-cracked specimens of 4340, H-11, D6AC, and 9-4-45 steels were tested in a distilled water environment. The average crack velocities were compared to measured hydrogen diffusivities in the steels. The resulting relationship, shown in Fig. 81, suggests that lower hydrogen diffusivities result in lower crack velocities. Thus, hydrogen trapping does not appear to explain crack growth kinetics.

117
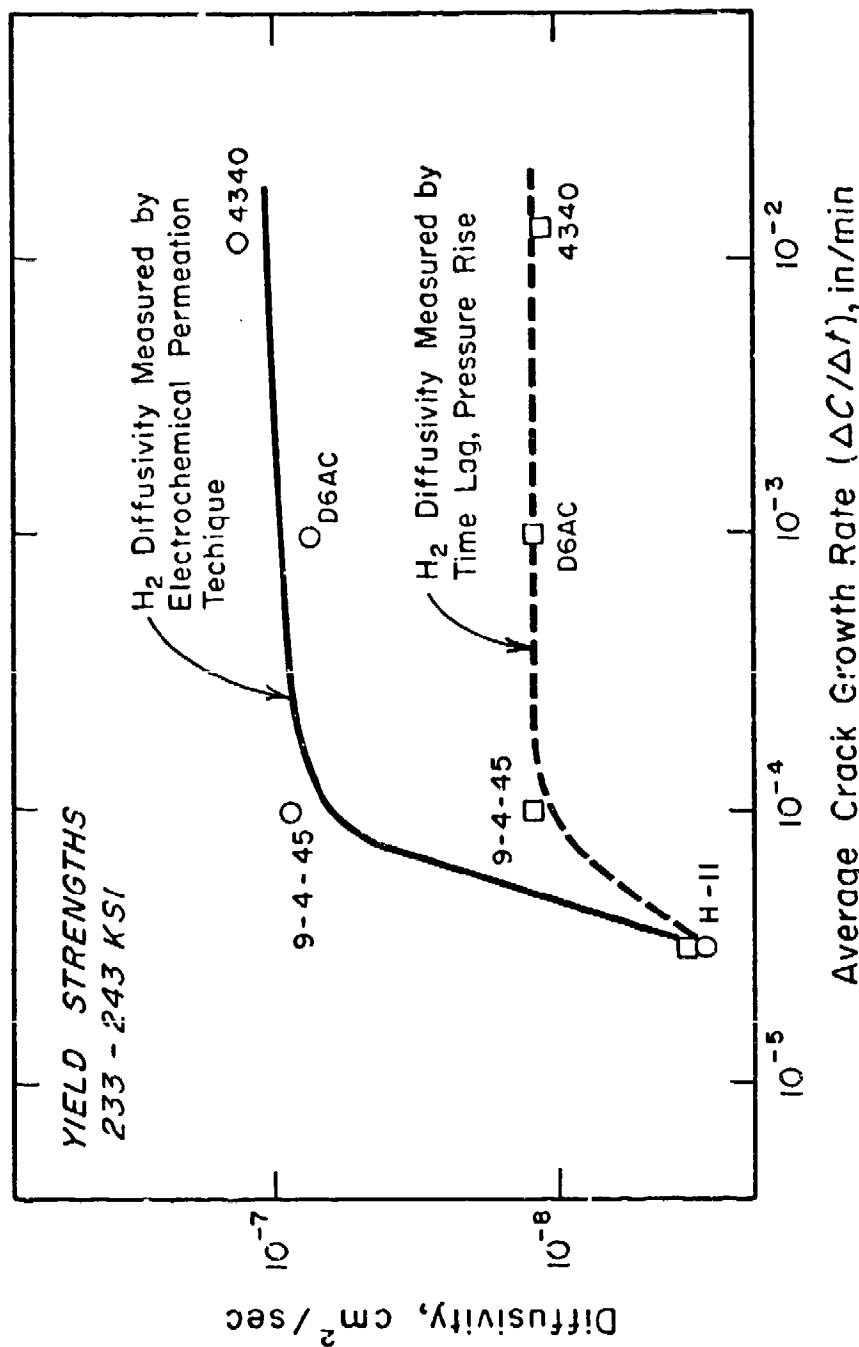
Fig. 81. Effect of Hydrogen Diffusivity on Crack Growth Rate [From the work of Kortovich and Steigerwald (103)]

118

Kikuta et al.[104] have shown that hydrogen-dislocation interaction may be related to the embrittlement phenomena. Notch tensile specimens of pure iron and HT80 steel were thermally charged with hydrogen and cold-rolled 10%. Internal friction measurements were then made. The notch tensile strength of each material was found to vary inversely with the height of the hydrogen-cold work peak, suggesting a significant hydrogen concentration in the stress field of a dislocation. The effect for pure iron is shown in Fig. 82. A hydrogen-dislocation interaction has also been suggested by Bastein et al.[105] and by Sturges et al.[106]

The application of an elastic tensile stress has been shown by Beck et al.[89] to enhance hydrogen permeation through steel. The observed effect has been attributed to a lowering of the chemical potential of hydrogen by a tensile stress field. Such an interaction suggests that regions of coherency strain, as well as dislocation stress fields, are favored locations for hydrogen in the steel.

It has not been established, however, that such trapping of hydrogen is responsible for the embrittlement of steel. Similarly, the inter-granular fracture mode observed in high-strength steels has not been adequately explained by such interaction of hydrogen with the defect structure in steels.
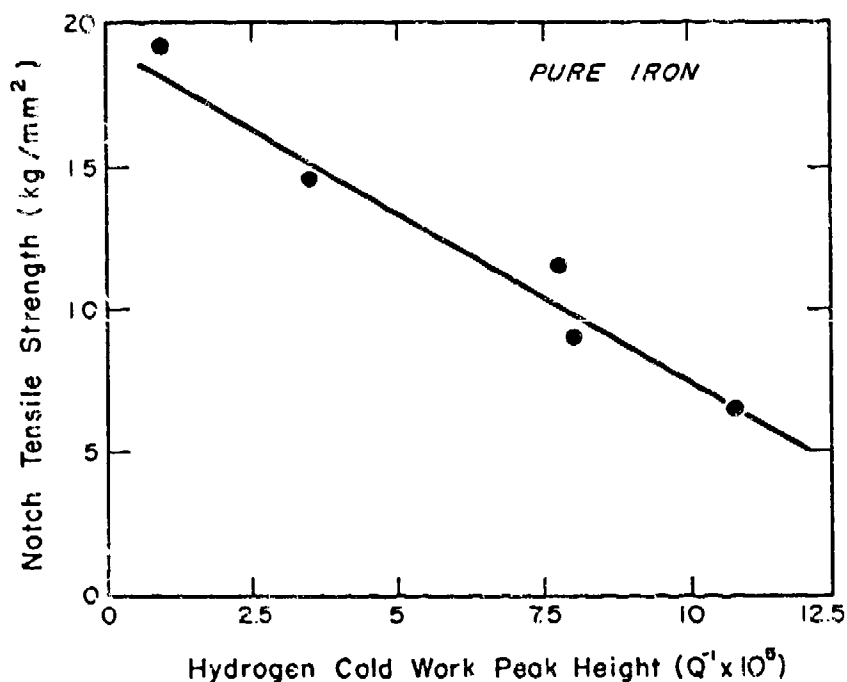
Fig. 82. Notch Tensile Strength of Aged Iron as a Function of the Hydrogen Cold-Work Peak Height [From the work of Kikuta et al. (104)]

119

REFERENCES

1. Sandoz, G., "High-Strength Steels," <u>Stress Corrosion Cracking in High-Strength Steels and in Titanium and Aluminum Alloys</u>, Naval Research Laboratory, Washington, D.C., (1972), 79.

2. Troiano, A. R., "The Role of Hydrogen and Other Interstitials in the Mechanical Behavior of Metals," (1959 Edward DeMille Campbell Memorial Lecture), <u>Trans. ASM</u>, <u>52</u> (1960), 54.

3. Bastein, P., and Azou, P., "Effect of Hydrogen on the Deformation and Fracture of Iron and Steel in Simple Tension," <u>Proc. First World Met. Congr.</u>, ASM, Cleveland, OH, (1951), 535.

4. Phelps, E. H., and Liginow, A. W., "Stress Corrosion of Steels for Aircraft and Missiles," <u>Corrosion</u>, <u>16</u> (1960), 325t.

5. Brown, B. F., "A New Stress Corrosion Cracking Test for High-Strength Alloys," <u>Mat'ls. Res. and Stds.</u>, <u>6</u> (1966), 129.

6. Brown, B. F.; Smith, J. A.; and Peterson, M. H., "Electrochemical Conditions at the Tip of an Advancing Stress-Corrosion Crack in AISI 4340 Steel," <u>Corrosion</u>, <u>26</u>:12 (1970), 539.

7. Hughes, P. C.; Lamborn, I.R.; and Liebert, B. B., "Delayed Fracture of a Low-Alloy Steel in Corrosive Environments," <u>J.I.S.I.</u>, <u>203</u> (1965), 156.

8. Steigerwald, E. A., and Benjamin, W. D., "Effect of Composition on the Environmentally Induced Delayed Failure of Precracked High-Strength," <u>Met. Trans.</u>, <u>2</u> (1971), 606.

9. Speidel, M. O., "Dynamic and Static Embirttlement of a High-Strength Steel in Water," <u>Hydrogen in Metals</u> International Conference in Paris, (May-June, 1972), 290.

10. Pourbaix, M., and de Zoubov, N., CEBELCOR Rapport CEFA/R.13.

11. Banerjee, B. R., "Fracture Micromechanics in High-Strength Steels," <u>Structure and Properties of Ultrahigh-Strength Steels</u>, ASTM STP 370, ASTM, (1965), 94.

12. Baker, A. J.; Lauta, F. J.; and Wei, R. P., "Relationships Between Microstructure and Toughness in Quenched and Tempered Ultrahigh-Strength Steels," <u>Structure and Properties of Ultrahigh-Steels</u>, ASTM STP 370, ASTM, (1965), 3.

13. Pascover, J. S., and Matas, S. J., "Relationships Between Structure and Properties in the 9Ni-4Co Alloy System," <u>Structure and Properties of Ultrahigh-Strength Steels</u>, ASTM STP 370, ASTM, (1965), 30.

14. Duckworth, W. E., "The Heat-Treatment of Low-Alloy Steels," Met. Rev., 13:128 (1968), 145.

15. Kelly, P. M., and Nutting, J., "Strengthening Mechanisms in Martensite," Physical Properties of Martensite and Bainite, Special Rep. 93, J.I.S.I., (1965), 166.

16. Benjamin, W. D., and Steigerwald, E. A., "Environmentally Induced Delayed Failures in Martensitic High-Strength Steels," Tech. Rep. AFML-TR-68-80, Wright Patterson Air Force Base, OH, (1968).

17. Klinger, L. J.; Barnet, W. J.; Fromberg, R. P.; and Troiaro, A. R., "The Embrittlement of Alloy Steel at High-Strength Levels," Trans. ASM, 46 (1954), 1557.

18. McGuire, M. F., Hehemann, R. F., and Troiano, A. R., "Stress-Corrosion Cracking and Hydrogen Embirttlement in 410 Stainless Steel," Hydrogen in Metals, International Conference in Paris, May-June, 1972, p. 325.

19. Lillys, P., and Nehrenberg, A. E., "Effect of Tempering on Stress-Corrosion Cracking and Hydrogen Embrittlement of Martensitic Stainless Steels," Trans. ASM, 48 (1956), 327.

20. Rickett, R. L.; White, W. F.; Walton, C. S.; and Butler, J. C., "Isothermal Transformation, Hardening, and Tempering of 12% Chromium Steel," presented at 33rd Annual Convention of ASM, Detroit, MI, (1951).

21. Bucher, J. H., Powell, G. W., and Spretnak, J. W., "A Micro-Fractographic Analysis of Fracture Surfaces in Some Ultra-High-Strength Steels," AIME Conf., 31, "Application of Fracture Toughness Parameter to Structural Metals," (1966), 323.

22. Davis, R. A., "Stress-Corrosion Cracking Investigation of Two Low Alloy, High-Strength Steels," Corrosion, 19 (1963), 45t.

23. Proctor, R. P. M., and Paxton, H. W., "The Effect of Prior-Austenite Grain-Size on the Stress-Corrosion Cracking Susceptibility of AISI 4340 Steel," Trans. ASM, 62 (1969), 989.

24. Carter, C. S., "The Effect of Silicon on the Stress Corrosion Resistance of Low Alloy High-Strength Steels," Corrosion, 25 (1969), 423.

25. Hancock, G. G., and Johnson, H. H., "Hydrogen, Oxygen, and Sub-critical Crack Growth in a High-Strength Steel," Trans. AIME, 236 (1969), 447.

26. Van der Sluys, W. A., "Mechanisms of Environment Induced Sub-critical Flaw Growth in AISI 4340 Steel," Engr. Fract. Mech., 1 (1969), 447.

27. Logan, H. L., *The Stress Corrosion of Metals*, John Wiley and Sons, NY, (1966), 280.

28. Brown, B. F., "The Application of Fracture Mechanics to Stress-Corrosion Cracking," *Met. Rev.*, 13 (1968), 171.

29. Dahlberg, E. P., "Report of NRL Progress," Naval Research Laboratory, Washington, D.C., (April, 1968), 25.

30. Wessel, E. T.; Clark, W. G.; and Wilson, W. K., "Engineering Methods for the Design and Selection of Materials Against Fracture," Final Tech. Rep. on U. S. Army Contract No. DA-30-069-AMC-602(T), (1966).

31. Brown, W. F., Jr., and Srawley, J. E., *Plane Strain Crack Toughness Testing of High-Strength Metallic Materials*, ASTM STP 410, ASTM, Phila, PA, (1966), 25.

32. Phelps, E. H., "A Review of the Stress-Corrosion Behavior of Steels with High-Yield Strength," *Proc. Conf. on Fund. Aspects of Stress-Corrosion Cracking*, The Ohio State University, (1967), 398.

33. Brown, B. F., "Stress-Corrosion Cracking of High-Strength Steels," *The Theory of Stress Corrosion Cracking in Alloys*, NATO Science Committee Research Evaluation Conference, Brussels, (1971), 186.

34. Sandoz, G., "A Unified Theory for Some Effects of Hydrogen Source, Alloying Elements, and Potential on Crack Growth in Martensitic AISI 4340 Steel," *Met. Trans.*, 3 (1972), 1169.

35. Colangelo, V. J., and Ferguson, M. S., "The Role of Strain Hardening Exponent in Stress-Corrosion Cracking of a High-Strength Steel," *Corrosion*, 25 (1969), 509.

36. Kerns, G. E., Ph.D. Dissertation, The Ohio State University, Columbus, OH, (1973).

37. Wang, M. T., and Staehle, R. W., "Effect of Heat Treatment and Stress Intensity Parameters on Crack Velocity and Fractography of AISI 4340 Steel," *Hydrogen in Metals*, International Conference in Paris, (May-June, 1972), 342.

38. Vaughan, D. A., and Phalen, D. I., "Reactions Contributing to the Formation of Susceptible Paths for Stress-Corrosion Cracking," *Stress Corrosion Testing*, ASTM STP 425, ASTM, (1967), 209.

39. Zackay, V. F.; Gerberich, W. W.; and McCoy, R. A., "On the Resistance of TRIP Steel to Hydrogen Embrittlement," *Met. Trans.*, 1 (1970), 2031.

40. Ault, R. T.; McDowell, K. O.; Hendricks, P. L.; and Ronald, T. M. F., "Increased Reliability of a High-Strength Steel Through Thermal-Mechanical Treatments," Trans. ASM, 60 (1967), 79.

41. Bressanelli, J. P., "Effects of Heat Treatments on the Resistance to Hydrogen Embrittlement of Type 410 Stainless Steel," Trans ASM, 58 (1965), 3.

42. Williams, D. P., and Nelson, H. G., "Embrittlement of 4130 Steel by Low-Pressure Gaseous Hydrogen," Met. Trans., 1 (1970), 63.

43. Sawicki, V. R., Jr., Ph.D. Dissertation, Cornell University, Ithaca, N.Y., (1971).

44. Proctor, R. P. M., and Paxton, H. W., "The Effect of Prior Austenite Grain Size on the Stress Corrosion Cracking Susceptibility of AISI 4340 Steel," Trans. ASM, 62 (1969), 989.

45. Webster, D., "The Improvement of Mechanical Properties of AFC77 by Austenite Grain Refinement," Trans. ASM, 62 (1969), 759.

46. Carter, C. S., "The Effect of Silicon on the Stress-Corrosion Resistance of Low Alloy High-Strength Steels," Corrosion, 25 (1969), 423.

47. Radhakrishnan, T. P., and Shreir, L. L., "Permeation of Hydrogen through Steel by Electrochemical Transfer - I. Influence of Catalytic Poisons," Electrochimica Acta, 11 (1966) 1007.

48. Wood, G. B., "A Study of Embrittlement of High-Strength Steels by Hydrogen Isotopes," J. Electrochemical Soc., 110 (1963) 867.

49. Farrell, K., "Cathodic Hydrogen Absorption and Severe Embrittlement in a High-Strength Steel," Corrosion, 26 (1970), 105.

50. Treseder, R. S. and Swanson, T. M., "Factors in Sulfide Corrosion Cracking of High-Strength Steels," Corrosion, 24 (1968), 31.

51. Hudgins, C. M.; McGlasson, R. L.; Mehdizadeh, P.; and Rosborough, W. M., "Hydrogen Sulfide Cracking of Carbon and Low Alloy Steels," Corrosion, 22 (1966), 238.

52. Tirman, A; Haney, E. G.; and Fugassi, P., "Environmental Effects of Sulfur and Sulfur Compounds on the Resistance to Stress-Corrosion Cracking of AISI 4340 Steel in Aqueous Chloride Solutions," Corrosion, 25 (1969), 342.

53. Fugassi, P., and Haney, E. G., "Effect of Heavy Metal Ions on Susceptibility of AISI 4340 Foil to Stress-Corrosion Cracking in Dilute Aqueous Hydrochloric Acid Solutions," Corrosion, 26 (1970), 118.

54. Brown, B. F., "Stress-Corrosion Cracking of High Strength Steels," The Theory of Stress-Corrosion Cracking in Alloys, NATO Science Committee, Research Evaluation Conference Brussels, (1971).

55. Brown, B. F. CEBELCOR, Bulletin E-76, Vol. 8 (1969), 1.

56. McGuire, M. F.; Hehemann, R. F.; and Troiano, A. R., "Stress-Corrosion Cracking and Hydrogen Embrittlement in 410 Stainless Steel," Hydrogen in Metals, International Conference in Paris, (May-June, 1972), 325.

57. Barth, C. F.; Steigerwald, E. A.; and Troiano, A. R., "Hydrogen Permeability and Delayed Failure of Polarized Martensitic Steel," Corrosion, 25 (1969), 353.

58. Troiano, A. R., and Fidelle, J. P., "Hydrogen Embrittlement in Stress-Corrosion Cracking," Hydrogen in Metals, International Conference in Paris, (May-June, 1972), 31.

59. Hanna, G. L.; Troiano, A. R.; and Steigerwald, E. A., "A Mechanism for the Embrittlement of High-Strength Steel By Aqueous Environments," Trans. ASM, 57 (1964), 668.

60. Speidel, M. O., "Branching of Sub-Critical Cracks in Metals," Hydrogen in Metals, International Conference in Paris, (May-June, 1972), 3.

61. Mostovoy, S.; Ripling, E. J.; Smith, H. R.; and Lingwall, R. G., "A Note on Stress-Corrosion Cracking Rates," Engr. Fract. Mech., 1 (1971), 291.

62. Landes, J. D., Ph.D. Dissertation, Lehigh University, Bethlehem, PA, (1970).

63. McIntyre, P., and Priest, A. H., "Accelerated Test Technique for the Determination of K_{Iscc} in Steels," British Steel Corp. Corporate Laboratories Rep. MG/31/72, (1972).

64. Kerns, G. E., and Staehle, R. W., "Slow Crack Growth in Hydrogen Sulfide Gas Environments," Scripta Met., 6 (1972), 631.

65. Johnson, H. H., and Willner, A. M., "Moisture and Stable Crack Growth in a High-Strength Steel," Appl. Mat. Res., 4 (1965), 34.

66. Truman, J. E.; Perry, R.; and Chapman, G. N., "Stress-Corrosion Cracking of Martensitic Stainless Steels," J.I.S.I., 202 (1964), 745.

67. Kerns, G. E., and Staehle, R. W., "Slow Crack Growth of a High-Strength Steel in Chlorine and Hydrogen Halide Gas Environments," Scripta Met., 6 (1972), 1189.

68. Wicks, C. E., and Block, F. E., Bulletin 605, U. S. Bureau of Mines, Washington, (1963).

69. Handbook of Chemistry and Physics, 48th Ed., The Chemical Rubber Company, Cleveland, OH, (1967).

70. JANAF Thermochemical Data, Dow Chemical Co., Midland, MI, Interim Tables.

71. Williams, D. P.; Nelson, H. G.; and Tetelman, A. S., "Embrittlement of a Ferrous Alloy in a Partially Dissociated Hydrogen Environment," Met. Trans., 2 (1971), 953.

72. Beck, W.; Bockris, J. O'M.; McBreen, J.; and Nanis, L., "Hydrogen Permeation in Metals as a Function of Stress, Temperature, and Dissolved Hydrogen Concentration," Proc. Roy Soc. (London), 290A (1966), 220.

73. McIntyre, P.; and Priest, A. H.; and Nicholson, C. E., "Hydrogen-Induced Sub-Critical Flaw Growth in Steels Under Static and Cyclic Loading Conditions," British Steel Corp. Corporate Laboratories Rep. MG/38/72, (1972).

74. Beachem, C. D., "A New Model for Hydrogen Assisted Cracking (Hydrogen 'Embrittlement')", Met. Trans., 3 (1972), 347.

75. Carter, C. S., "Stress-Corrosion Cracking Branching in High-Strength Steels," Engr. Fract. Mech., 3 (1971), 1.

76. Carter, C. S., 'Crack Extension in Several High-Strength Steels Loaded in 3-1/2% Sodium Chloride Solution," Document D6-19770, The Boeing Company, 1967.

77. Carter, C. S., "The Effect of Heat Treatment on the Fracture Toughness and Subcritical Crack Growth Characteristics of a 350-grade Maraging Steel," Met. Trans., 1 (1970), 1551.

78. Carter, C. S., unpublished data.

79. Zapffe, C. A., and Sims, C. E., "Hydrogen Embrittlement, Internal Stress, and Defects in Steel," Trans. AIME, 145 (1941), 225.

80. Tetelman, A. S., "The Mechanism of Hydrogen Embrittlement in Steel," Proc. Conf. on Fund. Aspects of Stress-Corrosion Cracking, The Ohio State University, (1967), 446.

81. Petch, N. J., "The Lowering of Fracture Stress Due to Surface Adsorption," *Phil. Mag.*, 1 (1956), 331.

82. Petch, N. J., and Stables, P., "The Delayed Failure of Metals Under Static Load," *Nature*, 169 (1952), 842.

83. Tetelman, A. S., and McEvily, A. J., Jr., *Fracture of Structural Materials*, John Wiley and Sons, N.Y., (1967), 57.

84. Trapnell, B. M. W., "The Activities of Evaporated Metal Films in Gas Chemisorption," *Proc. Roy. Soc. (London)*, A218 (1953), 566.

85. Gerberich, W. W., and Hartbower, C. E., "Monitoring Crack Growth of Hydrogen Embrittlement and Stress-Corrosion Cracking by Acoustic Emission," *Proc. Conf. on Fund. Aspects of Stress-Corrosion Cracking*, The Ohio State University, (1967), 446.

86. Dunegan, H. L., and Tetelman, A. S., "Non-Destructive Characterization of Hydrogen-Embrittlement Cracking by Acoustic Emission Techniques," *Engr. Fract. Mech.*, 2 (1971), 387.

87. Staehle, R. W., and Kerns, G. E., "Acoustic Emissions and Slow Crack Growth in High-Strength Steel," AGARD Conf. Proc. No. 98, (NATO), (1972), 17-1

88. Baker, G. S., Aerojet-General Corp. Tech. Rep. AFML-TR-67-266, (1968).

89. Beck, W.; Subramanyan, P. K.; Williams, F. S.; and Bockris, J. O'M., "The Effect of Stress on the Chemical Potential of Hydrogen in Iron and Steel," *Acta Met*, 19 (1971), 1209.

90. Roberts, M. W., and Ross, J. R. H., "Kinetics of the Dissociation of Hydrogen Sulfide by Iron Films," *Trans. Far. Soc.*, 62 (1966), 2301.

91. Palczewska, W., "The Effect of Catalytic Poisons on the Kinetics of Heterogeneous Recombination of Hydrogen Atoms," *Bulletin de L'Academie Polonaise des Sciences*, Series des Sciences Chimiques, 12.10 (1959), 743.

92. Palczewska, W., "Influence of Catalytic Promoters on the Permeation of Hydrogen From the Gas Phase Into Iron - II. The Effect of Temperature and Hydrogen Sulfide Concentration," *Bulletin de L'Academie Polonaise des Sciences*, Serie des sciences chimiques, 12:3 (1964), 183.

93. Porter, A. S., and Tompkins, F. C., "The Kinetics of Chemisorption of Hydrogen and Carbon Monoxide on Evaporated Iron Films," *Proc. Roy. Soc. (London)*, A217 (1953), 529.

94. Oriani, R. A., "Discussion of 'Embrittlement of 4130 Steel by Low-Pressure Gaseous Hydrogen'", Met. Trans., 1 (1970), 2346.

95. Johnson, H. H., and Sawicki, V., "The Effective Area Concept, Permeation, and Hydrogen Gas Crack Growth Kinetics, Met. Trans., 2 (1971), 3496.

96. Smithells, C. J., and Ransley, C. E., "The Diffusion of Gases Through Metals," Proc. Roy. Soc. (London), 150A (1935), 172.

97. Smialowski, M., "Effect of Electrolytic Charging Conditions On Hydrogen Penetration and Embrittlement of Various Steels," Hydrogen In Metals, International Conference in Paris, (May-June, 1972), 300.

98. Darken, L. S., and Smith, R. P., "Behavior of Hydrogen in Steel During and After Immersion in Acid," Corrosion, 5 (1949), 1.

99. Hill, M. L., and Johnson, E. W., "The Diffusivity of Hydrogen in Alpha Iron," Trans. AIME, 218 (1960), 1104.

100. Oriani, R. A., "The Diffusion and Trapping of Hydrogen in Steel," Acta Met., 18 (1970), 147.

101. Kim, C. D., and Loginow, A. W., "Techniques for Investigating Hydrogen-Induced Cracking of Steels with High-Yield Strength," Corrosion, 24 (1968), 313.

102. Bockris, J. O'M., and Subramanyan, P. K., "Hydrogen Embrittlement and Hydrogen Traps," J. Electrochem. Soc., 118 (1971), 1114.

103. Kortovich, C. S., and Steigerwald, E. A., "A Comparison of Hydrogen Embrittlement and Stress-Corrosion Cracking in High-Strength Steels," Engr. Fract. Mech., 4 (1972), 637.

104. Kikuta, Y.; Sugimoto, K.; Ochiai, S.; and Iwata, K., "The Interaction of Hydrogen and Dislocations, and Its Parallelism with Hydrogen Embrittlement in Iron and Steels," Hydrogen in Metals, International Conference in Paris, (May-June, 1972), 144.

105. Bastein, P., and Azou, P., Rev. Met., 49 (1952), 837.

106. Sturges, C. M., and Miodownik, A. P., "The Interaction of Hydrogen and Dislocations in Iron," Acta Met., 17 (1969), 1197.

PART II - EFFECTS OF ENVIRONMENTAL SPECIES AND METALLURGICAL STRUCTURE IN THE HYDROGEN ENTRY INTO STEEL

R. D. McCright

R. W. Staehle

INTRODUCTION

The entry of hydrogen into iron-base alloys is usually an undesired reaction because of the damage that hydrogen causes to the physical and mechanical properties of the metal. Species present in the environment have a profound effect on the quantity of hydrogen that can enter metals. A few cases of practical concern are sulfides in crude sour gas wells, residual traces of arsenic compounds in acids, cyanide in plating solutions, inhibitors added to pickling solutions. In all of these examples, the sulfide, cyanide, etc., caused a hydrogen-related problem that would not have existed in their absence. The purpose of this paper will be to examine the nature of the environmental species which influence hydrogen entry and the conditions under which they operate (pH, temperature, effect of metallurgical structure), and finally to discuss the mechanism.

THE HYDROGEN EVOLUTION AND HYDROGEN ABSORPTION REACTIONS

An understanding of the role of environmental species and metallurgical structure in the hydrogen entry problem depends on an understanding of the basic characteristics and considerations of the hydrogen evolution reaction (HER) and the hydrogen absorption reaction (HAR).

The Hydrogen Evolution Reaction

Many previous publications have described in detail the kinetics of the HER on various metals.[1,2,3] Because of the extreme variation of the exchange current density (some ten orders of magnitude) found for the HER on various metals, considerable changes in the reaction mechanism and energetics are thought to occur from one metal to another. Consideration of the mechanism of the HER is germane to the discussion of the hydrogen absorption reaction, because the latter is a side reaction.

Even a reaction as simple as the HER occurs in a number of consecutive steps; i.e., (1) transport of a hydrated proton $(H_3O)^+$ to the double layer, (2) loss of the water of hydration shield in the vicinity of the double layer, (3) adsorption of the proton to the electrode surface, (4) discharge (electronation) of the proton to an adsorbed hydrogen atom, (5a) chemical combination of two adjacent hydrogen adatoms to form a hydrogen molecule - possibility of surface migration between site of discharge and site of recombination,

(5b) electrodic combination of an adatom and a proton to form a hydrogen molecule, (6) desorption of H_2, (7) bubble formations as H_2 molecules coalesce, and (8) evolution of bubbles. Conditions of interest are usually such that steps (1) and (8) are rarely limiting. In addition, steps (2), (3), and (7) are thought not to affect the overall reaction rate. Therefore, the steps of interest are the discharge step, one of the combination steps (5a or 5b), and the desorption step. The combination and desorption steps are usually combined because of the weak affinity for H_2 to chemisorb. Thus, the HER occurs in two important steps; i.e., discharge followed by chemical or electrochemical combination. Either of these steps may be the rate-determining step (rds) or they may proceed in lock-chain fashion (coupled reaction).

McBreen and Genshaw[4] calculated the various rate expressions for the reaction paths. These rate expressions involve the overpotential and current density, quantities which are physically measurable. The energetics of the adsorption step affect these rate expressions. In Table I, where some of the derivations of these expressions are summarized, the Langmuir isotherm (all energy sites equal, no change in the heat of adsorption) and the Temkin isotherm (the heat of adsorption decreasing linearly in the algebraic sense with the coverage). The Langmuir isotherm is generally valid at low coverages and the Temkin at higher coverages.

The Hydrogen Absorption Reaction

Rate expressions for the absorption reaction are written in the form: rate = constant X concentration term. The "constant" involves a frequency term ν and an exponential term which in turn involves an activation energy for the absorption process. If the source of hydrogen is the monatomic gas that adsorbs to the metal surface, the rate of entry is

$$r = \nu \; \theta \; M_S \; \exp(-\Delta H^*/RT) , \qquad (1)$$

where M_S is the number of metal sites available for adsorption, θ is the fraction of these covered, and ΔH^* is the activation energy for the adsorption step.

Oftentimes the HAR is studied by permeating a thin metal specimen. The following equation obtains:

$$P = D(C_O - C_L)/L , \qquad (2)$$

where C_O is the subsurface concentration at the entry side, C_L is the concentration at a depth L, D is the diffusivity of hydrogen, and P is

Table I. Kinetic Derivatives for Mechanisms of the HER, Evaluated for $\beta = 1/2$

Mechanism	Tafel Slope $(-\partial\eta/\partial\ell n\,i)_{pH}$		Reaction Order $(-\partial\ell n\,i/\partial pH)_{\eta}$	
	Langmuir	Temkin	Langmuir	Temkin
rate-determining discharge followed by chemical desorption	$\dfrac{2RT}{F}$	$\dfrac{2RT}{F}$	1	1
discharge followed by rate-determining chemical desorption	$\dfrac{RT}{2F}$	$\dfrac{RT}{F}$	2	1
coupled discharge-chemical desorption	$\dfrac{2RT}{F}$	$\dfrac{3RT}{F}$	1	2/3
rate-determining discharge followed by electrodic	$\dfrac{2RT}{F}$	$\dfrac{RT}{F}$	1	3/2
discharge followed by rate-determining electrodic desorption	$\dfrac{2RT}{3F}$	$\dfrac{RT}{F}$	2	3/2
coupled discharge-electrodic desorption	$\dfrac{2RT}{F}$	$\dfrac{2RT}{F}$	1	1

131

the steady state permeation rate. It is seen from the equation that the entry concentration governs the magnitude of the gradient because C_L is generally made very low by experimental design.

Models of hydrogen entry

Two models for explaining hydrogen entry into the metal have been proposed. The first of these, which was developed by Bockris and Thacker[5,6] at the University of Pennsylvania, consider that the hydrogen enters in the same elementary form as it exists on the surface; that is, atomic or nascent hydrogen. In the second model hydrogen enters directly from a discharged proton (hydrogen ion) and does not pass through the intermediate adsorbed phase. These models are schematically depicted in Fig. 1.

In the Bockris-Thacker or "Pennsylvania" model the absorption step and chemical desorption (recombination) step are competing. The absorption step (step 4) is written as a "fast" step meaning that equilibrium is attained rapidly and the step proceeds with little activation energy. In the figure the k's are the specific rate constants for the various steps. The subscripts 1 and -1 refer to the discharge step and 4 and -4 to the absorption step. The chemical desorption step can be replaced by the electrodic desorption step (k_3 and k_{-3} rate constants) if that mechanism occurs.

In the Russian model the hydrogen ion is discharged and passes immediately into the metal with no intermediates involved. In other words, the HAR is competing for the same discharged protons as the HER. The specific rate constant for the absorption step in this model is denoted by the subscript 5.

Horiuti and Toya[7] have described two models of hydrogen chemisorption that relate to the two models of hydrogen entry. In the so-called r-type adsorption, shown in Fig. 2, the hydrogen adatoms are outside the electronic cloud but immediately atop a corresponding metal atom. The distance of the metal-hydrogen bond is about 2.5 Å. The bonding is largely covalent, with the hydrogen being the slightly negative member of the dipole. In the s-type adsorption, the hydrogen adatom is partly within the electronic cloud of the metal. The hydrogen behaves more like a proton dissolved in the surface layer and the bonding is more ionic, with hydrogen being positive. This situation represents a higher energy state than r-type adsorption, but lattice defects and other surface imperfections significantly reduce the energy and favor s-type adsorption. These adsorption variations influence the electrical resistivity of films, and from such measurements on nickel and platinum, r-type adsorption dominates at low hydrogen coverages and s-type at higher coverages. The entry model based on entry from adsorbed adatoms is analogous to r-type adsorption, while that for entry from protons corresponds to s-type adsorption.

(A) Absorption from H(ads)

$$H_2 + 2M$$

$$k_2 \Big\Updownarrow k_{-2}$$

$$H^+ + M + e^- \underset{K_{-1}}{\overset{K_1}{\rightleftharpoons}} MH(ads) \underset{K_{-4}}{\overset{K_4}{\rightleftharpoons}} MH(abs)$$

(B) Absorption from H^+

$$H_2 + 2M$$

$$K_2 \Big\Updownarrow K_{-2}$$

$$MH(ads)$$

$$H^+ + M + e^- \;\; K_1 / K_{-1}$$

$$K_5 \quad K_{-5} \quad MH(abs)$$
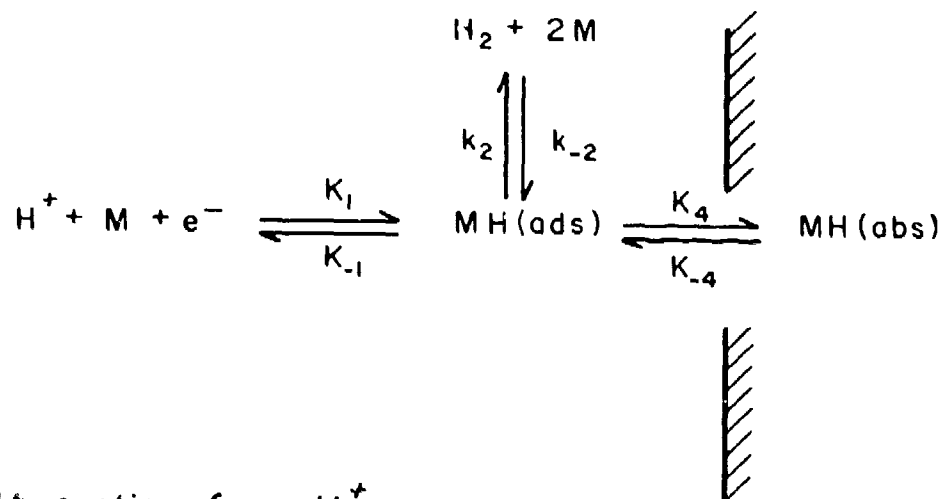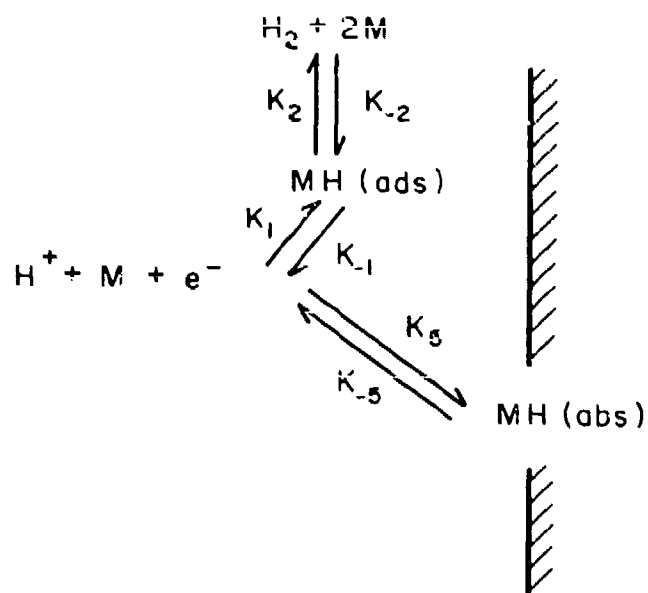
Fig. 1. Models for Hydrogen Entry into Metals: (A) Absorption from Atomic Hydrogen, (B) Absorption from Protons

133

r – Type Adsorption

Electronic Surface

Adatoms

Metal Atoms

s – Type Adsorption

Electronic Surface

Adatoms

Metal Atoms
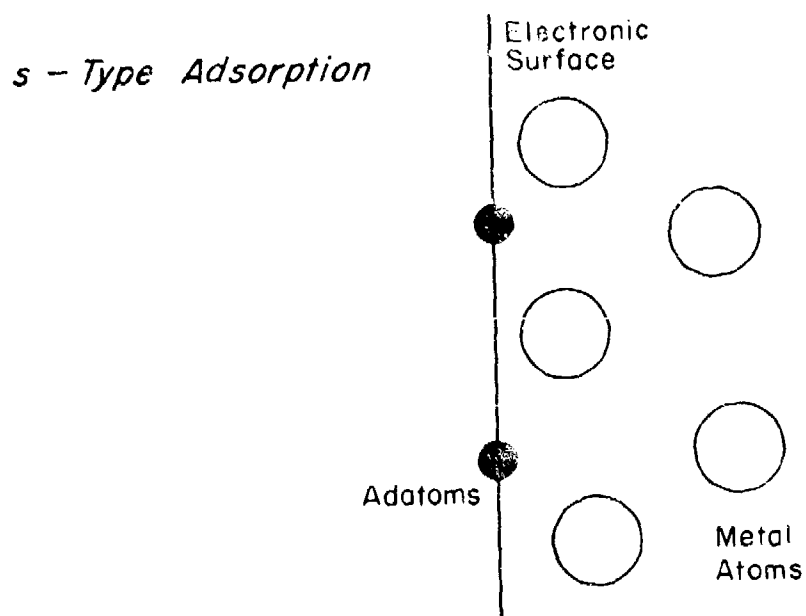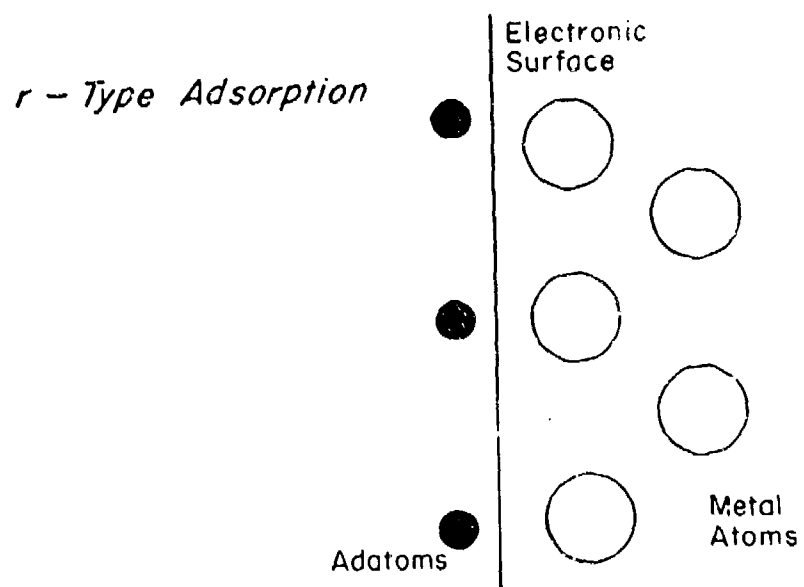
Fig. 2. Models for Chemisorbed Hydrogen

Energetics of the HAR

Bockris, Genshaw, and Fullenwider[8] considered the electrolytic hydrogen permeation into a number of metals and calculated the energy requirements for the reaction. The energy of the absorbed hydrogen should be the same regardless of its source (aqueous solution or gas), although the energy of the intermediate adsorbed phase may be different. These authors perform permeation experiments at several temperatures so that they were able to obtain a "heat of activation for permeation." By using equation

$$i^{\infty}_{p} = (ZFD \ C_{O}/L) , \tag{3}$$

and neglecting the dimensional change with temperature,

$$R\left[\partial \ell n \, i^{\infty}_{p}/\partial(1/T)\right] = R\left[\partial \ell n \, D/\partial(1/T)\right] + R\left[\partial \ell n \, C_{O}/\partial(1/T)\right] \tag{4}$$

and

$$\Delta H^{O}_{P}* = \Delta H^{O}_{D}* + \Delta H^{H}_{S} , \tag{5}$$

where $\Delta H^{O}_{P}*$ is the "heat of activation for permeation," and $\Delta H^{O}_{D}*$ is the "heat of activation for diffusion" hence the superscript. These terms are defined at zero overpotential; their difference gives the "heat of solution" for hydrogen in the metal, ΔH^{H}_{S}. For Fe the calculated heat of solution is 7.04 kcal/mole (based on the data of Bryan and Dodge) for absorption from the monatomic gas phase. A value of 5.0 kcal/mole was calculated for absorption from the solution phase at an overpotential of 300 mV cathodic. Considering the correction for overpotential, the value of ΔH^{H}_{S} in iron is about 8.5 kcal/mole and is endothermic.

The heat of solution determines the solubility of hydrogen in the metal. The more exothermic the heat of solution is, the greater the solubility. Some other values of ΔH^{H}_{S} calculated by these authors are -4.1 kcal/mole for Pd, -0.4 kcal/mole for Ni, and 0.3 kcal/mole for Pt. This is in the same order as the solubility of hydrogen in these metals: Pd > Ni > Pt > Fe.

Relationship of the HER and HAR

If the analysis of kinetic derivatives is carried out for the models of hydrogen entry presented above, the models lead to different predictions for the dependence of the entry rate on the experimental conditions of potential or current density maintained at the entry surface. Details of the analysis are given in previous papers[4,9] and

it will suffice here to give the results in tabulated form. In Table II the kinetic derivatives are given for the dependence of the steady state permeation current on the cathodic charging current. These are indicated for each of the mechanisms and adsorption isotherms discussed in relation to the kinetic derivates for the HER. Similarly, in Table III the kinetic derivatives are given for the dependence of the permeation current in the cathodic overpotential. All of these relationships pertain to absorption from the adsorbed phase (Model A in Fig. 1). For Model B, direct entry of hydrogen from the discharge step, the relationships are

$$-(\partial \eta / \partial \ln i_p^{\infty})_{pH} = \frac{RT}{F} \qquad (6)$$

and

$$(\partial \ln i_p^{\infty} / \partial \ln i)_{pH} = 2 \qquad (7)$$

This last prediction that the permeation current density depends on the square of the cathodic charging current has not been observed in permeation experiments. Rather, the dependence often observed is that the permeation current varies as the square root of the charging current. This information, along with the dependence $4RT/F$ of the cathodic overpotential with the permeation current, has led to the conclusion that hydrogen is absorbed from the adsorbed atomic phase. In addition, valuable information about the mechanism of the HER on iron has been obtained by measuring the hydrogen permeation through iron, determining the kinetic derivatives, and eliminating some of the ambiguities resulting from consideration of the kinetic derivatives of the HER alone (Table I). Such an analysis indicates that the mechanism of the HER on iron in acid solution is a coupled discharge-chemical desorption mechanism; in alkaline solutions the same mechanism prevails until overpotentials are about one volt, beyond which the rate determining step is electrodic desorption.[9,10] At least for the additives made to the solutions in this work (KI to H_2SO_4 and KCN to NaOH) the same mechanisms prevail in the presence of promoter species. Similarly, Shreir found that arsenic compounds[11] added to H_2SO_4 resulted in a dependence of the permeation current on the square root of the charging current, which is the same dependence which occurred in the un-poisoned solution. For selenium and tellurium additions some small deviation from the square root dependence was noted. Thus, it appears that additions of promoter compounds do not significantly change the over-all-mechanistic aspects of the HER, but that slight modifications of the potential energy barriers for the desorption step of hydrogen could lead to substantial increases in the HAR.

Although in aqueous solutions dependence of the permeation current on the charging current is less than order two predicted by the direct-discharge model, entry from the gas phase may occur through direct discharge of hydrogen into the metal.[12]

Table II. Relationship of Permeation Current (Steady State) to the Charging Current

Mechanism	$(\partial \ln i_p^\infty / \partial \ln i)_{pH}$	
	Langmuir Adsorption	Temkin Adsorption
Discharge RDS, Chemical Desorption	0	0
Discharge, Chemical Desorption RDS	1/2	1
Coupled Discharge-Chemical Desorption	1/2	1
Discharge RDS, Electrodic Desorption	-2	-1
Discharge Electrodic Desorption RDS	2/3	1
Coupled Discharge-Electrodic Desorption	0	0

Table III. Relationship of Permeation Current (Steady State) to the Overpotential

Mechanism	$-(\partial \eta / \partial \ln i_p^\infty)_{pH}$	
	Langmuir Adsorption	Temkin Adsorption
Discharge RDS Chemical Desorption	--	--
Discharge, Chemical Desorption RDS	$\dfrac{RT}{F}$	$\dfrac{RT}{F}$
Coupled Discharge-Chemical Desorption	$\dfrac{4RT}{F}$	$\dfrac{3RT}{2F}$
Discharge RDS, Electrodic Desorption	$\dfrac{RT}{F}$	$-\dfrac{RT}{2F}$
Discharge, Electrodic Desorption RDS	$\dfrac{RT}{F}$	$\dfrac{RT}{F}$
Coupled Discharge-Electrodic Desorption	--	--

Experimental determination of the HAR

Experimental determination of the rate of hydrogen entry into iron and iron base alloys falls into three categories of experiments. These are hydrogen permeation analysis, analytical determination of the hydrogen absorbed, and measurement of some physical or mechanical property of the metal which is influenced by absorbed hydrogen.

Consider the permeation analysis. In this type of experiment the metal functions as a membrane permeable to hydrogen. The source of hydrogen can be either a gas at elevated temperature and/or pressure or an aqueous solution with or without an applied cathodic potential. The amount of hydrogen permeating the specimen is measured by the pressure increase at the exit side in a partially evacuated enclosure or by measuring electrochemically the current increase at the exit side where a potential sufficiently anodic to oxidize the effusing hydrogen is maintained. The permeation experiment affords the advantage of charging the specimen and measuring the hydrogen entry rate in the same experiment. Also the experimenter can easily change the experimental boundary conditions (gas phase composition, temperature, applied potential, solution composition, pH) and thereby measure the direct influence of these variables on the permeation rate, and can even change conditions in the course of the experiment. This technique is quite sensitive; permeation currents on the order of 1 μA are readily measured, which corresponds to a flux of 10^{-11} moles H/sec.

The second general technique involves exposing the specimen to the environment causing hydrogenation of the specimen and then determining analytically the hydrogen content by vacuum extraction, usually at an elevated temperature, and measuring the volume of gas extracted. Since it is possible to estimate hydrogen contents to 0.001 ppm, this technique is quite sensitive. However, this process is very tedious with respect to the permeation experiment. Other difficulties arise with regard to accuracy because the specimen must be transported from the charging apparatus to the vacuum apparatus and some hydrogen may be lost from the specimen, particularly in the case of iron and other ferritic structures where the diffusivity of hydrogen and effusion rate from the structure are high.

The third category of experiment is one in which the specimen is hydrogenated and then undergoes a physical change. Among common physical and mechanical properties sensitive to hydrogen absorption and which have been measured are elongation, ductility, electrical resistivity, tensile strength, area reduction, and shear strength. Problems encountered are finding a suitably sensitive property, since the specimen must often be severely hydrogenated. Oftentimes, small concentrations of substances which decidedly accelerate the kinetics of the HAR must be added to the solution to ensure a measurable change in the property. A further point of discussion is whether the property change is determined in situ or after the hydrogen charging. In the latter case hydrogen may effuse out of the specimen. The great utility

of this type of experiment is that the information obtained is often directly applicable to practical problems of hydrogen damage to metals, whereas the permeation and analytical determinations give only the rate and amount of hydrogen present, which may cr may not be damaging.

ROLE OF ENVIRONMENTAL VARIABLES ON THE HAR

From a fundamental point of view the rate of the HAR depends on the chemical potential of the adsorbed and absorbed phases (or the proton and the absorbed phase if direct discharge occurs) and the concentration of adsorbed hydrogen. The difference in chemical potentials determines to a large extent the "activation energy" for absorption. The concentration of adsorbed hydrogen is usually expressed in terms of the fraction of surface sites. Neither of these variables - chemical potential and the resultant activation energy nor the surface coverage of hydrogen on a corrodible metal such as Fe are directly measurable.

From an experimental point of view the extent of the HAR is controlled by: (1) the potential of the metal (and hence the current density); (2) the pH and composition of the solution; (3) the presence of certain species called "promoters" that catalytically favor hydrogen absorption; (4) the temperature, and (5) the presence or absence of stress.

In the sections to follow, the above experimentally controllable variables will be described. When possible, their relation to the more fundamental terms will be discussed.

Effect of Potential

The electrochemical potential influences profoundly the HER and consequently the HAR. Not only does the potential enter into the rate equation in the exponential part, but also the potential affects the surface coverage in the pre-exponential part. From a thermodynamic point of view, the activity or fugacity of the hydrogen on the solution side of the interface establishes the boundary condition that in turn determines the concentration of dissolved hydrogen inside the metal. Many attempts have been made in applying Sievert's Law to the situation of cathodic charging, since the hydrogen content in the metal is amenable to analytical determination, whereas the "pressure" (or fugacity) envoking the concentration is not readily determinable. These attempts have led to calculations of pressures much in excess of the yield and even fracture stress of the metal. Locally high pressures may in fact exist in small asperities at the surface of the metal where hydrogen evolution occurs. Access of hydrogen away from these asperities is blocked and an enormous driving force is created. The concentration of hydrogen inside is locally supersaturated. Supersaturation is provoked by local plastic deformation and the resultant increase in solubility in these regions. In a way it is very difficult to correlate meaningfully data representative of the bulk (such as pressure and hydrogen content) when these localized processes dominate the situation.

139

This effect is exemplified in Fig. 3, where calculations of the theoretical pressure as a function of the overpotential and actual pressure determinations are shown. The pressure measurements were determined as a function of the potential by permeating and collecting the hydrogen through a thin iron membrane. Calculations of the virtual pressure in equilibrium with the hydrogen in the metal were also made. One can see the great divergence in the two pressures.[13]

Thus, although fundamentally crucial to establishing the conditions for hydrogen entry, the role of the potential was evaluated in a quantitatively predictable way is experimentally dependent.

Effect of Solution Composition

At the corrosion potential the hydrogen entry kinetics increases with the acidity of solution. In alkaline solutions a cathodic potential must be applied to effect hydrogen entry, since the corrosion potential in these solutions is above the reversible potential for hydrogen evolution. However, when hydrogen absorption rates from acid and alkaline solutions with the same applied overpotential or current are compared, the rate is much higher in the acid solution. Thus, the lower the pH is, the higher the entry rate will be.

All other experimental conditions being the same, the anion sometimes alters the hydrogen desorption reaction. In studying the pickling of low-carbon steel in various strong acids, Hudson[14] measured the corrosion rate and amount of hydrogen absorbed by the steel. The acids used were H_2SO_4, H_3PO_4, HCl and HNO_3. Very little hydrogen was absorbed during pickling in HNO_3 despite a high corrosion rate. Elsewhere, it is reported that hydrogen embrittlement effects are small or non-existent in HNO_3 because the nitrate ion is easily reduced by freshly discharged nascent hydrogen to NO_2, NO, N_2, or NH_3, depending on the circumstances. In some cases, nevertheless, nitric acid can provoke embrittlement when present in the concentration range 0.3 - 0.8 N. At stronger concentrations no embrittlement and little absorption result. The nitrate ion, especially at high concentrations, shifts the potential in the noble direction which lowers the kinetics of the HER and consequently the HAR.

With regard to HCl, H_2SO_4, and H_3PO_4 the hydrogen absorption rate at 38°C was generally lower in phosphoric acid than in the others for a range of acid concentrations between 0.05 and 10 N. as the temperature increased the absorption kinetics decreased; the highest rates were observed in H_2SO_4. However, when these data are compared on an intensive basis as the ratio of absorbed hydrogen to that theoretically produced by the corrosion of the steel, the ratio is highest for H_3PO_4 followed by H_2SO_4, then HCl. The ratio decreases with time and with increasing temperature owing to the rapid increase in the dissolution kinetics of the steel.
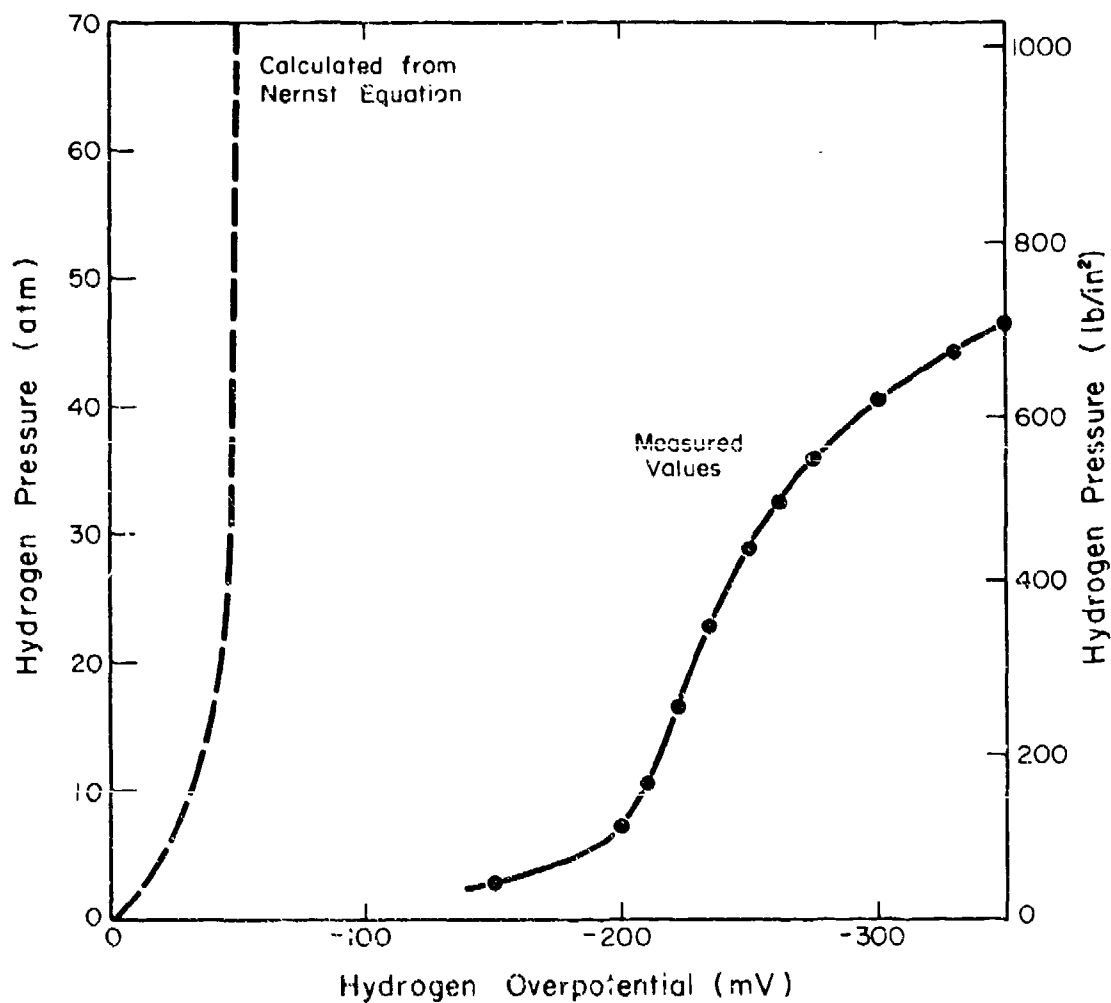
Fig. 3. Relationship Between Theoretical and Measured
Hydrogen Gas Pressures and Overpotential of an
Iron Cathode Polarized in 0.1N H_2SO_4 (from the
work of de Luccia et al., reported by Enyo[13])

At moderate pH values the presence of acetate seems to improve the hydrogen entry kinetics. The permeation rate of hydrogen cathodically charged from a pH 4.5 acetate buffer is considerably higher than that charged from a sulfate solution of comparable pH and ionic strength.[15]

Role of Hydrogen Promoters

A number of species have the effect of increasing the kinetics of the hydrogen entry into iron, steel, and ferritic alloys. The significant feature is that, in many cases, very small additions of these substances bring about a substantial increase in the hydrogen entry kinetics. The generic terms "cathode poison" and "cathodic promoter" are applied to these species because they are said to poison the evolution reaction and therefore promote hydrogen absorption.

Prominent among the species which have been found to promote hydrogen entry are certain compounds and elemental forms of Group V-A and VI-A elements of the Periodic Table. These are phosphorus, arsenic, antimony, and bismuth (V-A); and sulfur, selenium, and tellurium (VI-A). Other species which increase the hydrogen permeation are the halide ions in acid solution, cyanide ion in alkaline solutions, and the aromatic hydrocarbon naphthalene. Under some circumstances salts of heavy metals, such as mercury, tin, and lead, have been reported as enhancing hydrogen entry.

In surveying the above list of promoter species, certain properties common to at least a number of them are noted. These common properties suggest ways in which the species might act to promote hydrogen entry. Ions such as iodide, sulfide, and cyanide are known to adsorb strongly to metal surfaces. Many of the promoters form stable hydrides such as H_2S, H_2Te, H_2Se, PH_3, AsH_3, and SbH_3. In elemental form As, Sb, Bi, Hg, Pb, and Sn have bery low exchange current densities for the hydrogen evolution reaction. Another property, which is quite relevant here, is that these promoter species in certain forms are extremely toxic to biological entities (cyanide, arsenic compounds, H_2S, PH_3, Pb, and Hg).

Our purpose here will be to review significant details of the experimental circumstances under which these promoters act and to what extent they act. Then, we will use this information as a basis for mechanistic arguments.

Smialowski's work on Group V and VI promoters

Smialowski and colleagues[16],[17] measured the elongation of iron wires charged with hydrogen in the presence of promoters. Elongation is proportional to the amount of hydrogen absorbed. The elongation of an iron wire coil is an even more sensitive measurement, since the dilated metal lattice tends to increase the radius of curvature which causes the increase in length of the coil. Smialowski and Szklarska-Smialowska were able to get an elongation of more than three times the

original coil length for an iron coil charged in 1N H_2SO_4 at a current density of 18-36 mA/cm^2 at 20°C with arsenic additions (as As_2O_3) to the solution. These investigators performed similar experiments with the other elements of Group V-A and VI-A and made the correlation between coil elongation and periodicity as shown in Fig. 4. As, Sb, Bi, Se, and Te were added as the oxides; S was added as H_2S; and P as PH_3. S and P added in higher oxidation states (as $SO_4^=$ and $PO_4^=$) were ineffective in causing increased hydrogen absorption because of the high stability of these compounds even in the presence of the reducing potential. Because the form of the element appearing to cause the hydrogenation of the coil was either the hydride or a compound easily reduced to the hydride, these investigators concluded that the hydride form of the poison was a necessary condition for hydrogenation. When the data of Fig. 3 are calculated on an intensive basis (elongation per atom H) the order of effectiveness is

$$S > P > As > Se > Sb > Te > Bi ,$$
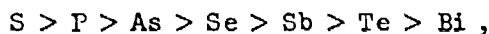
which is nearly the same as the stability of the hydrides (the higher the binding force, the more stable); i.e.,

$$S > P > Se > As > Sb .$$
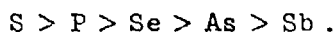
This listing also compares with the values of the standard redox potential for the elements and their hydrides (Table IV).

In another series of experiments[18] these investigators showed that adding the cathodic promoter to the solution during the charging (instead of already having it in solution) greatly increased the elongation of an iron wire. They used As_2O_3 and thiourea, which hydrolyzes to H_2S.

Because iron wire specimens which underwent torsion straining during cathodic polarization in H_2SO_4 with a small As_2O_3 addition (5.7 g As/ml) did not show a loss of ductility until they were polarized to potentials more negative than about -0.4 V_H, Angerstein-Kozlowska[20,21] concluded that arsine formation was necessary for causing enhanced hydrogenation and therefore embrittlement of the specimen. This potential corresponds to the reversible As/AsH_3 potential.

A further demonstration of the dependence of the efficacy of the promoter on pH was made recently by Smialowski.[22] He hydrogen-charged a rotating disc electrode of a ferritic Fe-5% Ni alloy below and above the limiting current density achieved in 0.1N Na_2SO_4 acidified to pH 2.6 under static conditions. He found that the permeation rate was drastically reduced near i_L when SeO_2 or thiourea was used as poisoners but that the permeation rate remained essentially independent
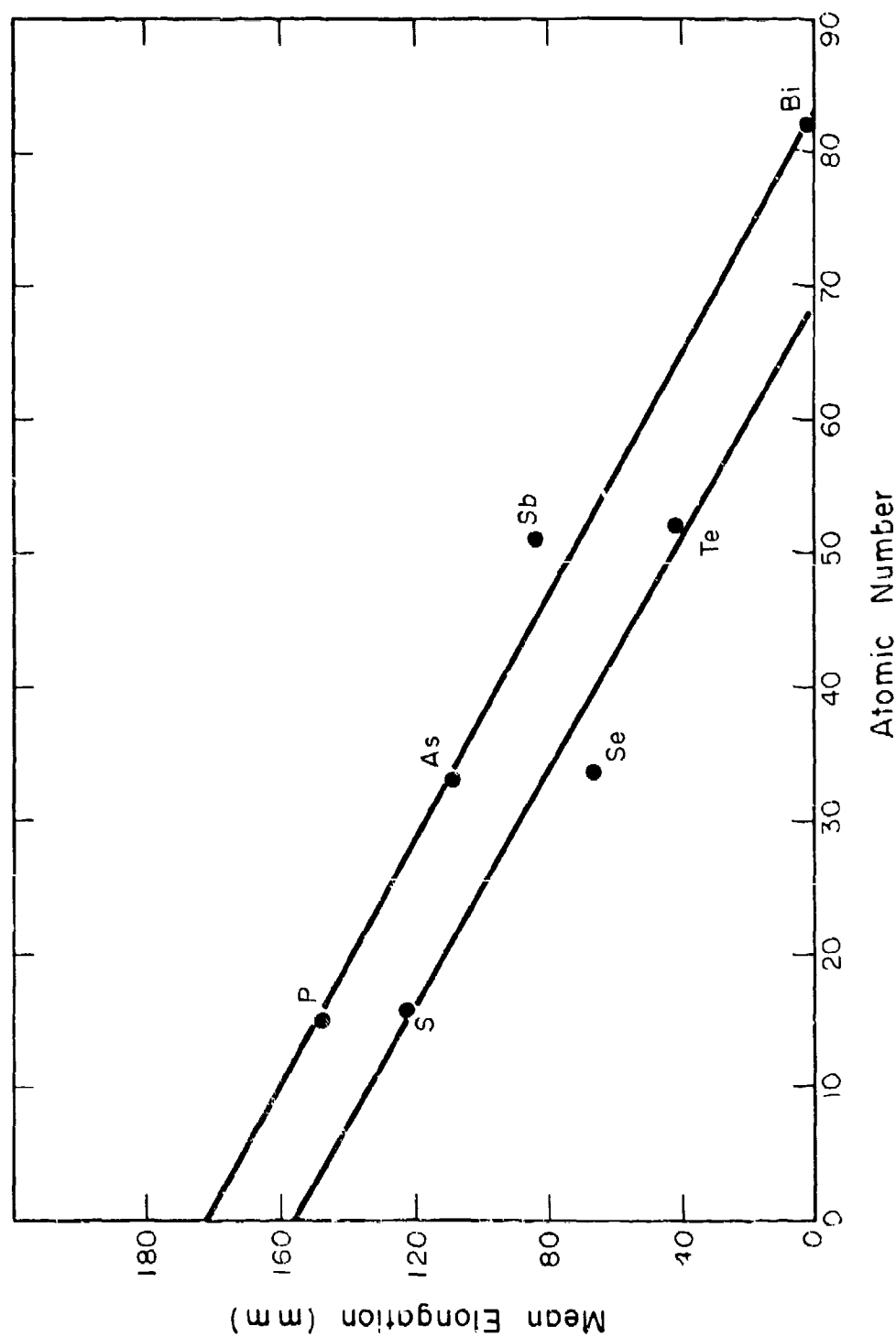
Fig. 4. Elongation of Iron Wires Polarized Cathodically in 1N H_2SO_4 Containing Various Promoter Elements; Correlation Between Elongation and Periodicity (from the work of Smialowski[18]

144

Table IV. Values of E_0^0 for Hydrogenation Promotion
Elements (From Pourbaix)[19]

Group V-A		Group VI-A	
P/PH_3	-0.110 V_H	S/H_2S	$+0.171$ V_H
As/AsH_3	-0.680	Se/H_2Se	-0.369
Sb/SbH_3	-0.510	Te/H_2Te	-0.717
Bi/BiH_3	-0.800		

of current, even above I_L, when As_2O_3 or Sb_2O_3 was employed. As i_L is
approached, the solution near the surface becomes more alkaline and the
hydrides H_2S and H_2Se become increasingly unstable, whereas AsH_3 and
SbH_3 are stable over the whole range of pH.

Shreir's work on Group V and VI elements

Newman and Shreir[23] investigated the phenomenology of promoter
additions to the charging solution. They measured the hydrogen content
in a vacuum-normalized high-strength steel (REX 539). The steel speci-
mens were exposed to solutions containing cathodic promoters at a cd of
0.5 mA/cm^2 for 24 hours to ensure saturation. In order to measure the
permeation over a number of pH's, they used a variety of solutions.
The solutions were previously deaerated with N_2 but were kept stagnant
during the 24-hour charge so as not to drive away any volatile hydride
that might form on the polarized steel electrode. The hydrogen content
of the charged steel was vacuum extracted at $300°C$. The amount of
hydrogen entering was proportional to the concentration of poisoner in
solution up to some critical concentration value beyond which the
hydrogen content was independent of increased concentration (for the
case of P, S, Se, and Te) or fell off slightly (for the case of As).
This critical concentration was independent of pH   The promoters were
added as $NaAsO_2$, Na_2SeO_3, Na_2TeO_3 (these are reduced to the hydride
electrochemically), and Na_2S and Ca_3P_2 (these hydrolyze to form the
hydride).

The pH dependence of the hydrogen content for As as the
poisoner was slight, while the other elements showed sharp maxima.
This effect is shown in Fig. 5. Even in solutions with no poisoner
present a maximum in hydrogen content was observed at a pH of about 2.
Thus, the authors concluded, water itself is a catalyst for hydrogena-
tion.

The authors concluded from their data that the hydride phase
is the one responsible for increased hydrogen entry. The bases for
this are as follows:
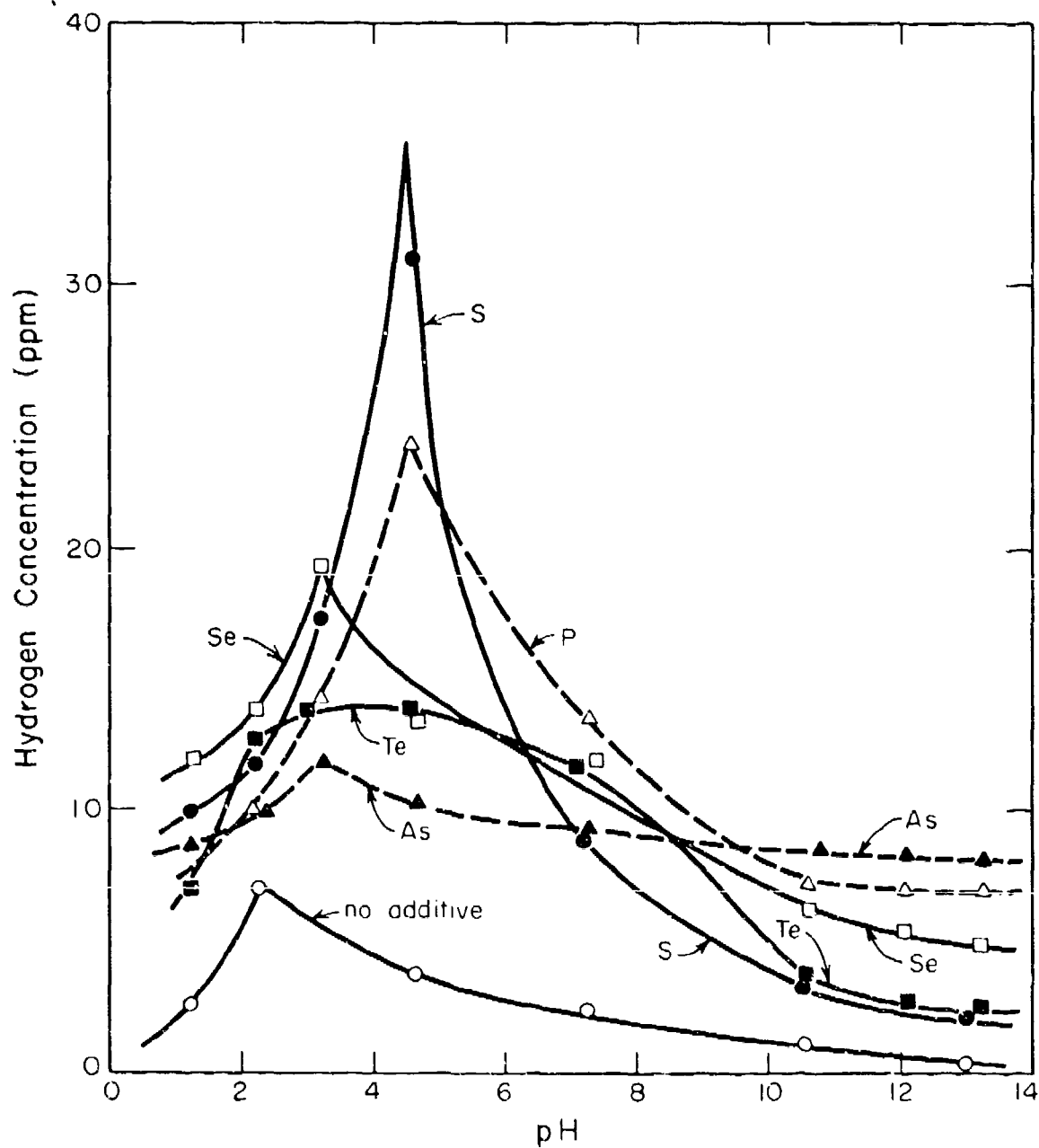
Fig. 5. Effect of pH on the Efficacy of Various Promoter
Elements in the Hydrogenation of Iron Specimens
(from the work of Newman and Shreir[23])

(A) AsH_3 is stable at all pH values and therefore pH should not greatly affect the poisoning effectiveness of As. Likewise, PH_3 is stable at all pH values. Although P did show a loss of effectiveness at the higher and lower pH's, this effect may be attributed to the formation of PH_3 from the subhydride (assuming the subhydride forms first and is a more effective poisoner);

$$P_2H_4 + 2H(ads) \rightarrow PH_3 .$$
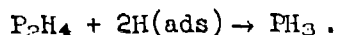
(B) For the Group VI-A elements, S, Se, and Te, their hydrides ionize according to the general reaction

$$H_2X \rightarrow H^+ + HX^-$$

and

$$HX^- \rightarrow H^+ + X^= .$$
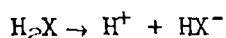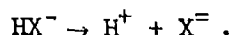
Thus, as the pH increases the dominant species will be in the sequence

$$H_2X \rightarrow HX^- \rightarrow X^= .$$
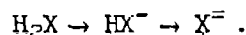
Assuming that H_2X is a better poisoner than HX^-, which in turn is better than $X^=$, the effectiveness of the element as a poisoner should fall off as pH increases. The assumption of the relative effectiveness of the above species is made considering that neutral H_2X will more readily adsorb to the negatively charged electrode than will the anions. At pH 6, HS^- begins to dominate. This compares with the pH 4.5 above which the effectiveness of the poison sharply declines.

(C) In order to explain the loss of effectiveness at very low pH's one would have to assume that in the competition for adsorption sites H_3O^+ would dominate over the promoter hydride. The effect of water and its ionized species H_3O^+ and OH^- shows that these can act as weak hydrogen promoters. Of course H_2O is analogous to H_2S and OH^- to HS^-; and, therefore, when H_2 and H_3O^+ are adsorbed on the surface the adsorption of the H(ads) is slightly greater than when H_3O^+ completely dominates at low pH or at high pH when H_2O and OH^- are present.

The conclusion from this paper concerning the relative effectiveness of the poisoners compared to one another at the condition corresponding to maximum hydrogen saturation in the sample (critical concentration of promoter - Table V) shows the order to be

147

Table V. Values of Promoter Concentrations at Which Maximum
Hydrogen Saturation is Attained in High-Strength
Steels (Data Taken from Newman and Shreir[23])

	Critical Concentration of Promoter		$[H]_{sat}$ (ppm)	pH at Which Maximum Saturation Occurs	pH at Which $H_2X/HX^- = 10/1$
	µg/ml	µmole/ml			
S	60	1870	33	4.5	6
Se	3	38.1	20	2.8	3
Te	45	5850	16	1.8	2.2
P	70	2170	23	3	-
As	1	13.4	12	2	-

$$S > P > Se > Te > As \; ,$$

which is in decreasing order to their bond strengths and binding energies
of the hydrides. However, if one tabulates the critical concentration
of promoter required to attain the maximum hydrogen absorption for the
respective promoter and converts the concentration to a mole basis, it
is apparent that a mole of As or Se in solution is more effective than
the other elements. These calculations are presented in Table V.

Radhakrishnan and Shreir[11] investigated the specific effects
of Group V and VI element additions to electrolytic hydrogen charging,
utilizing the Devanathan technique.[8] Their charging solution was
0.1N H_2SO_4 and the solution at the exit side was 0.1N NaOH. Thin
samples of shim steel (low carbon) were used as the membrane. The
variation in the steady-state permeation current as a function of the
charging current density for the various promoters is shown in Fig. 6.
For arsenic (added as $NaAsO_2$) a linear relationship between ip and the
square root of i_c obtains. Deviation from this behavior occurs for Se
and Te additions. Arsenic is the most effective of the poisoners
studied. The data depicted in Fig. 6 were obtained from the concentra-
tion of promoter which caused the greatest permeation rate. The linear
behavior observed for As seems to indicate that the coupled discharge-
recombination reaction (Table II) holds.

To test the hypothesis that arsine formation was necessary
for enhanced permeation, the authors produced arsine outside the
electrolytic cell containing the steel membrane in 0.1N H_2SO_4 and
bubbled it into the cell. No increase in hydrogen permeation resulted.
The following order of effectiveness was established (unit weight basis
of comparison):
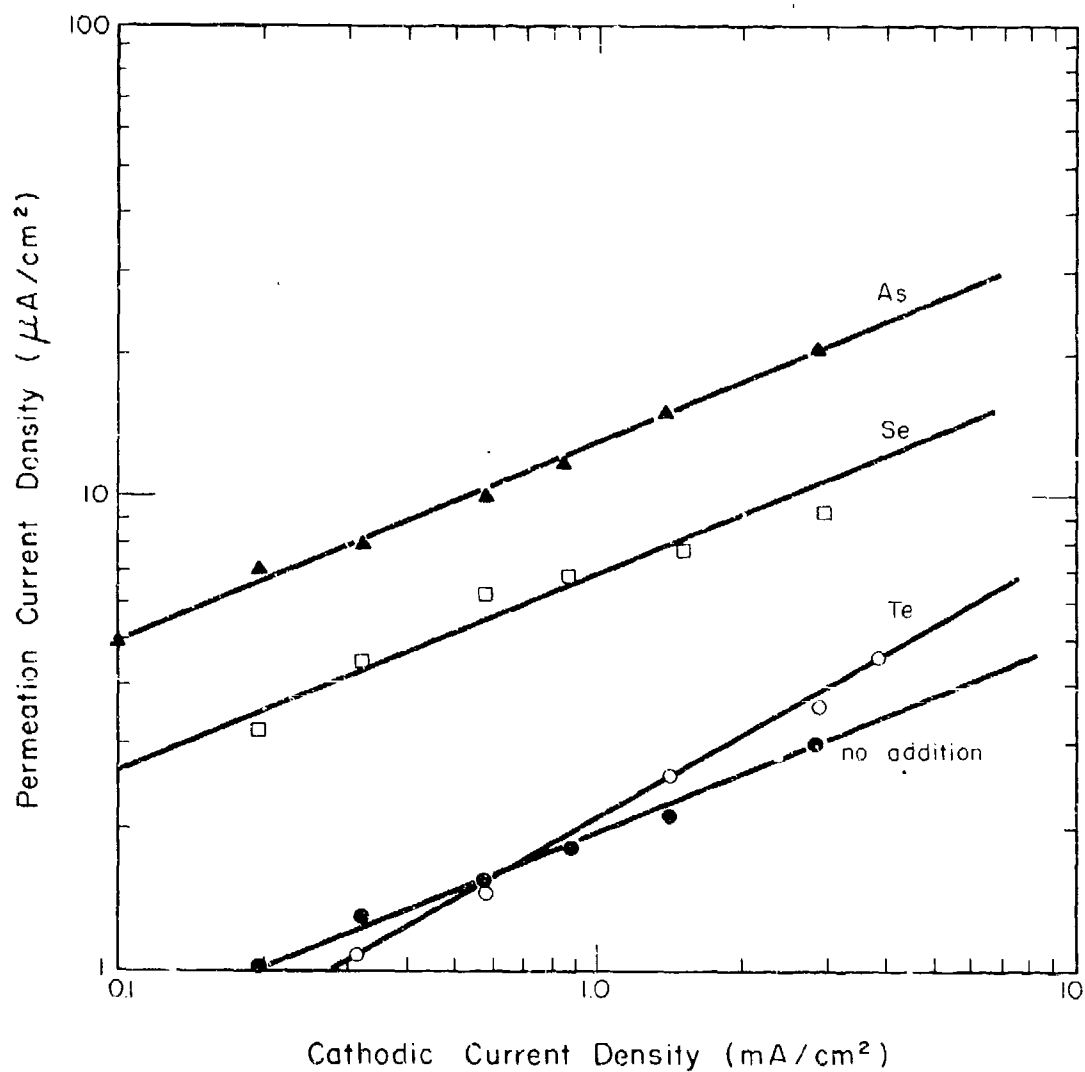
Fig. 6. Relationship Between the Applied Cathodic Charging Current Density and the Steady State Permeation Current; Shim Steel in $0.1N$ H_2SO_4 with Various Additions (from the work of Radhakrishnan and Shreir[11])

$$As > Se > Te > S > Bi \ .$$

The fact that sulfur did not enhance the permeation, as might be expected from the stability of its hydride, and that AsH_3 added to the solution did not increase the permeation rate suggests that the formation of a promoter hydride may not be necessary in all cases to promote hydrogenation. Matsuda and Franklin[24] were able to increase the amount of hydrogen absorbed by iron wires in 2N NaOH with addition of Na_2S when the concentration of the latter was greater than 10^{-5}M. The amount of increase was not large compared to the effect usually noted for acid solutions containing sulfide. Some of their results are shown in Fig. 7.

With regard to the role of electrochemical potential on the efficacity of promoter species, it is well known that sulfides increase the hydrogen entry at the corrosion potential of steel in acid media, potentials at which H_2S is thermodynamically stable. For instance, Kim and Loginow[25] permeated hydrogen through high-strength steel without applied potential to the surface exposed to an acetic acid-sodium chloride solution saturated with H_2S. Radhakrishnan and Shreir[11] noted that sulfide increased the background current in their electropermeation cell, this increase being due to a greater hydrogen entry rate at the corrosion potential.

Work at the OSU Corrosion Center on arsenic

From experiments performed in our own laboratory, when hydrogen was permeated into carbon steel specimens from solutions containing $NaAsO_2$, the effectiveness of the arsenite in promoting hydrogen entry depended on the electrochemical potential maintained at the charging surface.[15] One way of illustrating the effectiveness is by calculating the permeation efficiency which is the ratio of the steady-state permeation current density to the total cathodic current. Figures 8 and 9 taken from this work show the significant increase in permeation efficiency in the presence of arsenite at certain applied potentials. In a general way, the permeation efficiency decreases as the potential is made more active for promoter-free solutions, although the permeation rate itself increases with cathodic polarization. To a first approximation, permeation depends on the surface coverage, θ, of hydrogen atoms which increases with cathodic polarization. The recombination process which competes with permeation depends on θ. Thus, a smaller percentage of the available hydrogen enters the metal at large cathodic overpotentials but because the total current is large in this region, the permeation current is high.

When arsenite is present in the solution, permeation of hydrogen is suppressed at the corrosion potential. In the potential region of 100-300 mV cathodic to the corrosion potential, the permeation rate and the permeation efficiency from arsenite-containing solutions are less than those for the poison-free solutions. In this potential range, reduction of arsenite to elemental arsenic is occurring. Thus,
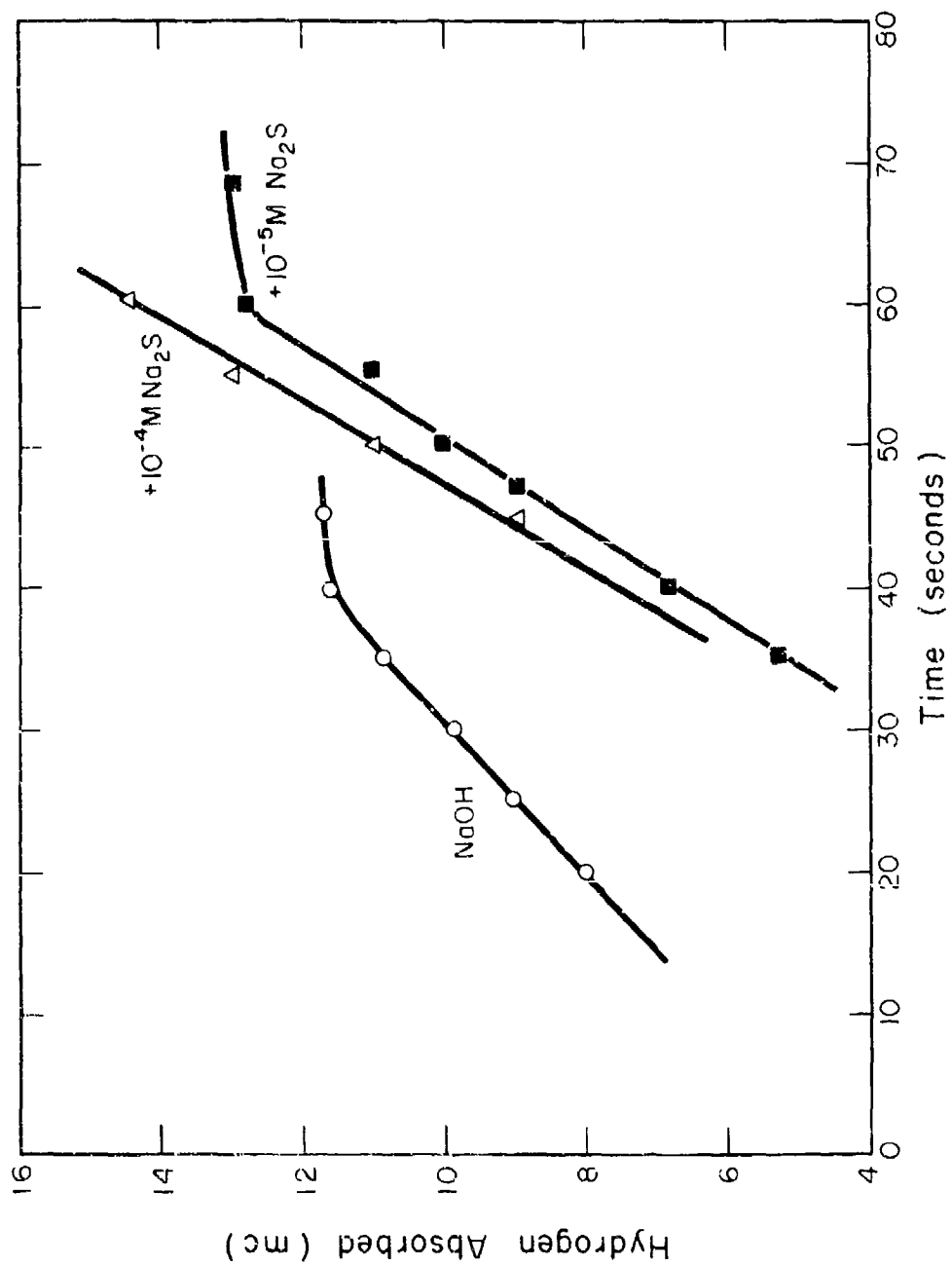
Fig. 7. Rate of Hydrogen Absorption in Iron Wires Polarized in 2N NaOH with and without Na_2S Additions (from the work of Matsuda and Franklin[24])

151
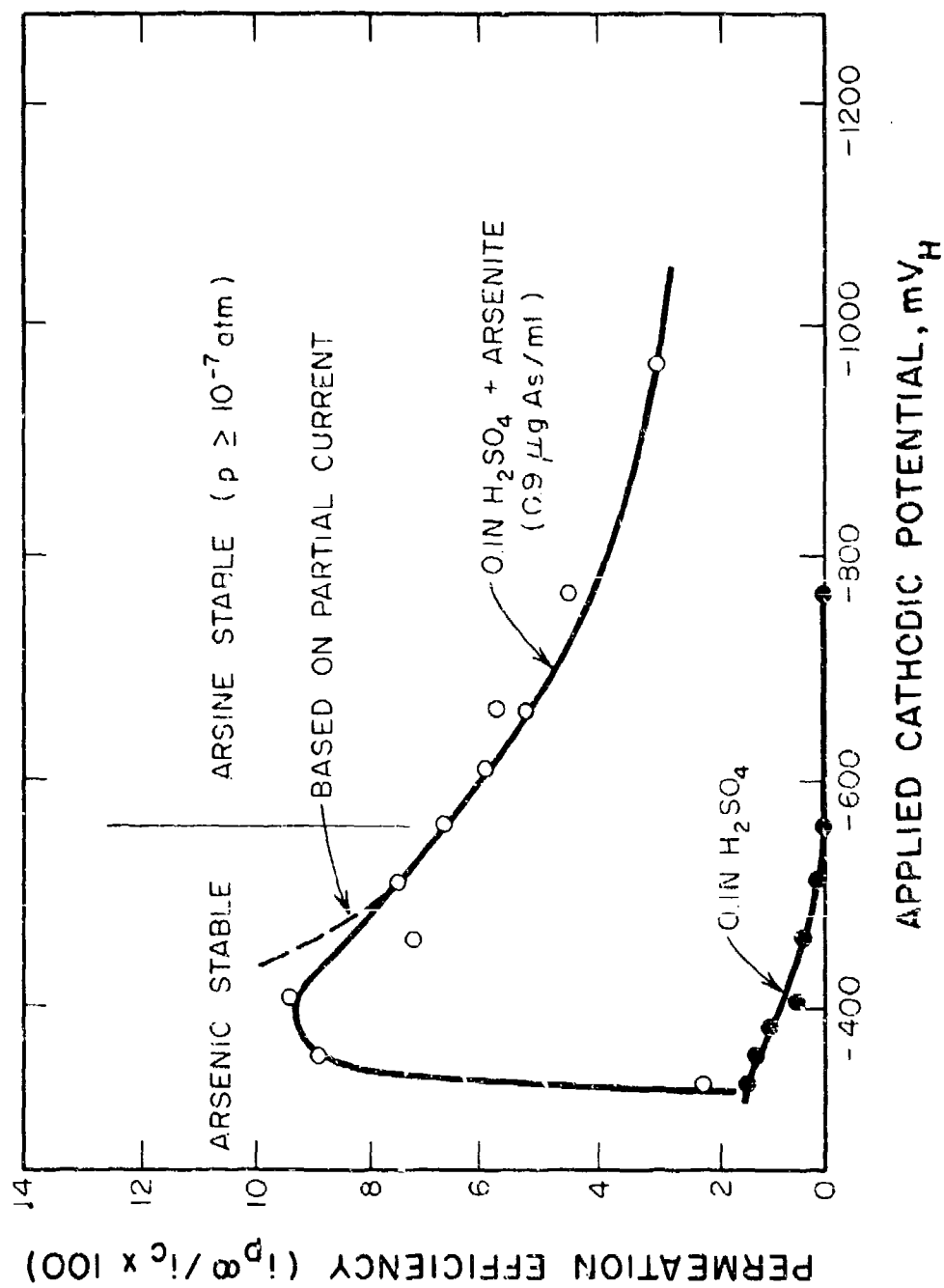
Fig. 8. Hydrogen Permeation Efficiency of Shim Steel Specimens Polarized
Cathodically in 0.1N H_2SO_4 with and without Arsenite Additions
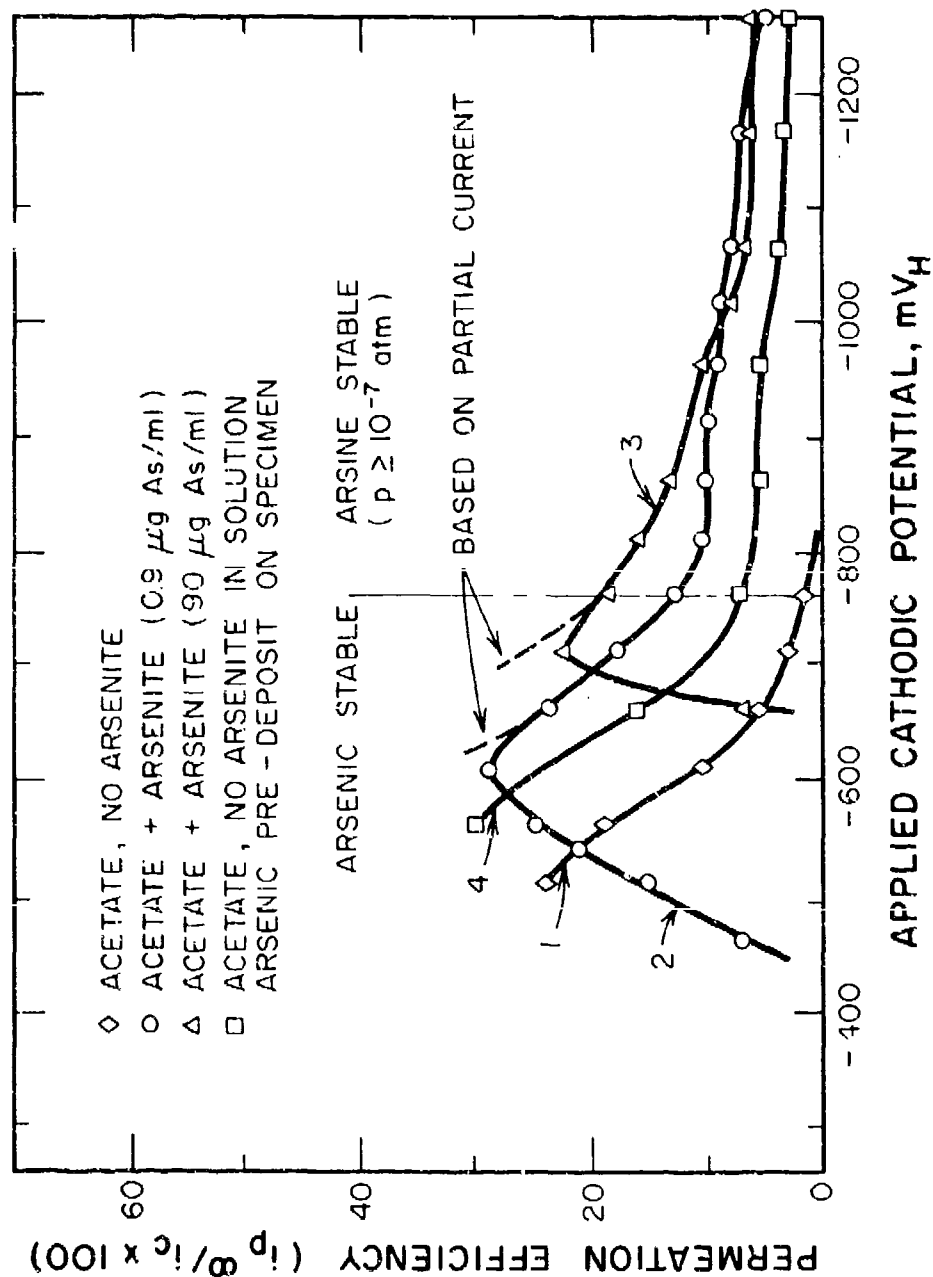
Fig. 9. Hydrogen Permeation Efficiency of Shim Steel Specimens Polarized Cathodically in Acetate Buffer Solutions with and without Arsenite Additions

153

arsenite acts as an inhibitor of the HAR at the corrosion potential and at small cathodic overpotentials. The extent of this inhibition depends on the arsenite concentration. As the concentration increases, a greater cathodic overpotential must be applied before hydrogenation of the specimen occurs. Once the steel specimen is sufficiently cathodically polarized, however, both the HER and HAR are accelerated. The permeation efficiency increases and reaches a maximum; a decrease in the permeation efficiency follows, as in the arsenite-free solutions. Figure 9 (curve 4) shows the effect of pre-depositing a thin plate of arsenic on the surface of the steel sample. The behavior is like that of the arsenite-free solution but the overall efficiencies are higher. The greatest permeation efficiencies take place when arsenic and hydrogen are co-reduced and this occurs at modest cathodic overpotentials.

The co-existence equilibrium potential between As at unit activity and AsH_3 at a fugacity of 10^{-7} atm is indicated in Figs. 8 and 9. From some of the work previously cited, it was concluded that formation of the hydride phase was a necessary condition for enhancement of the entry step. The particular value of 10^{-7} atm for AsH_3 was established by Angerstein-Kozlowska[30] who found that iron wires were not embrittled (torsion test) until the potential was made more negative than this co-existence potential. In the above figures it appears that significant hydrogen entry occurs before formation of arsine so that elemental arsenic or arsenite may be the species responsible for the effect. Solid arsenic sub-hydrides have also been reported.[26] It is reported that the current efficiency in producing AsH_3 electrochemically from As is only 1-2% in acid solution. This means that the reaction requires considerable overpotential before much arsine evolution occurs.[27] Other studies have also revealed very little arsine formation in spite of very negative potentials.[28-30] Thus, the presence of arsine may not be necessary for effecting hydrogenation in all cases involving arsenic compounds as poisons.

Corrosion-inhibiting properties of promoters

Hudson and Stragand[31] demonstrated the significance of arsenic compounds acting as inhibitors for the HAR as well as the HER and hence the dissolution reaction of the metal. At extremely small concentrations, arsenic (added as As_2O_3) accelerated the corrosion of a mild steel in a 2N H_2SO_4 pickling bath. At a concentration of 4 µg/ml the corrosion was inhibited and thus the HER. At concentrations of 8 µg/ml and greater, absorption of hydrogen was inhibited. The high sensitivity of the HER to the concentration of arsenic suggests two opposing tendencies. Increasing the i^0 for the HER accelerates the reaction. Adsorption of some species influences the adsorption of hydrogen, tending to increase the overpotential of the HER. Presumably, the first effect occurs at the lowest concentrations perhaps by an increase of the H+ concentration in the double layer. Greater concentrations of arsenite in solution result in adsorption of AsO_3^- or in its reduced form as elemental As.

Influence of Group V and VI elements
on polarization behavior

Polarization curves illustrate the corrosion-inhibiting properties of arsenic-containing solutions. The polarization curves, shown in Fig. 10, indicate that the anodic kinetics as well as the cathodic kinetics are greatly decreased. The HER is the principal cathodic reaction because the small concentration of promoter in solution dictates a small limiting current for the reduction of As^{+3} to As^{O}. However, the HER is suppressed until the potential is made several hundred millivolts cathodic. According to one explanation, the i^{O} for the HER on metallic arsenic is much smaller than that on iron ($\approx 10^{-12}$ A/cm^2 compared to 10^{-8} on Fe).[35] This increase in the overpotential increases the chemical potential for the adsorbed hydrogen, thus driving a larger fraction of it into the metal. Additionally, adsorption of the reduced arsenic interferes with hydrogen atom recombination. The S-shape of some of the polarization curves is indicative of adsorption effects.

Beloglazov[32] carried out a systematic investigation of the polarization behavior of promoter compounds added to $0.1N$ H_2SO_4. In Fig. 11 the curves are grouped into two classes, those which generally decrease the cathodic currents (As and Sb) and those which generally increase the cathodic currents (Se and Te). All of these promoters are added in an oxidized form so that reduction to the elemental phase or to the hydride occurs along with the HER. These are deposited on active parts of the polarized specimen, followed by H^+ discharge on the parts of the electrode covered by deposits of the promoter elements. The electron work function is less for As, Sb, Se, and Te than for Fe, thus favoring the discharge step on areas covered by these elements. Chemical or electrodic recombination of hydrogen adatoms occurs preferentially on the iron surface because the iron-hydrogen bond is less than the As-H, Se-H bonds, etc. For the smaller values of M-H bonds less activation energy is required to desorb and recombine the hydrogen adatoms.

There appears to be some conflicting explanations attached to the influence of the promoter species on the shape of the polarization curve. For transition metals like iron, according to Bockris and Conway,[33] as the work function of the metal increases, the exchange current density of the HER decreases (and therefore the "hydrogen overpotential" for a given current density). All of the promoter elements examined by Beloglazov have lower work functions than iron. Thus, these elements should decrease the overall HER kinetics on iron. Arsenic and antimony behaved in this fashion. On the other hand, if the metal-hydrogen bond energy is increased, the heat of adsorption for hydrogen is increased (in the sense that it becomes more exothermic). As a consequence, the overall HER kinetics are accelerated and the hydrogen overpotential at a given current density is decreased. Selenium and tellurium (at some potentials) behaved in this manner.
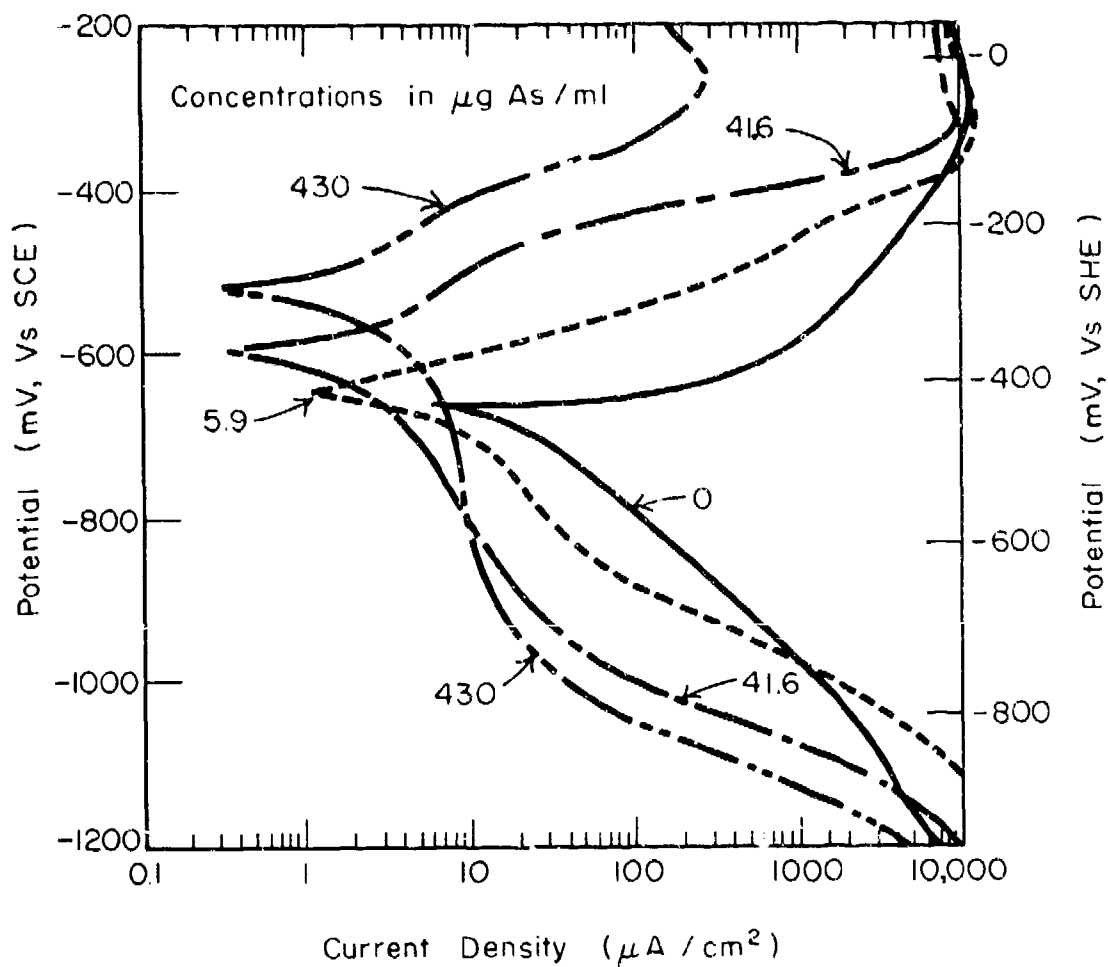
Fig. 10. Polarization Behavior of Shim Steel in Acetate Buffer Solutions with and without Arsenite Additions
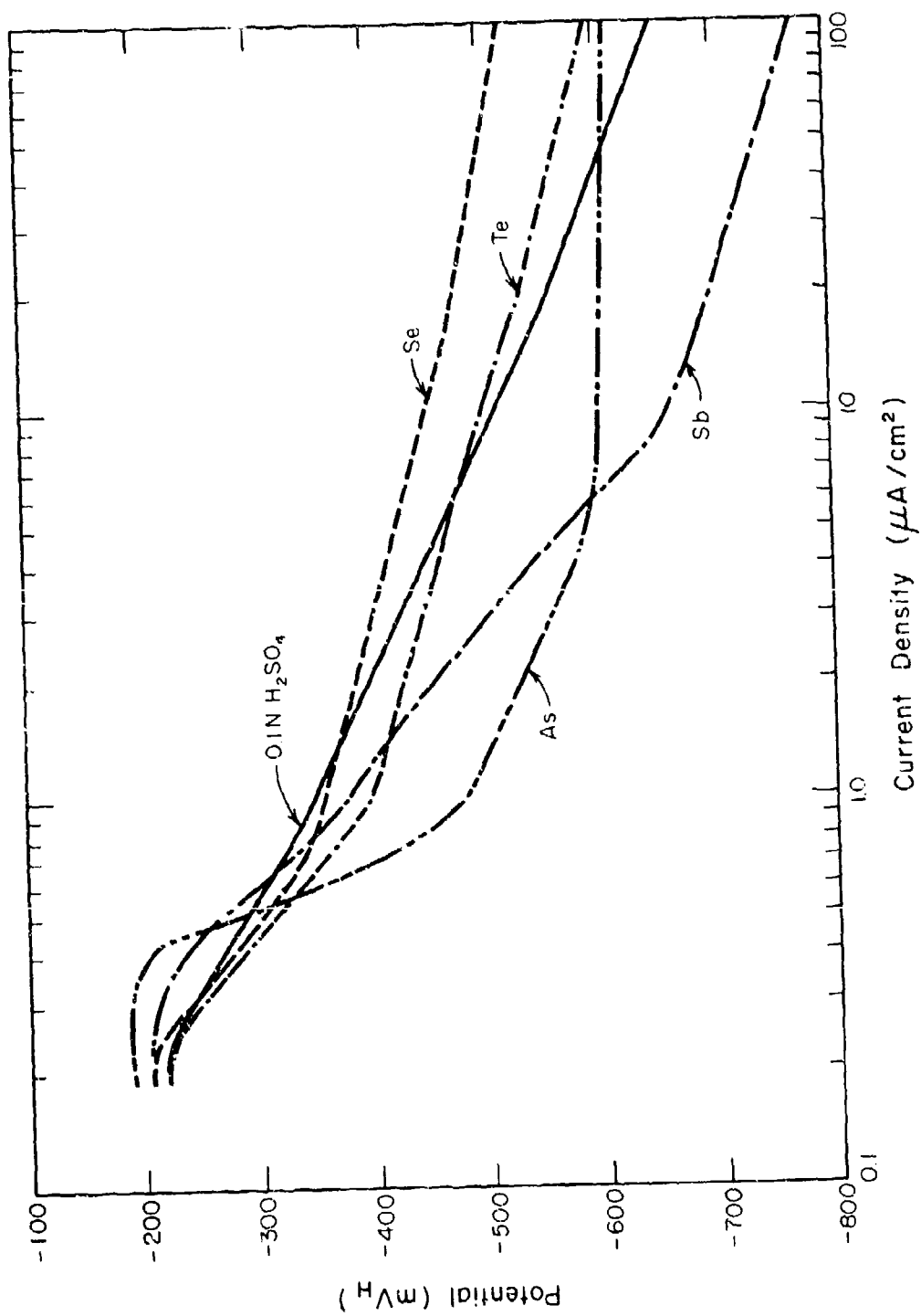
Fig. 11. Cathodic Polarization Behavior of Carbon Steel in 0.1N H_2SO_4 with and without Various Promoter Additions (from the work of Beloglazov[32])

Adsorption effects of promoter elements

Adsorption of specific molecules or ions occurs near the potential of zero charge. In the absence of all adsorbable substances the E_{pzc} for iron is about -400 mV_{SHE}.[34] Thus, the E_{pzc} is slightly cathodic to the corrosion potential of iron in acid solutions. Adsorption changes the shape of the electrocapillary curve (potential vs. surface energy) so that E_{pzc} is a function of the nature and concentration of the adsorbed species.

Adsorption effects change the course of polarization curves by adding an overpotential-type term due to the creation of the modified double layer.[35] Symbolically, for cathodic polarization,

$$\eta = \frac{-RT}{(1-\alpha)zF} \cdot \frac{i_c}{i_o} + \left(\frac{\alpha}{1-\alpha}\right)\psi , \qquad (8)$$

where ψ is the potential change of the metal due to the adsorbed species and has the same sign as the charge of the adsorbed species. Thus, adsorption of anions increases the cathodic overpotential. The sign of ψ for overall neutral molecules depends on the unequal charge distribution occurring among its component parts. The increase in overpotential results in S-shape polarization curves.

For comparison, the polarizability of a species is a useful index for ascertaining the adsorption tendency. The polarizability is a measure of the deformability of the charge distribution when the ion or molecule is placed in an electric field such as the double layer. Species with high polarizabilities respond more readily to the electric field and form a dipole with the surface metal atoms. The charge arrangement in the dipole tends to oppose the field.

The following Table gives some polarizabilities of species that are of interest in the hydrogenation of metals. The information is from West, who in turn collected it from various references.[35]

One sees from Table VI that anions are by far the most polarizable type of species and that cations are relatively weakly polarizable. This is consistent with observation that cations are not strongly adsorbed. Species more polarizable than water will tend to displace the latter when present in aqueous solutions.

Hydrides in gas phase hydrogen charging

If the hydrides of promoter elements are the form responsible for accelerating hydrogen entry, these hydrides ought to be effective in the gas phase. Experiments conducted by bombardment of H atoms with and without the presence of H_2S are summarized below. Specimens of

158

Table VI. Polarizabilities of Some Ions and Molecules of
Interest in Hydrogenation of Metals

Species	Polarizability (cm^2/mole)	Species	Polarizability (cm^2/mole)
S^-	22	$SO_4^=$	3.9
I^-	19.1	NO_3^-	3.6
HS^-	13.3	ClO_4^-	3.3
Br^-	12.5	F^-	2.6
Cl^-	8.9	NH_3^-	5.6
CNS^-	8.6	H_2O	3.7
CN^-	8.4	Pb^{++}	9.3
$O^=$	7.7	K^+	2.5
OH^-	4.9	Na^+	0.5

Armco Fe were exposed to the electrodelessly discharged H gas at room
temperature and 0.1 atm pressure. The permeation of hydrogen was
measured. In addition the hydrogen was partially ionized in some
experiments and this had a substantial influence on the permeation.
The results, using two specimen thicknesses, are given below.

Table VII. Steady State Permeation Rate of Hydrogen through
Armco Fe Bombarded by H Atoms (from Palczewska
and Ratajczykowa[1,2])

Species at Interface	Thickness = 0.078 cm	Thickness = 0.032 cm
H	1.3×10^{-8}	4.6×10^{-8}
$H + H_2S$	9.1×10^{-8}	2.5×10^{-7}
H^+	2.1×10^{-7}	3.3×10^{-6}
$H^+ + H_2S$	2.6×10^{-6}	6.3×10^{-6}

Permeation values are expressed as cm^3H/cm^2 surface·second. As
expected, the permeation values are greater for the thinner sample.
Addition of H_2S (concentration 0.2 mole %) increases the permeation
rate several-fold, but the most notable increase results when protons

are present. Also, H₂S increases the permeation rate in the presence of protons. These results indicate not only the efficacy of H₂S in gas phase charging, but also the importance of hydrogen entry as protons. Because H₂S catalyzes hydrogen entry from protons, it appears that H₂S may hinder proton-electron combination as it does atom-atom combination.

Other promoter species

When cyanide ion was added to a NaOH solution, the potential of the metal changed some 200 mV in the negative direction because of preferential adsorption of CN⁻.[36] This adsorption was verified by using C_{14} tracer in the cyanide. The characteristics of the surface concentration of cyanide as a fraction of the bulk concentration led the investigators to conclude that adsorption followed a Temkin or Freundlich isotherm; that is, the enthalpy of adsorption decreased with coverage of cyanide ion. The activation energy for cyanide adsorption increased with concentration. These two effects (decrease of H_{ads} and increase of E_a) would tend to decrease the tendency for further adsorption. This effect is important with regard to hydrogen entry because if the surface were completely covered, hydrogen-ion reduction would not occur. A subtle interaction between CN⁻ and H as adsorbates is required for enhancing entry of the latter. Desorption of cyanide occurs if the specimen is polarized more cathodically, but this is a slow and irregular process. Similarly, Bockris et al.[9] found an increase in the hydrogen permeation rate for hydroxide solutions containing cyanide.

Bockris et al. found that KI additions to 0.1N H₂SO₄ significantly increased the hydrogen permeation current in Armco iron specimens. The permeation rate increased at a given potential with an increase of the iodide concentration. The permeation current varied with the square root of the charging current in the same way as reported for arsenic.[11] From Table VI, iodide has a large polarizability and would be expected to chemisorb readily.

These same authors found a permeation current increase when naphthalene, an aromatic hydrocarbon, was added to sulfuric acid solution. However, the effect was not as large as for the above promoters because of the small solubility of naphthalene in water.

Elsewhere it is reported that lead, mercury, and tin salts act as hydrogen promoters.[11,47] These elements are co-reduced along with hydrogen during cathodic charging. In some cases they are reduced spontaneously as a displacement reaction with iron. Their effect as promoters is generally much smaller than the other species (Group V and VI elements, cyanide or iodide).

Hydrogen Entry Inhibiting Species

A few substances, when added to solution, substantially reduce the entry rate of hydrogen. The organic nitriles, as a class, have

this property. Some results obtained by Bockris et al.[9] where they added various concentrations of aliphatic nitriles (valeronitrile - $CH_3(CH_2)_3CN$) and aromatic nitriles (benzonitrile C_6H_5CN and naphthonitrile $C_{10}H_7CN$) to $0.1N$ H_2SO_4 are shown in Fig. 12. It is interesting to note that by itself naphthalene promotes entry as does cyanide ion. Elsewhere, acetonitrile is said to decrease hydrogen absorption.[24] These molecules probably adsorb vertically thereby restricting the access of hydrogen ions to the surface, the nitrile group being closest to the surface. Evidently, comparison of the adsorption characteristics of these molecules with those that promote hydrogen are important mechanistic clues. Dibenzyl sulfoxide is reported to be an effective inhibitor of hydrogen entry.[18] Some strong oxidizing species tend to discourage the HAR. The weak absorption effects in nitric acid have been previously noted. Chromate is also believed to lower the absorption rate of hydrogen, and dissolved oxygen may act similarly.

Effect of Strain

The effect of applying a uniaxial tensile stress to an Fe specimen during cathodic hydrogen charging has been investigated by Beck et al.[38] The effect of tensile strain increases the concentration of absorbed hydrogen because of dilation of the interstitial lattice sites where hydrogen lodges. The diffusivity of hydrogen did not change from the unstressed to the stressed condition so that the increase in permeability measured by these authors was due to the increase in solubility. From simple elasticity theory, the concentration in stressed material is given by

$$C_\sigma = C_0 \exp(6\sigma^2 V/2YRT) , \qquad (9)$$

where C_σ is the concentration under tensile stress σ, C_0 is the concentration in the absence of stress, V is the molar volume of iron, and Y is the yield stress. The factor 6 comes from the coordination of octahedral interstitial sites and the term $\sigma^2/2Y$ represents the elastic strain energy. When sheet specimens of high-strength steel were subjected to a static tensile stress during hydrogen charging, the increase in concentration measured during the experiment agreed closely with the result predicted from the above equation.

With regard to the promoter species, the presence or absence of these substances seems to be less important during dynamic straining. The work of Smialowski illustrates this point.[22] In these experiments he twisted wires in situ until fracture and defined an embrittlement index $F = (n - n_H)/n \times 100$, where n_H is the number of twists needed to fracture the hydrogenated specimen and n is the number of twists needed to fracture a non-hydrogenated specimen. In Fig. 13 taken from this paper, the effect of As_2O_3 or SeO_2 additions to H_2SO_4 increased the embrittlement of 0.56% C steel wires only slightly. In static
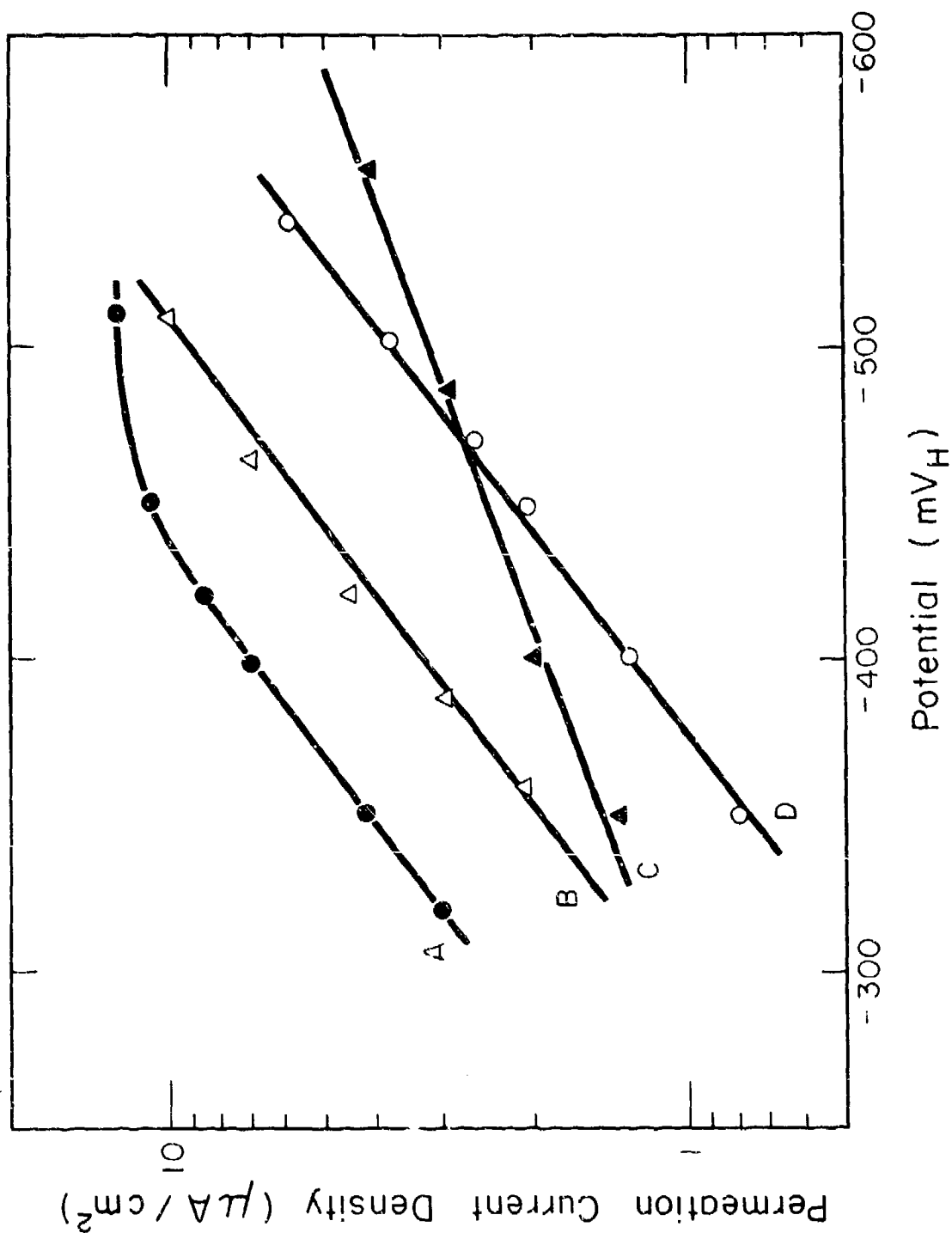
Fig. 12. Effect of Various Nitrile Additions to 0.1N H_2SO_4 in Reducing the Hydrogen Permeation in Armco Iron. (A) 0.1N H_2SO_4 Only; (B) + 10^{-1} M Valeronitrile; (C) + 10^{-4} M Naphthonitrile; (D) + 10^{-2} M Benzonitrile (from the work of Bockris, McBreen, and Nanis[3])
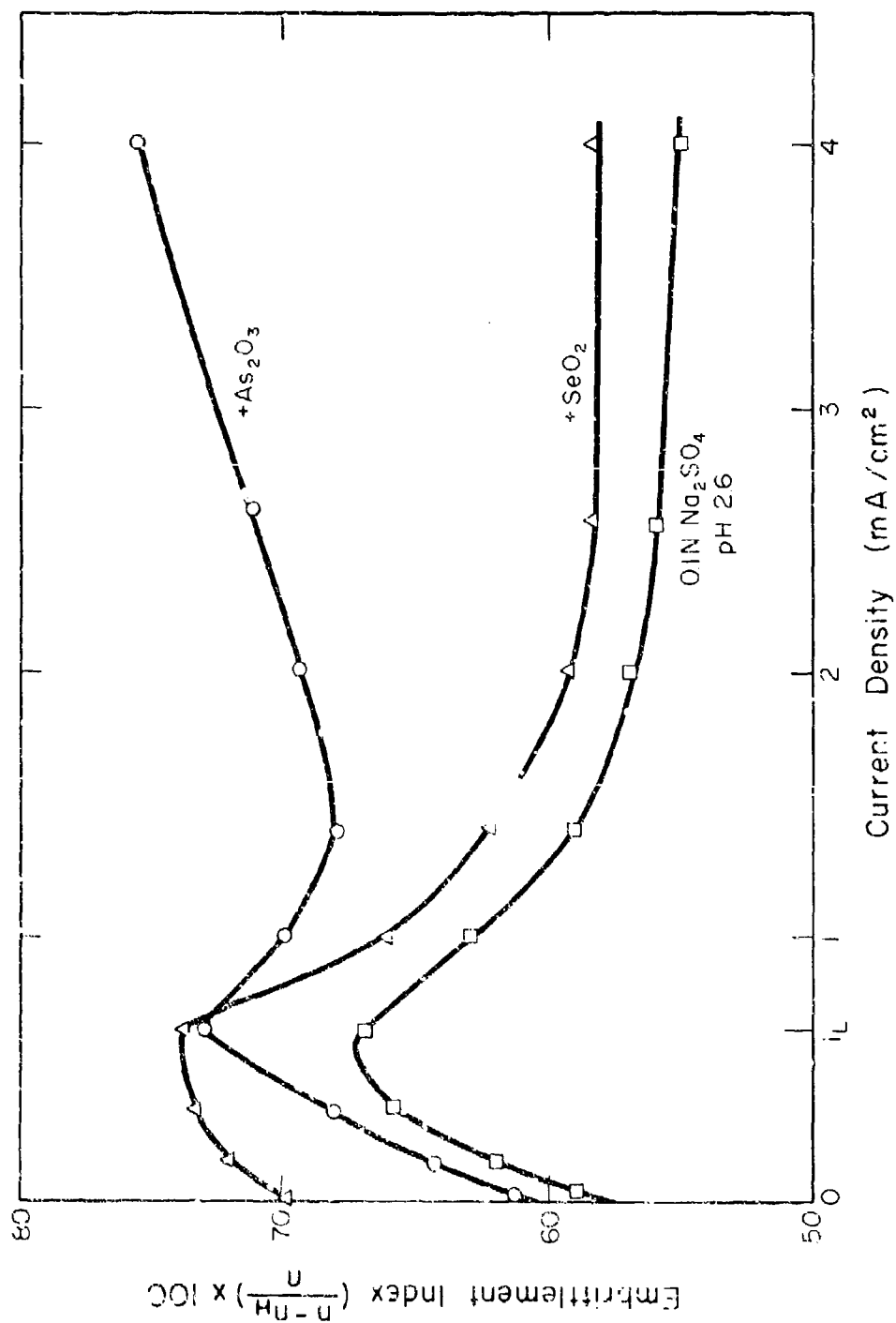
Fig. 13. Effect of Various Promoter Additions to Acidified Na_2SO_4 Solutions on the Embrittlement of Iron-Nickel Wires (from the work of Smialowski[22])

experiments, the presence of these compounds increases the hydrogen entry enormously and consequently the embrittlement tendency. The maximum embrittlement in the torsion experiments occurred near the static-limiting current density and the subsequent decrease in the embrittlement index at current densities beyond this value may be due to alkalinization.

Similar effects were noted when torsion-strained austenitic stainless steel wires were exposed to solutions containing poisons and without poisons. The embrittlement index for this steel was lower than that for the plain carbon steel.

The comparatively small increase in the embrittlement index in the presence of poisons suggests that slip bands form more rapidly than adsorption of these compounds. Thus, hydrogen entry takes place largely on uncontaminated and abundant fresh surfaces without benefit of the catalytic properties of the poisons.

Further Discussion on Mechanism
of Promotion

Unfortunately no clear-cut general explanation can be given as to why certain species act as hydrogenation promoters. A number of possible considerations are offered and discussed below.

(A) Adsorption strength of the species

Unquestionably promoter species are intimately attached to the surface but the question is why do some and not all strongly adsorbed species promote hydrogen entry. Obviously size and geometry of the adsorbed species determine the availability of other sites for hydrogen discharge and recombination. If coverage by the adsorbed species is nearly complete, then all cathodic reactions are inhibited and both the HER and HAR rates are drastically reduced. Therefore, promoter species are operative when their surface coverage is considerably less than unity.

The rate of hydrogen entry is expressed as $k_e x$, where x is the fraction of surface not covered by the promoter species, and the rate of hydrogen recombination by $k_r x p$, where p is the probability that adjacent sites are uncovered by poison. As the probability factor drops, entry is favored over recombination. Evidently, there is an optimum coverage factor for the promoter with regard to its effectiveness. If the coverage is too high, the entry rate is low because few sites remain for hydrogen adsorption. If the coverage is too small, the entry rate is low because the probability of adjacent hydrogen adatoms is high. These effects are noted in Newman and Shreir's and and Radhakrishnan and Shrier's papers where certain concentrations of promoters produce maximum absorption or permeation contents.

164

The geometry of the adsorbed species affects its ability to promote. Vertical adsorption of large molecules (organic nitriles) hinders the approach of hydrogen ions to the surface. Likewise, the geometry of the adsorption pattern is important. If large gaps of uncovered surface are left between adsorbed molecules, hydrogen atoms can adsorb and recombine in these gaps.[39]

(B) Structure of the double layer

Specific adsorption changes the structure and composition of the double layer. Vertical adsorption of large organic molecules may hinder hydrogen approach by increasing the thickness of the double layer with respect to the same molecules adsorbed horizontally. If adsorption increases the concentration of hydrogen ions in the double layer, hydrogen entry may be promoted. With regard to the double layer in its diffuse sense, adsorption of the promoter molecule would be positive end against the negatively polarized metal with the negative end of the molecule attracting hydrogen ions.

(C) Surface and bond energy considerations

Arguments have been offered proving that lowering of the metal-hydrogen bond energy in the presence of promoter species accelerates the HAR. On the contrary, arguments asserting an increase of promotion effect by raising the bond energy have also been made. The key idea is not so much the metal-hydrogen bond energy per se, but, rather, its effect on the activation energy for the desorption (recombination) step or the absorption step, these last two being competitive.

The essential concern is that the metal-hydrogen bond influences the heat of adsorption;

$$\Delta H_{ads} = 2E_{M-H} - E_{H-H},\qquad (10)$$

where E_{M-H} represents the metal-hydrogen bond and E_{H-H} the hydrogen-hydrogen bond. A more exothermic ΔH increases the extent of adsorption and entry should be enhanced by the higher concentration. Therefore an increase in the metal-hydrogen bond energy (in the algebraic sense) should promote entry. On the other hand, McBreen and Genshaw[4] advanced the idea that a lowering of the bond energy, (that is, a decrease in the algebraic sense) increased the activation energy for recombination, thereby promoting entry. Their argument was based on the slope of potential energy-distance (Morse) curves.

The presence of strongly adsorbed molecules may disturb the bonding between metal atoms so as to decrease their cohesiveness. Perturbations such as this may then increase hydrogen entry by increasing the lattice interstices near the surface. Thus, the hydrogen entering these expanded regions of the lattice would encounter less of

an activation barrier. From diffusion considerations of hydrogen in iron, the activation energy associated with this process is expansion of the interstitial site for accommodating the larger hydrogen atom.[38] Furthermore, the strong adsorption may create defects in the metal. Hydrogen atoms have a strong attraction to dislocations, for example, and an increase in the dislocation density near the surface may locally increase the entry rate.

(D) Uniqueness of the promoter hydride

The most pronounced effects for Group V and VI elements appear most generally where the hydrides of these elements are stable. These hydrides appear to adsorb strongly and compete with hydrogen for available sites. Adsorption of the hydride phase can result in an increase in the surface concentration of hydrogen by such a scheme as

$$2M + AsH_3 \rightarrow MAsH_2 + MH .$$
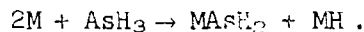
The experiments cited on charging from the gas phase emphasize the uniqueness of the hydride phase in catalyzing the hydrogen entry.[12] However, in a few cases involving As at potentials more positive than that corresponding to AsH_3 formation and S at alkaline pH's, enhanced entry occurred despite the lack of a stable hydride phase.

(E) Electronic structure considerations

Because the hydrogen absorption characteristics change from one transition metal to another, it is believed that the electronic structure, and in particular the d-electron band, influences significantly the solubility of hydrogen. Platinum, palladium, and nickel have higher hydrogen solubilities than iron. These first metals have a greater % of d-band character to the bonding. The cohesiveness of the metal is related to the metal-hydrogen bond energy by

$$E_{M-H} = \frac{1}{2} \left(E_{M-M} + E_{H-H} \right) + \text{ionic term} . \tag{11}$$

An increase in E_{M-M} increases E_{M-H}. The greatest cohesiveness is found in the middle of the transition group (Group V and VI). The cohesive properties decrease in going from these groups through Group VIII. The role of promoter species may be to increase the electron density of atoms near the surface. As a group the promoters are electron rich and may, for example, make "promoted" iron more electronically like nickel.

(F) General sense of poisoning action

The poisoning effect of the species described above has perhaps some relationship to poisoning in the biological sense.[2] Many of these species are extremely toxic. If many life processes occur by electrochemical mechanisms, the presence of "poisons" may encourage the breakdown of large molecules or prevent the combination of elementary entities such as nascent hydrogen and possibly oxygen. It is interesting to point out that, depending on the concentration, poisons can accelerate or decelerate reactions like the HER and this effect may be akin to the exhilarating effect of taking tiny doses of arsenic and the deadly effect to taking too much.

ROLE OF METALLURGICAL VARIABLES ON THE HAR

The metallurgical structure and composition influence the solubility of hydrogen. In general, it is difficult to assess the solubility without taking into account the diffusivity. The product of solubility and diffusivity is the permeability. This last entity in the quantity is usually determined experimentally.

The solubility, diffusivity, and permeability are strong functions of temperature and follow empirical Arrhenius type equations of the form

$$C = A_c p^{1/2} \exp(-B_c/RT) ,$$
$$D = A_D \exp(-B_D/RT) , \quad \text{and} \tag{12}$$
$$P = A_p \exp(-B_p/RT) .$$

Values of these constants are given in the following table for alpha iron, a high-steel, and an austenitic stainless steel. In particular, one notes the high value of the activation energy for diffusion in the austenitic material compared to the ferritic. At room temperature D in austenitic stainless steel is about 10^{-10} cm^2/sec compared to 10^{-5} cm^2/sec for pure iron. On the other hand, the solubility in the austenitic structure is much greater than in the ferritic.

Compositional Effects

The purpose of this section is to present some of this work, especially with respect to the compositional variable and how it influences permeability, diffusivity, or solubility.

Iron-chromium alloys

The permeation of Fe-Cr alloys was investigated by Bockris, Genshaw, and Fullenwider.[9] The permeation current increased with increasing temperature but decreased for increasing chromium content

Table VIII. Value of the Constants in Expressions for
Concentration, Diffusion, and Permeation
of Hydrogen in Iron and Iron-Base Alloys[40]

Materials	A_c	A_D	A_p	B_c	B_D	B_p
Alpha Iron	3.45×10^{-3}	2.33×10^{-3}	8.04×10^{-6}	27.6	6.68	34.3
4130 Steel Quenched and Tempered	2.29×10^{-3}	3.56×10^{-5}	8.17×10^{-6}	27.2	7.95	35.2
304 Stainless Steel	8.6×10^{-3}	2.72×10^{-2}	2.34×10^{-4}	9.6	54.4	64.0

units: A_c (complicated) B_c (kcal/mole)   C (moles/cm^3)

A_D (cm^2/sec) B_D (kcal/mole)   D (cm^2/sec)

A_p (moles/cm$^2 \cdot$sec) B_p (kcal/mole)   P (moles/cm$^2 \cdot$sec)

P (Newtons/m^2)

at a given temperature. Diffusivities and solubilities were calculable
from these data by analysis of the permeation current transients. It
was found that the diffusivity fell off sharply as the chromium content
increased, a 24% Cr alloy having a diffusivity of less than 1/1000 that
of iron at room temperature. The hydrogen solubility increases with
the chromium content at a given temperature. This panel shows how the
combined effects of diffusivity and solubility determine the permeability.
Although the solubility increases sharply with increased Cr in the alloy,
the diffusivity drops more abruptly, and, therefore, the permeability
decreases an order of magnitude or so.

Iron-nickel alloys

Beck et al [41] measured the hydrogen permeation in a series of
iron-nickel alloys and found that the solubility increased and the
diffusivity declined sharply with increasing nickel concentration. The
hydrogen solubility increased more slowly than it did for chromium
contents. This is shown in the following table.

Steels

The role of carbon in influencing the permeation, diffusion,
and solubility behavior in steels is not so clear, because the form of
the carbide is significant. Thus, it is difficult to sort out the role
of carbon alone from the role of the steel microstructure. In liquid

Table IX. Solubility of Hydrogen in Fe-Cr and
Fe-Ni Alloys at Room Temperature

Alloy	Solubility (moles/cm³)	(ppm)
Fe	1.5×10^{-8}	0.12
Fe, 5% Cr	1.0×10^{-6}	7.8
Fe, 12% Cr	2.0×10^{-6}	15.6
Fe, 18% Cr	2.5×10^{-6}	19.5
Fe, 5% Ni	2.0×10^{-8}	0.16
Fe, 10% Ni	9.0×10^{-8}	0.70
Fe, 15% Ni	1.2×10^{-7}	0.94
Fe, 20% Ni	3×10^{-7}	2.3
Fe, 40% Ni	7×10^{-6}	54.5

iron, carbon drastically reduces the hydrogen solubility.[42] The same chemical tenaency ought to be operable in the solid phase; however, this effect is obscured by the precipitation of carbon and subsequent metallurgical effects of the carbide that affect the local solubility of hydrogen (interfaces, strain fields, etc.).

It is the general conclusion that carbon reduces the hydrogen permeation through steel, regardless of the form in which the carbon appears. This is true at moderate temperatures, above 800°C the hydrogen permeation increases significantly after an incubation time. Decarburization by methane formation, which can ccur at these higher temperatures, is probably negligible at room temperatures.[43]

Room temperature determinations of the diffusivity in low carbon steels fall in the $10^{-5} - 10^{-8}$ cm²/sec range[44] as do those for pure iron. Radhakrishnan and Shreir performed electro-permeation experiments on a shim steel (0.17%C) and found that the permeability and diffusivity were lower for the steel than for pure iron (values of the latter being 5.5×10^{-6} cm²/sec for the steel and 1.4×10^{-5} cm²/sec for the iron, both in the annealed condition).[45]

The electro-permeation of AISI 4340 steel diaphragms was determined over the temperature range 10-75°C by Beck et al.[38] The room temperature diffusivity is 1×10^{-9} cm²/sec, much lower than the 10^{-5} cm²/sec value of D for alpha-Fe.

Metallurgical Effects

Effect of annealing and grain size

Radhakrishnan and Shreir[45] investigated the permeabilities between iron in the as-received (cold-rolled) conditions and in the

annealed condition. They found that the permeability increased for pure Fe (spectrographically pure iron, 5 mils thick) in the annealed condition. Beyond the initial annealing at 650°C for 1 hour there was no noticeable change in the permeation rate for specimens annealed at 600°F for up to 7 hours, at 700°C for up to 5 hours, and at 850°C for 4 hours followed by furnace cooling. The microstructure of the specimens showed grain growth with increased temperature and time at temperature. In the last condition the grains grew to the thickness of the specimen. Diffusivities calculated by analysis of the rise transient of the permeation current (ionization of dissolved hydrogen at exit surface) yielded values of 1.4×10^{-7} cm^2/sec for annealing at 650°C for one hour. Additional annealing time at this temperature or at higher temperatures had practically no effect on the diffusivity (or on the permeability). Evidently the as-received cold-rolled condition has a tendency to trap hydrogen and the initial annealing removes the source of the traps.

When these investigators performed the same experiment on shim steel (0.17%C) they found that the permeation current was lower for the annealed condition than for the "as-received" condition, however, the diffusivity of hydrogen was higher for the annealed specimen. In addition these experiments show that in the annealed state the diffusion is principally through the lattice and that increasing the grain size has no effect on the permeability.

Effect of microstructure

The form in which the carbon is present is very important with regard to the permeability. The results of three series of experiments are presented below in Table X. Each of the investigations used a different steel composition, but each one chosen was capable of being heat treated to several structures. To aid in making the comparisons, relative permeabilities were calculated from the given data, which were expressed in a variety of units. In all three cases the lowest permeability was detected for the martensitic structures. The bainitic structures had lower permeabilities than pearlitic structures but there is a difference in the results for the coarse and fine varieties of each. The effectiveness of the annealed and tempered structures in permeating hydrogen is generally high. As a very general conclusion from this, one could say that the more massive forms of carbide particles (spheroidite or globular cementite, pearlite, certain tempered carbides) offer considerably less resistance. Martensite, in which the carbon atoms are retained in a dilated and strained iron lattice affords the most resistance to hydrogen passage. Therefore, hydrogen permeability tends to increase with increasing temperature of formation or transformation of the microconstituent.

Smialowski[17] has found that the permeability of a steel is much higher when the permeation is measured perpendicular to the direction of rolling than when the permeation is measured parallel to the rolling direction. This indicates a probably importa t role of

Table X. Permeation of Hydrogen in Steels Heat Treated
to Produce Various Microstructures

Investigator	Steel Used	Metal Microstructure	Relative Permeability
Nosyreva[18]	0.84% C	Martensite	1
	0.5% Mn	Lower Bainite	1
		Globular cementite	3.59
		Troostite (fine, globular carbides)	3.91
		Annealed steel	4.78
		Sorbite (growth of troostite)	7
		Normalized steel	7.43
Baht and Lloyd[48]	0.59% C	Martensite	1
		Coarse lamellar Pearlite and ferrite	1.57
		Very fine pearlite and ferrite	2.79
Amiot[18]	0.26% C	Martensite	1
	0.25% Ni	Tempered Martensite (at 550°C)	1.04
		Fine bainite	1.57
		Coarse bainite	1.95
		Coarse lamellar pearlite	2.16
		Fine lamellar pearlite	2.98
		Spheroidite	3.25

Inclusions because the surface area of inclusions would be much larger
in the first case.

Effect of tempering

Using a Ni-Cr-Mo steel (0.13%C) that could be tempered to
different strength levels, Kim and Loginow[25] showed that the hydrogen
permeability remained about the same during cathodic charging for the
four strength levels tested, while the hydrogen diffusivity decreased
as the strength level increased. This means that the hydrogen content
must increase with strength level and this was confirmed in a separate
series of experiments in which specimens were hydrogenated until satu-
ration. These investigators used the electro-permeation technique, but
applied no external current to the entry side. Thus, hydrogen was
charged into the specimen at the open-circuit potential. They used an
environment on this side of a 3% NaCl, 0.5% CH_3COOH saturated with H_2S.

This environment is a particularly effective one for hydrogenation, causing the specimens to crack when stressed well below the yield strength. The following table summarizes some of the important results of their paper:

Table XI. Hydrogen Permeation in a High-Strength Steel
Tempered to Various Yield Strengths[25]

Tempering Temperature (°C)	Yield Strength (ksi)	Apparent Diffusivity (cm²/sec)	Hydrogen Content at Saturation (ppm)	Approximate Threshold Stress Below Which Specimen Did Not Crack (ksi)
550	150	6.3×10^{-7}	6.2	12
575	138	9.3×10^{-7}	5.5	16
675	103	17×10^{-7}	3.3	42
700	95	30×10^{-7}	2.8	46

They were able to estimate that of the total hydrogen content shown in the table, about 0.08 ppm was hydrogen dissolved in interstitial positions in the lattice. They assumed that this value did not change much with heat treatment, so that the concentration of "trapped" hydrogen increased with the yield strength. The decrease of diffusivity with yield strength underscores the importance of the trapping phenomenon at these higher strengths, and the greater susceptibility to hydrogen cracking emphasizes that trapped hydrogen is indeed detrimental. The authors noted that the particle size of the precipitate increased with the tempering temperature while the number of particles decreased with the result that there was more interfacial area in the high-strength conditions.

A different conclusion was reached by Bolton and Shreir[18] who measured the amount of hydrogen absorbed by a tempered high-strength steel and found that the hydrogen contents were higher for the specimens tempered at the higher temperatures (600°C compared to 200°C). They found a difference in the polarization behavior of the steel tempered at the higher temperature compared to that tempered at the lower temperature. At constant applied current there was an increase in the cathodic overpotential in acetate buffer pH 4 solutions for the 600°C tempered steel, while the overpotential dropped for iron, untempered martensite, and the steel specimens tempered at 200° and 400°C. They concluded that the entry rate was promoted by the higher overpotential. The hydrogen content was due to these factors: entry rate, interfacial area between the carbide and ferrite, and the internal stress. Evidently the steel tempered at the higher temperature had the highest

hydrogen content because of the first factor since the interfacial area
and stress decreased with softening.

REFERENCES

1. R. J. Barton, 47th Technical Proc. of the Am Electroplaters' Soc.,
   (1960), 116.

2. J. O'M. Bockris and A. K. N. Reddy, Modern Electrochemistry, Vol. 2,
   Plenum Press, New York (1970), (Chapter 10).

3. B. E. Conway, Theory and Principles of Electrode Processes, Ronald
   Press, New York (1965), (Chapter 8).

4. J. McBreen and M. A. Genshaw, Proc. of Conference: Fundamental
   Aspects of Stress Corrosion Cracking, The Ohio State University,
   (1967), editors R. W. Staehle, A. J. Forty, D. van Rooyen, Natl.
   Assoc. of Corrosion Engine~s, Houston (1969), p. 51.

5. J. O'M. Bockris and R. Thacker, Tech Report #3, ONR 551 (22),
   NR 036-028, Office of Naval Research (December 31, 1959).

6. J. O'M. Bockris and M. A. V. Devanathan, The Determination of the
   Coverage on Nickel and Steel During Electrolytic Hydrogen Evolution,
   Tech. Report #4, Office of Naval Research, NR 036-028 (February 28,
   1961).

7. J. Horiuti and T. Toya, Chemisorbed Hydrogen, Report from Research
   Instutute for Catalysis, Hokkaido University, Sapporo, Japan (1968).

8. J. O'M. Bockris, M. A. Genshaw, and M. Fullenwider, Electrochimica
   Acta, 15 (1970), 47.

9. J. O'M. Bockris, J. McBreen, and L. Nanis, J. Electrochem. Soc.,
   112 (1965), 1025.

10. M. A. V. Devanthan and Z. Stachurski, J. Electrochem Soc., 111
    (1964), 619.

11. T. P. Radhakrishnan and L. L. Snreir, Electrochimica Acta, 11
    (1966), 1007.

12. W. Palczewska and I. Ratajczykowa, Bull. Acad. Polon. Sci., ser.
    sci. chim. 14 (1966), 673.

13. M. Enyo, Electrochim Acta, 18 (1973), 155.

14. R. M. Hudson, Corrosion, 20 (1969), 24st.

15. R. D. McCright and R. W. Staehle, to be published, J. Electrochem Soc.

16. M. Smialowski, Hydrogen in Steel, Pergamon Press, Oxford and Addison-wesley Publishing Co., Reading, Mass., (1962).

17. M. Smialowski and Z. Szklarska-Smialowska, Bull. Academie Polonaise Sci Classe III, 2 (1954), 73.

18. A. R. Elsea and E. E. Fletcher, DMIC Report 219, Hydrogen Movement in Steel -- Entry, Diffusion and Elimination, Battelle Memorial Institute, (June 30, 1965).

19. M. Pourbaix, Atlas of Electrochemical Equilibria in Aqueous Solution, Pergamon Press, Oxford and Cebelcor, Brussels, (1966).

20. H. Angerstein-Kozlowska, Bull. Academie Polonaise Sci. Series: sci., chim., geol., et geogr., 7 (1959), 881.

21. H. Angerstein-Kozlowska, Bull. Academie Polonaise Sci. Series: sci., chim., geol., et geogr., 6 (1958), 739.

22. M. Smialowski, Congres International, L'Hydrogene dans les Metaux, Editions Science, Paris, (1972), p. 300.

23. J. F. Newman and L. L. Shreir, Corrosion Science, 9 (1969), 631.

24. F. Matsuda and T. C. Franklin, J. Electrochem. Soc., 112 (1965), 767.

25. C. D. Kim and A. W. Loginow, Corrosion, 24 (1968), 313.

26. W. L. Jolly, L. B. Anderson, and R. T. Betrami, J. Amer. Chem. Soc., 79 (1957), 2443.

27. H. W. Salzberg and B. Goldschmidt, J. Electrochem Soc., 107 (1960), 348.

28. G. Wranglen, J. Electrochem. Soc., 108 (1961), 1069.

29. I. A. Menzies and L. W. Owen, Electrochimica Acta, 11 (1966), 251.

30. R. Piontelli and G. Poli, J. Electrochem. Soc., 109 (1962), 551.

31. R. M. Hudson and G. L. Stragand, Corrosion, 18 (1962), 269t.

32. S. M. Beloglazov, Zhur. Fiz. Khim., 38 (1964), 427; [Russ. J. Phys. Chem., 223, (1964)].

33. B. E. Conway and J. O'M. Bockris, J. Chem. Phys., 26 (1957), 532.

34. N. E. Khomotov, *Russ. J. Phys. Chem.*, 36 (1962), 1475

35. K. M. West, Electrodeposition and Corrosion Processes, D. van Nostrand Co. Ltd., London (1965), (Chapters 2 and 3).

36. W. Beck, A. L. Glass, and E. Taylor, *J. Electrochem. Soc.*, 112 (1965), 53.

37. T. A. Bagotskaya, *Russ. J. Phys. Chem.*, 36 (1962), 2667.

38. W. Beck, J. O'M. Bockris, J. McBreen, and L. Nanis, *Proc. Royal Soc.* (London), A290 (1966), 220.

39. U. R. Evans, *J. Electrochem. Soc.*, 113 (1966), 637.

40. H. G. Nelson and J. E. Stein, NASA Technical Note, NASA TN D-7265 (April, 1973).

41. W. Beck, J. O'M. Bockris, M. A. Genshaw, and P. K. Subramanyan, *Metallurgical Transactions*, 2 (1971), 883.

42. M. Weinstein and J. F. Elliot, *Trans. Met. Soc. AIME*, 227 (1963), 382.

43. H. H. Podgurski, *Trans. Met. Soc. AIME*, 221 (1961), 389.

44. S. Wach, A. P. Midownik, and J. Mackowiak, *Corrosion Science*, 6 (1966), 271.

45. T. P. Radhakrishnan and L. L. Shreir, *Electrochimica Acta*, 12 (1967), 889.

46. U. V. Baht and H. K. Lloyd, *J. Iron and Steel Institute*, 165 (1950), 382.

47. M. Smialowski, private communication, March 24, 1973.

48. K. Bolton and L. L. Shreir, *Corrosion Science*, 3 (1963), 17.